UNIVERSITY OF CALIFORNIA
RIVERSIDE

Impact of Alternative Fuels and Emission Control Systems on Small Engines to Large Ocean Going Vessels

A Dissertation submitted in partial satisfaction
of the requirements for the degree of

Doctor of Philosophy

in

Chemical and Environmental Engineering

by

Jiacheng Yang

September 2018

Dissertation Committee:

Dr. David R. Cocker III, Co-Chairperson
Dr. Thomas Durbin, Co-Chairperson
Dr. Heejung Jung
Dr. Kent C. Johnson
Dr. Georgios Karavalakis

The Dissertation of Jiacheng Yang is approved:

_____

_____

_____

_____

Committee Co-Chairperson

_____

Committee Co-Chairperson

University of California, Riverside

Acknowledgements

I would like to thank many individuals for making this dissertation possible. I would like to thank my advisors Dr. David R. Cocker and Dr. Thomas Durbin for their endless support throughout the PhD program. I would like to express my gratitude to Dr. Thomas Durbin, Dr. Georgios Karavalakis, Dr. Kent Johnson, and Dr. J Wayne Miller for giving me the opportunity to join the emissions and fuels research group at CECERT. I would like to thank Dr. Heejung Jung for his guidance and participation as a committee member for my Ph.D. advancement to candidacy and final defense. I would like to thank Dr. Robert Russel, Dr. Akua Asa-Awuku, and Dr. Kelley Barsanti for their advice for my research. I would like to thank the UCR Chemical and Environmental Engineering department for accepting my application to PhD program at the time and providing a full fellowship in my first year. I would like to express my gratitude and appreciate to Dr. David Cocker, Dr. Thomas Durbin, Dr. Akua Asa-Awuku, and Dr. Matthew Barth for their financial support through teaching assistant assignments and a National Center for Sustainable Transportation (NCST) fellowship during my second year to make it possible for me to continuously studying in emissions and fuels research group.

I would also like to thank Mr. Don Pacocha, Mr. Edward O'Neil, Mr. Mark Villela, Mr. Daniel Sandez, Mr. Kurt Bumiller, Mr. Daniel Gomez, Ms. Lauren Aycock, and Mr. Joe Valdez for their help with various light duty, heavy duty, marine, and PEMS testing. I appreciate Dr. Yu Jiang, Mr. Patrick Roth, and Mr. Cavan McCaffery as my close team members for all of their help and support. I would also like to thank former and current graduate students, Dr. Tanfeng Cao, Dr. Yusuf Khan, Dr. Nick Gysel, Dr. Liem Pham, Dr.

Chengguo Li, Dr. Chia-Li Chen, Dr. Mary Kacarab, Dr. Emmanuel Fofie, Dr. Pedro Piqueras, Mr. Weihan Peng, Mr. Paul Van Rooy, Mr. Xinze Peng, Ms. Yue Lin, Mr. Jinwei Zhang and Mr. Hanwei Zhu for their help and advice over the last four years. Additionally, I would like to thank my undergraduate student team members, Mr. Anthony Gerigk, Mr. Miguel Robledo, Mr. Brian Estrada, Ms. Michelle Le, Ms. Grace Johnson, Ms. Kexin Liu, Ms. Tian Xia, Mr. Taymour Mohammed, and Mr. Daniel Zaragoza for their contribution to the programs that I worked on.

I would like to recognize the funding sources including the California Air Resources Board (CARB), the Coordinating Research Council (CRC), the International Council on Clean Transportation (ICCT), the Manufacturer of Emission Controls Association (MECA), and the South Coast Air Quality Management District (AQMD) that made this dissertation possible.

The text of Chapter 2 of this dissertation, in part or in full, is reprinted from Environmental Science & Technology, Volume 52; Jiacheng Yang, Patrick Roth, Thomas D. Durbin, Kent C. Johnson, David R. Cocker, Akua Asa-Awuku, Rasto Brezny, Michael Geller, and Georgios Karavalakis; Gasoline Particulate Filters as an Effective Tool to Reduce Particulate and Polycyclic Aromatic Hydrocarbon Emissions from Gasoline Direct Injection (GDI) Vehicles: A Case Study with Two GDI Vehicles, Pages 3275-3284, Copyright (2018), with permission from ACS Environmental Science & Technology.

The text of Chapter 5 of this dissertation, in part or in full, is reprinted from Science of The Total Environment, Volume 640-641; Jiacheng Yang, Thomas D. Durbin, Yu Jiang, Takeshi Tange, Georgios Karavalakis, David R. Cocker III, and Kent C. Johnson; A

comparison of a mini-PEMS and a 1065 compliant PEMS for on-road gaseous and particulate emissions from a light duty diesel truck, Pages 364-376, Copyright (2018), with permission from Elsevier.

The text of Chapter 6 of this dissertation, in part or in full, is reprinted from Fuel, Volume 184; Jiacheng Yang, Yu Jiang, Georgios Karavalakis, Kent C. Johnson, Sachin Kumar, David R. Cocker III, and Thomas D. Durbin; Impacts of dimethyl carbonate blends on gaseous and particulate emissions from a heavy duty diesel engine, Pages 681-688, Copyright (2016), with permission from Elsevier.

Dedication

I dedicate this work to my parents Shoubao Yang (杨守宝) and Xiuyun Tian (田秀云), my grandparent Chunli Yang (杨春礼) and Wenqiao lv (吕文桥), and my girlfriend Ziyao Geng (耿子瑶) for their love, encouragement, and support all through my life.

ABSTRACT OF THE DISSERTATION

Impact of Alternative Fuels and Emission Control Systems on Small Engines to Large Ocean Going Vessels

by

Jiacheng Yang

Doctor of Philosophy, Graduate Program in Chemical and Environmental Engineering
University of California, Riverside, September 2018
Dr. David R. Cocker III, Co-Chairperson
Dr. Thomas D. Durbin, Co-Chairperson

Emissions from internal combustion engines (ICEs) pose a big problem to human health and the environment, but they are controllable. This dissertation investigated the emissions from ICEs for a range of applications and the feasibility of reducing their emissions with various cutting edge emissions control systems (ECS) and alternative fuels. This included light-duty vehicles, heavy-duty diesel engines, small off-road diesel engines (SORDEs) and ocean going vessels (OGVs). The control technologies included gasoline particulate filters (GPFs) and scrubbers, and the alternative fuels included various ethanol blends and dimethyl carbonate (DMC).

It is important to investigate and understand the emissions from light-duty passenger vehicles since they represent the largest populations in the vehicle fleet. The rapid growth of gasoline direction injection (GDI) vehicles has increased concerns with particulate matter (PM) emissions. This dissertation investigated the impact of PM

emissions from current technology GDI engines with different ECS and alternative fuels. This dissertation also evaluated the toxicity of PM emitted from GDI engines. GPFs were found to have a great potential for PM reduction, with reductions of approximately 98%, and they could be an effective tool to control PM emissions from GDI engines. Also, this dissertation investigated the use of ethanol fuel at various level in flex fuel GDI engines. The results suggested that the use of higher ethanol contents in gasoline could provide significant reductions in PM emissions on the order of 90%. The physical, chemical, and toxicological properties of the PM emissions from current technology GDI vehicles were also investigated in this dissertation via various health assays. Our results showed the toxicity of PM emitted from GDI vehicles was relatively low in comparison to many ambient PM samples.

Diesel engines are the most significant source of NOx and PM. The use of alternative fuels or advanced aftertreatment such as diesel particulate filters (DPFs) and selective catalytic reduction (SCR) have shown significant emissions control capability for diesel engines. The use of sensor technology in monitoring emissions from diesel ICEs has been of great interest in recent years, this dissertation investigated the accuracy of nitrogen oxides (NOx), PM, and particle number (PN) sensors compared to a standard 1065-compliant portable emissions measurement system (PEMS). The results showed comparisons within 10% for NOx, and good comparisons for PM relative to the future 1 mg/mi emissions standard. The PN sensor did show a high bias due to a zero offset current, however, that has been corrected in the latest version of the instrument. This dissertation also investigated a highly oxygenated alternative diesel fuel (DMC) at various blend levels.

The results showed a 78% reduction in PM emissions with 30% DMC blend with regular diesel. The reduction of PM was significant and was comparable to the amount of reductions seen for DPFs.

This dissertation also evaluated the feasibility and effectiveness of equipping SORDEs in the range of 25-75 hp with advanced PM and/or NOx control systems. For those small engines, current regulations do not require ECS. Emissions benefits and engine performance with the addition of ECS were evaluated on an engine dynamometer over specific engine duty cycles. With the addition of advanced ECS, reductions of over 95% for PM and 50-70% of NOx were achieved. This information can be used to develop new regulations to control emissions from SORDEs.

Diesel engines in large OGVs are less controlled compare to light-duty passenger vehicles and heavy-duty trucks. The International Maritime Organization (IMO) has set various regulations for large OGVs to control their sulfur, PM, and NOx emissions. This dissertation investigated the performance of a cutting-edge sulfur scrubber ECS for reducing sulfur and PM emissions from a large container vessel. The results showed over a 97% reduction in sulfur species in gaseous phase as SO_2, however, only a 2-12% reduction was observed for sulfur species in the particulate phase as sulfuric acid particles. The results from this study could impact regulations and vessel operators decisions on whether to use scrubber systems or switch to low sulfur marine fuels.

Table of Contents

List of Figures

List of Tables

Acronyms and Abbreviations

AE .....Auxiliary Engines
Al.....Aluminum
AMPS.....Alternative Motive Power Systems
ARB .....Air Resources Board
ASE.....Accelerated Solvent Extraction
BC .....Black Carbon
BTEX .....Benzene, Toluene, Ethylbenzene, xylene
BSFC.....Brake Specific Fuel Consumption
C.....Carbon
Ca .....Calcium
CAI.....California Analytical Instruments
CAFE .....Corporate Average Fuel Economy
CARB.....California Air Resources Board
CE-CERT.....College of Engineering-Center for Environmental Research and Technology (University of California, Riverside)
CEMs .....Continuous Emissions Monitor
CFR.....Code of Federal Regulations
CH4.....Methane
CI.....Chemical Ionization
CL .....Closed Loop
CLD.....Chemiluminescence detector
CO .....Carbon Monoxide
CO_2.....Carbon Dioxide
COV .....Coefficient of Variation
CPC.....Condensation Particle Counter
cpsi .....cells per square inch
Cr.....Chromium
CS.....Catalytic Stripper
Cu.....Copper
CVS.....Constant Volume Sampling
DEF .....Diesel Emissions Fluid
DBE.....Double Bond Equivalent
DCM .....dichloromethane
DDC .....Detroit Diesel Corporation
DEP .....Diesel Exhaust Particles
DF .....Dilution Factor
DI .....Direct Injection

DMC .....DiMethyl Carbonate
DNPF 2,4-dinitrophenylhydrazine
DOC .....Diesel Oxidation Catalyst
DPF .....Diesel Particulate Filter
DRI.....Desert Research Institute
DTT.....Dithiothreitol
EC .....Elemental Carbon
ECAs.....Emissions Control Areas
ECC.....Environmental and Climate Change
ECS .....Emissions Control Systems
EFM .....Exhaust Flow Measurement
ES.....Exhaust gas scrubber
EEPS .....Engine Exhaust Particle Sizer
EI.....Electron Impact
ELISA .....Energy Independence and Security Act
EPA.....United States Environmental Protection Agency
EU .....European Union
Fe.....Iron
FFV .....Flexible Fuel Vehicles
FID .....Flame Ionization Detector
FMPS .....Fast Mobility Particle Sizer
FSN .....AVL Smoke Meter
FTP.....Federal Test Procedure
g/mi .....grams per mile
GC .....Gas Chromatography
GDI .....Gasoline Direct Injection
GFM.....Gravimetric filter module
GHG.....Greenhoue Gas
GPFs.....Gasoline Particulate Filters
HFO.....Heavy Fuel Oil
HMOX-1 .....Heme oxygenase 1
hp.....Horsepower
HPLC .....High performance liquid chromatograph
ICCT .....International Council on Clean Transportation
ICEs.....Internal Combustion Engines
IMO.....International Maritime Organization
IPSD.....Integrated Particle Size Distribution
I/M.....Inspection and Maintenance
ISO .....International Organization for Standardization
K.....Potassium

kW.....kilowatts
lbs.....pounds
LD.....Light Duty
MARPOL.....International Convention for the Prevention of Pollution from Ships
MDL.....Method Detection Limits
ME.....Main Propulsion Engine
MECA.....Manufacturers of Emissions Controls Association
MEL.....CE-CERT's Mobile Emissions Laboratory
MG.....Main Power Generator
MGO.....Marine Gas Oil
MFC.....Mass Flow Controller
MIL.....Malfunction Indicator Light
Mn.....Manganese
Mo.....Molybdenum
mpg.....miles per gallon
Mph.....Miles per Hour
MPO.....Myeloperoxidase
MSAT.....Mobile Source Air Toxics
MS.....Mass Spectrometry
MSS.....Micro Soot Sensor
MW.....MegaWatt
MY.....Model Year
Na.....Sodium
NCEM.....NTK Compact Emissions Meter
NEDC.....New European Drive Cycle
NDIR.....Nondispersive Infrared Analyzer
NDUV.....Non-dispersive ultraviolet radiation
Ni.....Nickel
NIOSH.....National Institute for Occupational Safety and Health
NRC.....National Research Council
NRTC.....Non-Road Transient cycles
NMHC.....Non-Methane HydroCarbons
NO.....Nitric Oxide
NO2.....Nitrogen Dioxide
NO_x.....Nitrogen Oxides
NTE.....Not to Exceed
O2.....Oxygen
OBD.....On-Board Diagnostics
OC.....Organic Carbon
OEM.....Original Equipment Manufacturer

OGVs .....Ocean Going Vessels
OIS .....OBD Inspection System
OGV .....Ocean Going Vessels
OL .....Open Loop
PAH.....Polycyclic Aromatic Hydrocarbons
EAQS .....Portable Emissions AcQuisition System
P .....Phosphorous
Pd .....Palladium
Pt .....Platinum
PDP-CVS .....Positive Displacement Pump-Constant Volume Sampling
PEMS .....Portable Emissions Measurement Systems
PFI.....Port Fuel Injection
PGE.....Platinum-Group Element
PGM.....Platinum Group Metal
PM.....Particulate Matter
PMI .....PM Index
PN .....Particle Number
ppm .....Parts per million
PTFE .....Polytetrafluoroethylene
qRT-PCR.....Quantitative Real Time-Polymerase Chain Reaction
RDE.....Real Driving Emissions
REE.....Rare Earth Elements
Rh.....Rhodium
RIA.....Regulatory Impact Analysis
ROS.....Reactive Oxygen Species
RPM.....Engine Revolutions Per Minute
S .....Sulfur
SCAQMD .....South Coast Air Quality Management District
SCR.....Selective Catalytic Reduction
SF-ICPMS.....Magnetic-sector inductively-coupled plasma mass spectrometry
SET .....Supplementary Emission Test
SI.....Supporting Information
SM.....Supplementary Material
SOF .....Soluble Organic Fraction
SORDEs.....Small Off-Road Diesel Engines
SOx .....Sulfur Oxide
SMPS .....Scanning Mobility Particle Sizer
TEUs .....Twenty-foot equivalent units
THC.....Total Hydrocarbons

TIGF	Teflon impregnated glass fiber
TNFα	Tumor Necrosis Factor Alpha
TRU	Transportation Refrigeration Unit
TWC	Three-Way Catalyst
UC	California Unified Cycle
UCR	University of California, Riverside
US	United States
USEPA	United States Environmental Protection Agency
UNCTAD	United Nations Conference on Trade and Development
ULSD	Ultra-Low Sulfur Diesel
USEPA	United State Environmental Protection Agency
V	Vanadium
VERL	CE-CERT's Vehicle Emissions Research Laboratory
VOC	volatile organic compounds
WIOC	Water Insoluble Organic Carbon
WLTC	Worldwide harmonized Light duty driving Test Cycle
WSOC	Water Soluble Organic Carbon

1. Introduction

Internal combustion engines (ICEs) are the most important sources for power generation for transportation, with gasoline and diesel engines being the most popular forms of ICEs. An estimated 2 billion of ICEs are currently deployed in global freight and ground transportation systems, which support trillions of dollars of economic growth [Heywood, 2018]. Gasoline and diesel engines have a wide range of applications, including generators, light-duty passenger vehicles, heavy duty trucks and equipment, locomotives, harbor craft and ocean going vessels. The need for gasoline and diesel engines is expected to grow in the near future, as projections have shown the demand for ICEs will continue to grow another 20% by 2040 [ExxonMobil, 2018].

The use of ICEs also has environmental impacts, however, which are important to understand. The transportation sector is the largest contributor of particulate matter (PM), nitrogen oxides (NOx), and carbon dioxide (CO_2) emissions [Pachauri and Reisinger, 2007]. Climate change has been attributed to an increase of anthropogenic greenhouse gas emissions mainly due to CO_2 emissions. Along with the reduction of PM and NOx emissions, reducing CO_2 and other greenhouse gases is an also key issue for regulatory agencies and industrial companies worldwide [Pachauri and Reisinger, 2007]. In the United States (US), the Corporate Average Fuel Economy (CAFE) standards are currently very demanding for automotive manufacturers, with requirements to raise the average fuel economy of new cars and trucks to 54.5 miles per gallon by 2025. In the European Union

(EU), similar mandates are set to decrease the CO_2 emissions to an average of 130 g/km. Based on the need to address global warming issues, higher in-cylinder compression ratio have become the key technology of spark ignition engine development to reduce CO_2 emissions by improving the engine efficiency [Alkidas, 2007].

Gasoline and diesel engines emit significant amounts of PM emissions as a result of inhomogeneous mixing that creates fuel-rich zones during combustion. This PM is also largely $PM_{2.5}$ (aerodynamic diameters less than 2.5 μm), which can penetrate more deeply into the lungs. Exposure to $PM_{2.5}$ increases the risk of chronic illnesses, such as lung cancer and cardiopulmonary disease. In California, diesel particulate matter (PM) has been classified as a toxic air pollutant since 1998 [CARB, 1998]. $PM_{2.5}$ suspended in the air can also reduce visibility in urban areas. On a federal level, the United States Environmental Protection Agency (USEPA) enacted stringent 2007 emission standards for heavy-duty diesel engines to reduce PM on-road to 0.0134 g/kWh [Johnson, 2016]. PM emissions from in-land diesel engines are well controlled with diesel particulate filters (DPFs) since 2007, however, the PM emissions from gasoline engines are becoming more of a concern due to the rapid growth of gasoline direct injection (GDI) engines in the light duty fleet. GDI engines offer better fuel economy, but the direct injection results in higher PM emissions compared to the traditional port fuel injection (PFI) engines. Black Carbon (BC), which is an important component of PM, also has specific adverse impacts on health, including contributing to cardiovascular and chronic lung diseases [Janssen et al., 2012; Winebrake et al., 2009].

Gasoline and diesel engines are also significant contributors to NOx emissions as a consequence of high in-cylinder combustion temperatures [Heywood, 2018; Karavalakis et al., 2014; Jiang et al., 2018; Yang et al., 2018]. NOx emissions from gasoline and diesel engines are formed with the nitrogen and oxygen in the air when nitrogen and oxygen are disassociated by high in-cylinder combustion temperatures. NOx emissions can increase the risk of respiratory diseases and it also react with ambient volatile organic compounds (VOC) to form ground level ozone [Jerrett et al., 2009]. Diesel engines tend to emit more NOx emissions than gasoline engines due to their higher compression ratios, which results in a higher in-cylinder combustion temperature and leaner combustion, which makes it more difficult to reduce NOx once formed. Thus, diesel engines emit higher levels of NOx and have become a dominant source of mobile related NOx emissions over the past decade. Gasoline and diesel engines together account for 60% of total NOx emissions for the national emissions inventory in the U.S. [EPA, 2008]. This is a particularly critical issue in regions such as the greater LA basin and New York city, where it is estimated that large reductions in diesel NOx are needed to meet the upcoming federal ozone standards in 2023 and 2030.

Ocean going vessels (OGVs) with large diesel engines play a major role in the global economy and international trade by contributing to 80% of global trade by volume and over 70% of global trade by value. Ship emissions generated by the merchant fleet are reported to represent a significant contribution to global anthropogenic emissions and lead to a change of the chemical composition of the atmosphere and of climate [Lawrence and Crutzen, 1999; Davis et al., 2001; Eyring et al., 2005]. As more goods are shipped, the

local and global anthropogenic emissions and impact from shipping increases. International shipping can also contribute to increased mortality in coastal regions. Some have estimated this impact to be 60,000 deaths from cardiopulmonary and lung cancer per annum [Corbett et al., 2007, USEPA, 2016]. Emissions from OGVs not only effect the population living near the ports and coastlines, but also those living hundreds of miles inland.

Sulfur emissions from OGVs have been a particular concern in causing health and environmental effects worldwide. PM and NOx emissions from large ocean going vessels are increasing concerns due to the progressively emissions reduction on in-land diesel engines with DPF and selective catalytic reduction (SCR). Marine BC emissions also associated with climatic effects that include influencing cloud formation, and melting of glaciers and sea ice, especially in the highly sensitive Arctic [Bond et al., 2013; Corbett et al., 2010; Lack and Corbett, 2012].

In order to manage and mitigate the impacts of ICEs on the environment, it is important to study how emissions are formed under a wide range of different conditions and from different sources. This dissertation represents a characterization of emissions from a number of different sources and conditions. This includes small off-road diesel engines, light duty GDI vehicles, heavy duty diesel engines, and large OGVs. The rest of this introduction provides background information on each of the main thesis topic area. Finally, the last section in the introduction provides and outline of different chapters in this thesis.

1.1. Investigates GPF Reduction Efficiency on Particles and PAHs from Light Duty GDI Vehicles

Although GDI vehicles offer the potential of improved fuel economy, less fuel pumping, and charge air cooling, they tend to produce higher PM emissions when compared with the traditional port fuel injection engines [Piock et. al, 2011; Karavalakis et. al, 2015; Su et. al, 2014]. In GDI engines, fuel is sprayed directly into the combustion chamber, which leads to incomplete fuel evaporation due to the limited time available for fuel and air mixing. This leads to pockets with high temperatures but insufficient oxygen, leading to pyrolysis reactions and soot formation. Additionally, as the fuel comes directly into contact with the cold cylinder walls and piston, a small amount of fuel may impinge on the piston, which during evaporation may lead to diffusion combustion and PM formation [Piock et. al, 2011, Stevens et. al, 2001; Karlsson and Heywood, 2001; He et. al, 2012]. The rapid market penetration of GDI vehicles has led governments to impose stricter standards to control PM emissions. California LEVIII and US Tier 3 regulations will begin a four year phase-in starting in 2015 and 2017, respectively, to a PM maximum of 3 mg/mile from the current 10 mg/mile LEVII limit. LEVIII will begin a four year phase-in of a tighter 1 mg/mile starting in 2025. In the EU, the Euro 6a particle number (PN) standard for GDI vehicles was reduced from $6x10^{12}$ particles/km to $6x10^{11}$ particles/km in September 2017.

Additionally, it is important to better understand the toxicity of the particles being formed in GDI combustion. Today, the literature is scarce about the toxic properties of PM emissions from GDI vehicles, such as those of polycyclic aromatic hydrocarbons (PAHs),

their oxygenated (oxy-PAHs), and nitrated derivatives (nitro-PAHs) [Munoz et. al, 2016; Maikawa et. al, 2016]. PAHs have long been recognized as one of the major soot precursors for soot particles, while they are also classified as carcinogenic and mutagenic compounds adsorbed onto the PM or partition in the semivolatile PM phase [Richter and Howard, 2000; Kim et. al, 2013]. Additionally, some oxy-PAH and nitro-PAH species have been recognized as similarly or more toxic than their parent PAHs [Lundstedt et. al, 2007].

1.2. Investigates Ethanol and Aromatic Content Impact on Particulate and Mobile Source Air Toxic (MSAT) Emissions from Flex-fuel GDI vehicles

The use of biofuels in the US and Europe has been promoted for the past several decades in an effort to reduce GHGs and other emissions from the transportation sector. Biomass-derived ethanol is the most popular biofuel in the US, where all gasoline sold contains up to 10% ethanol by volume (E10). Ethanol utilization is still on the rise in the US, with the US EPA allowing 15% of ethanol by volume (E15) to be sold in the market [EPA, 2011]. The favorable environment for growth of ethanol fuel use is also promoted by the Energy Independence and Security Act of 2007 (EISA) and the Renewable Fuel Standard mandates. In addition to lower concentrations of gasoline-ethanol blends, gasoline is allowed to contain between 51% and 83% ethanol by volume. Higher levels of ethanol can be used in flexible fuel vehicles (FFVs), which are designed for this purpose and are certified for emissions compliance by testing with E0 and E85.

One of the major drawbacks of GDI technology is the exacerbated PM emissions compared to PFI engines due to fuel impingement onto piston and cylinder walls. Understanding the impact of ethanol fueling on gaseous and particulate emissions from

GDI engines is not straightforward. Ethanol has the potential to suppress soot formation in GDI engines and in flames [Fatouraie et al., 2015; Khosousi et al., 2015]. Lemaire et al. [2010] studied the effects of adding ethanol to gasoline on soot formation in turbulent spray flames and observed suppressed soot formation with ethanol, not only by dilution effect, but also by chemical (oxygen) effect. Karavalakis and co-workers [2014] showed reductions in PM mass, black carbon, and particle number emissions when they tested E10, E15, and E20 blends in GDI vehicles over the Federal Test Procedure (FTP) and LA92 cycles. Maricq et al. [2012] documented only small reductions in PM mass and particle number emissions as the ethanol level in gasoline increased from 0 to 20% in tests of a GDI turbocharged vehicle, however, much higher reductions in both PM mass and particle number emissions were measured for ethanol contents >30%. In addition to particulate emissions, previous studies have shown that an increase in ethanol content in the fuel blends reduces the emissions of NOx, carbon monoxide (CO), non-methane hydrocarbons (NMHC), and total hydrocarbon (THC) [Hubbard et al., 2014; Dardiotis et al., 2015]. Other studies have shown that higher ethanol concentrations can lead to elevated formaldehyde and acetaldehyde emissions, which are potentially carcinogenic compounds to humans [Clairotte et al., 2013; Karavalakis et al., 2014]. Suarez-Bertoa et al. [2015] tested a flex fuel vehicle with direct injection on E5, E10, E15, E75, and E85 blends over the New European Drive Cycle (NEDC) and the Worldwide harmonized Light-duty driving Test Cycle (WLTC) and found sharp increases in CO, methane (CH_4), formaldehyde, acetaldehyde, and ethanol emissions. Karavalakis et al [2014] reported statistically significant reductions in CO, NMHC, and acetaldehyde emissions for E51 and E83 when

they tested one FFV with a direct injection engine and one FFV with a PFI engine over the FTP and LA92 cycles. The authors found lower benzene, toluene, ethylbenzene, xylene (BTEX) emissions with higher ethanol. The objective of this study is to investigate different ethanol concentrations, as well as the influence of higher gasoline aromatics content on the regulated emissions, PM mass, black carbon, and particle number emissions, and the mobile source air toxic pollutants.

1.3. Investigates Physical, Chemical, and Toxicological Characteristic of Particulate Emissions from Current Technology GDI Vehicles

The physiochemical and toxicological characteristics of the PM emissions are as, or more, relevant to potential human health impacts than the mass emission factors. However, toxicological impacts of PM emissions, especially from GDI engines, are poorly understood. Several studies have examined the nature of particulate emissions from GDI engines as a function of fuel type, fuel injection architecture, after-treatment control, and engine operating parameters [Chen et al., 2012; Chan et al., 2014; Barrientos et al., 2016]. Particles from GDI engines are generally formed from fuel and lubricant oil and are complex agglomerates of volatile and non-volatile substances, both organic and inorganic (sulfate, nitrate, metal species) in nature [Piock et al., 2011]. Karavalakis and co-workers [2015] documented that greater aromatic hydrocarbon content in gasoline resulted in higher PM mass, particle number, and black carbon emissions from a fleet of GDI and PFI vehicles. Pirjola et al. [2015] showed a clear effect of lubricant oil on particle emissions from a modern GDI vehicle. Badshah et al. [2016] reported that under cold-start conditions

the large majority of the total exhaust particles from GDI vehicles were solid soot and only a small fraction were semi-volatile.

A number of studies have shown that exposure to primary PM emissions from mobile sources is linked directly to adverse health implications [Bisig et al., 2018; Tzamkiozis et al., 2010; Seagrave et al., 2002]. Epidemiologic and toxicological studies have reported that elevated levels of PM are associated with cardiopulmonary mortality and morbidity [Araujo and Nel, 2009; Bates et al., 2015; Reed et al., 2008]. The underlying mechanisms via which PM exposure contributes to adverse human health outcomes have been the subject of intense study and our understanding is incrementally expanding. Increasing evidence suggests that transition metals present in PM (e.g., iron, manganese, vanadium), as well as certain organic species (e.g., quinones) generate reactive oxygen species (ROS), may be involved in producing respiratory symptoms [Rohr and Wyzga, 2012; Diaz et al., 2012; Charrier and Anastasio, 2012]. Diaz et al. [2012] showed that primary particles emitted from a gasoline vehicle might be able to cause a change in the breathing patterns of male Sprague Dawley rats. Lund and co-workers [2007] showed that inhalational exposure to gasoline engine emissions resulted in increased aortic mRNA expression of several genes, including matrix metalloproteinase-3 (MMP-3), MMP-7, and MMP-9, tissue inhibitor of metalloproteinases-2, endothelin-1 and heme oxygenase-1 (HO-1) in ApoE-/- mice (an animal model of atherosclerosis). The authors concluded that exposure to gasoline exhaust results in vascular remodeling, as well as increased expression of markers of oxidative stress, which may contribute to the progression of atherosclerosis. A recent study showed that exposure to GDI exhaust contributes to upregulation of genes

related to the metabolism of PAHs and oxidative stress [Maikawa et al., 2016]. There is a significant body of evidence documenting that insoluble PM can initiate inflammatory cascades in lung tissues with resulting morbidity, including carcinogenesis and endothelial dysfunction [Freire et al., 2013; Tamagawa et al., 2008]. The primary objectives of this study were to advance our understanding of the physical and chemical properties of particulate emissions from current technology GDI light-duty vehicles and provide a new primary assessment of the oxidative stress potential and inflammatory responses of the emitted PM.

1.4. **Investigates the Accuracy of Sensors for Light Duty On-road Measurement**

Portable Emissions Measurement Systems (PEMS) are tools that are designed to measure vehicle/truck emissions while operating on the road. The application and technology of PEMS has evolved considerably over the past 20 years. PEMS serve an important role in helping to better understand and characterize the differences between laboratory certification and other testing and real-world emissions. PEMS were incorporated into the regulatory process as part of the 1998 consent decree in the United States and the regulations for in-use compliance testing of heavy-duty vehicles within the Not-to-Exceed (NTE) areas of operation that were created as part of these proceedings [Federal Register 2003, 2005; US EPA, 2008]. This provided an impetus for the development of more commercial PEMS. PEMS have also been used extensively for measurements of emissions from heavy-duty trucks, light-duty vehicles, and construction equipment [Johnson, 2002; Gautam et al. 2001; Kishan et al., 2011; Frey et al. 2010; Cao

et al., 2016]. More recently, PEMS have been incorporated into regulations for Real Driving Emissions (RDE) testing in Europe [Vlachos et al., 2014].

Given the complexity and cost of 1065 compliant PEMS, there is a growing interest in the development of mini-PEMS that are not targeted at compliance with 1065 specifications, but still provide reliable emissions measurements, and are easy to deploy and less expensive. Mini-PEMS are simplified versions of the 1065 compliant PEMS. Such PEMS could have a number of applications in that they could be used to screen larger numbers of vehicles to identify and characterize potential emissions issues. This could be of use to both engine and vehicle manufacturers to identify potential issues under real-world conditions or for government agencies looking for issues that might require more extensive investigation as part of enforcement programs. Such PEMS could also be used for enforcement in applications such as Inspection and Maintenance (I/M) programs. Some simpler instruments designed to target only a single emissions component are already being applied in I/M type of applications. Opacity has been used extensively as a surrogate for PM emissions in a number of different areas. More recently, the Swiss SR941.242 Regulation in Europe is requiring biannual testing of off-road diesel machinery equipped with DPFs for compliance with a particle number (PN) mini-PEMS. The goal of this study was to compare emissions measurements between a 1065 compliant PEMS, and one of the current generation mini-PEMS.

1.5. Evaluates the Impacts of Dimethyl Carbonate Blends on Gaseous and Particulate Emissions from a Heavy Duty Diesel Engine

There is a growing interest in the use of renewable oxygenated fuels either as replacements of, or additives to, petroleum-based transportation fuels in ICEs. Oxygenated biofuels, such as ethanol and fatty acid methyl esters, are attractive because they offer GHGs emission benefits, reduce the tendency to form soot and black carbon emissions, help address climate change, and reduce the dependence on fossil fuel resources [Karavalakis et al., 2014; Hajbabaei et al., 2014; Ratcliff et al., 2016]. Carbonate esters (which consist of a carbonyl group connecting two alkyl groups) are promising fuels for use in compression ignition engines [Kumar and Sarayanan, 2016; Sivalakshmi and Balusamy, 2012]. Dimethyl carbonate [$CH_3OC(=O)OCH_3$, DMC] is a fuel that generates interest primarily due to its high oxygen content (53% by weight) [Pacheco and Marshall, 1997]. DMC is non-toxic, biodegradable, and highly miscible with diesel fuel. An additional benefit is that DMC can be produced from methanol and CO_2 in the presence of a catalyst (usually potassium chloride) providing a sink for the GHGs, CO_2 [Souza et al., 2014]. The molecular structure of DMC includes oxygen atoms paired up with carbon atoms to form CO. Hence, the absence of carbon-carbon bonds in the fuel moiety will contribute to hydrocarbon oxidation rather than participation in soot growth reactions [Glaude et al., 2005].

There have been studies of the combustion performance and emissions of diesel engines operating on DMC blends with petroleum diesel fuel [Sun et al., 2016; Kocis et al., 2000; Kozak et al., 2009]. Fundamental chemical kinetic studies have shown that when

DMC is tested in a flame much of the oxygen in the dimethyl carbonate goes directly to CO_2, which reduces the effectiveness of DMC for soot reduction in diesel engines [Glaude et al., 2005; Sun et al., 2016]. Rubino and Thomson [1999] observed a marked reduction of soot precursors, such as acetylene and benzene, when using a counter-flow propene/air diffusion flame to study the inhibition of soot formation with DMC. This systematic tendency of DMC to reduce soot was also confirmed in older studies, where soot and smoke emissions declined almost linearly with increasing DMC content [Miyamoto et al., 1998; Murayama et al., 1995]. Cheung et al. [2011] investigated DMC-diesel blends in a direct injection diesel engine and found small differences in gaseous emissions, with some increases in CO and THC especially at lighter engine loads. They also found significant reductions in PM mass and particle number emissions with higher DMC concentrations, especially at higher engine loads. Huang et al. [2003] studied the combustion and emissions characteristics of a diesel engine fueled with DMC-diesel blends and found that the engine's thermal efficiency increases and the emissions of PM, THC, and CO decrease. Similar reductions in PM emission were also seen in other studies with DMC-diesel blends, as well as the potential of reducing benzene and 1,3-butadiene emissions [Rounce et al., 2010]. Motivated by previous studies published in the open literature as well as by the concerns regarding global climate change caused by GHG emissions and the contribution of heavy-duty diesel engines to PM emissions, the present work investigates the impact of DMC blending on the regulated emissions, mobile source air toxics (MSATs) that include some aromatics and carbonyl compounds, and particulate emissions.

1.6. Evaluates the Feasibility and Emissions Benefit of Equipping Small Off-road Diesel Engines with Advanced PM and/or NOx Aftertreatment

Emissions from off-road diesel engines are a significant contributor to the emissions inventory in California, especially with respect to toxic PM and NOx. Small off-road diesel engines comprise approximately 20-40% of the population of all off-road diesel engines within the State, and are responsible for an equivalent portion of those emissions. As aftertreatment systems (DPFs and SCR) have been implemented for large off-road diesel engines; however, the impact of emissions from small off-road engines with less controls on the emissions inventory is expected to increase. The existing standards for tier 4 off-road engines were developed based on a regulatory impact analysis (RIA) conducted back in 2004, and do not require aftertreatment for NOx below 75 hp or PM below 25 hp. Since aftertreatment control devices for diesel vehicles and equipment are considerably more common now, the use of these strategies for <37kW engines may be considerably more viable than the time of the previous RIA, which could warrant renewed consideration for adopting more stringent exhaust standards for the <37kW sector.

Estimates of the potential emissions inventory benefits of adding advanced emissions controls to SORDEs were made using estimated of expected reduction efficiencies for DPFs and SCRs. For these calculations, DPFs were estimated to reduce PM by 90%, while SCR was estimated to reduce NOx emissions by 60 to 85%. The objective of this study is to evaluate the potential effectiveness, feasibility, and cost effectiveness of implementing regulations on mobile off-road diesel engines with rated powers of less than 37 kilowatts (kW) that will require the use of advanced emission control strategies, such

as DPFs and SCR. This study includes a demonstration of selected aftertreatment technologies on actual engines and verification of the emissions performance of these devices through a series of emissions tests.

1.7. Evaluates the Scrubber Efficiency on Removing Sulfur Species Emissions from Ocean Going Vessels

International shipping is attractive because of the low cost per ton of delivered goods. One driver of the low delivery cost is that the diesel engines OGVs are designed to burn the lowest cost fuels available, so called bunker fuels. These fuels are a blend of distillable refinery streams with the non-distillable portions of crude and as a result have a high content of sulfur, polycyclic aromatic hydrocarbons and heavy metals. Burning fuels with high sulfur contents lead to high levels of sulfur oxide emissions that can harm the respiratory system and make breathing difficult, especially for asthmatics [Li et al., 2014]. Furthermore, SOx reacts with compounds in the atmosphere to form small particles that may penetrate deeply into sensitive parts of the lungs and cause additional health problems. Several investigators have reported a connection between fuel sulfur content and PM emissions [Fridell and Salo, 2014; Winnes and Fridell, 2009]. For comparison, it should be noted that a switch from heavy fuel oil (HFO) to a marine gas oil (MGO) resulted in a 75% PM mass reduction [Winners and Fridell, 2009]. Due to the increased concern about ship emissions near ports, the International Maritime Organization (IMO) reduced the maximum sulfur limit for marine fuels in 2012 to 3.5 wt% and in 2020 to 0.5 wt%, [IMO; Fridell and Salo, 2014].

In addition to lowering the sulfur levels for all marine fuels, the IMO also identified environmentally sensitive areas, called Emission Control Areas (ECAs), where after January 2015 SOx emissions must be the same or less than if the ship burned a fuel with 0.1% sulfur. Currently, there are four ECAs around North America and Western Europe and more ECAs are planned. Within ECAs, vessels with exhaust gas cleaning system may burn fuels with up to 3.5% sulfur as long as the ratio of SOx to CO_2 exhaust emissions are the same or less as if the ship burned a fuel with 0.1% sulfur. When operating ships within ECAs, vessel owners have to decide whether to burn a fuel with <0.1% sulfur or install a scrubber in order to burn a fuels with up to 3.5% sulfur. Soon, in 2020, vessel owners will have to burn fuels with <0.5% sulfur globally or install an exhaust gas scrubber (EGS). For both cases, the choice of either low-sulfur fuel or a scrubber depends on a number of factors and is a tradeoff of operating versus capital expenses. Factors entering that decision include the relative cost of the fuels, the amount of time spent in ECAs, the ship's fuel consumption, its age and the cost of adding a scrubber [UNCTAD, 2015]. The installed cost of a wet scrubber system is in the range of $2 to $5 million depending on vessel and scrubber design [UNCTAD, 2015]. Many have found that installing a seawater scrubber to offset the higher operating expense of low sulfur fuel is a proven strategy [IMO, 2009]. So, EGS use is expected to increase before 2020 when the new sulfur limits for marine fuels are implemented.

Many studies show that scrubbers were highly effective for controlling SOx at either laboratory or power plant levels [Caiazzo et al., 2013; Andreasen and Mayer, 2007; Oikawa et al., 2003]. However, ship results are sparse. Available results show SOx

reductions > 95% and PM mass reductions ranging from 45-80%. [Fridell and Salo, 2014; Hansen, 2012; USEPA, 2011]. The significant difference in scrubber efficiencies for SOx and PM is not surprising given that the mechanism and design principles for removing SOx and PM are different [Cooper and Alley, 2010], and that the vessels are installing scrubbers designed to remove SO2 rather than PM. Given the ECA regulation, the approaching new sulfur limits, and an increasing number of installed/planned EGS systems, there is an immediate need to understand whether EGS provides both the SOx and the PM emission control as intended in Regulation 14 of MARPOL Annex VI. Data from this research will provide information on whether EGS is an acceptable environmental path for both SOx and PM with the high-sulfur, residual marine fuels. Data can also be useful in the current debate on whether all marine fuels should be limited to 0.5% sulfur in 2020.

1.8. **Outline of Dissertation**

Chapter 2 presents an assessment the gaseous, particulate, and genotoxic pollutants from two current technology gasoline direct injection vehicles when tested in their original configuration and with a catalyzed GPF. Testing was conducted over the LA92 and US06 Supplemental Federal Test Procedure (US06) driving cycles on typical California E10 fuel. Our results showed dramatic reductions in PM mass, black carbon, and total and solid particle number emissions with the use of GPFs for both vehicles over the LA92 and US06 cycles. The use of a GPF did not show any fuel economy and CO_2 emission penalties, while the emissions of THC, CO, and NOx were generally reduced. Particle size distributions were primarily bimodal in nature, with accumulation mode particles dominating the distribution profile and their concentrations being higher during the cold-start period of the

cycle. PAHs and nitrated PAHs were quantified in both the vapor and particle phases of the PM, with the GPF-equipped vehicles practically eliminating most of these species in the exhaust. For the stock vehicles, 2-3 ring compounds and heavier 5-6 rings compounds were observed in the PM, whereas the vapor phase was dominated mostly by 2-3 ring aromatic compounds.

Chapter 3 presents the influence of low-, mid-, and high-ethanol fueling, as well as the influence of the aromatic hydrocarbons in the fuel blend, on the regulated and greenhouse gas emissions, the mobile source air toxic pollutants, and the particulate emissions from a current model flexible fuel vehicle equipped with a gasoline direct injection engine. This study utilizes four fuels in total, including a baseline US EPA Tier E10 fuel, one E10 fuel with higher aromatics content than the baseline E10, an E30 fuel that was splash-blended with the Tier 3 E10, and an E78 fuel. The findings of this study showed that the higher ethanol blends, namely the E30 and E78, led to statistically significant THC, NMHC, CO, and NOx emissions reductions compared to the high aromatics E10 fuel. The emissions CO_2 were higher of the high aromatics E10 than the Tier 3 E10, E30, and E78 blends. A fuel economy penalty was also observed for lower energy content E30 and E78 blends compared to both E10 fuels. PM mass, black carbon, and total and solid particle number emissions showed statistically significant reductions for the E30 and E78 fuels compared to both E10 fuels. Results also showed that the high PM Index/high aromatics E10 produced more particulate emissions than the low PM Index E10, as well as higher populations of accumulation (soot) mode particles. Acetaldehyde formation favored by the higher ethanol content in the fuel, whereas benzene, toluene,

ethylbenzene, and xylenes emissions enhanced their formation with the high aromatics E10 and reduced with E30 and E78 fuels.

Chapter 4 presents the assessment of the physical, chemical and toxicological characteristics of particulate emissions from four light-duty gasoline direct injection vehicles when operated over the LA92 driving cycle. Our results showed that particle mass and number emissions increased markedly during accelerations. For three of the four vehicles tested, particle mass and number emissions were markedly higher during cold-start and the first few accelerations following the cold-start period than during the hot running and hot-start segments of the LA92 cycle. For one vehicle (which had the highest emissions overall) the hot-start and cold-start PM emissions were similar. Black carbon emissions were also much higher during the cold-start conditions, indicating severe fuel wetting leading to slow evaporation and pool burning, and subsequent soot formation. Particle number concentrations and black carbon emissions showed large reductions during the urban and hot-start phases of the test cycle. The oxidative potential of PM was quantified with both a chemical and a biological assay, and the gene expression impacts of the PM in a macrophage model with PCR and ELISA analyses. Inter- and intra-vehicle variability in oxidative potential per milligram of PM emitted was relatively low for both oxidative assays, suggesting that real-world emissions and exposure can be estimated with distance-normalized emission factors. The PCR response from signaling markers for oxidative stress (e.g., NOX1) was greater than from inflammatory, AhR, or MAPK signaling. Protein production associated with inflammation (TNFα) and oxidative stress (HMOX-1) were quantified and displayed relatively high inter-vehicle variability,

suggesting that these pathways may be activated by different PM components. Correlation of trace metal concentrations and oxidative potential suggests a role for small, insoluble particles in inducing oxidative stress.

Chapter 5 presents the comparison of emissions measurements between a 1065 compliant PEMS, and the NTK Compact Emissions Meter (NCEM) capable of measuring NOx, PM, and solid PN. Both units were equipped on a light-duty diesel truck and tested over local, highway, and downtown driving routes. The results indicate that the NOx measurements for the NCEM were within approximately ±10% of those the 1065 compliant PEMS, which suggests that the NCEM could be used as a screening tool for NOx emissions. The NCEM showed larger differences for PM emissions on an absolute level, but this was at PM levels well below the 1 mg/mi level. The NCEM differences ranged from -2% to +26% if the comparisons are based on a percentage of the 1.0 mg/mi standard. Larger differences were also seen for PN emissions, with the NCEM measuring higher PN emissions, which can primarily be attributed to a zero current offset that we observed for the NCEM, which has been subsequently improved in the latest generation of the NCEM system. The comparisons between the 1065 compliant PEMS and the NCEM suggest that there could be applications for the NCEM or other mini-PEMS for applications such as identification of potential issues by regulatory agencies, manufacturer evaluation and validation of emissions under in-use conditions, and potential use in I/M programs, especially for heavy-duty vehicles.

Chapter 6 presents the investigation of an alternative fuel blend for diesel. DMC is an oxygenate fuel that can be used in petroleum diesel that is been lightly studied, but could

provide significant reductions in PM emissions from internal combustion engines. This study evaluated the emissions impacts of 5%, 12.5%, 20%, and 30% blends of DMC in a California diesel fuel. DMC showed PM reductions increased with increasing DMC blend levels, ranging from 30% to 78% for the DMC5 to DMC30 blends. In contrast, particle number emissions increased with increasing DMC levels, which could be attributed to the enhanced formation of small nucleation particles as the levels of larger accumulation particles were reduced. NO_x emissions showed increases of 3.2% and 3.1%, respectively, for the higher 20% and 30% blends, but no statistically significant differences for the 5% and 12.5% blends. CO emissions showed strong reductions from 26.3% to 60.9% with DMC blending, while THC emissions showed increases from 32.5% to 137% with DMC. Most of the hydrocarbon species showed increases with increasing DMC blend levels, including benzene and most mono-aromatic hydrocarbons. Similarly, formaldehyde and acetaldehyde showed statistically significant increases with DMC blending relative to diesel fuel. The CO_2 emissions and brake specific fuel consumption (BSFC) increased with increasing DMC blend levels compared to diesel fuel.

Chapter 7 presents the potential effectiveness, feasibility, and cost effectiveness of implementing regulations on mobile off-road diesel engines with rated powers of less than 37 kW that will require the use of advanced emission control strategies, such as DPFs and SCR. This study includes a demonstration of selected aftertreatment technologies on actual engines and verification of the emissions performance of these devices through a series of emissions and durability tests.

Chapter 8 provides emission measurements of gaseous, PM, sulfur species, and elemental and organic carbon from a Tier 0 large ocean going vessel with cutting-edge scrubber systems. This vessel was operating with high sulfur content fuel with a scrubber system to compliance in the IMO regulated ECA area. The scrubber system is designed to reduce sulfur emissions to an equivalent level as low sulfur fuel. Our results indicates that the scrubber system has over 95% reduction in SOx, but very limited reductions on sulfur from the particle phase. This is due to the natural formation of the nanosized nucleation mode sulfuric acid particles under such conditions that they can not be eliminated by the scrubber system. Considering sulfur emissions as a whole, both gaseous and particulates, the scrubber systems equivalent sulfur emissions were still higher than those achieved by using low sulfur.

1.9. **References**

Alkidas, A. C. Combustion advancements in gasoline engines. Energy Conversion and Management 2007, 48, 2751-2761.

Andreasen, A., & Mayer, S. (2007). Use of seawater scrubbing for SO2 removal from marine engine exhaust gas. Energy & Fuels, 21(6), 3274-3279.

Araujo JA, Nel AE. Particulate matter and atherosclerosis: role of particle size, composition and oxidative stress. Part Fibre Toxicol 2009;24.

Badshah H, Kittelson D, Northrop W. Particle emissions from light-duty vehicles during cold-cold start. SAE Technical Paper, 2016; 2016-01-0997.

Barrientos, E.J.; Anderson, J.E.; Maricq, M.M.; Boehman, A.L. Particulate matter indices using smoke point for vehicle emissions with gasoline, ethanol blends, and butanol blends. Combustion and Flame 2016, 167, 308-319.

Bates JT, Weber RJ, Abrams J, Verma V, Fang T, Klein M, Tolbert PE. Reactive oxygen species generation linked to sources of atmospheric particulate matter and cardiorespiratory effects. Environ. Sci. Technol. 2015;49:13605-13612.

Bisig C, Comte P, Gudel M, Czerwinski J, Mayer A, Muller L, Petri-Fink A, Rothen-Rutishauser B. Assessment of lung cell toxicity of various gasoline engine exhaust using a versalite in vitro exposure system. Environmental Pollution 2018;235:263-271.

Bond, T.C., Doherty, S.J., Fahey, D.W., Forster, P.M., Berntsen, T., DeAngelo, B.J., Flanner, M.G., Ghan, S., Kärcher, B., Koch, D., Kinne, S., 2013. Bounding the role of black carbon in the climate system: A scientific assessment. J. Geophys. Res. 118, 5380-5552.

Caiazzo, G., Langella, G., Miccio, F., & Scala, F. (2013). An experimental investigation on seawater SO2 scrubbing for marine application. Environmental Progress & Sustainable Energy, 32(4), 1179-1186.

California Air Resources Board: Resolution 98-35: Identification of particulate emissions from diesel-fueled engines as a toxic air contaminant; http://www.arb.ca.gov/regact/diesltac/res98-35. California Air Resources Board, 1998.

Cao, T., Durbin, T.D., Cocker III, D.R., Wanker, R., Schimpl, T., Pointner, V., Oberguggenberger, K., Johnson, K.C., 2016. A Comprehensive Evaluation of a Gaseous Portable Emissions Measurement System with a Mobile Reference Laboratory, Emissions Control Sci. & Technol. 2, 173-180.

Chan TW, Meloche E, Kubsh J, Brezny R. Black carbon emissions in gasoline exhaust and a reduction alternative with a gasoline particulate filter. Environ. Sci. Technol. 2014;48:6027-6034.

Charrier JG, Anastasio C. On dithiothreitol (DTT) as a measure of oxidative potential for ambient particles: evidence for the importance of soluble transition metals, Atmos. Chem. Phys. 2012;12:9321-9333.

Chen L, Stone R, Richardson D. A study of mixture preparation and PM emissions using a direct injection engine fueled with stoichiometric gasoline/ethanol blends. Fuel 2012;96:120-130.

Cheung CS, Zhu R, Huang Z. Investigation on the gaseous and particulate emissions of a compression ignition engine fueled with diesel-dimethyl carbonate blends. Science of the Total Environment 2011;409:523-529.

Clairotte, M.; Adam, T.W.; Zardini, A.A.; Manfredi, U.; Martini, G.; Krasenbrink, A.; Vicet, A.; Tournie, E.; Astorga, C. Effects of low temperature on the cold start gaseous emissions from light duty vehicles fueled by ethanol-blended gasoline. Applied Energy 2013, 102, 44-54.

Cooper, C. D., & Alley, F. C. (2010). Air pollution control: A design approach. Waveland Press.

Corbett, J. J., Winebrake, J. J., Green, E. H., Kasibhatla, P., Eyring, V., & Lauer, A. (2007). Mortality from ship emissions: a global assessment. Environmental science & technology, 41(24), 8512-8518.

Corbett, J.J., Winebrake, J.J., Green, E.H., 2010. An assessment of technologies for reducing regional short-lived climate forcers emitted by ships with implications for Arctic shipping. Carbon Manage. 1, 207-225.

Dardiotis, C.; Fontaras, G.; Marotta, A.; Martini, G.; Manfredi, U. Emissions of modern light duty ethanol flex-fuel vehicles over different operating and environmental conditions. Fuel 2015, 140, 531-540.

Davis, D. D., G. Grodzinsky, P. Kasibhatla, J. Crawford, G. Chen, S. Liu, A. Bandy, D. Thornton, H. Guan, and S. Sandholm (2001), Impact of ship emissions on marine boundary layer NOx and SO2 distributions over the Pacific Basin, Geophys. Res. Lett.,28, 235–238.

Diaz EA, Chung Y, Papapostolou V, Lawrence J, Long MS, Hatakeyama V, Gomes B, Calil Y, Sato R, Koutrakis P, Godleski JJ. Effects of fresh and aged vehicular exhaust emissions on breathing pattern and cellular responses-pilot single vehicle study. Inhalation Toxicology 2012;25:288-295.

EPA. Ethanol Waivers (E15 and E10). Environmental Protection Agency; 2011.

Eyring, V., Köhler, H. W., Lauer, A., & Lemper, B. (2005). Emissions from international shipping: 2. Impact of future technologies on scenarios until 2050. Journal of Geophysical Research: Atmospheres, 110(D17).

Fatouraie, M.; Wooldridge, M.S.; Petersen, B.R.; Wooldridge, S.T. Effects of ethanol on in-cylinder and exhaust gas particulate emissions of a gasoline direct injection spark ignition engine. Energy and Fuels 2015, 29, 3399-3412.

Federal Register, 2003. Proposed Settlement Agreement, Federal Register 68:113, June 12 2003, pp. 35211–35212.

Federal Register, 2005. Control of Emissions of Air Pollution From New Motor Vehicles: In-use Testing for Heavy-duty Diesel Engines and Vehicles, Federal Register, June 14, 2005, vol. 70 No. 113.

Freire J, Ajona D, De Biurrun G, Agorreta J, Segura V, Guruceaga E, Bleau AM, Pio R, Blanco D, Montuega LM. Silica-induced chronic inflammation promotes lung carcinogenesis in the context of an immunosuppressive microenvironment. Neoplasia 2013;15:913-924.

Frey, H.C., Rasdorf, W., Lewis, P., 2010b. Comprehensive field study of fuel use and emissions of nonroad diesel construction equipment. Transp. Res. Rec. 2158, 69e76.

Fridell, E., & Salo, K. (2014). Measurements of abatement of particles and exhaust gases in a marine gas scrubber. Proceedings of the Institution of Mechanical Engineers, Part M: Journal of Engineering for the Maritime Environment, 1475090214543716.

Gautam, M., Clark, N.N., Riddle, W., Nine, R., Wayne, W.S., Maldonado, H., Agrawal, A., Carlock, M., 2002. Development and initial use of a heavy-duty diesel truck test schedule for emissions characterization. In Proceedings of Society of Automotive Engineers (SAE) Fuels and Lubricants Meeting; SAE Paper 2002-01-1753. SAE: Warrendale, PA.

Glaude PA, Pitz WI, Thomson MJ. Chemical kinetic modeling of dimethyl carbonate in an opposed-flow diffusion flame. Proceedings of the Combustion Institute 2005;30:1111-1118.

Hajbabaei, M, Karavalakis G, Johnson KC, Guthrie J, Mitchell A, Durbin TD. Impacts of biodiesel feedstock and additives on criteria emissions from a heavy-duty engine. Fuel Processing Technology 2014;126:402-414.

Hansen JP. Exhaust gas scrubber installed onboard MV Ficaria Seaways (Public test report). København: Environmental Protection Agency, Danish Ministry of Environment, 2012.

He, X.; Ratcliff, M.A.; Zigler, B.T. Effects of gasoline direct injection engine operating parameters on particle number emissions. Energy and Fuels 2010, 26, 2014-2027.

Heywood, J. B. (2018). Internal combustion engine fundamentals.

Huang ZH, Jiang DM, Zeng K, Liu B, Yang ZL. Combustion characteristics and heat release analysis of a direct injection compression ignition engine fuelled with diesel-dimethyl carbonate blends. Proc. Instn. Mech. Engrs. Part D: J. Automobile Engineering 2003;217:595-605.

Hubbard, C.P.; Anderson, J.E.; Wallington, T.J. Ethanol and air quality: Influence of fuel ethanol content on emissions and fuel economy of flexible fuel vehicles. Environ. Sci. Technol. 2014, 48, 861-867.

International Maritime Organization (IMO), Marine Environment Protection Committee 184(59), adopted on July 17 2009, http://www.imo.org/blast/blastDataHelper.asp?data_id=26469&filename=184(59).pdf

Janssen, N.A., Hoek, G., Simic-Lawson, M., Fischer, P., Van Bree, L., Ten Brink, H., Keuken, M., Atkinson, R.W., Anderson, H.R., Brunekreef, B., Cassee, F. R. 2012. Black carbon as an additional indicator of the adverse health effects of airborne particles compared with PM10 PM 2.5. Environ. Health Perspect. 119, 1691-1699.

Jerrett, M., Burnett, R.T., Pope III, C.A., Ito, K., Thurston, G., Krewski, D., Shi, Y., Calle, E. and Thun, M., 2009. Long-term ozone exposure and mortality. New England Journal of Medicine, 360(11), 1085-1095.

Jiang, Y., Yang, J., Cocker, D., Karavalakis, G., Johnson, K. C., & Durbin, T. D. (2018). Characterizing emission rates of regulated pollutants from model year 2012+ heavy-duty diesel vehicles equipped with DPF and SCR systems. *Science of the Total Environment*, *619*, 765-771.

Johnson, D., 2002. ROVER – Real-time On-road Vehicle Emissions Reporter. Presentation for the Mobile Source Technical Review Committee, February.

Johnson T. Vehicular emissions in review. SAE Int. J. Engines 2016;9:doi:10.4271/2016-01-0919.

Karavalakis, G., Short, D., Vu, D., Villela, M., Russell, R., Jung, H., ... & Durbin, T. (2014). Regulated emissions, air toxics, and particle emissions from SI-DI light-duty vehicles operating on different iso-butanol and ethanol blends. *SAE International Journal of Fuels and Lubricants, 7*(1), 183-199.

Karavalakis, G.; Short, D.; Vu, D.; Russell R.L.; Asa-Awuku, A.; Jung, H.; Johnson, K.C.; Durbin, T.D. The impact of ethanol and iso-butanol blends on gaseous and particulate emissions from two passenger cars equipped with spray-guided and wall-guided direct injection SI (spark ignition) engines. Energy 2015, 82, 168-179.

Karlsson, R.B.; Heywood, J.B. Piston fuel film observations in an optical access GDI engine. SAE Technical Paper 2001, 2001-01-2022.

Khosousi, A.; Liu, F.; Dworkin, S.B.; Eaves, N.A.; Thomson, M.J.; He, X., Dai, Y.; Gao, Y.; Liu, F.; Shuai, S.; Wang, J. Experimental and numerical study of soot formation in laminar coflow diffusion flames off gasoline/ethanol blends. Combustion and Flame 2015, 162, 3925-3933.

Kim, K.H.; Jahan, S.A.; Kabir, E.; Brown, R.J.C. A review of airborne polycyclic aromatic hydrcarbons (PAHs) and their human health effects. Environ. Int. 2013, 60, 71-80.

Kishan, S., Fincher, S., Sabisch, M., 2011. Populations, Activity and Emissions of Diesel Nonroad Equipment in EPA Region 7, Final Report for the US EPA and the CRC E-70 Program by Eastern Research Group. EPA Contract No. EP-C-06e080.

Kocis D, Song K, Lee H, Litzinger T. Effects of dimethoxymethane and dimethylcarbonate on soot production in an optically-accessible DI diesel engine. SAE Technical Paper 2000;2000-01-2795.

Kozak M, Merkisz J, Bielaczyc P, Szczotka A. The influence of oxygenated diesel fuels on a diesel vehicle PM/NOx emission trade-off. SAE Technical Paper 2009;2009-01-2996.

Kumar BR, Saravanan S. Partially premixed low temperature combustion using dimethyl carbonate (DMC) in a DI diesel engine for favorable smoke/NOx emissions. Fuel 2016;180:396-406.

Lack, D.A., Corbett, J.J., 2012. Black carbon from ships: a review of the effects of ship speed, fuel quality and exhaust gas scrubbing. Atmos. Chem. Phys. 12, 3985-4000.

Lawrence, M. G., & Crutzen, P. J. (1999). Influence of NOx emissions from ships on tropospheric photochemistry and climate. Nature, 402(6758), 167-170.

Lemaire, R.; Therssen, E.; Desgroux, P. Effect of ethanol addition in gasoline and gasoline-surrogate on soot formation in turbulent spray flames. Fuel 2010;89:3952-3959.

Li, R., Kou, X., Tian, J., Meng, Z., Cai, Z., Cheng, F., & Dong, C. (2014). Effect of sulfur dioxide on inflammatory and immune regulation in asthmatic rats. Chemosphere, 112, 296-304.

Lund, A.K.; Knuckles, T.L.; Akata, C.O.; Shohet, R.; McDonald, J.D.; Gigliotti, A.; Seagrave J.C.; Campen, M.J. Gasoline exhaust emissions induce vascular remodeling pathways involved in atherosclerosis. Toxicological Sciences 2007, 95, 485-494.

Lundstedt, S.; White, P.A.; Lemieux, C.L.; Lynes, K.D.; Lambert, I.B.; Öberg, L.; Haglund, P.; Tysklind, M. Sources, fate, and toxic hazards of oxygenated polycyclic aromatic hydrocarbons (PAHs) at PAH-contaminated sites. Ambio 2007, 36, 475-485.

Maikawa, C.L.; Zimmerman, N.; Rais, K.; Shah, M.; Hawley, B.; Pant, P.; Jeong, C.H.; Delgado-Saborit, J.M.; Volkens, J.; Evans, G.; Wallace, J.S.; Godri Pollitt, K.J. Murine precision-cut lung slices exhibit acute responses following exposure to gasoline direct injection engine emissions. Science of the Total Environment 2016, 568, 1102-1109.

Maricq, M.M.; Szente, J.J.; Jahr, K. The impact of ethanol fuel blends on PM emissions from a light-duty GDI vehicle. Aerosol Science and Technology 2012, 46, 576-583.

Miyamoto N, Ogawa H, Nurun NM, Obata K, Arima T. Smokeless, low NOx, high thermal efficiency, and low noise diesel combustion with oxygenated agents as main fuel. SAE Technical Paper 1998;980506.

Mizan, T. (2018). 2018 Outlook for Energy: A View to 2040. Presentation at 28th CRC Real World Emissions Workshop, Garden Grove, CA, March.

Munoz, M.; Heeb, N.V.; Haag, R.; Honegger, P.; Zeyer, K.; Mohn, J.; Comte, P.; Czerwinski, J. Bioethanol blending reduces nanoparticle, PAH, and alkyl- and nitro-PAH emissions and the genotoxic potential of exhaust from a gasoline direct injection flex-fuel vehicle. Environ. Sci. Technol. 2016, 50, 11853-11861.

Murayama T, Zheng M, Chikahisa T, Oh Y-T, Fujiwara Y, Tosaka S, Yamashita M, Yoshitake H. Simultaneous reductions of smoke and NOx from a DI diesel engine with EGR and dimethyl carbonate. SAE Technical Paper 1995;952518.

Oikawa K, Yongsiri C, Takeda K, et al. Seawater flue gas desulphurization: its technical implication and performance results. Environ Prog 2003; 22: 67–73

Pachauri, R.K. and Reisinger, A. IPCC 2007: Climate Change 2007: Synthesis report. Contribution of Working Groups I, II, and III to the Fourth Assessment Report of the Intergovernmental Panel on Climate Change, IPCC, Geneva, Switzerland.

Pacheco MA Marshall CL. Review of dimethyl carbonate (DMC) manufacture and its characteristics as fuel additive. Energy and Fuels 1997;11:2-29.

Piock, W.; Hoffmann, G.; Berndorfer, A.; Salemi, P.; Fusshoeller, B. Strategies towards meeting future particulate matter emission requirements in homogeneous gasoline direct injection engines. SAE Int. J. Engines 2011, 4, 1455-1468.

Pirjola, L.; Karjalainen, P.; Heikkila, J.; Saari, S.; Tzamkiozis, T.; Ntziachristos, L.; Kulmala, K.; Keskinen, J.; Ronkko, T. Effects of fresh lubricant oils on particle emissions emitted by a modern gasoline direct injection passenger car. Environ. Sci. Technol. 2015, 49, 3644-3652.

Ratcliff MA, Burton J, Sindler P, Christensen E, Fouts L, Chupka GM, McCormick RL. Knock resistance and fine particle emissions for several biomass-derived oxygenates in a direct-injection spark-ignition engine. SAE Technical Paper 2016;2016-01-0705.

Reed MD, Barret EG., Campen MJ, Divine KK, Gigliotti AP, McDonald JD, Seagrave JC, Mauderly JL, Seilkop SK, Swenberg JA. Health effects of subchronic inhalation exposure to gasoline engine exhaust. Inhalation Toxicology 2008;20:1125-1143.

Richter, H.; Howard, J. B. Formation of polycyclic aromatic hydrocarbons and their growth to soot-a review of chemical reaction pathways. Prog. Energy Combust. Sci. 2000, 26, 565-608.

Rohr AC, Wyzga RE. Attributing health effects to individual particulate matter constituents. Atmospheric Environment 2012;62:130-152.

Rounce P, Tsolakis A, Leung P, York APE. A comparison of diesel and biodiesel emissions using dimethyl carbonate as an oxygenated additive. Energy and Fuels 2010;24:4812-4819.

Rubino L, Thomson MJ. The effect of oxygenated additives on soot precursor formation in a couterflow diffusion flame. SAE Technical Paper 1999;1999-01-3589.

Seagrave JC., McDonald JD, Gigliotti AP, Nikula KJ, Seilkop SK Curevich M, Mauderly JL. Mutagenicity and in vivo toxicity of combined particulate and semivolatile organic fractions of gasoline and diesel engine emissions. Toxicological Sciences 2002;70:212-226.

Sivalakshmi S, Balusamy T. Effects of Dimethylcarbonate-biodiesel blends on the combustion, performance and exhaust emissions of a DI diesel engine. SAE Technical Paper 2012;2012-01-0870.

Souza LFS, Ferreira PRR, de Medeiros JL, Aves RMB, Araujo OQF. Production of DMC from CO_2 via indirect route: Technical-economical-environmental assessment and analysis. ACS Sustainable Chem. Eng. 2014;2:62-69.

Stevens, E.; Steeper, R. Piston wetting in an optical DISI engine: Fuel films, pool fires, and soot generation. SAE Technical Paper 2001, 2001-01-1203.

Su, J.; Lin, W.; Sterniak, J.; Xu, M.; Bohac, S.V. Particulate matter emission comparison of spark ignition direct injection (SIDI) and port fuel injection (PFI) operation of a boosted gasoline engine. J. Eng. Gas Turbines Power 2014, 136, 091513-1-091513-6.

Suarez-Bertoa, R.; Zardini, A.A.; Keuken, H.; Astorga, C. Impact of ethanol containing gasoline blends on emissions from a flex-fuel vehicle tested over the Worldwide Harmonized Light duty Test Cycle (WLTC). Fuel 2015, 143, 173-182.

Sun W, Yang B, Hansen N, Westbrook CK, Zhang F, Wang G, Moshammer K, Law CK. An experimental and kinetic modeling study on dimethyl carbonate (DMC) pyrolysis and combustion. Combustion and Flame 2016;164:224-238.

Tamagawa E, Bai N, Morimota K, Gray C, Mui T, Yatera K, Zhang X, Xing L, Li Y, Laher I, Sin DD, Man SFP, van Eeden SF. Particulate matter exposure induces persistent lung inflammation and endothelial dysfunction. American Journal of Physiology: Lung Cellular and Molecular Physiology, 2008;295:L79-L85.

Tzamkiozis T, Stoeger T, Cheung K, Ntziachristos L, Sioutas C, Samaras Z. Monitoring the inflammatory potential of exhaust particles from passenger cars in mice. Inhalation Toxicology 2010;22:59-69.

United Nations Conference on Trade and Development (UNCTAD), Review of Maritime Transport 2015

U.S. Environmental Protection Agency, 2008. Determination of PEMS measurement allowances for gaseous emissions regulated under the heavy-duty diesel engine in-use testing program. Revised Final Report EPA420-R-08-005. United States Environmental Protection Agency, Arlington, US.

United States Environmental Protection Agency (USEPA). Exhaust gas scrubber washwater effluent. EPA-800-R-11-006, November 2011. Washington, DC.

Vlachos, T., Bonnel, P., Perujo, A., Weiss, M. et al., 2014. In-Use Emissions Testing with Portable Emissions Measurement Systems (PEMS) in the Current and Future European Vehicle Emissions Legislation: Overview, Underlying Principles and Expected Benefits, SAE Int. J. Commer. Veh. 7(1), 2014-01-1549, doi:10.4271/2014-01-1549.

Winebrake, J.J., Corbett, J.J., Green, E.H., Lauer, A., Eyring, V. 2009. Mitigating the health impacts of pollution from oceangoing shipping: an assessment of low-sulfur fuel mandates. Environ. Sci. Technol. 43, 4776-4782.

Winnes, H., & Fridell, E. (2009). Particle emissions from ships: dependence on fuel type. Journal of the Air & Waste Management Association, 59(12), 1391-1398.

Yang, J., Roth, P., Durbin, T. D., Johnson, K. C., Cocker III, D. R., Asa-Awuku, A., ... & Karavalakis, G. (2018). Gasoline Particulate Filters as an Effective Tool to Reduce Particulate and Polycyclic Aromatic Hydrocarbon Emissions from Gasoline Direct Injection (GDI) Vehicles: A Case Study with Two GDI Vehicles. *Environmental science & technology*, *52*(5), 3275-3284.

2. Gasoline Particulate Filters as an Effective Tool to Reduce Particulate and Polycyclic Aromatic Hydrocarbon Emissions from Gasoline Direct Injection (GDI) Vehicles: A Case Study with Two GDI Vehicles

2.1. **Abstract**

We assessed the gaseous, particulate, and genotoxic pollutants from two current technology gasoline direct injection vehicles when tested in their original configuration and with a catalyzed gasoline particulate filter (GPF). Testing was conducted over the LA92 and US06 Supplemental Federal Test Procedure (US06) driving cycles on typical California E10 fuel. The use of a GPF did not show any fuel economy and carbon dioxide (CO_2) emission penalties, while the emissions of total hydrocarbons (THC), carbon monoxide (CO), and nitrogen oxides (NOx) were generally reduced. Our results showed dramatic reductions in particulate matter (PM) mass, black carbon, and total and solid particle number emissions with the use of GPFs for both vehicles over the LA92 and US06 cycles. Particle size distributions were primarily bimodal in nature, with accumulation mode particles dominating the distribution profile and their concentrations being higher during the cold-start period of the cycle. Polycyclic aromatic hydrocarbons (PAHs) and nitrated PAHs were quantified in both the vapor and particle phases of the PM, with the GPF-equipped vehicles practically eliminating most of these species in the exhaust. For the stock vehicles, 2-3 ring compounds and heavier 5-6 rings compounds were observed in the

PM, whereas the vapor phase was dominated mostly by 2-3 ring aromatic compounds.

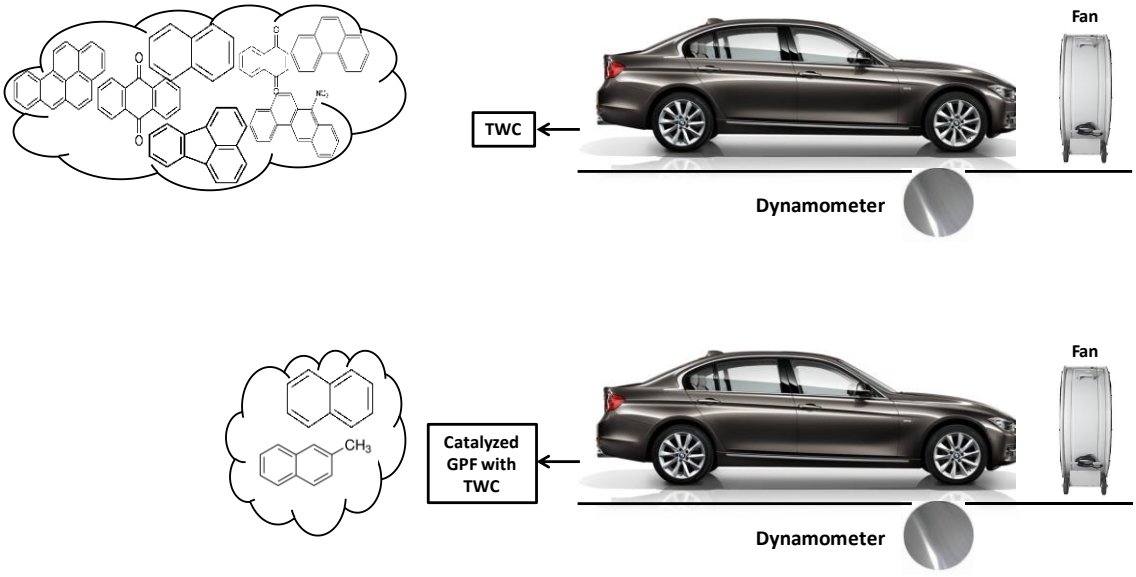

Graphic Abstract

2.2. **Introduction**

Climate change has been attributed to an increase of anthropogenic greenhouse gas emissions, with the transportation sector being the largest contributor of carbon dioxide (CO_2) emissions (Pachauri and Reisinger, 2007). Reducing CO_2 and other greenhouse gases is a key issue for regulatory agencies and industrial companies worldwide (Pachauri and Reisinger, 2007). In the United States (US), the Corporate Average Fuel Economy (CAFE) standards are currently very demanding for automotive manufacturers, with requirements to raise the average fuel economy of new cars and trucks to 54.5 miles per gallon by 2025. In the European Union (EU), similar mandates are set to decrease the CO_2 emissions to an average of 130 g/km. Based on the need to address global warming issues, gasoline direct injection (GDI) concepts have become the key technology of spark ignition

engine development to reduce CO_2 emissions by improving the engine efficiency (Alkidas, 2007).

Although GDI vehicles offer the potential of improved fuel economy, less fuel pumping, and charge air cooling, they tend to produce higher particulate matter (PM) emissions when compared with the traditional port fuel injection engines (Piock et. al, 2011; Karavalakis et. al, 2015a; Su et. al, 2014). In GDI engines, fuel is sprayed directly into the combustion chamber, which leads to incomplete fuel evaporation due to the limited time available for fuel and air mixing, resulting in pockets with high temperatures but insufficient oxygen, leading to pyrolysis reactions and soot formation. Additionally, as the fuel comes directly into contact with the cold cylinder walls and piston, a small amount of fuel may impinge on the piston, which during evaporation may lead to diffusion combustion and PM formation (Piock et. al, 2011, Stevens et. al, 2001; Karlsson and Heywood, 2001; He et. al, 2012). The rapid market penetration of GDI vehicles has led governments to impose stricter standards to control PM emissions. California LEVIII and US Tier 3 regulations will begin a four year phase-in starting in 2015 and 2017, respectively to a PM maximum of 3 mg/mile from the current 10 mg/mile LEVII limit. LEVIII will begin a four year phase-in of a tighter 1 mg/mile starting in 2025. In the EU, the Euro 6a particle number (PN) standard for GDI vehicles was reduced from $6x10^{12}$ particles/km to $6x10^{11}$ particles/km in September 2017.

Meeting the strictest PM standard, of 1 mg/mile and the European PN limit with GDI vehicles will likely be a challenge for automotive manufacturers. PM reductions in GDI platforms may be achieved by a combination of measures including alternative fuel

formulations, fuel injection strategies, and the use of gasoline particulate filters (GPFs). Several studies have reported that the use of oxygenated fuels (i.e., ethanol) have generally beneficial impacts on PM emissions (Barrientos et. al, 2016; Maricq et.al, 2012; Karavalakis et. al, 2015b). Other studies have shown that centrally-mounted injection systems have lower mass and number emissions than wall-guided injection systems, due to the fact that the injector is located close to the spark plug leading to better fuel evaporation and less wall wetting effects (Karavalakis et. al, 2015b; Oh and Bae, 2013). The use of GPFs in GDI vehicles may still be needed to meet future tightened regulations, and an increasing number of studies are focusing in this research area (Maricq et. al, 2013; Chan et. al, 2012; Lambert et. al, 2016). This is particularly true for the EU where the strict PN emissions standard for diesel particulate filter (DPF) equipped diesel vehicles was essentially translated to GDI vehicles. The stringent PN limit combined with the Real Driving Emissions (RDE) requirements that came into effect with Euro 6c has led to numerous OEMs reporting wide deployment of GPFs across their new vehicle fleets. Mamakos et al. (2013a) showed that the installation of GPFs in GDI vehicles is both feasible and cost effective. In a different study, Mamakos et al. (2013) reported that GPFs had filtration efficiencies in excess of 89% for PN emissions for a Euro 6 technology GDI vehicle over the New European Driving Cycle (NEDC) and the Common Artemis Driving Cycle (CADC). Chan et al. (2014) also showed large reductions in black carbon and solid particle number (SPN) emissions with the use of a GPF with a GDI vehicle tested over the US Federal Test Procedure (FTP) and the US06 Supplemental Federal Test Procedure (SFTP or US06) cycles. Choi et al. (2013) reported lower PN emissions for a GPF-

equipped GDI vehicle in another study, but the filtration efficiency of 57% was lower than what has previously been reported in studies (Mamakos et.al ,2013; Chan et. al, 2014; Spiess et. al, 2013).

It is important to better understand the toxicity of the particles being formed in GDI combustion. Today, the literature is scarce about the toxic properties of PM emissions from GDI vehicles, such as those of polycyclic aromatic hydrocarbons (PAHs), their oxygenated (oxy-PAHs), and nitrated derivatives (nitro-PAHs) (Munoz et. al, 2016; Maikawa et. al, 2016). PAHs have long been recognized as one of the major soot precursors for soot particles, while they are also classified as carcinogenic and mutagenic compounds adsorbed onto the PM or partition in the semivolatile PM phase (Richter and Howard, 2000; Kim et. al, 2013). Additionally, some oxy-PAH and nitro-PAH species have been recognized as similarly or more toxic than their parent PAHs (Lundstedt et. al, 2007).

This study aims to better characterize the toxicity of PM from GDI vehicles and the potential for catalyzed GPFs to reduce this toxicity. This study assessed the PM mass and particle number (PN) emissions and chemical constituents, such as PAHs and nitro-PAHs, in the particle- and vapor-phases of exhaust from two current technology GDI vehicles tested in their original configuration and when equipped with GPFs. The vehicles were tested over the LA92 and US06 test cycles on a chassis dynamometer, with the resulting exhaust samples being characterized for toxic species. The emissions results will be presented and discussed in the context of the influences of driving conditions, aftertreatment system, and engine technology.

2.3. **Experimental Section**

2.3.1. **Test Vehicles and Driving Cycles**

This study utilized two 2016 model year passenger cars. GDI_1 was equipped with a 2.0 liter (L) wall-guided direct injection spark ignition Atkinson cycle engine and GDI_2 was equipped with a 1.5 L downsized turbocharged centrally-mounted direct injection engine. Both vehicles were operated stoichiometrically, and were equipped with three-way catalysts (TWCs). GDI_1 and GDI_2 were certified to meet LEV III SULEV30 (PZEV) and LEV II emissions standards and had 14,780 and 24,600 miles at the start of the campaign, respectively.

After the baseline emissions were measured, both vehicles were retrofitted with a catalyzed GPF installed in place of the underfloor TWC. The original close-coupled catalysts were retained in their stock location. The catalyzed GPFs were provided by the Manufacturers of Emissions Controls Association (MECA). The GPFs were sized based on the engine displacement of each vehicle and they were catalyzed with precious metal loadings typical of underfloor catalysts matching the certification levels of the two vehicles. Both GPFs were 4.66” in diameterand 4.5” in length, with an 8 mil wall thickness and a cell density of 300 cells per square inch (cpsi). The GPFs had a TWC washcoat with approximately 1.0 g/liter loading of palladium (Pd) and rhodium (Rh) (Pd:Rh ratio of 4:1).

Both vehicles were tested over duplicate LA92s and US06 cycles on typical California E10 fuel. The LA92 test cycle or the California Unified Cycle (UC) is a dynamometer driving schedule for light-duty vehicles developed by the California Air Resources Board (CARB). The LA92 consists of three phases (i.e., cold-start, urban, and

hot-start phases) and has a three-bag structure similar to the FTP cycle. The LA92 is characterized by higher speeds, higher accelerations, fewer stops per miles, and less idle time than the FTP. The US06 was developed to reflect aggressive, high speed, and high acceleration driving behavior. Unlike the LA92, it is a hot-start test typically run with a prep cycle to ensure the vehicle is warmed up. For this study, two US06 preconditioning cycles followed by a 10-minute soak period were performed as prep prior to conducting the actual US06 emission test cycles.

2.3.2. **Emissions Testing**

All tests were conducted in CE-CERT's Vehicle Emissions Research Laboratory (VERL), on a Burke E. Porter 48-inch single-roll electric dynamometer. A Pierburg Positive Displacement Pump-Constant Volume Sampling (PDP-CVS) system was used to obtain standard bag measurements for total hydrocarbons (THC), carbon monoxide (CO), nitrogen oxides (NO_x), non-methane hydrocarbons (NMHC), and carbon dioxide (CO_2). Bag measurements were made with a Pierburg AMA-4000 bench. PM mass, total and solid PN, particle size distributions, elemental and organic carbon (EC/OC) fractions, and black carbon emissions were also measured. Total and solid particles were counted with a TSI 3776 ultrafine CPC and downstream of a catalytic stripper with a TSI 3776 ultrafine CPC, respectively, where both were connected to an ejector dilutor that was used to collect samples from the CVS tunnel. Solid particle counts were also measured in the raw exhaust before the CVS with a TSI NPET 3795 to evaluate the filtration efficiencies of the GPFs. Detailed information on the methods used to collect and analyze these emissions is provided in the Supporting Information (SI). Analyses of PAH and nitro-PAH species were

performed at the Desert Research Institute, Reno, NV. PAH and nitro-PAH samples were collected on pre-cleaned Teflon impregnated glass fiber (TIGF) filters (100 mm). Semi-volatile organic compounds were collected on cleaned Amberlite XAD-4 polyaromatic absorbent resin (Aldrich Chemical Company, Inc.) that was packed into a glass cartridge. The samples collected on each filter-XAD sampling train were extracted separately with high purity dichloromethane and then acetone, followed by an accelerated solvent extraction (ASE). A Varian 4000 Ion Trap in electron impact (EI) mode was used for PAH analysis, and a Varian 1200 triple quadrupole GC/MS operating in negative chemical ionization (CI) mode was used for nitro-PAH compounds. Negative CI offers superior sensitivity for the analysis of nitro-PAHs (approximately 100 times higher than EI or positive CI) and other compounds with electron-withdrawing substituents, but not for regular PAH and hydrocarbons. More details on the analysis methods of PAH and nitro-PAH compounds can be found elsewhere (Hu et. al, 2007).

2.4. **Results and Discussion**

2.4.1. **Gaseous Emissions and Fuel Economy**

Table 2-1 shows the gas-phase emissions and fuel economy results for the two GDI vehicle with and without the GPFs. The installation of the catalyzed GPFs into the exhaust systems for both GDI vehicles led to some differences in the regulated emission levels and fuel economy, as shown in Table 2-1. A clear reduction was observed for CO, THC, NMHC, and NOx emissions with the use of GPFs on both the LA92 and US06 cycles. Spiess et al. (2013) and Xia et al. (2017) also showed gas-phase emission improvements with the use of a catalyzed GPF, especially for NOx emissions. The reductions in THC,

CO, and NOx emissions over the LA92 cycle with the catalyzed GPFs compared to the stock configuration were 37%, 26%, and 17%, for GDI_1 and 62%, 71%, and 88% for GDI_2. NOx, THC, and CO conversion occurs mainly on the TWC. It appeared that the catalyzed GPFs, which has TWC coatings and precious metals loadings similar to the original underfloor converter, provided additional catalytic active surface, which enhanced the conversion of NOx, THC, and CO emissions. For the cold-start phase of LA92, the reductions in emissions with the GPFs compared to the stock configuration emission levels were not as pronounced due to the catalyst being below its light-off temperature (Table S2-1, SI). A small, but statistically significant, increase in CO_2 emissions was seen for the GDI_2/GPF configuration compared to GDI_2 without the GPF, although there were no statistically significant differences in fuel economy between these two configurations. CO_2 emissions and fuel economy did not show statistically differences between the stock and GPF equipped vehicles for the other cases.

Table 2-1 Regulated emissions and fuel economy, expressed in g per miles and miles per gallon, respectively, over the LA92 and US06 cycles

	GDI_1	GDI_1/GPF	GDI_2	GDI_2/GPF
		LA92 cycle		
THC	0.010±0.001	0.006±0.001	0.062±0.003	0.024±0.001
NHMC	0.008±0.001	0.005±0.001	0.054±0.003	0.019±0.001
CO	0.189±0.017	0.141±0.043	0.665±0.038	0.195±0.010
NO_x	0.010±0.001	0.008±0.000	0.066±0.003	0.008±0.001
CO_2	271.3±13.7	254.2±0.7	339.2±2.5	330.7±11.0
Fuel Economy	31.8±1.6	33.9±0.1	25.3±0.2	26.0±0.8
		US06 cycle		
THC	0.007±0.000	0.006±0.003	0.040±0.002	0.008±0.002
NHMC	0.005±0.000	0.004±0.002	0.029±0.001	0.002±0.001
CO	0.235±0.332	0.225±0.184	4.210±0.462	1.456±0.213
NO_x	0.002±0.003	0.007±0.005	0.138±0.008	0.004±0.000
CO_2	248.1±3.4	243.8±21.0	334.9±1.2	340.0±0.8
Fuel Economy	34.8±0.5	35.5±3.0	25.3±0.1	25.2±0.0

2.4.2. **PM Mass, Black Carbon, and Particle Number Emissions**

Figure 2-1 (a-b) shows the PM mass, organic carbon (OC) and elemental carbon (EC) fractions, and black carbon emissions for both vehicles over the LA92 and US06 cycles. PM mass emissions were lower for the wall-guided GDI_1 vehicle compared to the centrally- mounted GDI_2 vehicle. This was likely due to the higher compression ratio for GDI_1 (14.0:1) compared to GDI_2 (10.0:1), which probably resulted in an earlier fuel injection, leading to the formation of a more homogeneous air-fuel mixture due to the availability of sufficient time for mixture preparation, as well as the higher in-cylinder temperature, which increased the oxidation of particles in the combustion chamber, resulting in lower PM emissions for GDI_1. It also has to be noted that GDI_1 is certified to more stringent LEV III standards compared to GDI_2, which is certified to a LEV II standard. Vehicle weight, engine size, and calibration strategy can play a role on PM

emissions. PM mass and black carbon emissions were drastically reduced with the GPFs, with these reductions being on the order of 97% and 99% for GDI_1/GPF and 98% and 100% for GDI_2/GPF on the LA92 and US06 cycles, respectively. Previous chassis dynamometer studies also showed reductions in PM mass from GDI vehicles with the use of GPFs (Mamakos et. al, 2013b; Chan et. al, 2014; Choi et. al, 2013; Czerwinski et. al, 2017).

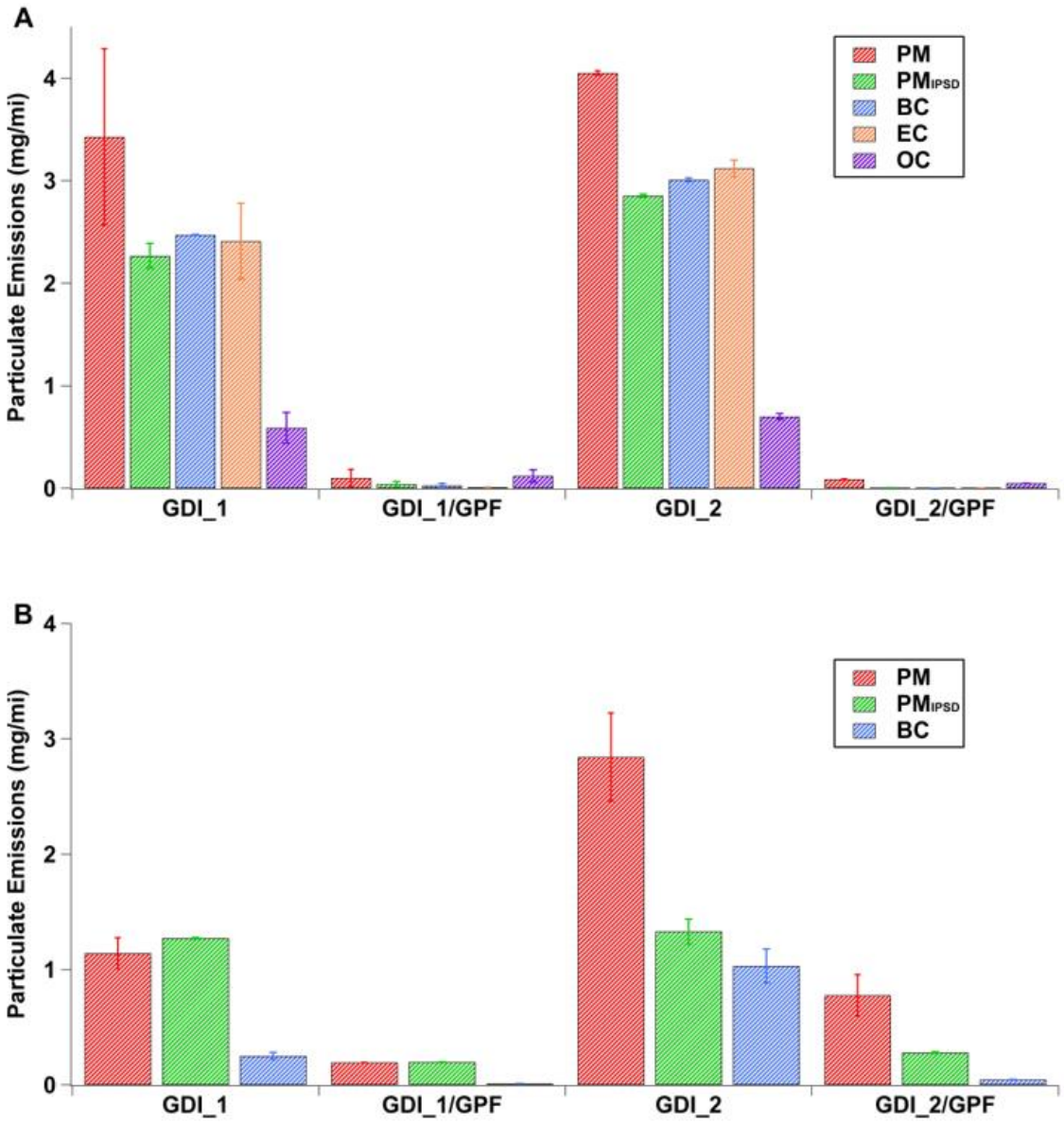

Figure 2-1 Gravimetric PM mass, PM mass calculated based on the IPSD method, black carbon, and EC/OC emissions over the LA92 cycle (a) and gravimetric PM mass, PM mass calculated based on the IPSD method, and black carbon emissions over the US06 cycle for both vehicles (b)

PM mass emissions were also calculated using the integrated particle size distribution (IPSD) method, which is an alternative metric for measuring PM mass from real-time mobility-based particle size distributions that are converted into mass distributions by applying a size-resolved particle effective density, as shown in previous

studies (Quiros et. al, 2015; Xue et. al, 2016). The PM mass reduction based on the IPSD method was 34% and 30% for GDI_1 and GDI_2, and 60% and 94% for GDI_1/GPF and GDI_2/GPF, respectively, lower than the gravimetric PM mass over the LA92, but similar to the black carbon or soot emissions (Figure 2-1a). The underestimation for the IPSD method compared to the gravimetric PM mass implies that most of the PM was EC or black carbon in nature and that the semivolatile components of PM were not taken into account with the IPSD measurement. These components can condense onto the filters collecting PM mass, but not be measured by the IPSD method. For the US06 cycle, the IPSD method agreed well with the gravimetric PM mass for GDI_1, but underestimated the gravimetric PM mass for GDI_2. The PM mass composition from both vehicles was dominated by EC, as confirmed by the black carbon emission measurements, whereas OC constitutes only a small fraction of PM. However, when both vehicles were retrofitted with the GPFs, the OC fraction was found to be higher than the EC fraction of the PM. The GPFs proved capable of eliminating most of the black carbon or soot particles, but not all of the semivolatile organic compounds.

Total and solid (> 23nm) PN emissions are shown in Figure 2-2a. For both vehicles, total and solid PN counts are in line with the gravimetric PM mass. The cold-start phase of the LA92 generated significantly higher PN emissions than the hot-running and hot-start phases, due to incomplete combustion, as shown by the THC emissions (Table S2-1, SI), and liquid fuel impingement onto the cold piston bowl and cylinder surfaces (He et. al, 2012). As expected, PN emissions during hot-start operation were markedly lower due to the increased fuel temperature and temperature of the engine parts that promote almost

complete fuel vaporization and better fuel-air mixing. The use of GPFs resulted in larger reductions for both total and solid PN emissions; for GDI_1/GPF the filtration efficiencies were 95% for both total and solid PN, while for GDI_2/GPF the filtration efficiencies were 97% for total PN and 99% for solid PN. Interestingly, both total and solid PN emissions for the stock and GPF-equipped vehicles are of similar magnitude, suggesting that most of the emitted particles were solid in nature with diameters larger than 23 nm.

Total and solid PN emissions over the US06 are shown in Figure 2-2b. For GDI_1/GPF, the reductions in total and solid PN emissions were 83% and 85%, respectively, compared to 34% and 71% for GDI_2/GPF. Solid particle counts measured in the raw exhaust significantly decreased with the use of GPFs indicating filtration efficiencies in the range of 86%-92% for both vehicles. It is theorized that the low reductions in PN emissions when measured with the TSI CPCs for GDI_2/GPF were an artifact of potential CVS and exhaust transfer line contamination. GDI_2/GPF systematically showed higher exhaust and CVS inlet temperatures than GDI_1/GPF, as shown in Figure S2-1 (SI). The high speed and high load driving conditions for the US06, coupled with temperatures above 250 °C for more than 10 minutes, will likely lead to the desorption or pyrolysis of stored volatile and solid particles, as well as other organic material by the hot exhaust gaseous from the exhaust transfer line and the CVS tunnel

surfaces. This phenomena has also been observed previously in studies using the US06 cycle (Maricq et. al, 1999).

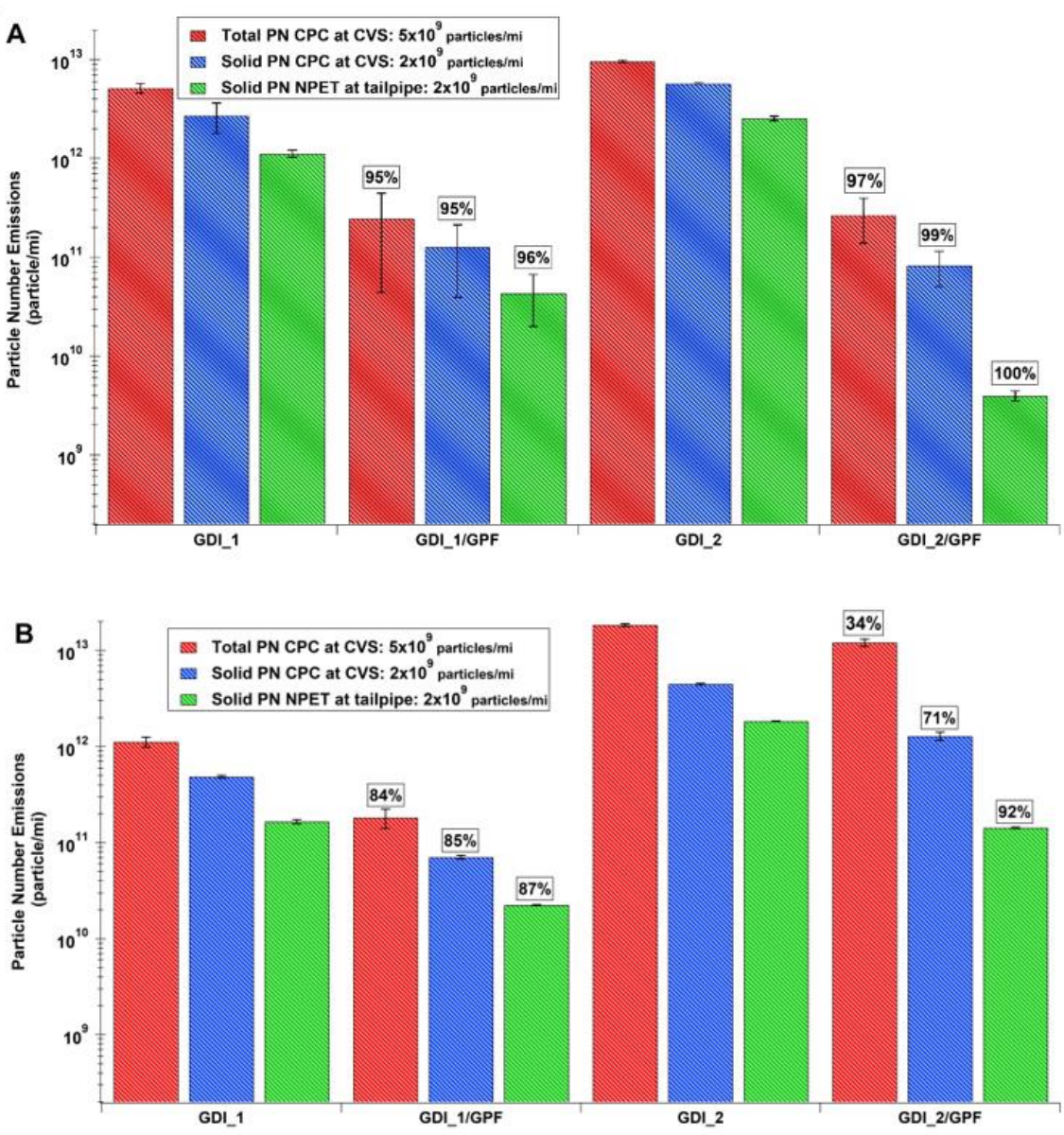

Figure 2-2 (a)(b) Total and solid particle number emissions over the LA92 cycle (a) and US06 cycle (b) for both test vehicles

2.4.3. **Particle Size Distributions**

Average particle size distributions are illustrated in Figure 2-3 for GDI_1, and in Figure S2-2 (SI) for GDI_2. The particle size distribution profile for GDI_1 was bimodal in nature with accumulation or soot mode particles dominating over nucleation mode particles. Particle populations were centered in the accumulation mode between 40 to 120 nm in diameter. Similar particle distribution profiles with higher concentrations of accumulation mode particles and a much smaller nucleation mode from GDI vehicles have been shown in other studies (Koczak et. al, 2016; Zhang and McMahon, 2012). The cold-start emissions during the first 200 seconds represent a significant fraction of the total emitted particles over the entire LA92, especially for GDI_1 (Figure 2-3a).

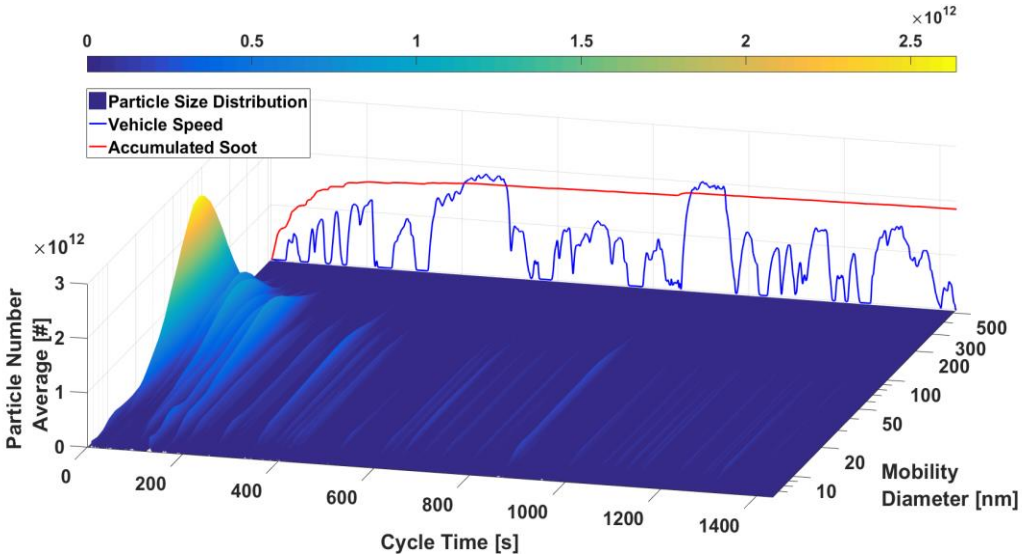

Figure 2-3 (a) Transient particle size distribution for phases 1 and 2 of the LA92 for GDI_1. The speed-time profile and the accumulated soot mass are also included for visual reference

For GDI_2, high levels of accumulation mode particles were seen for a longer duration of phase 1, up to 400 seconds. During cold-start operation, a significant portion

of the injected fuel lands on the cold combustion chamber surfaces. Since the combustion chamber walls are at lower temperature than the saturation temperature of most of the species of the injected fuel, the result is the formation of fuel films that fail to evaporate completely, creating overly fuel rich zones that are responsible for the high levels of particle emissions during cold-start (Stevens et. al, 2001; Cheng et. al, 2001). Typically, cold-start operation favors the formation of accumulation mode particles consisting of carbonaceous chain agglomerates (Badshah et. al, 2016). The cold fuel can lead to poor fuel vaporization and mixture deficiencies resulting in pool fires and diffusive combustion and the formation of soot particles in the accumulation mode (Piock et. al, 2011; Badshah et. al, 2016; Chen et. al 2017). It is clear that after 250-300 seconds the particle concentrations were drastically reduced due to the warm-up of the engine and exhaust surfaces. Overall, the drop in particle size and concentrations was likely due to better fuel vaporization, less wall wetting, and avoidance of pool fires. Sharp reductions were also observed for the nucleation mode particles for both vehicles after the first 400 seconds. It is assumed that the TWC was above its light-off temperature and thus capable in oxidizing volatile organic hydrocarbons from unburned fuel that primarily constitute the nucleation mode.

The hot-start particle concentrations for both vehicles were about an order of magnitude lower compared to cold-start emissions (Figure 2-3b). For GDI_1, the nucleation mode was prominent for phase 3 compared to phases 1 and 2 of the LA92, with the particle size distribution being bimodal and trimodal in nature. In contrast, GDI_2

showed a dominance of accumulation mode particles and practically the absence of a nucleation mode during hot-starts.

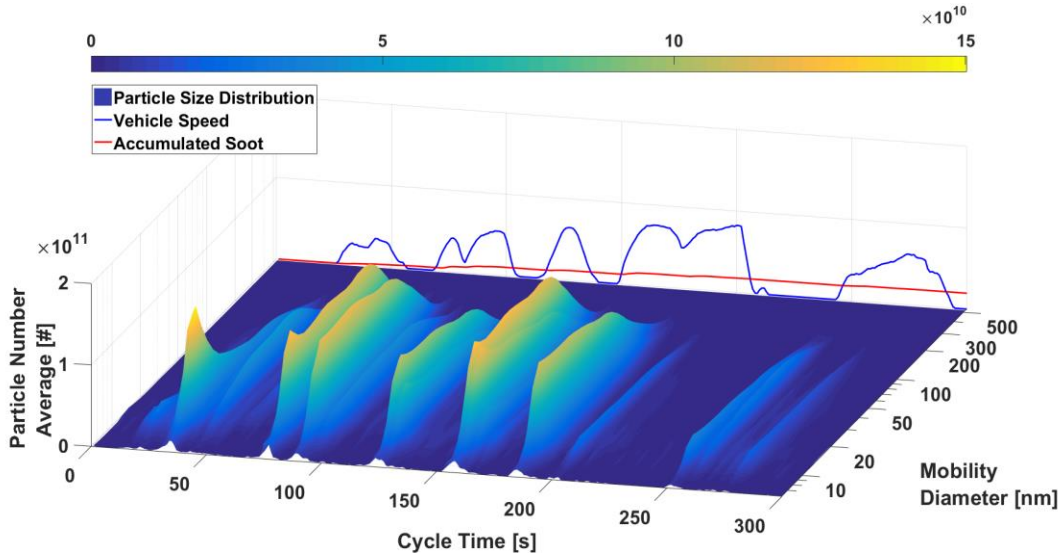

Figure 2-4 (b) Transient particle size distribution for phase 3 of the LA92 for GDI_1. The speed-time profile and the accumulated soot mass are also included for visual reference

The results reported here for the GPF-equipped vehicles showed particle concentrations orders of magnitude lower than the stock vehicles for all phases of the LA92. In fact, only cold-start showed some spikes of accumulation mode particles for GDI_1/GPF (Figure 2-3c), whereas hot-start emissions were at the noise level of the measurement. Similarly, GDI_2/GPF showed larger peaks for nucleation mode particles, but at very low concentrations and close to the noise levels (Figure S2-4, SI).

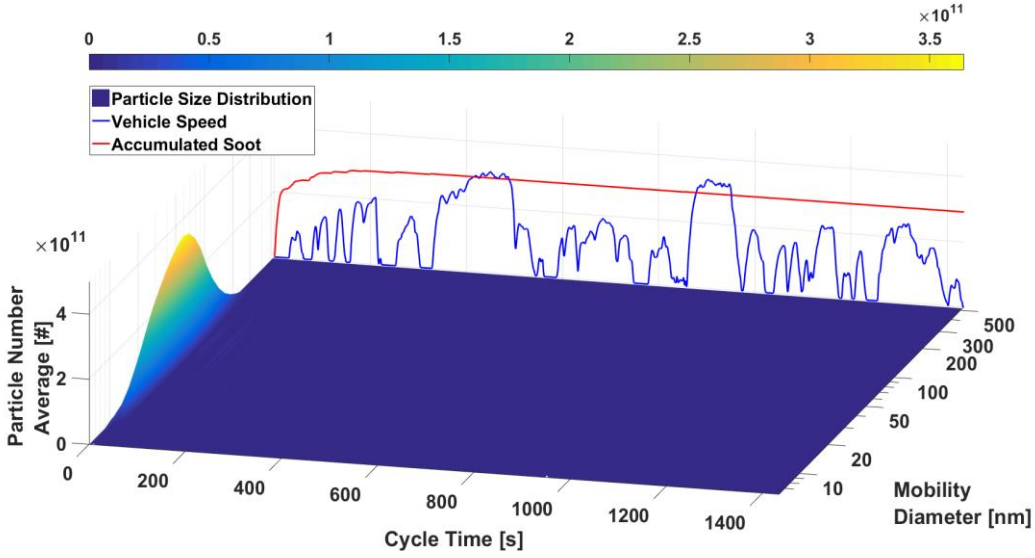

Figure 2-5 (c) Transient particle size distribution for phases 1 and 2 of the LA92 for GDI_1/GPF. The speed-time profile and the accumulated soot mass are also included for visual reference

The particle size distributions for both vehicles over the US06 cycles are shown in Figures S2-5 (a-b) through S2-6 (a-b), SI. The particle size distributions for the US06 are vehicle dependent and exhibited substantial differences compared to the LA92 cycle, with the majority of the particle populations centered in the nucleation mode. There was a shift of the accumulation mode towards smaller diameter particles for GDI_1, while the accumulation mode disappeared leaving the nucleation mode dominating the particle sizing profile for GDI_2. For GDI_1, the nucleation and soot particle number concentrations were lower for the GPF configuration as they were more effectively removed by the GPF. For GDI_2, a burst of nucleation mode particles was observed for both configurations. Previous studies have shown elevated particle number emissions over US06 operation, suggesting a possible filter regeneration event (Chan et. al, 2016). As previously discussed, the higher

nucleation particle populations with the GPF were attributed to CVS contamination issues from hydrocarbon deposits on the walls rather than GPF regeneration mechanisms, as shown elsewhere (Saffarpour et. al, 2015). These hydrocarbon deposits and other organic material will likely lead to particles nucleation in the dilution tunnel (Maricq et. al, 1999). Maricq et al. (2017) also showed significant nucleation mode exhaust particle emissions from GDI vehicles during US06 operation, which was associated with sulfate promoting semivolatile hydrocarbons to nucleate instead of condensing onto soot particles.

2.4.4. **PAH and Nitro-PAH Emissions**

Emissions of particle- and vapor-phase PAHs categorized by families of compounds for substituted, non-substituted, oxygenated, and phenyl PAHs are shown in Figure 2-4 and Figure 2-5, respectively.

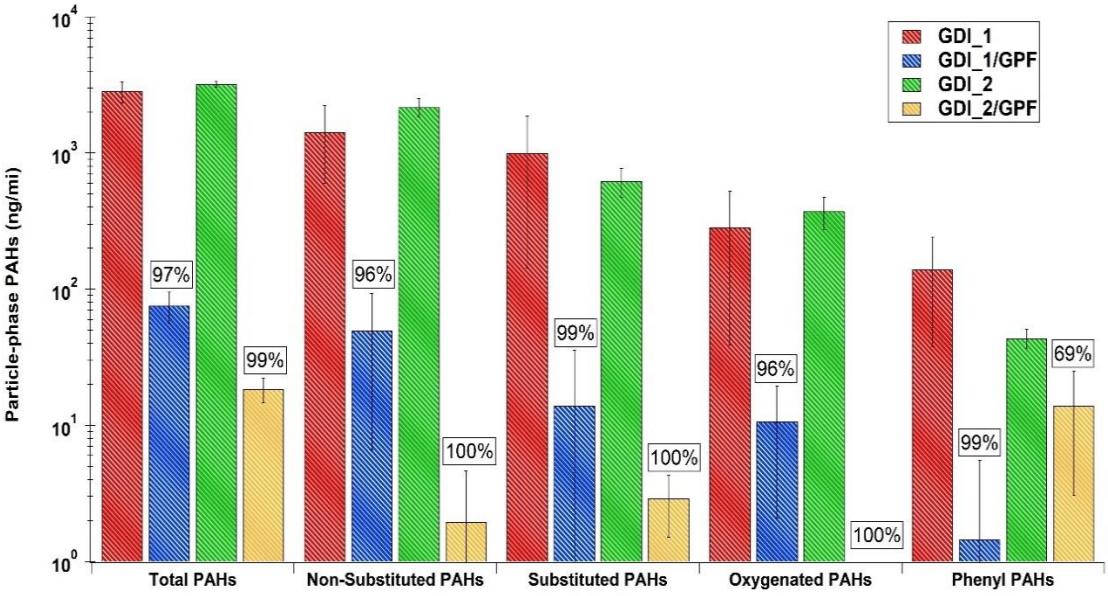

Figure 2-6 Total particle-phase PAH emissions, expressed in ng/mile, for both test vehicles over the LA92 cycle

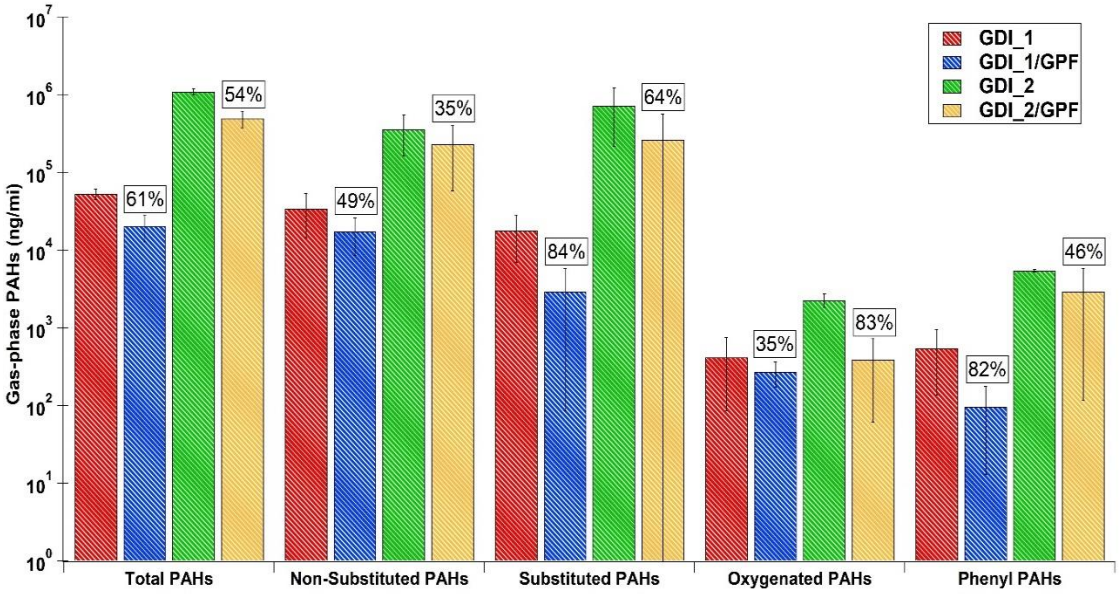

Figure 2-7 Total gas-phase PAH emissions, expressed in ng/mile, over the LA92 cycle

The individual particle- and vapor-phase PAH compounds are listed in Tables S2-2 through S2-3 in SI. Particle-phase PAH emissions showed large overall reductions with the application of GPFs for both vehicles, which were on the order of 97% and 99% for GDI_1/GPF and GDI_2/GPF, respectively. The GPFs practically eliminated PAH emissions in the particle-phase, with their levels being below the detection limit. For the stock vehicles, 2-3 member ring compounds dominated the distribution of PAHs, with lower levels of high molecular weight species. Higher concentrations of heavier PAHs with up to 6 rings were detected in the exhaust of GDI_2 compared to GDI_1. Compounds like methyl-pyrenes, methyl-phenanthrenes, benzo(*ghi*)fluoranthene, benzo(*a*)pyrene, indeno[123-*cd*]pyrene, coronene, etc., were found in significantly higher levels in GDI_2 exhaust than GDI_1. This is in agreement with the higher PM mass of this vehicle, since PAHs with four or more fused rings play an important role in contributing to PM mass

formation (An et. al, 2016a). Interestingly, total particle-phase PAH emissions for the stock GDI_2 were higher than the stock GDI_1, whereas GDI_2/GPF showed much lower total particle-phase PAH emissions relative to GDI_1/GPF, indicating a higher filtration efficiency for this vehicle. It should be stressed that the PAH species (benzo(*a*)pyrene, benzo(*a*)anthracene, benzo(*b*)fluoranthene, benzo(*k*)fluoranthene, chrysene, dibenzo(*a,h*)anthracene, benzo(*ghi*)perylene, and indeno(1,2,3-*cd*)pyrene) are considered to be carcinogenic and toxic to humans by the International Agency for Research on Cancer (IARC) and the US EPA, and they were found in relatively high concentrations in the particle phase (International Agency for Research on Cancer, 2010). Some of the heavier PAHs seen in the present experiment, were also observed in a previous chassis dynamometer study using a GDI vehicle (Storey et. al, 2014). Although benzo(*a*)pyrene is considered as a Class 1 carcinogen by the IARC, other heavier PAHs such as dibenzo(*a,h*)pyrene possess a carcinogenic potential about 10 times higher that of benzo(*a*)pyrene (Maricq et. al, 2017). These findings suggest that GDI exhaust could possess high potency due to the presence of heavier PAH emissions, even at low concentrations in the sample.

It should be noted that both vehicles presented a diverse profile in their PAH distribution, with light, medium, and heavier molecular weight PAHs being abundant in the exhaust. In the absence of oxygen and at temperatures above 400 °C the hydrocarbon molecules from fuel or lubricating oil are decomposed into smaller active radicals (H, OH, CH_3, C_2H_4, C_2H_2) that form PAH molecules (An et. al, 2016b; Slavinskaya et. al, 2012). Lighter and medium molecular weight PAHs, such as phenanthrene, fluoranthene and

pyrene, were likely sourced from pyrosynthesis routes of n-alkanes in the fuel through reactions of naphthalene and indene with acetylene (hydrogen abstraction C_2H_2 addition, HACA mechanism) or cyclopentadienyl (Lea-Langton et. al, 2013). Heavier PAHs, such as benzo(a)pyrene, benzo(*b*+*j*+*k*)fluoranthene, benzo(*a*)anthracene, benzo(*ghi*)fluoranthene, indeno[123-*cd*]pyrene, and coronene, could be attributed to the pyrolysis from the incomplete combustion of larger fuel fragments and the lubricant oil (Munoz et. al, 2016). In GDI engines, the lubricating oil can penetrate the combustion chamber either via the cylinder walls or via the intake ports and contribute to PM and PAH formation, primarily due to its higher evaporation temperature that results in incomplete vaporization. Non-combusted PAHs from fuel pyrolysis condense and accumulate in the lubricating oil, which acts as a sink for PAHs (Brandenberger et. al, 2005).

As shown in Figure 2-4, the total particle-phase PAHs by category showed the following distribution for both vehicles: non-substituted > substituted > oxygenated > phenyl. Naphthalene was the predominant non-substituted PAH compound in the particle phase for both vehicle configurations, followed by phenanthrene, fluoranthene, pyrene, benzo(*ghi*)fluoranthene, benzo(*b*+*j*+*k*)fluoranthene, and others. These PAH species were likely produced from the thermal cracking of fuel directly injected into the cylinder. For the substituted PAH emissions, methyl-, dimethyl-, and trimethyl-naphthalenes, methyl- and dimethyl-phenanthrenes, and methyl-pyrenes were the dominant compounds in the exhaust. The predominant particle-phase oxy-PAH compounds for both vehicles were 9-fluorenone, perinaphthenone, anthraquinone, and dibenzofuran. While the stock GDI_2 had the highest total oxy-PAH concentrations, the addition of the GPF eliminated these

species from the exhaust. For the total phenyl PAH emissions, GDI_1 showed higher concentrations relative to GDI_2, with biphenyl being the dominant species in the exhaust.

The total vapor-phase PAH emissions were found in significantly higher concentrations than the particle-phase emissions, with GDI_2 showing higher concentrations of tailpipe vapor-phase PAHs than GDI_1. The predominantly semi-volatile PAHs were mainly those with two and three-member rings, with a small amount of four-member ring PAHs. Heavier PAHs of four or more rings were predominantly adsorbed in the particle (soot) phase. Naphthalene was the largest contributor to the total vapor-phase PAHs, followed by methyl-, ethyl-, and dimethyl-naphthalene. Unlike for the particle-phase PAHs, where total PAH emissions decreased by more than 97% with the GPF addition, the reductions in the vapor-phase were generally lower. Specifically, the reductions for the total vapor-phase substituted, non-substituted, oxygenated, and phenyl PAHs emissions were 84%, 49%, 35%, and 82% for GDI_1/GPF, while for GDI_2/GPF were 64%, 35%, 83%, and 46%, respectively. These results suggest that PAHs existing in the vapor-phase are not eliminated by the GPF as effectively as those associated with the particle-phase over the LA92 cycle. It has to be noted that substantial reductions of vapor-phase PAHs with a GPF are not expected; however, the catalyzed GPFs provided the additional catalytically active coating resulting in the partial oxidation of the vapor-phase PAH species.

Particle-phase nitro-PAH emissions were found in much lower concentrations than their parent PAHs, as shown in Figure 2-6 and in Tables S2-4 and S2-5 in SI.

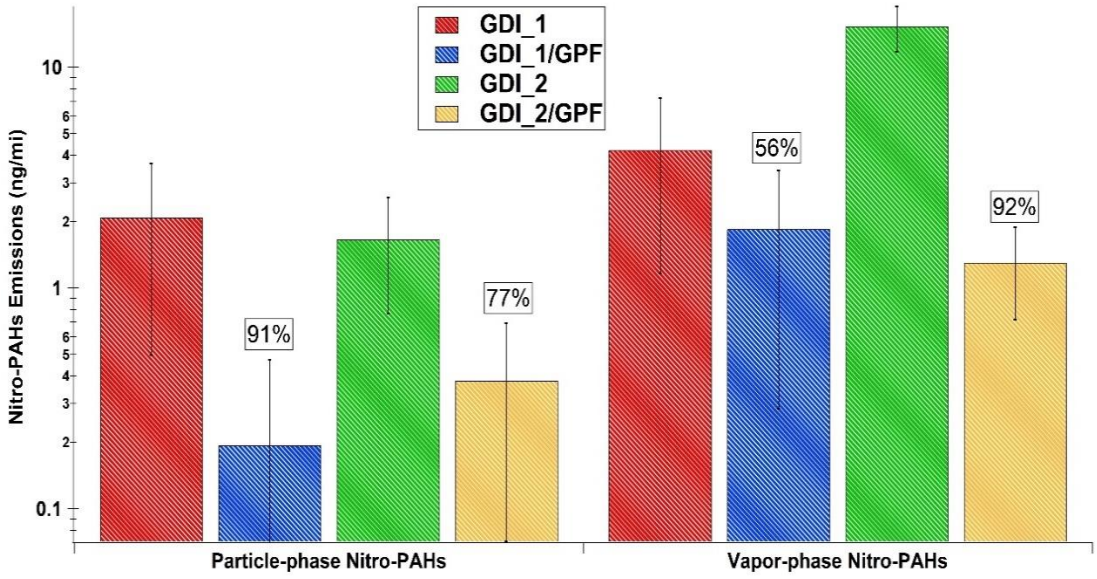

Figure 2-8 Total particle- and gas-phase nitrated PAH emissions for both test vehicles over the LA92 cycle

The reductions in total nitro-PAH emissions were 91% and 77%, respectively, for GDI_1/GPF and GDI_2/GPF. For the stock vehicles, the most prevalent nitro-PAH species in the particle phase were 1-nitronaphthalene, 2-nitronaphthalene, 9-nitroanthracene, 1-nitropyrene, 2-nitrofluoranthene, and 2,7-dinitrofluorene. Although the emissions of the most volatile two ring species were higher than those of the three and four ring nitro-PAHs for GDI_1, some heavier nitro-PAHs for GDI_2, such as 2-nitrofluoranthene and 2,7-dinitrofluorene, showed higher emissions than the lighter nitronaphthalenes. Interestingly, some species only detected for both vehicles with the GPFs suggesting that these nitro-PAHs formed *de novo* in the GPF system via selective nitration reactions. Similar to the parent PAHs, the vapor-phase nitro-PAH emissions were seen in higher concentrations than the particle-phase emissions. The reductions in total vapor-phase nitro-PAH emissions with the use of GPF were 56% and 92%, respectively, for GDI_1 and GDI_2. The lighter

two-member ring species of 1-nitronaphthalene and 2-nitronaphthalene were the most dominant in the exhaust followed by 1-methyl-6-nitronaphthalene and 9-nitroanthracene. The compounds of 1-nitropyrene and 4-nitropyrene were also found in the vapor-phase, with both being four-member ring species that usually exist in the particle phase. 1-nitropyrene is both toxic and mutagenic, while nitropyrenes are generally precursors for the more potent and mutagenic dinitropyrenes (Heeb et. al, 2008).

2.5. **Conclusions and Implications**

Our results demonstrate that current technology GDI vehicles could be an important source for on-road ultrafine particles and black carbon emissions and ultimately a contributor to urban air pollution. This study revealed that catalyzed GPFs can improve the conversion efficiency for NOx, THC, and CO emissions and have no measurable impact on CO_2 emissions and fuel economy. This is one of the few studies revealing that GDI vehicles could significantly contribute to PAH and nitrated PAH emissions and to our knowledge, the only one that looked at remediation of these toxics using a catalyzed gasoline particulate filter. We found that the use of catalyzed GPFs could significantly reduce the PM mass and black carbon emissions, as well as total and solid particle number emissions without having a measurable impact on the vehicle's GHG emissions and fuel economy. The catalyzed GPF significantly reduced the particle-phase PAHs and nitro-PAHs emissions, especially the less volatile or highly reactive PAH species. On the other hand, the vapor-phase PAHs did not show the same filtration efficiency as the PM-bound compounds. This study showed that GDI vehicle exhaust is characterized by diverse PAH distribution profile, ranging from 3-6 ring species. The projected increased penetration of

GDI vehicles in the US market, suggests that future health studies aimed at characterizing the toxicity of GDI emissions are needed to understand the health risks associated with non-GPF-equipped GDI PM emissions. The fact that GPF adoption from US vehicle manufacturers is not as dynamic as in the EU, due to the more stringent European PN standard especially over real-driving emissions (RDE) testing, should raise concerns about the lack of societal and air quality benefits from the GDI fleet.

2.6. **Acknowledgements**

The authors thank the following organizations and individuals for their valuable contributions to this study. We acknowledge funding from the South Coast Air Quality Management District (SCAQMD) under contract 15625 and the Manufacturers of Emission Controls Association (MECA) under contract 15040420. The authors thank Mr. Mark Villela and Mr. Daniel Gomez of the University of California, Riverside for their contribution in contacting this research program. We also thank MECA for providing the catalyzed GPF for this program and also for their technical support and guidance.

2.7. **References**

Alkidas, A. C. Combustion advancements in gasoline engines. Energy Conversion and Management 2007, 48, 2751-2761.

An, Y.-Z.; Pei, Y-.Q.; Qin, J.; Zhao, H.; Teng, S.-P.; Li, B. Development of a PAH (polycyclic aromatic hydrocarbon) formation model for gasoline surrogates and its application for GDI (gasoline direct injection) engine CFD (computational fluid dynamics) simulation. Energy 2016a, 94, 367-379.

An, Y.-Z.; Teng, S.-P.; Pei, Y-.Q.; Qin, J.; Li, X.; Zhao, H. An experimental study of polycyclic aromatic hydrocarbons and soot emissions from a GDI engine fueled with commercial gasoline. Fuel 2016b, 164, 160-171.

Andersson, J.T.; Achten, C. Time to say goodbye to the 16 EPA PAHs? Toward an up-to-date use of PACs for environmental purposes. Polycyclic Aromatic Compounds 2015, 35, 330-354.

Badshah, H.; Kittelson, D.; Northrop, W. Particle emissions from light-duty vehicles during cold-cold start. SAE Int. J. Engines 2016, 9, 1775-1785.

Barrientos, E.J.; Anderson, J.E.; Maricq, M.M.; Boehman, A.L. Particulate matter indices using smoke point for vehicle emissions with gasoline, ethanol blends, and butanol blends. Combustion and Flame 2016, 167, 308-319.

Brandenberger, S.; Mohr, M.; Grob K.; Neukom, H.P. Contribution of unburned lubricating oil and diesel fuel to particulate emission from passenger cares. Atmospheric Environment 2005, 39, 6985-6994.

Chan, T.W.; Meloche, E.; Kubsh, J.; Rosenblatt D.; Brezny, R.; Rideout, G. Evaluation of a gasoline particulate filter to reduce particle emissions from a gasoline direct injection vehicle. SAE Int. J. Fuels Lubr. 2012, 5, 1277-1290.

Chan, T. W.; Meloche, E.; Kubsh, J.; Brezny, R. Black carbon emissions in gasoline exhaust and a reduction alternative with a gasoline particulate filter. Environ. Sci. Technol. 2014, 48, 6027-6034.

Chan, T.W.; Saffaripour, M.; Liu, F.; Hendren, J.; Thomson, K.A.; Kubsh, J.; Brezny, R.; Rideout, G. Characterization of real-time particle emissions from a gasoline direct injection vehicle quipped with a catalyzed gasoline particulate filter during filter regeneration. Emiss. Control Sci. Technol. 2016, 2, 75-88.

Chen, L.; Liang, Z.; Zhang, X.; Shuai, S. Characterizing particulate matter emissions from GDI and PFI vehicles under transient and cold start conditions. Fuel 2017, 189, 131-140.

Cheng, Y.; Wang, J.; Zzhuang, R.; Wu, N. Analysis of Combustion behavior during colddstart and warm-up process of SI gasoline engine. SAE Technical Paper 2001; 2001-01-3557.

Choi, K.; Kim, J.; Ko, A.; Myung, C.L.; Park, S.; Lee, J. Size-resolved engine exhaust aerosol characteristics in a metal foam particulate filter for GDI light-duty vehicle. Journal of Aerosol Science 2013, 57, 1-13.

Czerwinski, J.; Comte, P.; Heeb, N., Mayer, A.; Hensel, V.; Nanoparticle emissions of DI gasoline cars with/without GPF. SAE Technical Paper 2017; 2017-01-1004.

He, X.; Ratcliff, M.A.; Zigler, B.T. Effects of gasoline direct injection engine operating parameters on particle number emissions. Energy and Fuels 2010, 26, 2014-2027.

Heeb, N.V.; Schmid, P.; Kohler, M.; Gujer, E.; Zennegg, M.; Wenger, D.; Wichser, A.; Ulrich, A.; Gfeller, U.; Honegger, P.; Zeyer, K.; Emmenegger, L.; Petermann, J.L.; Czerwinski, J.; Mosimann, T.; Kasper, M.; Mayer, A. Secondary effects of catalytic diesel particulate filters: conversion of PAHs versus formation of nitro-PAHs. Environ. Sci Technol. 2008, 42, 3773-3779.

Hu, S.; Herner, J.D.; Robertson, W.; Kobayashi, R.; Chang, M.C.; Huang, S.M.; Zienlinska, B.; Kado, N.; Collins, J.F.; Rieger, P.,; Huai, T.; Ayala, A. Emissions of polycyclic aromatic hydrocarbons (PAHs) and nitro—PAHs from heavy-duty diesel vehicles with DPF and SCR. J Air Waste Manag Assoc 2013, 63, 984-996.

International Agency for Research on Cancer. Working Group on the Evaluation of Carcinogenic Risks to Humans, IARC monographs on the evaluation of carcinogenic risks to humans. Ingested nitrate and nitrite, and cyanobacterial peptide toxins. In IARC Monographs on the Evaluation of Carcinogenic Risks to Humans; World Health Organisation: Geneva, Switzerland, 2010; Volume 94.

Karavalakis, G.; Short, D.; Vu, D.; Russell, R.; Hajbabaei, M.; Asa-Awuku, A.; Durbin, T.D. Evaluating the effects of aromatics content in gasoline on gaseous and particulate matter emissions from SI-PFI and SI-DI vehicles. Environ. Sci. Technol. 2015b, 49, 7021-7031.

Karavalakis, G.; Short, D.; Vu, D.; Russell R.L.; Asa-Awuku, A.; Jung, H.; Johnson, K.C.; Durbin, T.D. The impact of ethanol and iso-butanol blends on gaseous and particulate emissions from two passenger cars equipped with spray-guided and wall-guided direct injection SI (spark ignition) engines. Energy 2015a, 82, 168-179.

Karlsson, R.B.; Heywood, J.B. Piston fuel film observations in an optical access GDI engine. SAE Technical Paper 2001, 2001-01-2022.

Kim, K.H.; Jahan, S.A.; Kabir, E.; Brown, R.J.C. A review of airborne polycyclic aromatic hydrcarbons (PAHs) and their human health effects. Environ. Int. 2013, 60, 71-80.

Koczak, J.; Boehman, A.; Brusstar, M. Particulate emissions in GDI vehicle transients: An examination of FTP, HWFET, and US06 measurements. SAE Technical Paper, 2016, 2016-01-0992.

Lambert, C.K.; Bumbaroska, M.; Dobson, D.; Hangas, J.; Pakko, J.; Tennison, P. Analysis of high mileage gasoline exhaust particle filters. SAE Technical Paper 2016; 2016-01-0941.

Lea-Langton, A.R.; Ross, A.B.; Bartle, K.D.; Andrews, G.E.; Jones, J.M.; Li, H.; Pourkashanian, M.; Williams, A. Low temperature PAH formation in diesel combustion. Journal of Analytical and Applied Pyrolysis 2013, 103, 119-125.

Lundstedt, S.; White, P.A.; Lemieux, C.L.; Lynes, K.D.; Lambert, I.B.; Öberg, L.; Haglund, P.; Tysklind, M. Sources, fate, and toxic hazards of oxygenated polycyclic aromatic hydrocarbons (PAHs) at PAH-contaminated sites. Ambio 2007, 36, 475-485.

Maikawa, C.L.; Zimmerman, N.; Rais, K.; Shah, M.; Hawley, B.; Pant, P.; Jeong, C.H.; Delgado-Saborit, J.M.; Volkens, J.; Evans, G.; Wallace, J.S.; Godri Pollitt, K.J. Murine precision-cut lung slices exhibit acute responses following exposure to gasoline direct injection engine emissions. Science of the Total Environment 2016, 568, 1102-1109.

Mamakos, A.; Steininger, N.; Martini, G.; Dilara, P.; Drossinos, P. Cost effectiveness of particulate filter installation on direct injection gasoline vehicles. Atmospheric Environment 2013a, 77, 16-23.

Mamakos, A.; Martini, G.; Marotta, A.; Manfredi, U. Assessment of different technical options in reducing particle emissions from gasoline direct injection vehicles. Journal of Aerosol Science 2013b, 63, 115-125.

Maricq, M.M.; Chase, R.E.; Podsiadlik D.H.; Vogt, R. Vehicle exhaust particle size distributions: a comparison of tailpipe and dilution tunnel measurements. SAE Technical Paper 1999; 1999-01-1461.

Maricq, M.M.; Szente, J.J.; Jahr, K. The impact of ethanol fuel blends on PM emissions from a light-duty GDI vehicle. Aerosol Science and Technology 2012, 46, 576-583.

Maricq, M. M.; Szente, J. J.; Adams, J.; Tennison, P.; Rumpsa, T. Influence of mileage accumulation on the particle mass and number emissions of two gasoline direct injection vehicles. Environ. Sci. Technol. 2013, 47, 11890-11896.

Maricq, M.M.; Szente, J.J.; Harwell, A.L.; Loos, M.J. Impact of aggressive drive cycles on motor vehicle exhaust PM emissions. Journal of Aerosol Science 2017, 133, 1-11.

Munoz, M.; Heeb, N.V.; Haag, R.; Honegger, P.; Zeyer, K.; Mohn, J.; Comte, P.; Czerwinski, J. Bioethanol blending reduces nanoparticle, PAH, and alkyl- and nitro-PAH emissions and the genotoxic potential of exhaust from a gasoline direct injection flex-fuel vehicle. Environ. Sci. Technol. 2016, 50, 11853-11861.

Nadezhda, A.; Slavinskaya, N.A.; Riedel, U.; Dworkin, S.B.; Thomson, M.J.; Detailed numerical modeling of PAH formation and growth in non-premixed ethylene and ethane flames. Combustion and Flame 2012, 159, 979-995.

Oh, H.; Bae, C. Effects on the injection timing on spray and combustion characteristics in a spray-guided DISI engine under lean-stratified operation. Fuel 2013, 107, 225-235.

Pachauri, R.K. and Reisinger, A. IPCC 2007: Climate Change 2007: Synthesis report. Contribution of Working Groups I, II, and III to the Fourth Assessment Report of the Intergovernmental Panel on Climate Change, IPCC, Geneva, Switzerland.

Piock, W.; Hoffmann, G.; Berndorfer, A.; Salemi, P.; Fusshoeller, B. Strategies towards meeting future particulate matter emission requirements in homogeneous gasoline direct injection engines. SAE Int. J. Engines 2011, 4, 1455-1468.

Quiros, D.C.; Zhang, S.; Sardar, S.; Kamboures, M.A.; Eiges, D.; Zhang, M.; Jung, H.S.; Mcarthy, M.J.; Chang, M.C.O.; Ayala, A.; Zhu, Y.; Huai, T.; Hu, S. Measuring particulate emissions of light duty passenger vehicles using integrated particle size distribution (IPSD). Environ. Sci. Technol. 2015, 49, 5618-5627.

Richter, H.; Howard, J. B. Formation of polycyclic aromatic hydrocarbons and their growth to soot-a review of chemical reaction pathways. Prog. Energy Combust. Sci. 2000, 26, 565-608.

Saffaripour, M.; Chan, T.W.; Liu, F.; Thomson, K.A.; Smallwood, G.J.; Kubsh, J.; Brezny, R. Effect of drive cycle and gasoline particulate filter on the size and morphology of soot particles emitted from a gasoline-direct-injection vehicle. Environ. Sci. Technol. 2015, 49, 11950-11958.

Spiess, S.; Wong, K.F.; Richter, J.M.; Klingmann, R. Investigations of emissions control systems for gasoline direct injection engines with a focus on removal of particulate emissions. Topics in Catalysis 2013, 434-439.

Stevens, E.; Steeper, R. Piston wetting in an optical DISI engine: Fuel films, pool fires, and soot generation. SAE Technical Paper 2001, 2001-01-1203.

Storey, J.M.; Lewis, S.; Szybist, J.; Thomas, J.; Barone, T.; Eibl, M.; Nafziger, E.; Kaul, B. Novel Characterization of GD engine exhaust for gasoline and mid-level gasoline-alcohol blends. SAE Int. J. Fuels Lubr. 2014, 7, 571-579.

Su, J.; Lin, W.; Sterniak, J.; Xu, M.; Bohac, S.V. Particulate matter emission comparison of spark ignition direct injection (SIDI) and port fuel injection (PFI) operation of a boosted gasoline engine. J. Eng. Gas Turbines Power 2014, 136, 091513-1-091513-6.

Xia, W.; Zheng, Y.; He, X.; Yang, D.; Shao, H.; Remias, J.; Roos, J.; Wang, Y. Catalyzed gasoline particulate filter (GPF) performance: effect of driving cycle, fuel, catalyst coating. SAE Technical Paper 2017; 2017-01-2366.

Xue, J.; Quiros, D.; Wang, X.; Durbin, T.D.; Johnson, K.C.; Karavalakis, G.; Hu, S.; Huai, T.; Ayala, A.; Jung, H.S. Using a new inversion matrix for a fast-sizing spectrometer and a photo-acoustic instrument to determine suspended particulate mass over a transient cycle for light-duty vehicles. Aerosol Science and Technology 2016, 50, 1227-1238.

Zhang, S.; McMahon, W. Particulate emissions for LEV II light-duty gasoline direct injection vehicles. SAE Int. J. Fuels Lubr. 2012, 5, 637-646.

2.8. **Supporting Information**

2.8.1. **Emissions Analysis**

PM measurements were made on both a mass and number basis. PM mass samples were collected cumulatively over the entire length of the LA92 cycle, with one sample collected for each test. Total PM mass samples were collected using 47-mm polytetrafluoroethylene (PTFE) filters (Whatman) and weighed with a 1065-compliant microbalance in a temperature and humidity controlled clean chamber meeting 1065 requirements. Buoyancy corrections for barometric pressure differences were also made for the PM filter weights as per CFR 1065.

Total particle number was measured using a TSI 3776 ultrafine-Condensation Particle Counter (CPC) with a 2.5 nm cut point. The instrument operated at a flowrate of 1.5 L/min. Solid particle number counts were measured with the use of a catalytic stripper. The catalytic stripper both vaporizes volatile species and oxidizes them, and hence more efficiently removes volatiles from the sample than thermal treatment alone. For this study, the catalytic stripper used was 40 mm long with a diameter of 17 mm and was based on a cordierite monolith with a 400 cpsi cell density and a 6 mils substrate thickness. It had both oxidation and sulfur storage capability, but its exact chemical composition was unknown. The particular unit was characterized according to the protocol outlined by Amanatidis et al. (2013) and was deemed appropriate for the measurements of this study. The particles were counted downstream of the catalytic stripper with a TSI 3776 ultrafine CPC at a flow rate of 1.5 L/min. An ejector diluter was used to collect particle number samples from the CVS tunnel for the GDI vehicles.

Real-time particle size distributions were obtained using an Engine Exhaust Particle Sizer (EEPS) spectrometer. The EEPS (TSI 3090, firmware version 8.0.0) was used to obtain real-time second-by-second size distributions between 5.6 to 560 nm. Particles were sampled at a flow rate of 10 L/min, which is considered to be high enough to minimize diffusional losses. They were then charged with a corona charger and sized based on their electrical mobility in an electrical field. Concentrations were determined through the use of multiple electrometers. In this study, the measured electrometer currents over 22 electrometers were inverted to particle size distributions into 32 bins using two inversion matrices, known as Default Matrix or Soot Matrix (Xue et. al, 2015). A detailed mathematical description of how the inversion matrix converts electrometer signals to size distributions is given elsewhere (Wang et. al, 2016). PM mass measurements based on the integrated particle size distribution (IPSD) method were made according to Xue et al. (2016).

Real-time soot or black carbon emissions were measured using an AVL Micro-Soot Sensor (MSS). The MSS is an instrument that measures soot mass concentration at a frequency of one-Hertz basis using a photo acoustic detection technique, where the light-absorbing PM components (such as soot particles) are exposed to laser light that is periodically modulated at the acoustical resonant frequency (Schindler et. al, 2004). The instrument is designed to measure soot concentrations down to ~5$\mu g/m^3$, and operates at a flow rate of 2 L/min.

Elemental and organic carbon (EC/OC) fractions were collected on 2500 QAT-UP Tissuquartz (Pall Gelman, Ann Arbor, MI) filters. Quartz fiber filters were pre-cleaned to

remove carbonaceous contaminants by firing at 600 ºC for 5 hours. A Thermal/Optical Carbon Aerosol Analyzer (Sunset Laboratory, Forest Grove, OR) operating using the NIOSH (National Institute of Occupational Safety and Health) Method 5040 was used to analyze the OC and EC fractions.

2.8.2. **Polycyclic Aromatic Hydrocarbon (PAH) and Nitrated PAH Analysis**

Analysis of PAH and nitro-PAH species was performed at the Desert Research Institute (DRI), Reno, NV. PAH and nitro-PAH species for both the vapor- and particle-phase PM were collected in duplicate samples for the baseline and each control technology. The SVOC collected on each filter-XAD sampling train were extracted separately with high-purity, HPLC-grade dichloromethane (DCM) followed by acetone by accelerated solvent extraction (ASE). The ASE method pressurized and heated the media for 15 min/cell at 1500 psi and 80°C. The following deuterated internal standards were added to the media (XAD and filters) prior to extraction: naphthalene-d_8, acenaphthylene-d_8, phenanthrene-d_{10}, anthracene-d_{10}, chrysene-d_{12}, pyrene-d_{10}, benz[a]anthracene-d_{12}, benzo[a]pyrene-d_{12}, benzo[e]pyrene-d_{12}, benzo[k]fluoranthene-d-$_{12}$, benzo[g,h,i]perylene-d_{12}, coronene-d_{12}, 1-nitronaphthalene-d_7, 2-nitrobiphenyl-d_9, 1-nitrofluorene-d_9, 9-nitroanthracene-d_9, 3-nitrofluoranthene-d_9, 1-nitropyrene-d_9, 9-nitrochrysene-d_{11}, 6-nitrobenzo[a]pyrene-d_{11}. Extracts were concentrated to ~1mL by rotary evaporation at 35-45°C under gentle vacuum, and filtered through a 0.2 µm PTFE disposable filter (Whatman Pura disc TM 25TF). Filtrate was collected in a 4 mL amber glass vial for a total volume of ~4 mL (including flask rinse with solvent). Approximately 500 µl of hexane was added at this

time, and the extracts were reduced in volume under a gentle stream of ultra-high purity (UHP) nitrogen (with a Chrompack CP-Gas-Clean moisture filter) to ~250 μL.

The XAD cartridge extracts were analyzed separately by electron impact (EI) GC/MS for PAHs using a Varian 4000 GC/MS system equipped with a CP-8400 autosampler. A 1 μL injection onto a 30-m 5% phenylmethylsilicone fused-silica capillary column (DB-5MS+DG, J&W Scientific, Folsom CA) was performed. Compounds and corresponding deuterated internal standards were quantified by selective ion monitoring (SIM). Additional analyses were performed for filter PAH and nitro-PAH on a Scion 456 GC interfaced with a Scion TQ triple quadrupole MS/MS and equipped with CP-8400 autosampler, due to the superior sensitivity of this instrument. The PAH method utilized the same capillary column mentioned previously, while the nitro-PAH method required a 30-m DB-17MS column (J&W Scientific, Folsom CA). Negative ion chemical ionization (NICI) with methane as a reagent gas was utilized for nitro-PAH analysis to enhance detection sensitivity.

Method detection limits (MDLs) for PAHs and nitro-PAHs are about 10 ng/sample. Replicate analysis was performed on 10% of samples and used to assess measurement uncertainty. Uncertainties were calculated as the larger of the average of replicate precision [p = (2*abs(r1 - r2)/(r1 + r2)] or the limit of resolution (1 ng/sample). The uncertainties depend on sample matrix and concentration, but on average were about 10% of the sample concentration.

2.8.3. **Supplementary Tables**

Table S2-1. Regulated emissions for each phase of the LA92 cycle for both test vehicles

		GDI_1	GDI_1/GPF	GDI_2	GDI_2/GPF
THC (g/mi)	Cold-start	0.160±0.006	0.116±0.017	0.440±0.065	0.395±0.012
	Hot-running	0.001±0.000	0.000±0.000	0.037±0.000	0.001±0.000
	Hot-start	0.005±0.000	0.004±0.002	0.103±0.004	0.035±0.002
NHMC (g/mi)	Cold-start	0.131±0.006	0.093±0.011	0.384±0.060	0.336±0.013
	Hot-running	0.001±0.000	0.000±0.000	0.032±0.000	0.000±0.000
	Hot-start	0.000±0.000	0.000±0.001	0.084±0.003	0.019±0.002
CO (g/mi)	Cold-start	2.330±0.206	1.526±0.575	2.453±0.860	1.349±0.148
	Hot-running	0.075±0.008	0.065±0.012	0.536±0.023	0.126±0.012
	Hot-start	0.034±0.013	0.055±0.038	0.963±0.194	0.207±0.067
NOx (g/mi)	Cold-start	0.017±0.001	0.015±0.001	0.173±0.059	0.096±0.008
	Hot-running	0.009±0.002	0.008±0.000	0.063±0.000	0.003±0.000
	Hot-start	0.008±0.001	0.004±0.001	0.028±0.002	0.003±0.001
CO_2 (g/mi)	Cold-start	470.3±34.5	417.8±7.4	534.1±2.9	540.1±21.6
	Hot-running	253.4±12.3	238.9±0.9	318.6±3.3	309.4±10.2
	Hot-start	349.8±15.1	324.7±4.0	455.4±3.6	444.9±15.3

Table S2-2. Individual particle-phase PAH compounds, expressed in ng/mile, for both test vehicles over the LA92 cycle

ng/mi	GDI_1				GDI_2			
Non-substituted PAHs	Without GPF		With GPF		Without GPF		With GPF	
Naphthalene	507.41 ± 404.8		26.86 ± 25.33		227.03 ± 62.22		1.95 ± 2.67	
Acenaphthylene	36.77 ± 20.4		0.00 ± 0.00		24.79 ± 12.80		0.00 ± 0.00	
Acenaphthene	0.00 ± 0.0		0.00 ± 0.00		0.00 ± 0.00		0.00 ± 0.02	
Fluorene	29.76 ± 4.5		0.00 ± 0.00		0.00 ± 0.00		0.00 ± 0.00	
Phenanthrene	248.73 ± 180.9		4.38 ± 0.25		84.75 ± 5.16		0.00 ± 0.00	
Anthracene	50.82 ± 29.4		0.00 ± 0.00		26.06 ± 0.46		0.00 ± 0.00	
Fluoranthene	129.51 ± 52.0		3.12 ± 1.56		113.71 ± 17.25		0.00 ± 0.00	
Pyrene	135.91 ± 56.5		2.07 ± 0.06		126.13 ± 13.05		0.00 ± 0.00	
Benzo(a)fluorene	9.59 ± 4.5		0.00 ± 0.00		20.21 ± 1.87		0.00 ± 0.00	
Benzo(b)fluorene	7.99 ± 2.3		0.00 ± 0.00		18.67 ± 0.30		0.00 ± 0.00	
benzo(c)phenanthrene	3.20 ± 0.0		0.00 ± 0.00		20.21 ± 1.87		0.00 ± 0.00	
Benzo(ghi)fluoranthene	76.75 ± 18.1		1.06 ± 1.49		264.45 ± 4.50		0.00 ± 0.00	
Cyclopenta(c,d)pyrene	33.58 ± 6.8		0.00 ± 0.00		141.33 ± 30.71		0.00 ± 0.00	
Benz(a)anthracene	22.38 ± 4.5		0.00 ± 0.00		125.88 ± 17.76		0.00 ± 0.00	
Chrysene-Triphenylene	17.59 ± 6.8		0.00 ± 0.00		112.00 ± 2.58		0.00 ± 0.00	
Benzo(b+j+k)fluoranthene	30.38 ± 6.8		2.07 ± 0.06		233.01 ± 44.62		0.00 ± 0.00	
Benzo(a)fluoranthene	0.00 ± 0.0		0.00 ± 0.00		12.45 ± 0.20		0.00 ± 0.00	
BeP	9.59 ± 0.0		0.00 ± 0.00		62.17 ± 7.79		0.00 ± 0.00	
BaP	14.39 ± 2.3		0.00 ± 0.00		114.97 ± 20.13		0.00 ± 0.00	
Perylene	1.60 ± 2.3		9.11 ± 12.88		21.75 ± 4.05		0.00 ± 0.00	
Indeno[123-cd]fluoranthene	0.00 ± 0.0		0.00 ± 0.00		3.11 ± 0.05		0.00 ± 0.00	
dibenz(a,h)acridine	0.00 ± 0.0		0.00 ± 0.00		0.00 ± 0.00		0.00 ± 0.00	
dibenz(a,j)acridine	0.00 ± 0.0		0.00 ± 0.00		0.00 ± 0.00		0.00 ± 0.00	
Indeno[123-cd]pyrene	11.19 ± 2.3		0.00 ± 0.00		93.18 ± 20.49		0.00 ± 0.00	
Dibenzo(ah+ac)anthracene	0.00 ± 0.0		1.01 ± 1.43		10.87 ± 2.02		0.00 ± 0.00	
Dibenzo(a,j)anthracene	0.00 ± 0.0		0.00 ± 0.00		7.76 ± 2.07		0.00 ± 0.00	
Benzo(b)chrysene	0.00 ± 0.0		0.00 ± 0.00		7.76 ± 2.07		0.00 ± 0.00	
Picene	0.00 ± 0.0		0.00 ± 0.00		9.30 ± 4.25		0.00 ± 0.00	
Benzo(ghi)perylene	31.98 ± 9.0		0.00 ± 0.00		181.71 ± 38.85		0.00 ± 0.00	
Anthanthrene	0.00 ± 0.0		0.00 ± 0.00		20.21 ± 1.87		0.00 ± 0.00	
Dibenzo(a,l)pyrene	0.00 ± 0.0		0.00 ± 0.00		0.00 ± 0.00		0.00 ± 0.00	

Coronene	8.00	±	2.3	0.00	±	0.00	62.17	±	7.79	0.00	±	0.00
Dibenzo(a,e)pyrene	0.00	±	0.0	0.00	±	0.00	6.22	±	0.10	0.00	±	0.00
Dibenzo(a,i)pyrene	0.00	±	0.0	0.00	±	0.00	0.00	±	0.00	0.00	±	0.00
Dibenzo(a,h)pyrene	0.00	±	0.0	0.00	±	0.00	0.00	±	0.00	0.00	±	0.00
Dibenzo(b,k)fluoranthene	0.00	±	0.0	0.00	±	0.00	18.64	±	4.10	0.00	±	0.00
Substituted PAHs												
2-methylnaphthalene	390.69	±	366.31	7.41	±	12.76	228.67	±	51.19	0.00	±	0.00
1-methylnaphthalene	116.37	±	117.58	3.16	±	4.23	58.61	±	14.42	0.00	±	0.00
2,6+2,7-dimethylnaphthalene	54.02	±	56.53	0.00	±	0.00	19.84	±	0.35	0.00	±	0.00
1,3+1,6+1,7dimethylnaphth	41.57	±	49.75	0.00	±	0.00	18.60	±	8.50	0.00	±	0.00
1,4+1,5+2,3-dimethylnaphth	9.59	±	13.57	0.00	±	0.00	0.00	±	0.00	0.00	±	0.00
1,2-dimethylnaphthalene	0.00	±	0.00	0.00	±	0.00	0.00	±	0.00	0.00	±	0.00
1,8-dimethylnaphthalene	0.00	±	0.00	0.00	±	0.00	0.00	±	0.00	0.00	±	0.00
1-ethyl-2-methylnaphthalene	0.00	±	0.00	0.00	±	0.00	0.00	±	0.00	0.00	±	0.00
2,3,5+I-trimethylnaphthalene	0.00	±	0.00	0.00	±	0.00	0.00	±	0.00	0.00	±	0.00
B-trimethylnaphthalene	4.45	±	4.52	0.00	±	0.00	0.00	±	0.00	0.00	±	0.00
A-trimethylnaphthalene	18.84	±	15.83	0.00	±	0.00	2.70	±	2.13	0.00	±	0.00
C-trimethylnaphthalene	4.45	±	4.52	0.00	±	0.00	0.00	±	0.00	0.00	±	0.00
1+2ethylnaphthalene	43.17	±	56.53	0.00	±	0.00	23.29	±	6.22	0.97	±	1.37
2-ethyl-1-methylnaphthalene	1.60	±	2.26	0.00	±	0.00	0.00	±	0.00	0.00	±	0.00
E-trimethylnaphthalene	1.60	±	2.26	0.00	±	0.00	1.57	±	2.23	0.00	±	0.00
2,4,5-trimethylnaphthalene	0.00	±	0.00	0.00	±	0.00	0.00	±	0.00	0.00	±	0.00
F-trimethylnaphthalene	6.40	±	4.52	0.00	±	0.00	1.57	±	2.23	0.00	±	0.00
1,4,5-trimethylnaphthalene	0.00	±	0.00	0.00	±	0.00	0.00	±	0.00	0.00	±	0.00
J-trimethylnaphthalene	0.00	±	0.00	0.00	±	0.00	0.00	±	0.00	0.00	±	0.00
A-Methylfluorene	12.79	±	9.04	0.00	±	0.00	0.00	±	0.00	0.00	±	0.00
B-Methylfluorene	0.00	±	0.00	0.00	±	0.00	0.00	±	0.00	0.00	±	0.00
1-Methylfluorene	6.40	±	4.52	0.00	±	0.00	3.11	±	0.05	0.00	±	0.00
2-methylphenanthrene	25.58	±	13.57	1.06	±	1.49	7.80	±	2.33	0.00	±	0.00
3-methylphenanthrene	38.03	±	20.35	1.18	±	1.56	22.91	±	4.00	1.96	±	0.04
2-methylanthracene	17.59	±	2.26	0.00	±	0.00	15.56	±	0.25	0.00	±	0.00
4,5-methylenephenanthrene	28.78	±	18.09	0.00	±	0.00	1.54	±	2.17	0.00	±	0.00
9-methylphenanthrene	27.18	±	20.35	0.00	±	0.00	4.65	±	2.13	0.00	±	0.00
1-methylphenanthrene	31.63	±	15.83	0.12	±	0.06	10.54	±	4.60	0.00	±	0.00
9-methylanthracene	0.00	±	0.00	0.00	±	0.00	0.00	±	0.00	0.00	±	0.00
A-dimethylphenanthrene	6.40	±	0.00	0.00	±	0.00	7.76	±	2.07	0.00	±	0.00
B-dimethylphenanthrene	4.80	±	2.26	0.00	±	0.00	3.11	±	0.05	0.00	±	0.00

1,7-dimethylphenanthrene	7.99	±	6.78	0.00	±	0.00	4.69	±	2.28	0.00	±	0.00
3,6-dimethylphenanthrene	4.80	±	6.78	0.00	±	0.00	4.69	±	2.28	0.00	±	0.00
D-dimethylphenanthrene	4.80	±	2.26	0.00	±	0.00	3.08	±	4.35	0.00	±	0.00
E-dimethylphenanthrene	4.45	±	0.00	0.00	±	0.00	1.17	±	0.05	0.00	±	0.00
C-dimethylphenanthrene	22.39	±	22.61	1.01	±	1.43	21.82	±	4.75	0.00	±	0.00
B-MePy/MeFl	17.59	±	2.26	0.00	±	0.00	32.66	±	1.67	0.00	±	0.00
1-MeFl+C-MeFl/Py	1.60	±	2.26	0.00	±	0.00	7.80	±	2.33	0.00	±	0.00
1+3-methylfluoranthene	7.99	±	6.78	0.00	±	0.00	9.30	±	4.25	0.00	±	0.00
4-methylpyrene	11.19	±	2.26	0.00	±	0.00	20.28	±	6.93	0.00	±	0.00
C-MePy/MeFl	14.39	±	6.78	0.00	±	0.00	35.81	±	2.78	0.00	±	0.00
D-MePy/MeFl	6.40	±	0.00	0.00	±	0.00	18.71	±	4.70	0.00	±	0.00
1-methylpyrene	6.40	±	0.00	0.00	±	0.00	12.48	±	4.60	0.00	±	0.00
3-methylchrysene	0.00	±	0.00	0.00	±	0.00	13.99	±	1.97	0.00	±	0.00
5+6-methylchrysene	0.00	±	0.00	0.00	±	0.00	3.11	±	0.05	0.00	±	0.00
7-methylbenzo(a)pyrene	0.00	±	0.00	0.00	±	0.00	1.54	±	2.17	0.00	±	0.00
Oxygenated PAHs												
Dibenzofuran	75.01	±	65.58	0.00	±	0.00	5.79	±	4.15	0.00	±	0.00
9-fluorenone	108.38	±	101.75	0.12	±	0.06	38.51	±	0.66	0.00	±	0.00
Xanthone	12.79	±	18.09	5.19	±	1.62	9.34	±	0.15	0.00	±	0.00
Acenaphthenequinone	0.00	±	0.00	0.00	±	0.00	0.00	±	0.00	0.00	±	0.00
Perinaphthenone	57.21	±	38.44	0.08	±	2.86	193.08	±	66.98	0.00	±	0.00
Anthraquinone	24.89	±	18.09	5.35	±	4.11	47.55	±	11.84	0.00	±	0.00
9-Anthraaldehyde	1.60	±	2.26	0.00	±	0.00	3.15	±	4.45	0.00	±	0.00
Benzanthrone	0.00	±	0.00	0.00	±	0.00	63.78	±	1.16	0.00	±	0.00
Benz(a)anthracene-7,12-dione	3.20	±	0.00	0.00	±	0.00	12.38	±	8.60	0.00	±	0.00
Phenyl PAHs												
3-methylbiphenyl	23.78	±	4.52	0.00	±	0.00	0.00	±	0.00	0.00	±	0.00
4-methylbiphenyl	18.15	±	6.78	0.32	±	2.74	5.00	±	6.42	2.95	±	1.48
2-phenylnaphthalene	20.79	±	11.31	0.00	±	0.00	24.90	±	0.40	0.00	±	0.00
Biphenyl	66.81	±	61.05	1.13	±	1.37	13.62	±	0.25	0.00	±	0.00
2-methylbiphenyl	10.15	±	18.09	0.00	±	0.00	0.00	±	0.00	10.69	±	9.47

Table S2-3. Individual gas-phase PAH compounds, expressed in ng/mile, for both test vehicles over the LA92 cycle

ng/mi	GDI_1				GDI_2			
Non-substituted PAHs	Without GPF		With GPF		Without GPF		With GPF	
naphthalene	32881 ± 18908		17010 ± 8564		339292 ± 184527		229738 ± 172108	
Acenaphthylene	262 ± 140		16 ± 5		10229 ± 7255		801 ± 663	
Acenaphthene	172 ± 104		39 ± 47		852 ± 67		346 ± 383	
Fluorene	210 ± 127		23 ± 21		1121 ± 68		22 ± 29	
Phenanthrene	212 ± 88		76 ± 17		2572 ± 597		98 ± 12	
Anthracene	22 ± 5		6 ± 0		418 ± 79		9 ± 1	
Fluoranthene	0 ± 0		0 ± 0		337 ± 43		0 ± 0	
Pyrene	4 ± 0		6 ± 2		436 ± 38		17 ± 4	
Retene	0 ± 0		0 ± 0		0 ± 0		3 ± 1	
benzo(a)fluorene	0 ± 0		0 ± 0		20 ± 11		0 ± 0	
benzo(b)fluorene	0 ± 0		0 ± 0		14 ± 2		0 ± 0	
benzo(c)phenanthrene	0 ± 0		0 ± 0		8 ± 2		1 ± 1	
Benzo(ghi)fluoranthene	0 ± 0		0 ± 0		73 ± 32		0 ± 0	
Cyclopenta(c,d)pyrene	0 ± 0		0 ± 0		12 ± 17		0 ± 0	
Benz(a)anthracene	2 ± 2		0 ± 0		16 ± 4		1 ± 1	
Chrysene-Triphenylene	0 ± 0		0 ± 0		5 ± 2		0 ± 0	
Benzo(b+j+k)fluoranthene	2 ± 2		0 ± 0		3 ± 0		1 ± 1	
Benzo(a)fluoranthene	0 ± 0		0 ± 0		0 ± 0		0 ± 0	
BeP	0 ± 0		0 ± 0		0 ± 0		0 ± 0	
BaP	0 ± 0		0 ± 0		0 ± 0		0 ± 0	
Dibenzothiophene	5 ± 2		4 ± 3		14 ± 6		2 ± 0	
Dibutyl phthalate	125 ± 213		0 ± 0		264 ± 44		138 ± 362	
Substituted PAHs								
2-methylnaphthalene	8618 ± 5479		1547 ± 1511		390402 ± 290615		157967 ± 187511	
1-methylnaphthalene	4725 ± 2921		1110 ± 1051		177406 ± 118496		76477 ± 81765	
2,6+2,7-dimethylnaphthalene	680 ± 402		14 ± 23		25868 ± 15530		3915 ± 4876	
1,3+1,6+1,7dimethylnaphth	1126 ± 642		37 ± 59		45875 ± 28110		7461 ± 9131	
1,4+1,5+2,3-dimethylnaphth	332 ± 206		18 ± 3		11972 ± 7127		1908 ± 2311	
1,2-dimethylnaphthalene	139 ± 104		5 ± 1		13285 ± 12941		845 ± 1047	
1,8-dimethylnaphthalene	0 ± 0		0 ± 0		0 ± 0		0 ± 0	
1-ethyl-2-methylnaphthalene	66 ± 29		16 ± 15		1573 ± 1231		122 ± 123	
2,3,5+I-trimethylnaphthalene	112 ± 45		0 ± 0		2548 ± 1271		207 ± 158	

B-trimethylnaphthalene	210	±	102	0	±	0	4395	±	2361	450	±	471
A-trimethylnaphthalene	249	±	54	0	±	0	6602	±	3779	682	±	740
C-trimethylnaphthalene	159	±	79	1	±	2	3600	±	2015	293	±	258
1+2ethylnaphthalene	693	±	387	76	±	104	24031	±	14764	8259	±	10185
2-ethyl-1-methylnaphthalene	4	±	5	0	±	0	206	±	80	29	±	38
E-trimethylnaphthalene	101	±	32	0	±	0	2023	±	1080	179	±	163
2,4,5-trimethylnaphthalene	129	±	45	19	±	0	1236	±	639	165	±	141
F-trimethylnaphthalene	65	±	45	0	±	0	1495	±	716	110	±	99
1,4,5-trimethylnaphthalene	4	±	5	4	±	3	303	±	196	7	±	7
J-trimethylnaphthalene	34	±	5	12	±	7	505	±	267	75	±	47
A-Methylfluorene	30	±	25	4	±	4	242	±	48	0	±	0
B-Methylfluorene	11	±	0	2	±	3	53	±	29	3	±	1
1-Methylfluorene	21	±	2	0	±	0	157	±	32	3	±	12
2-methylphenanthrene	5	±	2	1	±	1	126	±	9	4	±	0
3-methylphenanthrene	1	±	0	0	±	0	111	±	22	0	±	3
2-methylanthracene	0	±	0	0	±	0	81	±	12	0	±	0
4,5-methylenephenanthrene	17	±	5	3	±	1	179	±	25	5	±	1
9-methylphenanthrene	4	±	7	8	±	2	108	±	33	8	±	5
1-methylphenanthrene	0	±	0	2	±	2	129	±	42	9	±	1
9-methylanthracene	0	±	0	0	±	0	9	±	0	0	±	0
A-dimethylphenanthrene	0	±	0	0	±	0	42	±	7	0	±	0
B-dimethylphenanthrene	0	±	0	0	±	0	22	±	14	1	±	1
1,7-dimethylphenanthrene	0	±	0	0	±	0	34	±	25	0	±	0
3,6-dimethylphenanthrene	0	±	0	0	±	0	23	±	16	0	±	0
D-dimethylphenanthrene	0	±	0	0	±	0	26	±	2	6	±	3
E-dimethylphenanthrene	0	±	0	0	±	0	26	±	3	0	±	0
C-dimethylphenanthrene	0	±	0	0	±	0	82	±	23	2	±	3
B-MePy/MeFl	0	±	0	0	±	0	36	±	2	0	±	0
1-MeFl+C-MeFl/Py	0	±	0	0	±	0	14	±	2	0	±	0
1+3-methylfluoranthene	0	±	0	0	±	0	11	±	2	0	±	0
4-methylpyrene	2	±	2	1	±	1	16	±	4	0	±	0
C-MePy/MeFl	0	±	0	0	±	0	26	±	6	0	±	0
D-MePy/MeFl	0	±	0	1	±	1	5	±	2	0	±	0
1-methylpyrene	0	±	0	0	±	0	11	±	2	0	±	0
3-methylchrysene	0	±	0	0	±	0	0	±	0	0	±	0
5+6-methylchrysene	0	±	0	0	±	0	0	±	0	0	±	0
7-methylbenz(a)anthracene	0	±	0	0	±	0	0	±	0	0	±	0

7,12-dimethylbenz(a)anthracene	0 ± 0	0 ± 0	0 ± 0	0 ± 0
3-methylcholanthrene	0 ± 0	0 ± 0	0 ± 0	0 ± 0
7-methylbenzo(a)pyrene	0 ± 0	0 ± 0	0 ± 0	0 ± 0
Oxygenated PAHs				
Dibenzofuran	369 ± 310	150 ± 62	1426 ± 220	314 ± 303
9-fluorenone	38 ± 11	86 ± 22	655 ± 130	46 ± 8
Xanthone	2 ± 2	31 ± 10	73 ± 8	16 ± 5
Perinaphthenone	2 ± 2	0 ± 0	80 ± 69	6 ± 8
Anthraquinone	0 ± 0	0 ± 0	19 ± 6	7 ± 1
9-Anthraaldehyde	2 ± 2	0 ± 0	5 ± 2	1 ± 1
Phenyl PAHs				
Biphenyl	541 ± 405	90 ± 81	3882 ± 57	2649 ± 2415
3-methylbiphenyl	0 ± 0	0 ± 0	731 ± 103	170 ± 300
4-methylbiphenyl	0 ± 0	0 ± 0	684 ± 62	83 ± 77
Bibenzyl	0 ± 0	0 ± 0	0 ± 0	0 ± 0
2-phenylnaphthalene	2 ± 2	5 ± 2	106 ± 11	6 ± 0

Table S2-4. Individual particle-phase nitrated PAH compounds, expressed in ng/mile, for both test vehicles over the LA92 cycle

ng/mile	GDI 1		GDI 2	
	Without GPF	With GPF	Without GPF	With GPF
1-Nitronaphthalene	0.195±0.122	0±0	0.058±0.005	0±0
5-Methyl-1-nitronaphthalene	0.015±0.016	0.002±0.003	0.014±0.003	0.005±0.007
2-Nitronaphthalene	1.006±0.914	0±0	0.287±0.033	0±0
2-Nitrobiphenyl	0.07±0.046	0.001±0.002	0.016±0.005	0±0
2-Methyl-4-nitronaphthalene	0.049±0.07	0±0	0±0	0.014±0.019
1-Methyl-4-nitronaphthalene	0.035±0.023	0±0	0.005±0.01	0±0
1-Methyl-6-nitronaphthalene	0.101±0.065	0.008±0.012	0.041±0.001	0±0
3-Nitrobiphenyl	0.079±0.052	0±0	0.017±0.016	0±0
4-Nitrobiphenyl	0.075±0.076	0±0	0.136±0.245	0.033±0.099
1,3-Dinitronaphthalene	0±0	0.049±0.069	0±0	0.142±0.019
1,5-Dinitronaphthalene	0±0	0.004±0.006	0±0	0.003±0.004
5-Nitroacenaphthene	0.062±0.007	0.015±0.022	0.086±0.017	0.02±0.008
2-Nitrofluorene	0±0	0±0	0±0	0±0
4-Nitrophenanthrene	0±0	0±0	0±0	0±0
9-Nitroanthracene	0.218±0.041	0±0	0±0	0.086±0.122
9-Nitrophenanthrene	0.011±0.016	0±0	0.034±0.012	0±0
1,8-Dinitronaphthalene	0±0	0±0	0.013±0.018	0±0
3-Nitrophenanthrene	0.003±0.004	0±0	0.026±0.009	0±0
2-Nitrophenanthrene	0±0	0±0	0.01±0.014	0±0

2-Nitroanthracene	0±0	0±0	0±0	0±0
1-Nitrofluoranthene	0±0	0±0	0±0	0±0
7-Nitrofluoranthene	0±0	0±0	0±0	0±0
2-Nitrofluoranthene	0.02±0.058	0.073±0.133	0.173±0.125	0±0
3-Nitrofluoranthene	0±0	0±0	0±0	0±0
4-Nitropyrene	0.021±0.03	0±0	0.092±0.025	0.011±0.015
8-Nitrofluoranthene	0±0	0±0	0±0	0±0
1-Nitropyrene	0.118±0.042	0.041±0.034	0.222±0.016	0.068±0.016
2-Nitropyrene	0±0	0±0	0±0	0±0
2,7-Dinitrofluorene	0±0	0±0	0.352±0.228	0±0
2,7-Dinitrofluoen-9-one	0±0	0±0	0±0	0±0
7-Nitrobenz(a)anthracene	0±0	0±0	0.084±0.119	0±0
6-Nitrochrysene	0±0	0±0	0±0	0±0
3-Nitrobenzanthrone	0±0	0±0	0±0	0±0
1,3-Dinitropyrene	0±0	0±0	0±0	0±0
1,6-Dinitropyrene	0±0	0±0	0±0	0±0
1,8-Dinitropyrene	0±0	0±0	0±0	0±0
6a+1e-nitrobenzo(e)pyrene	0±0	0±0	0±0	0±0
3-Nitrobenz(e)pyrene	0±0	0±0	0±0	0±0

Table S2-5. Individual gas-phase nitrated PAH compounds, expressed in ng/mile, for both test vehicles over the LA92 cycle

ng/mile	GDI 1		GDI 2	
	Without GPF	With GPF	Without GPF	With GPF
1-Nitronaphthalene	0.9±0.078	0.489±0.309	5.372±1.256	0.582±0.113
5-Methyl-1-nitronaphthalene	0.117±0.035	0.033±0.014	0.263±0.073	0.052±0.031
2-Nitronaphthalene	2.127±1.529	0.737±0.825	7.326±0.63	0±0
2-Nitrobiphenyl	0.292±0.113	0.228±0.031	0.952±0.104	0.277±0.031
2-Methyl-4-nitronaphthalene	0±0	0±0	0±0	0±0
1-Methyl-4-nitronaphthalene	0.097±0.366	0±0	0±0	0±0
1-Methyl-6-nitronaphthalene	0.139±0.06	0.085±0.063	0.333±0.345	0.084±0.051
3-Nitrobiphenyl	0.036±0.142	0.062±0.022	0.235±0.159	0±0
4-Nitrobiphenyl	0.063±0.089	0±0	0.16±0.227	0.088±0.051
1,3-Dinitronaphthalene	0±0	0±0	0±0	0±0
1,5-Dinitronaphthalene	0±0	0±0	0.033±0.046	0±0
5-Nitroacenaphthene	0±0	0±0	0±0	0±0
2-Nitrofluorene	0.001±0.007	0±0	0.035±0.008	0.007±0.007
4-Nitrophenanthrene	0±0	0±0	0±0	0.025±0.036
9-Nitroanthracene	0.405±0.572	0.185±0.262	0.488±0.483	0.137±0.193
9-Nitrophenanthrene	0±0	0±0	0.017±0.024	0.018±0.025
1,8-Dinitronaphthalene	0±0	0±0	0.016±0.022	0±0
3-Nitrophenanthrene	0±0	0±0	0.011±0.015	0±0
2-Nitrophenanthrene	0±0	0±0	0±0	0±0

2-Nitroanthracene	0±0	0±0	0±0	0±0
1-Nitrofluoranthene	0±0	0±0	0±0	0±0
7-Nitrofluoranthene	0±0	0±0	0±0	0±0
2-Nitrofluoranthene	0±0	0±0	0.013±0.018	0±0
3-Nitrofluoranthene	0±0	0±0	0±0	0±0
4-Nitropyrene	0.043±0.061	0.012±0.017	0.029±0.041	0.017±0.024
8-Nitrofluoranthene	0±0	0±0	0±0	0±0
1-Nitropyrene	0±0	0.015±0.022	0.08±0.113	0.018±0.025
2-Nitropyrene	0±0	0±0	0±0	0±0
2,7-Dinitrofluorene	0±0	0±0	0±0	0±0
2,7-Dinitrofluoen-9-one	0±0	0±0	0±0	0±0
7-Nitrobenz(a)anthracene	0±0	0±0	0±0	0±0
6-Nitrochrysene	0±0	0±0	0±0	0±0
3-Nitrobenzanthrone	0±0	0±0	0±0	0±0
1,3-Dinitropyrene	0±0	0±0	0±0	0±0
1,6-Dinitropyrene	0±0	0±0	0±0	0±0
1,8-Dinitropyrene	0±0	0±0	0±0	0±0
6a+1e-nitrobenzo(e)pyrene	0±0	0±0	0±0	0±0
3-Nitrobenz(e)pyrene	0±0	0±0	0±0	0±0

Table S2-6. Metal emissions for the LA92 cycle for both test vehicles

ug/mi	GDI_1 Without GPF	GDI_1 With GPF	GDI_2 Without GPF	GDI_2 With GPF
Na	4.04 ± 2.39	0.00 ± 0.00	1.38 ± 1.95	0.00 ± 0.00
Mg	0.05 ± 0.07	0.26 ± 0.37	0.58 ± 0.83	0.38 ± 0.54
Al	1.31 ± 1.85	0.23 ± 0.33	0.18 ± 0.26	0.93 ± 1.06
Si	2.17 ± 0.13	4.26 ± 1.70	2.14 ± 1.07	1.30 ± 0.05
P	2.04 ± 2.89	0.00 ± 0.00	0.58 ± 0.70	0.00 ± 0.00
S	1.56 ± 1.23	0.05 ± 0.08	0.78 ± 0.03	0.21 ± 0.20
Cl	3.39 ± 0.45	0.15 ± 0.21	1.97 ± 0.40	0.17 ± 0.06
K	0.06 ± 0.09	0.00 ± 0.00	0.06 ± 0.09	0.05 ± 0.07
Ca	5.44 ± 5.14	0.31 ± 0.12	3.39 ± 1.59	0.26 ± 0.31
Ti	0.00 ± 0.00	0.00 ± 0.00	0.00 ± 0.00	0.00 ± 0.00
V	0.04 ± 0.03	0.07 ± 0.01	0.08 ± 0.02	0.02 ± 0.03
Cr	0.47 ± 0.01	0.07 ± 0.06	0.11 ± 0.15	0.07 ± 0.06
Mn	0.07 ± 0.10	0.14 ± 0.08	0.19 ± 0.02	0.00 ± 0.00
Fe	4.45 ± 4.49	0.75 ± 0.06	0.82 ± 0.39	0.96 ± 0.34
Co	0.02 ± 0.03	0.00 ± 0.01	0.00 ± 0.00	0.00 ± 0.00
Ni	0.57 ± 0.81	0.02 ± 0.04	0.03 ± 0.02	0.00 ± 0.00
Cu	0.15 ± 0.04	0.00 ± 0.00	0.06 ± 0.09	0.03 ± 0.05
Zn	1.32 ± 1.49	0.02 ± 0.02	1.08 ± 0.50	0.02 ± 0.03
Ga	0.03 ± 0.05	0.00 ± 0.00	0.04 ± 0.06	0.00 ± 0.00
Ge	0.00 ± 0.00	0.00 ± 0.00	0.00 ± 0.00	0.03 ± 0.04
As	0.00 ± 0.00	0.02 ± 0.02	0.01 ± 0.01	0.00 ± 0.00
Se	0.00 ± 0.00	0.00 ± 0.01	0.00 ± 0.00	0.00 ± 0.00
Br	1.29 ± 0.36	0.03 ± 0.00	0.37 ± 0.05	0.03 ± 0.01
Rb	0.02 ± 0.02	0.04 ± 0.03	0.00 ± 0.00	0.02 ± 0.03
Sr	0.00 ± 0.00	0.04 ± 0.05	0.00 ± 0.00	0.00 ± 0.00
Y	0.48 ± 0.41	0.00 ± 0.00	0.02 ± 0.02	0.00 ± 0.00
Zr	4.96 ± 5.86	0.07 ± 0.10	0.04 ± 0.05	0.02 ± 0.00
Mo	0.65 ± 0.02	0.00 ± 0.00	0.00 ± 0.00	0.00 ± 0.00
Pd	0.08 ± 0.02	0.08 ± 0.11	0.00 ± 0.00	0.07 ± 0.09
Ag	0.00 ± 0.00	0.18 ± 0.25	0.00 ± 0.00	0.00 ± 0.00
Cd	0.00 ± 0.00	0.00 ± 0.00	0.00 ± 0.00	0.00 ± 0.00
In	1.31 ± 0.22	0.03 ± 0.04	0.04 ± 0.05	0.00 ± 0.00
Sn	0.15 ± 0.21	0.03 ± 0.05	0.00 ± 0.00	0.16 ± 0.23
Sb	0.42 ± 0.22	0.00 ± 0.00	0.00 ± 0.00	0.28 ± 0.13
Ba	1.02 ± 0.59	0.00 ± 0.00	0.00 ± 0.00	0.00 ± 0.00
La	0.64 ± 0.40	0.14 ± 0.20	0.00 ± 0.00	0.00 ± 0.00
Hg	0.00 ± 0.00	0.05 ± 0.07	0.00 ± 0.00	0.00 ± 0.00
Pb	0.15 ± 0.21	0.00 ± 0.00	0.00 ± 0.00	0.00 ± 0.00
SUM	38.35 ± 29.84	7.06 ± 4.00	13.94 ± 8.34	5.02 ± 3.33

2.8.4. **Supplementary Figures**

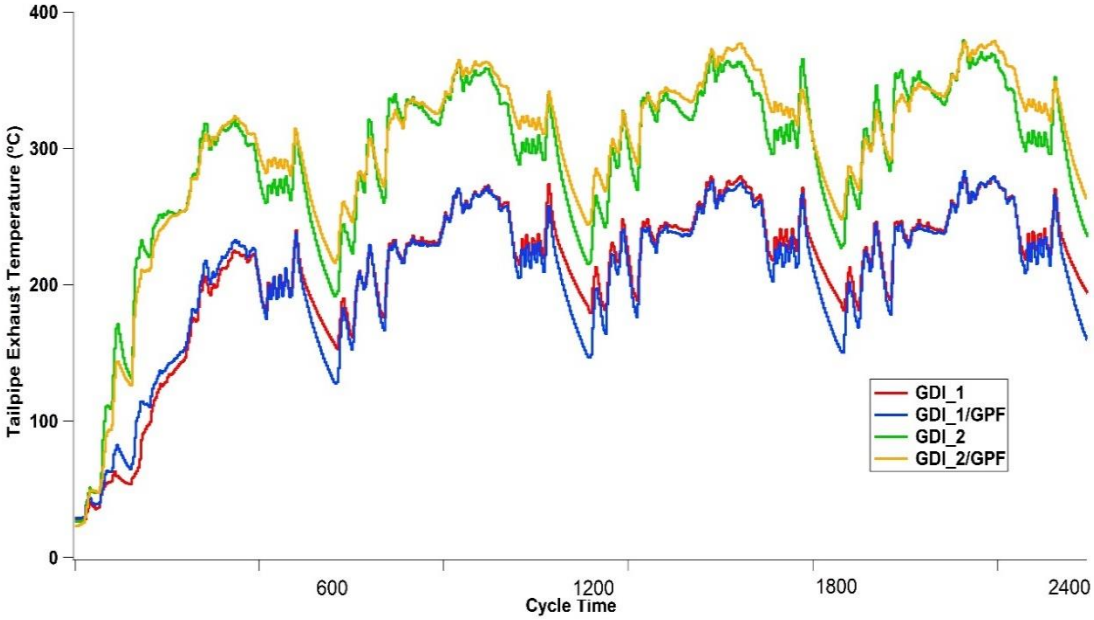

Figure S2-1. Exhaust temperatures (°C) for both test vehicles when operated over the US06 cycle in their stock configurations and with GPFs

A

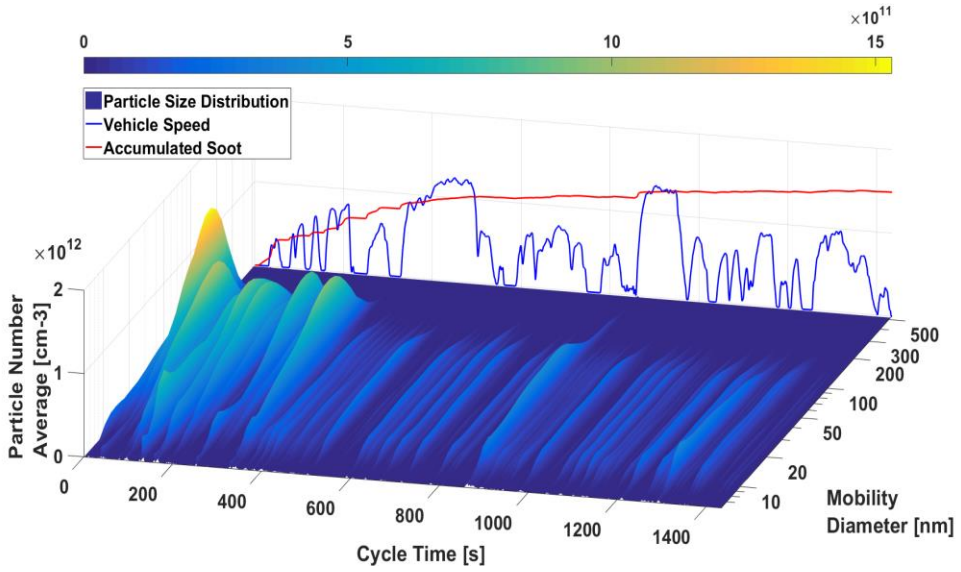

B

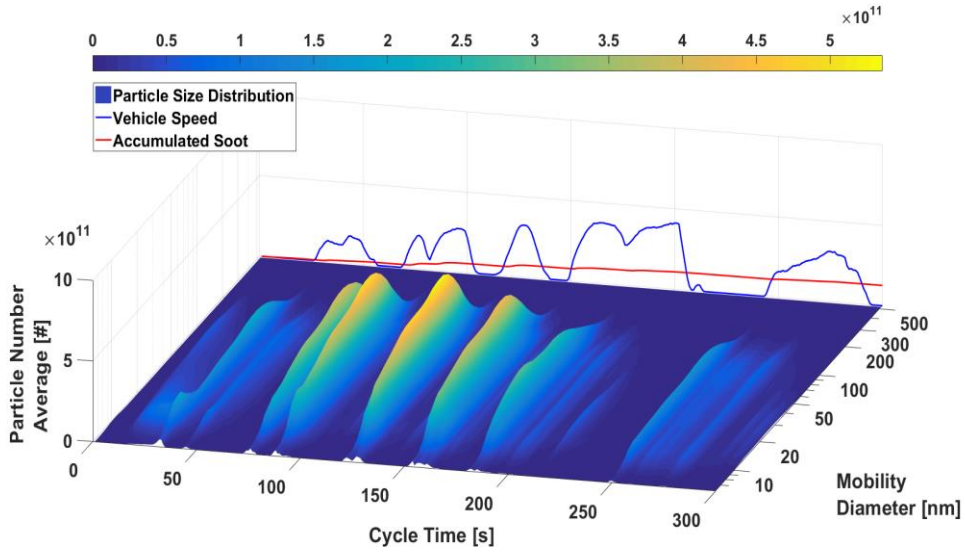

Figure S2-2 (a-b) Transient particle size distribution for phases 1 and 2 of the LA92 for GDI_2 (a); particle size distribution for phase 3 of the LA92 for GDI_2 (b); The speed-time profile and the accumulated soot mass are also included for visual reference

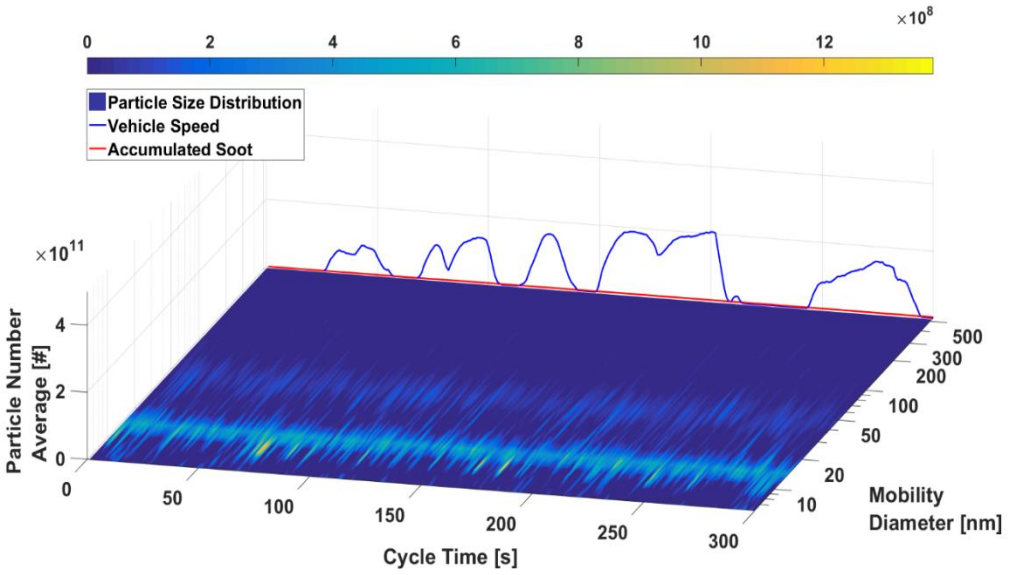

Figure S2-3 Transient particle size distribution for phase 3 of the LA92 for GDI_1/GPF; The speed-time profile and the accumulated soot mass are also included for visual reference

A

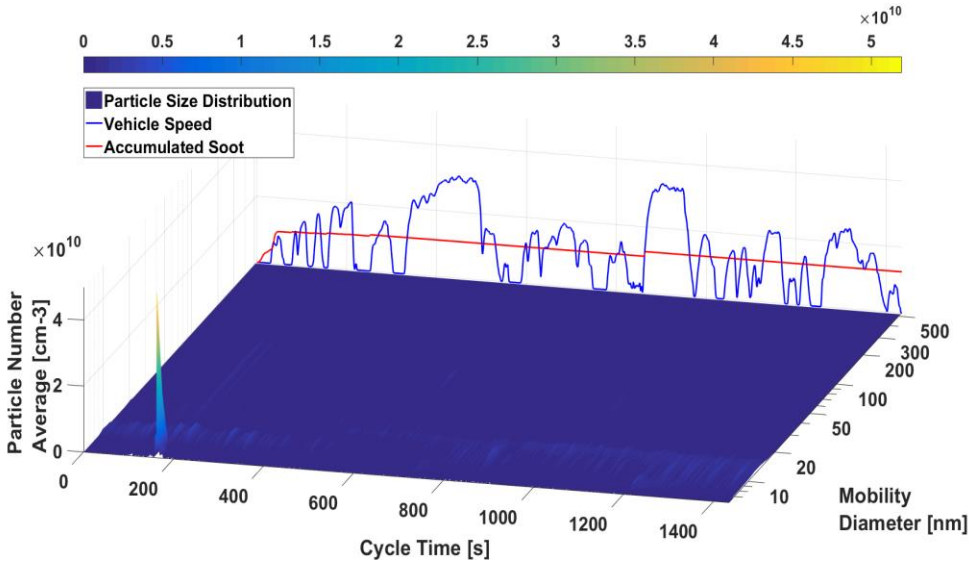

B

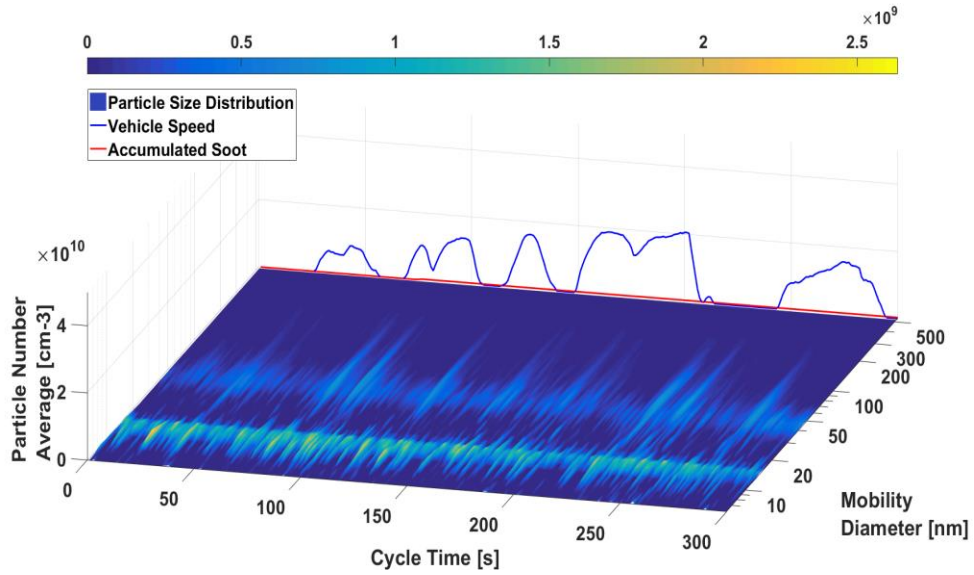

Figure S2-4 (a-b) Transient particle size distribution for phases 1 and 2 of the LA92 for GDI_2/GPF (a); particle size distribution for phase 3 of the LA92 for GDI_2/GPF (b); The speed-time profile and the accumulated soot mass are also included for visual reference

A

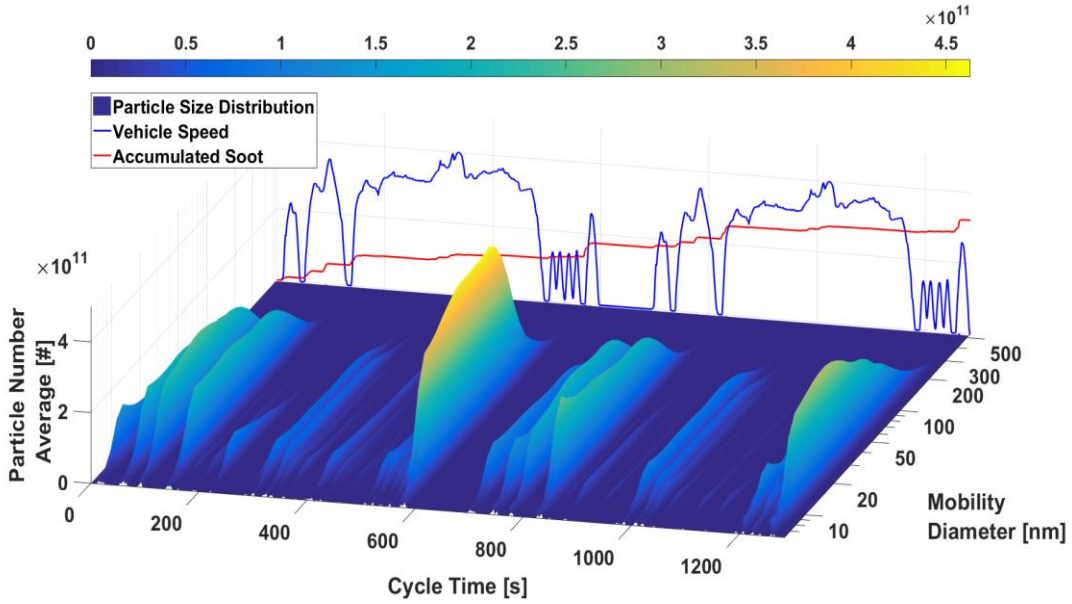

B

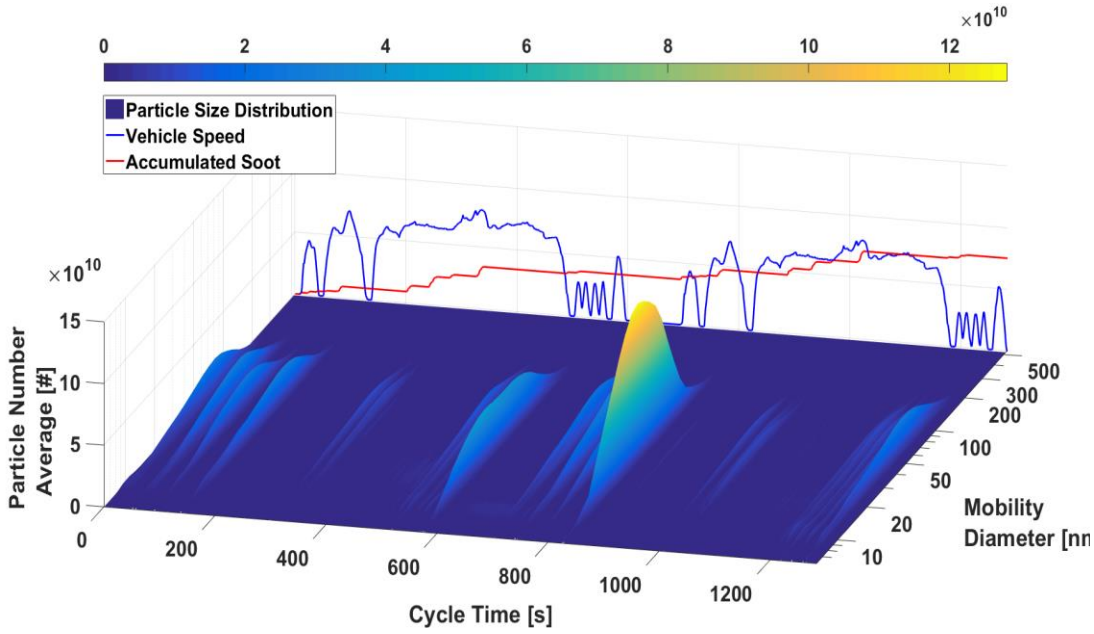

Figure S2-5 (a-b) Transient particle size distribution for the stock GDI_1 (a) the GPF-equipped GDI_1 (b) over the US06 cycle; The speed-time profile and the accumulated soot mass are also included for visual reference

A

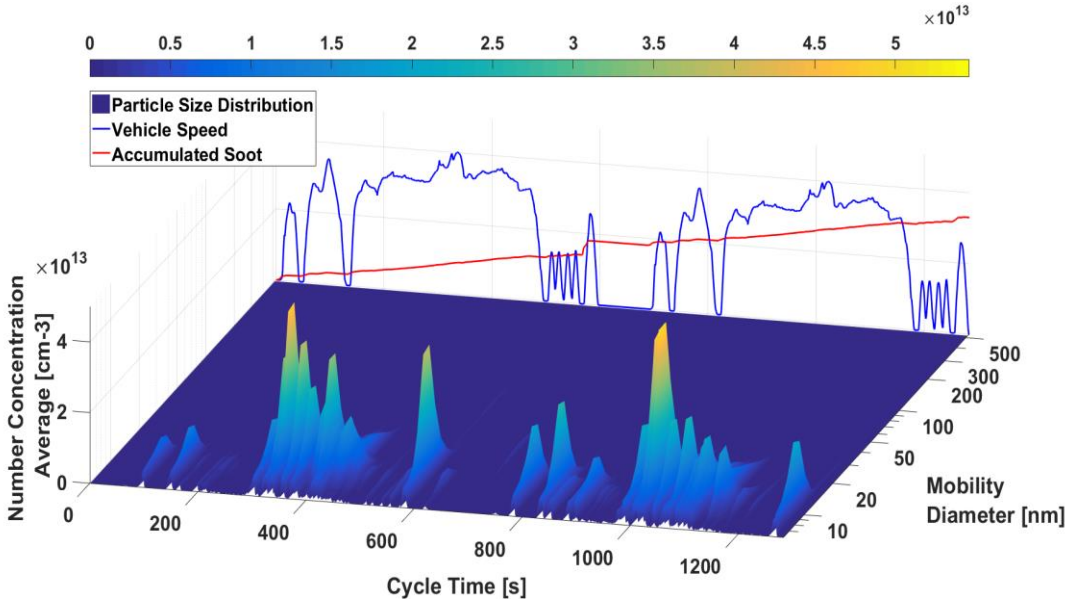

B

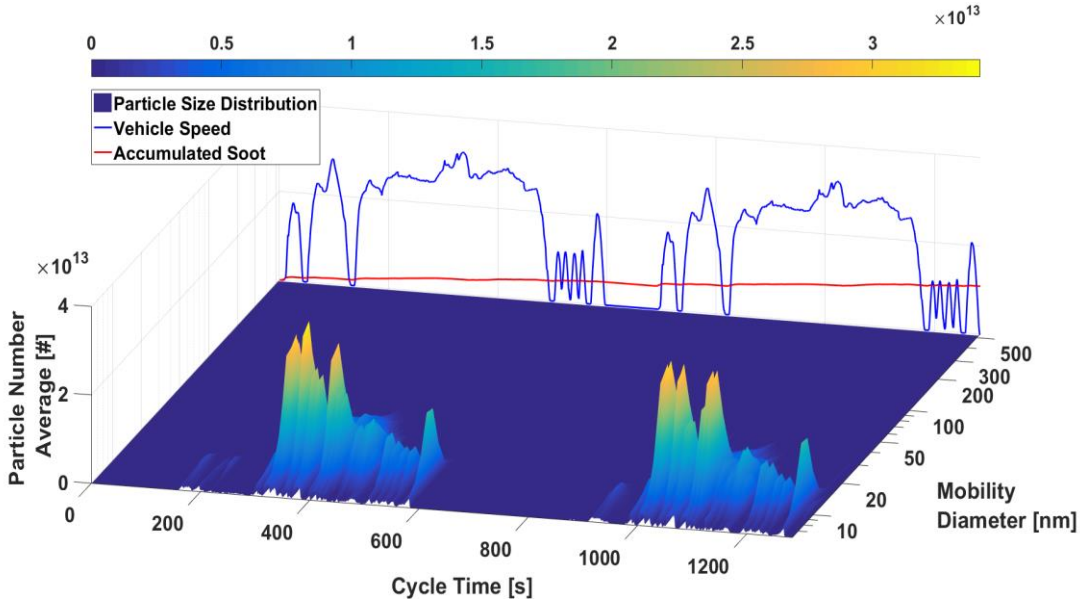

Figure S2-6 (a-b) Transient particle size distribution for the stock GDI_2 (a) the GPF-equipped GDI_2 (b) over the US06 cycle; The speed-time profile and the accumulated soot mass are also included for visual reference

2.8.5. **Supplementary References**

Amanatidis, S.; Ntziachristos, L.; Giechaskiel, B.; Katsaounis, D.; Samaras, Z.; Bergmann, A. Evaluation of an Oxidation Catalyst ("Catalytic Stripper") in Eliminating Volatile Material from Combustion Aerosol. Journal of Aerosol Science, 2013, 57, 144-155.

Schindler, W.; Haisch, C.; Beck, H.A.; Niessner, R.; Jacob, E.; Rothe, D. A Photoacoustic Sensor System for the Time Resolved Quantification of Diesel Soot Emission. SAE Technical Paper 2004, 2004-01-0969.

Xue, J.; Li, Y.; Wang, X. L.; Durbin, T. D.; Johnson, K. C.; Karavalakis, G.; Awuku, A.; Villeta, M.; Quiros, D.; Hu, S. H.; Huai, T.; Ayala, A.; Jung, H. J. Comparison of Vehicle Exhaust Particle Size Distributions Measured by SMPS and EEPS During Steady-state Conditions. Aerosol Sci. Technol. 2015, 49, 984-996.

Wang, X.L.; Grose, M.; Avenido, A.; Stolzenburg, M.R.; Caldow, R.; Osmondson, B.L.; Chow, J.C.; Watson, J. G. Improvement of Engine Exhaust Particle Sizer (EEPS) Size Distribution Measurement - I. Algorithm and Applications to Compact Aerosols. J. Aerosol Sci., 2016, 92, 95-108.

Xue, J.; Quiros, D.; Wang, X.; Durbin, T.D.; Johnson, K.C.; Karavalakis, G.; Hu, S.; Huai, T.; Ayala, A.; Jung, H.S. Using a new inversion matrix for a fast-sizing spectrometer and a photo-acoustic instrument to determine suspended particulate mass over a transient cycle for light-duty vehicles. Aerosol Sci. Technol., 2016, 50, 1227-1238.

3. Investigation of the effect of mid- and high-level ethanol blends on the particulate and the mobile source air toxic (MSAT) emissions from a GDI flex fuel vehicle

3.1. Abstract

This study examines the influence of low-, mid-, and high-ethanol fueling, as well as the influence of the aromatic hydrocarbons in the fuel blend, on the regulated and greenhouse gas emissions, the mobile source air toxic pollutants, and the particulate emissions from a current model flexible fuel vehicle equipped with a gasoline direct injection engine. This study utilizes four fuels in total, including a baseline US EPA Tier E10 fuel, one E10 fuel with higher aromatics content than the baseline E10, an E30 fuel that was splash-blended with the Tier 3 E10, and an E78 fuel. Testing was conducted over triplicate cold-start and hot-start LA92 cycles. The findings of this study showed that the higher ethanol blends, namely the E30 and E78, led to statistically significant total hydrocarbon (THC), non-methane hydrocarbon (NMHC), carbon monoxide (CO), and nitrogen oxides (NOx) emissions reductions compared to the high aromatics E10 fuel. The emissions of carbon dioxide (CO_2) were higher of the high aromatics E10 than the Tier 3 E10, E30, and E78 blends. A fuel economy penalty was also observed for lower energy content E30 and E78 blends compared to both E10 fuels. Particulate matter (PM) mass, black carbon, and total and solid particle number emissions showed statistically significant

reductions for the E30 and E78 fuels compared to both E10 fuels. Results also showed that the high PM Index/high aromatics E10 produced more particulate emissions than the low PM Index E10, as well as higher populations of accumulation (soot) mode particles. Acetaldehyde formation favored by the higher ethanol content in the fuel, whereas benzene, toluene, ethylbenzene, and xylenes emissions enhanced their formation with the high aromatics E10 and reduced with E30 and E78 fuels.

3.2. **Introduction**

The use of biofuels in the United States (US) and Europe have been promoted for the past several decades in an effort to reduce greenhouse gas (GHG) and other emissions from the transportation sector. Biomass-derived ethanol is the most popular biofuel in the US, where all gasoline sold contains up to 10% ethanol by volume (E10). Ethanol utilization is still on the rise in the US, with the US Environmental Protection Agency (EPA) allowing 15% of ethanol by volume (E15) to be sold in the market [EPA, 2011]. The favorable environment for growth of ethanol fuel use is also promoted by the Energy Independence and Security Act of 2007 (EISA) and the Renewable Fuel Standard mandates. In addition to lower concentrations of gasoline-ethanol blends, gasoline is allowed to contain between 51% and 83% ethanol by volume. Higher levels of ethanol can be used in flexible fuel vehicles (FFVs), which are designed for this purpose and are certified for emissions compliance by testing with E0 and E85.

Another pathway to reduce net GHG emissions from the transportation sector and meet the federal Corporate Average Fuel Economy (CAFE) standard is to improve the engine's thermal efficiency, which will reduce fuel consumption and carbon dioxide

(CO_2) emissions. Today, this technology can be achieved through the gasoline direct injection (GDI) platform that has increased in popularity in the US, and is expected to eventually dominate the market by replacing traditional port fuel injection (PFI) engines [Alkidas, 2007]. One of the major drawbacks of GDI technology is the exacerbated particulate matter (PM) emissions compared to PFI engines due to fuel impingement onto piston and cylinder walls. Direct injection involves the direct spray of fuel into the combustion chamber. Late evaporation of this fuel can lead to localized poor air-fuel mixing or diffusion-governed combustion that favors PM formation [Piock et al., 2011; Stevens and Steeper, 2011].

Overall, pollutant formation is a complex function of fuel type and fuel composition, as well as combustion chemistry and physics. For example, it is expected that different fuels will produce different levels of PM emissions [Khalek et al., 2010; Sobotowski et al., 2015; Leach et al., 2018]. The hydrocarbon composition, especially the content and distribution of aromatics, and the distillation characteristics strongly affects PM formation [Yao et al., 2017; Leach et al., 2013; Karavalakis et al., 2015]. Aikawa et al. [2010] developed an empirical method called the PM Index (PMI) that correlates PM emissions with the vapor pressure and the double bond equivalent (DBE) of the fuel components. Their results showed that aromatics with high boiling points and high DBE values increased PM mass and particle number emissions.

Understanding the impact of ethanol fueling on gaseous and particulate emissions from GDI engines is not straightforward. Ethanol has the potential to suppress soot formation in GDI engines and in flames [Fatouraie et al., 2015; Khosousi et al., 2015].

Lemaire et al. [2010] studied the effects of adding ethanol to gasoline on soot formation in turbulent spray flames and observed suppressed soot formation with ethanol, not only by dilution effect, but also by chemical (oxygen) effect. Karavalakis and co-workers [2014] showed reductions in PM mass, black carbon, and particle number emissions when they tested E10, E15, and E20 blends in GDI vehicles over the Federal Test Procedure (FTP) and LA92 cycles. Maricq et al. [2012] documented only small reductions in PM mass and particle number emissions as the ethanol level in gasoline increased from 0 to 20% in tests of a GDI turbocharged vehicle, however, much higher reductions in both PM mass and particle number emissions were measured for ethanol contents >30%. In addition to particulate emissions, previous studies have shown that an increase in ethanol content in the fuel blends reduces the emissions of nitrogen oxides (NOx), carbon monoxide (CO), non-methane hydrocarbons (NMHC), and total hydrocarbon (THC) [Hubbard et al., 2014; Dardiotis et al., 2015]. Other studies have shown that higher ethanol concentrations can lead to elevated formaldehyde and acetaldehyde emissions, which are potentially carcinogenic compounds to humans [Clairotte et al., 2013; Karavalakis et al., 2014]. Suarez-Bertoa et al. [2015] tested a flex fuel vehicle with direct injection on E5, E10, E15, E75, and E85 blends over the New European Drive Cycle and the Worldwide harmonized Light-duty driving Test Cycle (WLTC) and found sharp increases in CO, methane (CH4), formaldehyde, acetaldehyde, and ethanol emissions. Karavalakis et al [2014] reported statistically significant reductions in CO, NMHC, and acetaldehyde emissions for E51 and E83 when they tested one FFV with a direct injection engine and one FFV with a PFI engine over the FTP and

LA92 cycles. The authors found lower benzene, toluene, ethylbenzene, xylene (BTEX) emissions with higher ethanol.

The objective of this study is to investigate different ethanol concentrations, as well as the influence of higher gasoline aromatics content on the regulated emissions, PM mass, black carbon, and particle number emissions, and the mobile source air toxic pollutants. Testing was performed on a GDI flex fuel vehicle over cold-start and hot-start LA92 test cycles on a chassis dynamometer. The results of this work are discussed in the context of the impacts of ethanol concentration, aromatics content, and driving operation.

3.3. **Experimental**

3.3.1. **Test Fuels and Vehicles**

A total of four fuels were employed in this study, including an E10 blend with a of total aromatics content of 28.1 vol %, which served as the baseline fuel. While the baseline E10, hereinafter denoted as E10, was manufactured to be representative of US EPA Tier 3 E10 test fuel, its total aromatics content was slightly higher than the EPA specification. For comparison purposes, this study also utilized an E10 fuel with a higher 36.7 vol % fraction of aromatics (hereinafter denoted as E10HA). Two higher ethanol blends, namely E30 and E78, were also used to investigate the effects of higher ethanol fueling in tailpipe emissions. The E30 fuel was a splash-blend of the E10 fuel with an additional 20% ethanol. The E78 fuel was blended following the US EPA Tier 3 and the California Air Recourses Board (CARB) certification requirements for E85 fuels. The blending level was selected in order to meet the ASTM D5798 Reid vapor pressure (RVP) requirement. The main properties of the test fuels are given in Table 3-1.

Table 3-1 Main physicochemical properties of the test fuels

Property	Test Method	E10	E10HA	E30	E78
Research Octane Number	ASTM D2699	92.1	93.5	100.5	
Motor Octane Number	ASTM D2700	84	83.9	87.5	
Octane Rating		88.1	88.7	94	
Sulfur Content (wt. %)	ASTM D5453	8	7.2	6	3
Total Aromatics (vol %)	ASTM D5769	28.1	36.7	22	5.5
C6 Aromatics (Benzene) (vol %)	ASTM D5769	0.599	0.565	0.457	0.2
C7 Aromatics (Toluene) (vol %)	ASTM D5769	7.583	9.143	5.897	1.4
C8 Aromatics (vol %)	ASTM D5769	6.548	7.266	5.109	1.2
C9 Aromatics (vol %)	ASTM D5769	6.124	10.229	4.808	1.8
C10+ Aromatics (vol %)	ASTM D5769	5.56	7.023	4.395	0.8
Olefins Content	ASTM D6550	8.498	10.634	6.45	1.5
Hydrogen Content (wt. %)	ASTM D5291	13.59	13.21	13.33	13.07
Carbon Content (wt. %)	ASTM D5291	82.77	83.19	75.28	59.41
Oxygen Content (wt. %)	ASTM D4815	3.63	3.59	11.39	27.52
C/H Ratio		6.09	6.297	5.647	4.545
Net Heat of Combustion (MJ/Kg)	ASTM D240	41.94	41.65	38.17	30.30
Density at 15.56 °C (g/cc)	ASTM D4052	0.7494	0.7544	0.7597	0.7830
RVP at 100 F (psi)	ASTM D5191	8.89	9.39	8.20	5.05
Distillation (°C)	ASTM D86				
IBP		35	34.5	36.5	49.9
10%		51.7	53.5	57	71.1
50%		94	96.3	74.5	77.4
70%		129.1	130	78.8	77.9
90%		163.5	165.9	158.1	78.6
95%		179.1	181.8	175.7	79.4
FBP		203.5	209.1	198.8	168.2
Ethanol Content (vol%)	ASTM D4815	9.86	9.85	31.44	78.27

Testing was conducted on a 2016 model year FFV passenger car with a 2.0L I-4 spark ignition, direct injection, wall-guided engine. The engine had a rated horsepower of 160 hp at 6500 rpm, a torque of 198 Nm at 4450 rpm, and a compression ratio of 12.0 to 1. The vehicle was equipped with a three-way catalyst (TWC), was flexible-fuel capable, and was certified under Federal Tier 2 Bin 5 emission standards. It had accumulated 22,854 miles at the beginning of the test campaign.

3.3.2. **Driving Cycle and Measurement Protocol**

The GDI FFV was exercised over triplicate cold-start and hot-start LA92 test cycles. The LA92 test cycle or the California Unified Cycle (UC) is a dynamometer driving schedule for light-duty vehicles developed by the California Air Resources Board (CARB). The LA92 consists of three phases (i.e., cold-start, urban, and hot-start phases) and has a three-bag structure similar to the FTP cycle. The LA92 is characterized by higher speeds, higher accelerations, fewer stops per miles, and less idle time than the FTP.

The 6 tests on a particular fuel were conducted sequentially once the vehicle was changed to operate on that fuel, and the fuel was not changed to another fuel during this time. The preconditioning procedure was similar to that specified in the Code of Federal Regulations (40 CFR 86.132-00). For each fuel change there were multiple drain and fills and 2 LA4s along with idle periods between the testing on each fuel to condition the vehicle and ensure no carryover effects.

3.3.3. **Emissions Testing**

All tests were conducted in CE-CERT's Vehicle Emissions Research Laboratory (VERL), on a Burke E. Porter 48-inch single-roll electric dynamometer. A Pierburg Positive Displacement Pump-Constant Volume Sampling (PDP-CVS) system was used to obtain standard bag measurements for THC, CO, NOx, NMHC, and CO_2. Bag measurements were made with a Pierburg AMA-4000 bench. PM mass, volatile and solid particle number, particle size distributions, and black carbon emissions were also measured. Detailed information on the methods used to collect and analyze these emissions is provided in the Supporting Information (SI).

Samples for carbonyl analysis were collected onto 2,4-dinitrophenylhydrazine (DNPH) coated silica cartridges (Waters Corp., Milford, MA). A Sierra mass flow controller (MFC) controlled the flow to 1.0 L/min through the cartridge. Analysis of DNPH cartridges for 14 C1-C8 carbonyl compounds was performed at the Organic Analytical Laboratory of the Desert Research Institute and is described elsewhere [Khlystov et al., 2016]. Briefly, DNPH cartridges were eluted with 2 mL of acetonitrile (HPLC grade, EMD Millipore Corporation, Billerica, MA, USA) and analyzed with an HPLC system (Waters 2690 Alliance System with 996 Photodiode Array Detector) following a modified US-EPA TO-11A method (U.S.EPA, 1999). The HPLC response was calibrated with certified calibration mixture purchased from AccuStandard Inc. (New Haven, CT 06513, USA).

Hydrocarbon species were collected using a 6 L specially-prepared SUMMA passivated canister, which was connected to the CVS system. Analysis of the hydrocarbon species was conducted using a Gas Chromatography/Mass Spectrometry/Flame Ionization Detector (GC/MS/FID) analytical system with the standard PAMS Protocol Compendium Method TO-15.

3.4. **Results and Discussion**

3.4.1. **Regulated Emissions**

Figure 3-1 shows the cold-start and hot-start regulated emissions over the LA92 test cycle on the different test fuels. For the cold-start emissions, THC and NMHC followed the same patterns, with E30 and E78 blends being lower than E10 and E10HA. The higher ethanol blends did not show any statistically significant differences in THC and NMHC emissions compared to the baseline E10, whereas both E30 and E78 showed statistically

significant differences compared to E10HA. The hot-start THC and NMHC emissions followed the same trends as found for the cold-start LA92, but at lower concentrations.

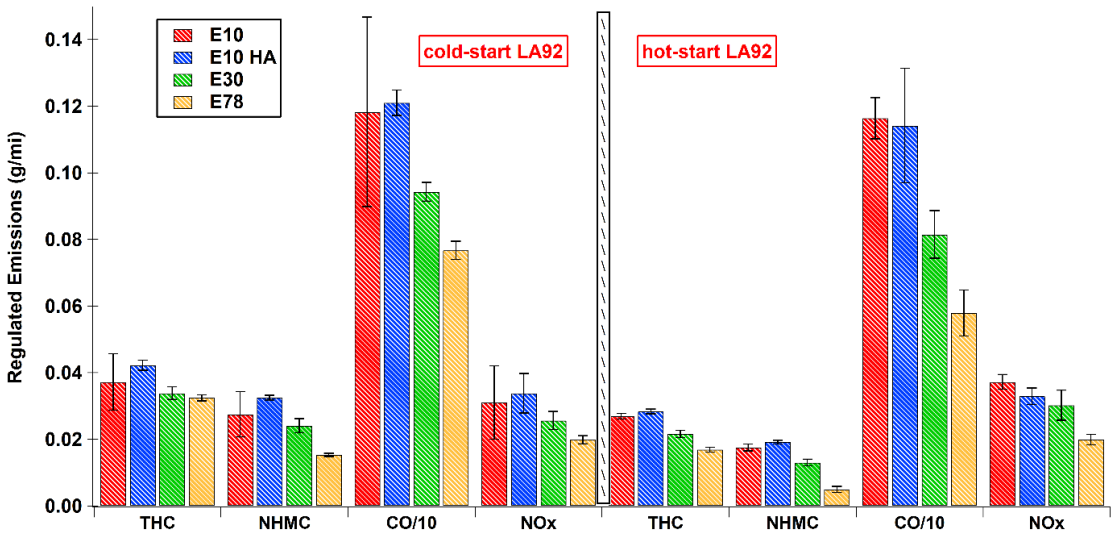

Figure 3-1 Regulated emissions for all test fuels over the cold-start and hot-start LA92 cycles. Data presented as mean ± standard deviation, N=3.

The lower hot-start THC and NMHC emissions for E30 and E78 blends were statistically significant different compared to both E10 and E10HA, whereas E10HA showed marginally statistically significant higher hot-start THC and NMHC emissions than E10. The lower THC and NMHC emissions with higher ethanol blends were primarily due to the higher oxygen content in the ethanol, which increased the local oxygen in the fuel-rich regions leading to more complete combustion [Liu et al., 2011; Catapano et al., 2014]. Ethanol also has a lower molecular weight compared to gasoline, so ethanol requires less time for complete atomization and vaporization, resulting in a more homogeneous air-fuel mixture [Catapano et al., 2016]. Consistent with previous studies, our results showed trends of higher THC and NMHC emissions for the higher aromatics E10 fuel [Karavalakis et al., 2015; USEPA, 2013; Goodfellow et al., 1996]. Overall, aromatic hydrocarbons are

more difficult to oxidize and vaporize than simpler molecules, such as alkanes or ethanol, resulting in more fuel wetting in the cylinder walls and thus higher THC emissions.

Cold-start and hot-start LA92 CO emissions did not show any differences between the two E10 fuels. For the cold-start LA92, the E10HA showed statistically significant higher CO emissions than E30 and E78, while the E10 fuel showed statistically significant higher CO emissions than E78. For the hot-start LA92, CO emissions for both E10 fuels showed statistically significant increases compared to E30 and E78 blends. The reduction in CO emissions with the higher ethanol blends may be attributed to the fact that ethanol has less carbon than gasoline, as well as to the higher oxygen content in the fuel blend, which improves the oxidation of CO in the fuel-rich regions of the combustion chamber, ensuring more efficient combustion [Najafi et al., 2009].

For both cold-start and hot-start LA92 cycles, NOx emissions decreased with an increase in ethanol content. For the cold-start LA92, the E10HA showed higher NOx emissions at a statistically significant level compared to E30 and E78. Although no differences in NOx emissions were seen between the E10 fuels for the cold-start LA92, a marginally statistically significant increase of 12% for E10 compared to E10HA was observed over the hot-start LA92. For the hot-start LA92, both E10 fuels were higher at a statistically significant level than E78. Previous studies have also shown NOx reductions with higher ethanol blends [Clairotte et al., 2013; Yassine and La Pan, 2012], but higher NOx with increasing aromatics [Han et al., 2018]. The lower NOx emissions for the higher ethanol fuels could be due to the lower adiabatic temperature for oxygenated fuels. In addition, higher ethanol blends have a higher latent heat of vaporization and lower heating

value, which can lead to a reduction in the local temperature of the air-fuel mixture at the end of the injection compared to lower ethanol blends, affecting the formation of thermal NOx [Iodice et al., 2018; Turner et al., 2011].

The CO_2 emissions followed similar patterns for both the cold-start and hot-start LA92 cycles, showing an inverse relationship to CO emission levels, as shown in Figure 3-2. The E10HA fuel showed higher CO_2 emissions at a statistically significant level compared to E10, E30, and E78. Compared to E10HA, E10, E30, and E78 showed CO_2 reductions of 9%, 10%, and 6%, respectively. The higher CO_2 emissions for the E78 fuel relative to E30 was due to the higher oxygen content in the E78 blend, which improved the combustion. As expected, the influence of higher aromatics content for E10HA led to more CO_2 emissions than E10 because of the higher carbon/hydrogen ratio for this fuel. This finding is in agreement with previous studies [Karavalakis et al., 2015; Goodfellow et al., 1996].

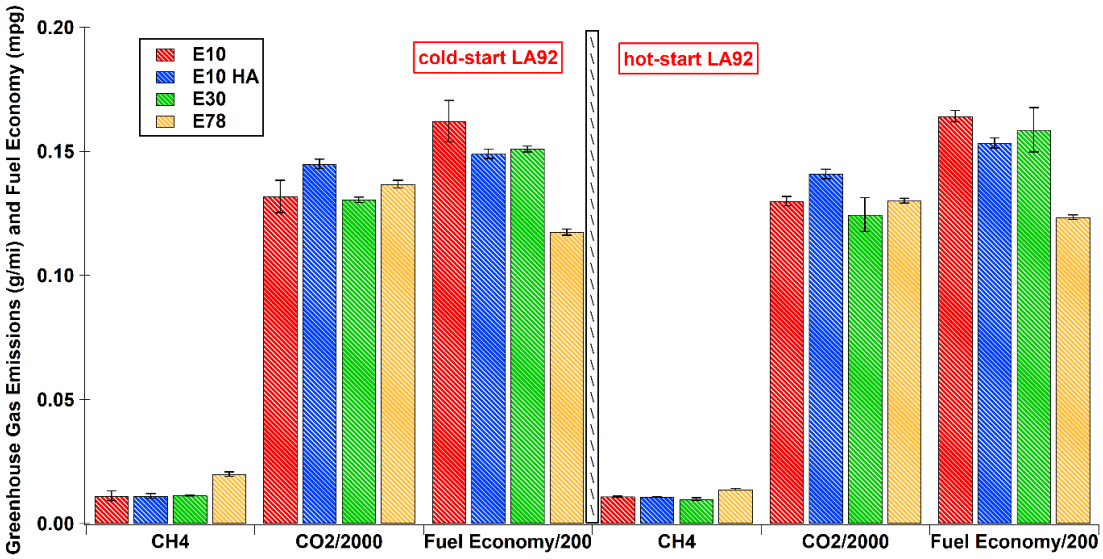

Figure 3-2 Greenhouse gas emissions of CO_2 and CH_4, and carbon balanced fuel economy over the cold-start and hot-start LA92 cycles. Data presented as mean ± standard deviation, N=3.

Emissions of CH_4 did not show any differences between the fuels for either the cold-start LA92 or the hot-start LA92, with the exception of the E78 fuel (Figure 3-2). Tailpipe CH4 emissions for the E78 showed statistically significant increases than all the other test fuels for both test cycles. More CH4 emissions for high ethanol blends have been observed in previous studies with FFVs [Hubbard et al., 2014; Clairotte et al., 2013]. CH4 emissions are particularly difficult to oxidize in the TWC and are primarily formed during the cold-start when the catalyst is below its light-off temperature [Poulopoulos et al., 2001]. CH4 is also formed from the decomposition of acetaldehyde over rhodium (Rh)-doped TWCs [Idriss, 2004].

Fuel economy was calculated based on the carbon balance method and the unique properties for each different test fuel. The results reported here showed statistically

significant reductions in fuel economy with E30 and E78 blends compared to the E10 blend (Figure 3-2). The reductions in fuel economy were 8% for E30, 15% for E78, and 8% for E10HA over the cold-start LA92. Similar reductions in fuel economy for the high ethanol blends and the E10HA fuel were seen over the hot-start LA92, ranged from 4% to 12%. The lower fuel economy for the E30 and E78 blends was attributed to the lower energy content per gallon for these fuels compared to the E10 fuels.

3.4.2. PM Mass, Particle Number, and Particle Size Distribution

Figure 3-3 shows the PM mass and black carbon emissions over the cold-start and hot-start LA92 cycles.

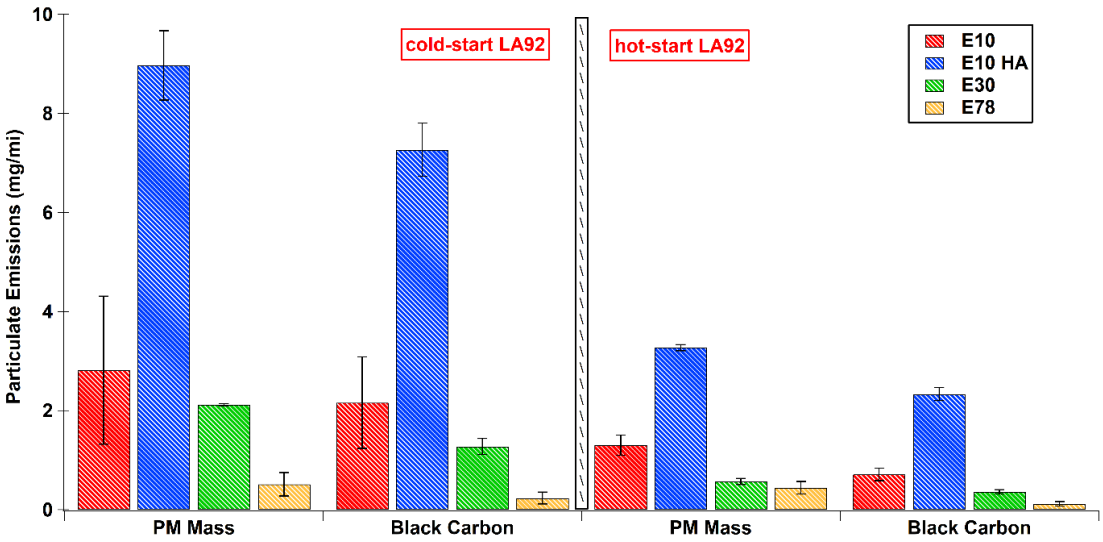

Figure 3-3 PM mass and black carbon emissions. Data presented as mean ± standard deviation, N=3.

Our results are in line with previous studies, showing that PM mass and black carbon emissions were higher over cold-start conditions due to the fact that a high fraction of these pollutants is emitted during the early phases of the cycle when the engine is cold

and fuel injection results to inhomogeneous mixing between air and fuel into the combustion cylinder [Khalek et al., 2010, Zhang and McMahon, 2012]. For both the cold-start and hot-start LA92 cycles, the use of higher ethanol led to large decreases in PM mass emissions compared to the E10 fuels, with E78 showing the lowest PM mass concentrations at 0.51 mg/mile. For the cold-start LA92, the higher PMI E10HA fuel (PMI=2.517) produced higher PM mass than the other fuels and a statistically significant increase of 218% relative to the lower PMI E10 (PMI=1.945). The E30 (PMI=1.528) and E78 (PMI not available) blends showed statistically significant reductions in PM mass of 76% and 94%, respectively, compared to E10HA. For the hot-start LA92, both the high and low PMI E10 fuels showed statistically significant increases in PM mass emissions than the E30 and E78 fuels. The high PMI E10 exhibited 151% higher PM mass than the low PMI E10 at a statistically significant level.

Analogous to the PM mass, black carbon emissions showed large reductions with E30 and E78 blends compared to both E10 fuels. For the cold-start LA92, black carbon emissions showed statistically significant reductions of 82% and 92% for E30 and E78, respectively, compared to the high PMI E10HA fuel. The difference between the high PMI E10HA and the low PMI E10 in black carbon emissions was 70% at a statistically significant level. Similar statically significant reductions in black emissions were also seen for the hot-start LA92 for the high ethanol blends compared to the E10 fuels, and for E10HA compared to the E10.

Total and solid particle number emissions are shown in Figure 3-4 (a-b). For the cold-start LA92, the reductions in total particle and solid number emissions ranged from

A

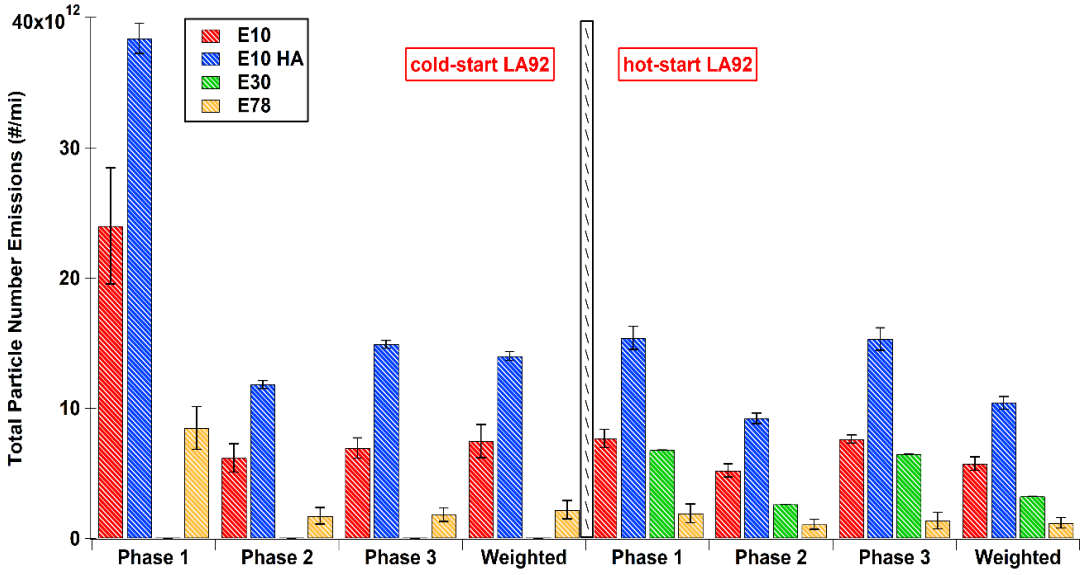

B

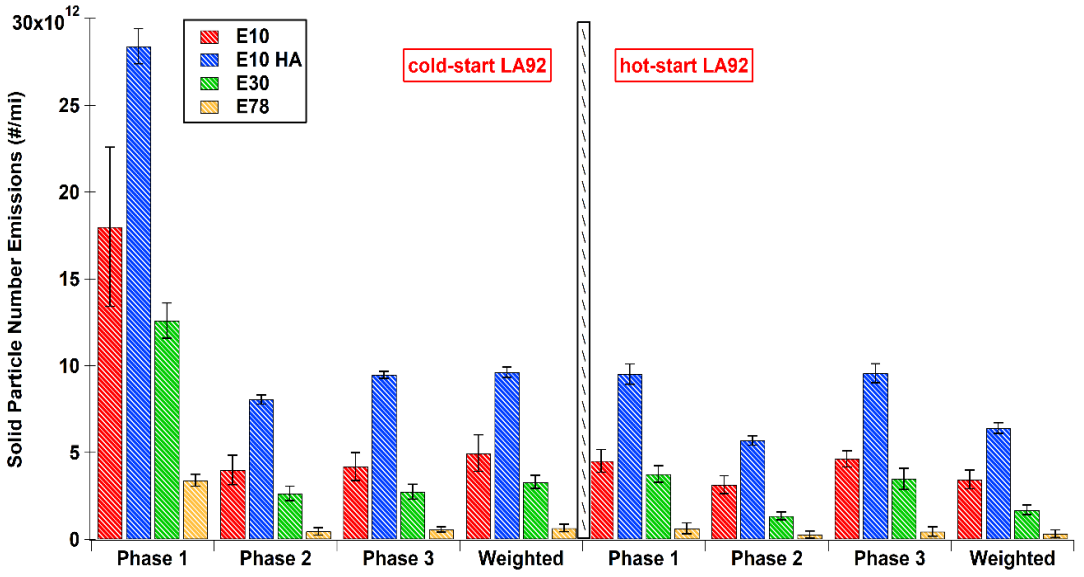

Figure 3-4 (a-b) Total (a) and solid particle (b) number emissions over both the weighted cold-start and hot-start LA92s and their individual phases

47%-84% and from 45-89%, respectively, while for the hot-start LA92 the reductions ranged from 49%-93% and from 46%-95%, respectively. The cold-start phase (bag 1) of the LA92 dominated the formation of both total and solid particle number emissions. During the cold-start phase of the LA92, the cold engine with its cold walls and components make fuel evaporation much more difficult. Because the TWC is below its light-off temperature, more fuel is introduced in the cold combustion chamber to heat up the catalyst resulting in mixture inhomogeneity and diffusive combustion from fuel pools [Piock et al., 2011]. For the hot-running (bag 2) and hot-start (bag 3) phases, total and solid particle number emissions were found in lower concentrations than in bag 1. Higher fuel temperatures and piston surface temperatures promote better fuel vaporization and a more homogeneous air-fuel mixture [He et al., 2010].

Particulate emissions from the GDI FFV were lowest when operating with the higher ethanol blends. Our results are in agreement with the majority of the published literature showing a positive effect of ethanol on particulate emissions from GDI engines [Karavalakis et al., 2014; Maricq et al., 2012; Wang et al., 2014; Jin et al., 2017]. The reductions in particulate emissions with E30 and E78 fuels were likely due to dilution effects, resulting from aromatic content reduction in the fuel, as opposed to the increased oxygen content of ethanol that enhanced soot oxidation. Aromatics and polyaromatics have a higher sooting tendency than non-aromatic hydrocarbons [Ladommatos et al., 1996]. Diluting the aromatics in the fuel stream for the higher ethanol blends will lower the soot precursor formation and reduce the soot surface growth through the HACA (hydrogen abstraction acetylene addition) mechanism [Khosousi et al., 2015, Wu et al., 2006].

As previously discussed, aromatics content and fuel volatility had a strong influence on particulate emissions for the two E10 fuels. The high PMI E10HA fuel had a higher content of total aromatics than the lower PMI E10, and contained higher concentrations of compounds with high boiling points and DBE values. The higher the boiling point and DBE of the aromatic species in the fuel, the more particulate emissions increase. Due to the higher boiling points of aromatic hydrocarbons, they are more difficult to vaporize during combustion compared to other hydrocarbons (alkanes and olefins) or oxygenates (i.e., ethanol) because aromatics burn at higher adiabatic flame temperatures. In addition, the distillation temperatures of T90 and T95 are higher for the E10HA fuel relative to E10, indicating that this fuel contains more of heavier hydrocarbon fractions that are more difficult to evaporate. This will likely result to poor air-fuel mixture and diffusion combustion (pool fire) of liquid fuel, leading to higher soot emissions. Previous studies have also shown increased particulate emissions with higher aromatic content gasoline fuels [Khalek et al., 2010; Yao et al., 2017; Leach et al., 2013; Karavalakis et al., 2015; Chan et al., 2017; Zhu et al., 2017].

Figure 3-5 and Figure 3-6 illustrate the particle size distribution characteristics for all test fuels over the cold-start and hot-start LA92s, respectively. For most fuels, the particle size distributions showed bimodal profiles, consisting of a nucleation mode (10-23 nm) and an accumulation mode (23-100 nm). For all test fuels and both cycles, the nucleation mode was centered at around 15 nm, whereas the accumulation mode was centered at 70-80 nm. The cold-start LA92 produced much higher particle populations in the accumulation mode, but not in the nucleation mode.

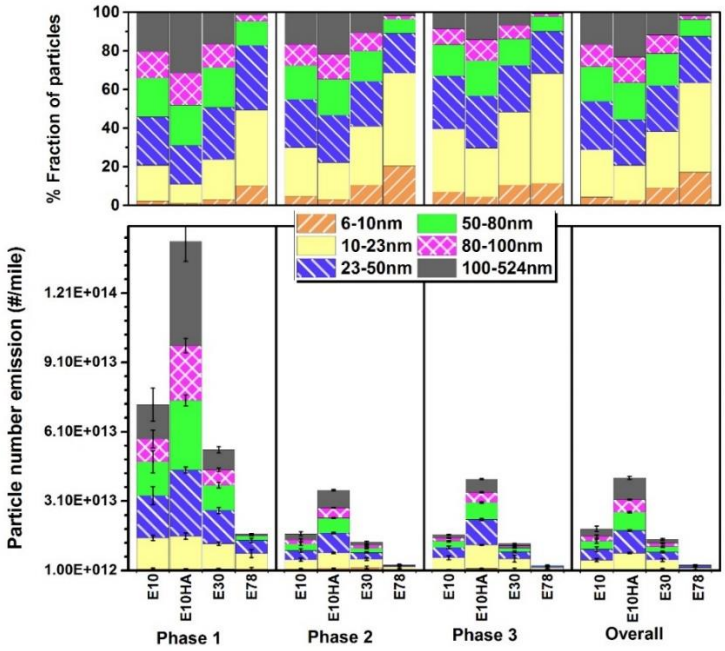

Figure 3-5 Particle size distribution profile for the test fuels over the entire cold-start LA92 cycle and its individual phases

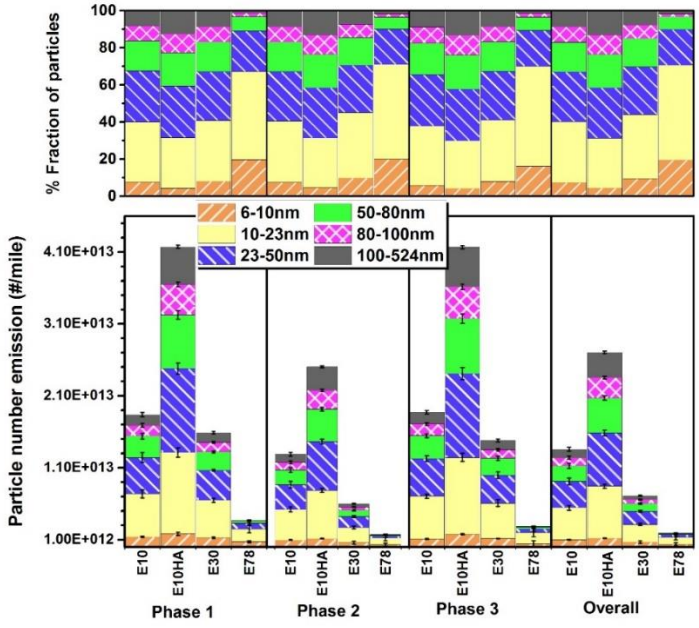

Figure 3-6 Particle size distribution profile for the test fuels over the entire hot-start LA92 cycle and its individual phases

This suggests that fuel-rich combustion during cold-start conditions contributes to the formation and growth of soot particles in the accumulation mode [He et al., 2010, Badshah et al., 2016]. For both LA92 cycles, the E30 and E78 fuels showed reductions of accumulation mode particles compared to E10, with these reductions for the cold-start LA92 being 29.7% and 88.6% for E30 and for the hot-start LA92 at 50.5% and 92.3% for E78, respectively. The high PMI E10HA fuel showed increases in the accumulation mode particles compared to E10 on the order of 123.2% and 116.8%, respectively, for the cold-start and hot-start LA92s. The use of E30 and E78 produced reductions in nucleation mode particles with respect to E10 of 9.3% and 66.1% for the cold-start LA92 and at 44.7% and 78% for the hot-start LA92, respectively. For the E78 fuel, the soot mode was practically eliminated, with the nucleation mode particles dominating the particle size distribution profile at 46% over the cold-start LA92 and at 51% over the hot-start LA92. Our findings are consistent with previous studies showing that with increasing alcohol content, peak particle number concentrations and particle size are decreased [Catapano et al., 2016, Wang et al., 2014, Szybist et al., 2011]. It is worth noting that the particle size distribution profile for the hot-running and hot-start segments for both the cold-start and hot-start LA92 cycles were very similar, with the main differences in particle sizing observed for the cold-start segment or bag 1 for both cycles.

The increased oxygen content, which suppresses soot formation, and more importantly, the dilution of aromatics in the fuel lower the rates of soot precursor formation and thus the accumulation mode particles [Salamanca et al., 2012]. It is theorized that ethanol slows down the coagulation process leading to soot by reducing the formation of

polycyclic aromatic hydrocarbons, which are precursors to soot particles. It is important to note that for both driving cycles the E30 and E78 fuels exhibited higher concentrations of nucleation mode particles and a lower formation of soot particles, suggesting the high ethanol blends primarily contributed to nucleation mode particles via the available soot surface area on which hydrocarbons adsorb or condense, favoring nucleation. The sooting tendency of E10HA was considerably higher than that for the low PMI E10 fuel, which can be ascribed to the higher aromatics content of this fuel. The particle size distributions of E10HA were dominated by the accumulation soot mode over both cycles, ranged at 56.2% for the cold-start LA92 and 55.7% for the hot-start LA92. These findings are in agreement with the higher PM mass and black carbon emissions for the higher PMI E10HA fuel relative to the lower PMI E10.

3.4.3. **Aldehyde Emissions**

Figure 3-7 shows the aldehyde emissions for both the cold-start and hot-start LA92 cycles. Formaldehyde and acetaldehyde were the most dominant aldehydes in the exhaust followed by m-tolualdehyde. Previous studies have also shown that formaldehyde and acetaldehyde emissions are the principal aldehydes from ethanol exhaust [Clairotte et al., 2013; Karavalakis et al., 2014; Suarez-Bertoa et al., 2015, Costagliola et al., 2013]. The concentrations of aldehyde emissions were found to be significantly higher over the cold-start LA92 compared to the hot-start LA92 cycle. This result was as expected, since aldehydes emissions are primarily formed during initial part of the cycles (bag 1) when the TWC is below its light-off temperature. The impact of ethanol was particularly strong in acetaldehyde emissions, with E30 and E78 showing higher acetaldehyde emissions at a

statistically significant level compared to both E10 fuels. For the cold-start LA92, the increases in acetaldehyde emissions for E30 and E78 were 206% and 595% compared to E10HA and 139% and 443% compared to E10. For the hot-start LA92, acetaldehyde emissions increased by 222% for E30 and 335% for E78 relative to E10HA, and by 92% for E30 and 158% for E78 relative to E10. Acetaldehyde emissions did not show any statistically significant effects between the two E10 fuels. These observations are in agreement with other studies and a building consensus that acetaldehyde is produced from the partial oxidation of ethanol [Karavalakis et al., 2014, Jin et al., 2017; Zervas et al., 2002]. Ethanol combustion will result to hydrogen abstraction, which will form radicals that react with either oxygen or unimolecularly decompose yielding acetaldehyde [Haas et al., 2009].

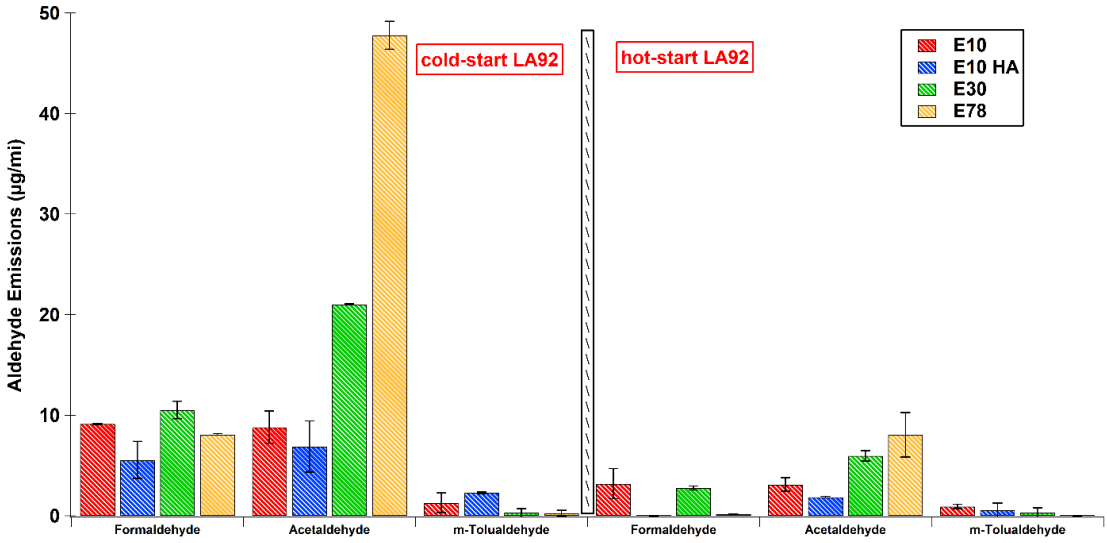

Figure 3-7 Aldehyde emissions over the cold-start and hot-start LA92 cycles

Formaldehyde emissions showed statistically significant effects for some fuels, but not for others. For the cold-start LA92, E30 showed a marginally statistically significant

increase in formaldehyde emissions of 47% compared to E10HA, whereas E78 showed a statistically significant reduction in formaldehyde emissions of 12% compared to E10. The E10HA trended lower for formaldehyde emissions than E10, but these differences were not statistically significant. A reduction in aromatics could lead to lower formaldehyde and acetaldehyde emissions because these compounds do not participate in their formation pathways [Zervas et al., 2002, Petit and Montagne, 1993]. Formaldehyde could be formed from the breakdown of the C-C bond in the initial step of ethanol combustion. Both increases [Clairotte et al., 2013; Jin et al., 2017] and decreases [Storey et al., 2014] in formaldehyde emissions with higher ethanol blends have been reported in previous studies. Emissions of the aromatic m-tolualdehyde also showed strong and statistically significant reductions for E30 (87%) and E78 (90%) compared to E10HA, but not compared to E10. The addition of oxygen and the lower content of aromatics in the fuel, such as m/p-xylenes, yielded lower m-tolualdehyde emissions.

3.4.4. **Monoaromatic and VOC Emissions**

The monoaromatic hydrocarbons of benzene, toluene, ethylbenzene, m/p-xylenes, and o-xylene (collectively known as BTEX), as well as 1,3-butadiene are shown in Figure 3-8. Other volatile organic compounds (VOCs) measured over both driving cycles are shown in Table S3-1 in SI. For the cold-start LA92, the use of E30 and E78 fuels resulted in large and statistically significant reductions in BTEX emissions compared to the high PMI E10HA, but not always compared to the low PMI E10 fuel. In most cases, BTEX levels for E30 were similar to E10, indicating that neither ethanol nor aromatics played a dominant role in their formation during the cold-start LA92. The E78 blend showed the

lowest BTEX emissions compared to both E10 fuels over both driving cycles. Compared to E10HA, the statistically significant reductions in BTEX emissions for E30 ranged from 40%-49% and for E78 ranged from 67%-84%. The lower BTEX emissions for E30 and E78 blends were largely due to the lower aromatics content in these fuels, as opposed to the fuel-bound oxygen assisting the hydrocarbon oxidation process. The E10HA trended higher for BTEX emissions compared to E10, but not at a statistically significant level. Previous studies have also shown lower BTEX emissions with ethanol fuels in gasoline engines [Jin et al., 2017, Costagliola et al., 2013]. For 1,3-butadiene emissions, the only statistically significant reduction was seen for E78 (72%) relative to E10HA. Generally, 1,3-butadiene is produced by the partial combustion of olefins in the fuel and it has been reported that it decreases its concentrations with oxygenates [Poulopoulos et al., 2001]. The E10HA fuel had the highest total olefins levels and E78 the lowest among the test fuels. It has also been reported that cyclohexane (higher concentration in E10HA than E78) is a major compound that participates in the formation of 1,3-butadiene [Petit and Montagne, 1993].

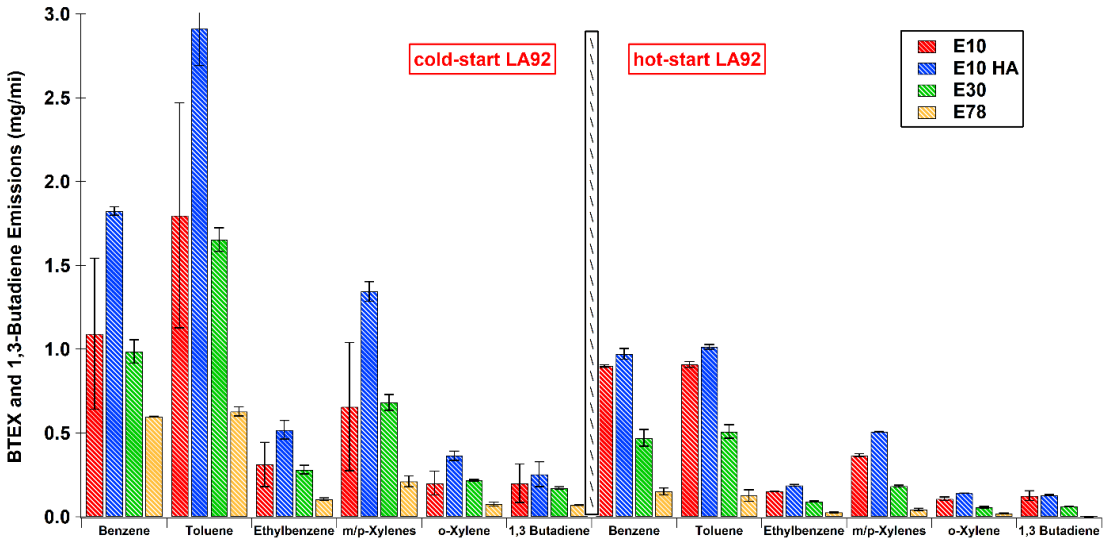

Figure 3-8 BTEX (benzene, toluene, ethylbenzene, and xylenes) and 1,3-butadiene emissions over the cold-start and hot-start LA92 cycles

BTEX and 1,3-butadiene emissions were found in lower concentrations over the hot-start LA92. The warm engine and catalyst better facilitate the oxidation of these species. Emissions of 1,3-butadiene for E78 were below the detection limit of the method, while the 1,3-butadiene emissions for E30 were statistically significant lower than both E10 fuels. It should be noted that the impacts of fuel aromatics and oxygen content were stronger during the hot-start LA92 than the cold-start conditions. During the cold-start LA92, fuel volatility contributed to the formation of monoaromatic emissions, especially for the fuels with higher T90 and T95 distillation temperatures. It is possible that partially unburned heavier fuel fractions escaped the cold catalyst forming BTEX emissions. In addition, the cold-start period of the cycle appeared to negatively influence the variability of some pollutants, an effect that is not obvious for the hot-start LA92. For the hot-start LA92, BTEX emissions for the E30 and E78 blends showed statistically significant reductions compared to both E10 fuels. For all BTEX species, the high PMI E10HA was

statistically significant higher compared to the low PMI E10. The benzene, toluene, ethylbenzene, and xylenes contents were lower for the high compared to low aromatic fuels, indicating that these emissions were closely related to the content of aromatics in the fuel. The benzene levels for the two E10 fuels, however, were about the same, suggesting that benzene is formed by the dealkylation of toluene and xylenes during combustion (methyl group for toluene and xylene, and ethyl group for ethylbenzene) [Zhang et al., 2008]. Cyclohexane is also a precursor for benzene formation [Zervas et al., 2004], and the use of ethanol has been shown to decrease benzene formation [Poulopoulos et al., 2001, Jin et al., 2017].

Ethylene and acetylene are important hydrocarbon precursors due to their ability to form soot via the HACA mechanism [Sanchez et al., 2012]. Both ethylene and acetylene were higher for E10HA and E78 fuels. Both pollutants can be produced during combustion from C2 radicals formed through H-abstractions and β-scissions, and from fuel aromatics. While ethanol usually decreases the formation of these pollutants, more ethylene and acetylene emissions were seen for E78 fuel. This finding is not in agreement with the very low PM mass and black carbon emissions for the E78 fuel compared to the other fuels. Ethane emissions trended higher for E10HA and E78. Ethane formation is enhanced by cyclohexane, but it also appears that ethanol is oxidized to ethane. Propylene emissions decreased with E30 and E78, with E10HA showing the highest propylene concentrations. The compounds n-pentane and 2,2,4-trimethylpentane (isooctane) were found in relatively high concentrations for all test fuels, and their emission levels were primarily dependent on the concentrations in the fuel. Isopentane and 1-butene were found in high

concentrations for the E10 fuels and the E30 blends, but in low levels for E78. The formation of isopentane and 1-butene were mainly enhanced by isooctane, where both E10 fuels and the E30 had higher levels than E78 [Zervas et al., 2004]. The compounds 1-hexene and n-hexane were also detected in higher levels for the two E10 fuels and the E30 compared to E78. Both species are exclusively enhanced from unburned fuel components [Zervas et al., 1999]. Several monoaromatic species, such as m-ethyltoluene, p-ethyltoluene, o-ethyltoluene, 1,3,5-trimethylbenzene, and 1,2,4-trimethylbenzene were detected in lower concentrations than the BTEX species. The use of E78 decreased their emissions, with the higher PMI E10HA fuel showing higher concentrations of these pollutants.

3.5. **Conclusions**

This study evaluated the gaseous and particulate emissions from a FFV equipped with a wall-guided direct injection gasoline engine. Testing was conducted over cold-start and hot-start LA92 cycles when the vehicle was operated on two E10 fuels with different levels of aromatic hydrocarbons, an E30, and an E78 blend. Our results showed that the use of higher ethanol blends resulted in lower THC, NMHC, CO, and NOx emissions from a current technology GDI FFV. The higher aromatics E10 fuel showed higher THC and NMHC emissions than the lower aromatic E10 fuel, suggesting the formation of these pollutants was more sensitive to fuel aromatics than CO and NOx emissions. The GHG emissions of CO_2 and CH4 showed some increases with the E78 blend compared to the other fuels. This could potentially be a concern for high concentration ethanol blends considering the global warming potential for both the CO_2 and CH4 gases. As expected,

the vehicle experienced a fuel economy penalty with the higher ethanol blends due to their lower energy content per gallon compared to the E10 fuels.

The results reported in this study also demonstrated strong PM mass, black carbon, total, and solid particle number emissions reductions with the higher ethanol blends and the lower PMI E10 fuel compared to the high PMI E10HA. The higher PMI fuel led to increased populations of accumulation mode particles, with the E78 blend having an almost unimodal particle distribution dominated by nucleation mode particles. Ethanol fuels showed a clear increase in acetaldehyde emissions, but mixed results for formaldehyde emissions. The fuel effect on BTEX and 1,3-butadiene emissions was particularly strong, with aromatics being the main driver for their formation. Fuels with lower aromatics and higher ethanol contents showed lower BTEX and 1,3-butadiene emissions. Overall, this study provides valuable insights on the impacts of ethanol content and gasoline composition on the exhaust emissions from a current technology GDI FFV.

3.6. **Acknowledgements**

We acknowledge funding from the South Coast Air Quality Management District (SCAQMD) under contract 15625 and ICM Inc. under contract 16070832. The authors thank Mr. Mark Villela and Mr. Daniel Gomez of the University of California, Riverside for their contribution in conducting the emissions testing for this program.

3.7. **References**

Alkidas, A. C. Combustion advancements in gasoline engines. Energy Conversion and Management 2007, 48, 2751-2761.

Aikawa, K.; Sakurai, T.; Jetter, J. J. Development of a predictive model for gasoline vehicle particulate matter emissions. SAE Int. J. Fuels Lubr. 2010, 3, 610-622.

Badshah, H.; Kittelson, D.; Northrop, W. Particle emissions from light-duty vehicles during cold-cold start. SAE Int. J. Engines 2016, 9, 1775-1785.

Catapano, F.; Di Iorio, S.; Sementa, P.; Vaglieco, B.M. Characterization of ethanol-gasoline blends combustion processes and particle emissions in a GDI/PFI small engine. SAE Technical Paper 2014, 2014-01-1382.

Catapano, F.; Sementa, P.; Vaglieco, B.M. Air-fuel mixing and combustion behavior of gasoline-ethanol blends in a GDI wall-guided turbocharged multi-cylinder optical engine. Renewable Energy 2016, 96, 319-332.

Chan, T.W.; Lax, D.; Gunter, G.C.; Hendren, J.; Kubsh, J.; Brezny, R. Assessment of the Fuel Composition Impact on Black Carbon Mass, Particle Number Size Distributions, Solid Particle Number, Organic Materials, and Regulated Gaseous Emissions from a Light-Duty Gasoline Direct Injection Truck and Passenger Car. Energy and Fuels 2017, 31, 10452-10466.

Clairotte, M.; Adam, T.W.; Zardini, A.A.; Manfredi, U.; Martini, G.; Krasenbrink, A.; Vicet, A.; Tournie, E.; Astorga, C. Effects of low temperature on the cold start gaseous emissions from light duty vehicles fueled by ethanol-blended gasoline. Applied Energy 2013, 102, 44-54.

Costagliola, M.A.; De Simio, L.; Pratti, M.V. Combustion efficiency and engine out emissions of a S.I. engine fueled with alcohol/gasoline blends. Applied Energy 2013, 111, 1162-1171.

Dardiotis, C.; Fontaras, G.; Marotta, A.; Martini, G.; Manfredi, U. Emissions of modern light duty ethanol flex-fuel vehicles over different operating and environmental conditions. Fuel 2015, 140, 531-540.

EPA. Ethanol Waivers (E15 and E10). Environmental Protection Agency; 2011.

Fatouraie, M.; Wooldridge, M.S.; Petersen, B.R.; Wooldridge, S.T. Effects of ethanol on in-cylinder and exhaust gas particulate emissions of a gasoline direct injection spark ignition engine. Energy and Fuels 2015, 29, 3399-3412.

Goodfellow, C. L.; Gorese, R. A.; Hawkins, M. J.; McArragher, J. S. European Programme on Emission, Fuels and Engine Technologies – Gasoline Aromatics/E100 Study. SAE Technical Paper 1996, 961072.

Haas, F.M.; Chaos, M.; Dryer, F.L. Low and intermediate temperature oxidation of ethanol and ethanol-PRF blends: An experimental and modeling study. Combustion and Flame 2009, 156, 2346-2350.

Han, Y.; Hu, S.; Sun, Y.; Sun, X.; Tan, M.; Xu, Y.; Tian, J.; Li, R.; Shao, S. Compositional effect of gasoline on fuel economy and emissions. Energy Fuels 2018, 32, 5072-5080.

He, X.; Ratcliff, M.A.; Zigler, B.T. Effects of gasoline direct injection engine operating parameters on particle number emissions. Energy and Fuels 2010, 26, 2014-2027.

Hubbard, C.P.; Anderson, J.E.; Wallington, T.J. Ethanol and air quality: Influence of fuel ethanol content on emissions and fuel economy of flexible fuel vehicles. Environ. Sci. Technol. 2014, 48, 861-867.

Idriss, H. Ethanol reactions over the surfaces of noble metal/cerium oxide catalysts. Platinum Metals Rev. 2004, 48, 105-115.

Iodice, P.; Langella, G.; Amoresano, A. Ethanol in gasoline fuel blends: Effect on fuel consumption and engine out emissions of SI engines in cold operating conditions. Applied Thermal Engineering 2018, 130, 1081-1089.

Jin, D.; Choi, K.; Myun, C.L.; Lim, Y., Lee, J.; Park, S. The impact of various ethanol-gasoline blends on particulates and unregulated gaseous emissions characteristics from a spark ignition direct injection (SIDI) passenger vehicle. Fuel 2017, 209, 702-712.

Karavalakis, G.; Short, D.; Russell, R.L.; Jung, H.; Johnson, K.C.; Asa-Awuku, A.; Durbin, T.D. Assessing the Impacts of Ethanol and Iso-butanol on Gaseous and Particulate Emissions from Flexible Fuel Vehicles. Environ. Sci. Technol. 2014, 48, 14016-14024.

Karavalakis, G.; Short, D.; Vu, D.; Villela, M.; Asa-Awuku, A.; Durbin, T.D. Evaluating the regulated emissions, air toxics, ultrafine particles, and black carbon from SI-PFI and SI-DI vehicles operating on different ethanol and iso-butanol blends. Fuel 2014, 128, 410-421.

Karavalakis, G.; Short, D.; Vu, D.; Russell, R.; Hajbabaei, M.; Asa-Awuku, A.; Durbin, T.D. Evaluating the effects of aromatics content in gasoline on gaseous and particulate matter emissions from SI-PFI and SI-DI vehicles. Environ. Sci. Technol. 2015, 49, 7021-7031.

Khalek, I. A.; Bougher, T.; Jetter J. J. Particle emissions from a 2009 gasoline direct injection engine using different commercially available fuels. SAE Int. J. Fuels Lubr. 2010, 3, 623-637.

Khlystov, A.; Samburova V. Flavoring Compounds Dominate Toxic Aldehyde Production During E-cigarette Vaping. Environ. Sci. and Technol. 2016, 50, 13080-13085.

Khosousi, A.; Liu, F.; Dworkin, S.B.; Eaves, N.A.; Thomson, M.J.; He, X., Dai, Y.; Gao, Y.; Liu, F.; Shuai, S.; Wang, J. Experimental and numerical study of soot formation in laminar coflow diffusion flames off gasoline/ethanol blends. Combustion and Flame 2015, 162, 3925-3933.

Ladommatos, N.; Rubenstein, P.; Bennett, P. Some effects of molecular structure of single hydrocarbons on sooting tendency. Fuel 1996, 75, 114-124.

Leach, F.; Stone, R.; Richardson, D. The influence of fuel properties on particulate number emissions from a direct injection spark ignition engine. SAE Technical Paper 2013, 2013-01-1558.

Leach, F.C.P.; Stone, R.; Richardson, D.; Turner, J.W.C.; Lewis, A.; Akehurst, S.; Remmert, S.; Cambell, S.; Cracknell, R. The effect of oxygenate fuels on PN emissions from a highly boosted GDI engine. Fuel 2018, 225, 277-286.

Lemaire, R.; Therssen, E.; Desgroux, P. Effect of ethanol addition in gasoline and gasoline-surrogate on soot formation in turbulent spray flames. Fuel 2010;89:3952-3959.

Liu, F.-J.; Liu, P.; Wei, Y.-J.; Liu, S.-H. Regulated and unregulated emissions from a spark-ignition engine fuelled with low-blend ethanol-gasoline mixtures. Proceedings of the Institution of Mechanical Engineers, Part D: Journal of Automobile Engineering 2011, 226, 517-528.

Maricq, M.M.; Szente, J.J.; Jahr, K. The impact of ethanol fuel blends on PM emissions from a light-duty GDI vehicle. Aerosol Science and Technology 2012, 46, 576-583.

Najafi, G.; Ghobadian, B.; Tavakoli, T.; Buttsworth, D.R.; Yusaf, T.F.; Faizollahnejad, M. Performance and exhaust emissions of a gasoline engine with ethanol blended fuels using artificial neural network. Applied Energy 2009, 86, 630-639.

Petit, A.; Montagne, X. Effects of the gasoline composition on exhaust emissions of regulated and speciated pollutants. SAE Technical Paper 1993, 932681.

Piock, W.; Hoffmann, G.; Berndorfer, A.; Salemi, P.; Fusshoeller, B. Strategies towards meeting future particulate matter emission requirements in homogeneous gasoline direct injection engines. SAE Int. J. Engines 2011, 4, 1455-1468.

Poulopoulos, S.G.; Samaras, D.P.; Philipopoulos, C.J. Regulated and unregulated emissions from an internal combustion engine operating on ethanol-containing fuels. Atmospheric Environment 2001, 35, 4399-4406.

Salamanca, M.; Sirignano, M.; D'Anna, A. Particulate formation in premixed and counter-flow diffusion ethylene/ethanol flames. Energy and Fuels 2012, 26, 6144-6152.

Sanchez, N.E.; Callejas, A.; Millera, A.; Bilbao, R.; Alzueta, M.U. Polycuclic aromatic hydrocarbon (PAH) and soot formation in the pyrolysis of acetylene and ethylene: Effect of the reaction temperature. Energy and Fuels 2012, 26, 4823-4829.

Sobotowski, R.A.; Butler, A.D.; Guerra, Z. A pilot study of fuel impacts on PM emissions from light-duty gasoline vehicles. SAE Technical Paper, 2015, 2015-01-9071.

Stevens, E.; Steeper, R. Piston wetting in an optical DISI engine: Fuel films, pool fires, and soot generation. SAE Technical Paper 2001, 2001-01-1203.

Storey, J.; Lewis, S.; Szybist, J.; Thomas, J.;; Barone, T.; Eibl, M.; Nafziger, E.; Kaul, B.. Novel characterization of GDI engine exhaust for gasoline and mid-level gasoline-alcohol blends. SAE Technical Paper 2014; 2014-01-1606.

Suarez-Bertoa, R.; Zardini, A.A.; Keuken, H.; Astorga, C. Impact of ethanol containing gasoline blends on emissions from a flex-fuel vehicle tested over the Worldwide Harmonized Light duty Test Cycle (WLTC). Fuel 2015, 143, 173-182.

Szybist, J.P.; Youngquist, A.D.; Barone, T.L.; Storey, J.M.; Moore, W.R.; Foster, M.; Confer, K. Ethanol blends and engine operating strategy effects on light-duty spark-ignition engine particle emissions. Energy and Fuels 2011, 25, 4977-4985.

Turner, D.; Xu, H.; Cracknell, R.F.; Natarajan, V.;, Chen, X. Combustion performance of bio-ethanol at various blend ratios in a gasoline direct injection engine. Fuel 2011, 90, 1999-2006.

U.S. Environmental Protection Agency. Assessing the effect of five gasoline properties on exhaust emissions from light-duty vehicles certified to Tier 2 standards: Analysis of data from EPAct phase 3 (EPAct/V2/E-89). Final Report. EPA-420-R-13-002, April, 2013, http://www.epa.gov/otaq/models/moves/epact.htm

Wang, C.; Xu, H.; Herreros, J.M.; Wang, J.; Cracknell, R. Impact of fuel and injection system on particle emissions from a GDI engine. Applied Energy 2014, 132, 178-191.

Wu, J.; Song, K.H.; Litzinger, T.; Lee, S.-Y.; Santoro, R.; Linevsky, M.; Colket, M.; Liscinsky, D. Reduction of PAH and soot in premixed ethylene-air flames by addition of ethanol. Combustion and Flame 2006, 144, 675-687.

Yao, C.; Dou, Z.; Wang, B.; Liu, M.; Lu, H.; Feng, J.; Feng, L. Experimental study of the effect of heavy aromatics on the characteristics of combustion and ultrafine particle in DISI engine. Fuel 2017, 203, 290-297.

Yassine, M.K.; La Pan, M. Impact of ethanol fuels on regulated tailpipe emissions. SAE Technical Paper 2012, 2012-01-0872.

Zervas, E.; Montagne, X.; Lahaye, J. The influence of gasoline formulation on specific pollutant emissions. Journal of the Air & Waste Management Association 1999, 49, 1304–1314.

Zervas, E.; Montagne, X.; Lahaye, J. Emission of alcohols and carbonyl compounds from a spark ignition engine. Influence of fuel and air/fuel equivalence ratio. Environ. Sci. Technol. 2002, 36, 2414-2421.

Zervas, E.; Montagne, X.; Lahaye, J. Influence of fuel and air/fuel equivalence ratio on the emission of hydrocarbons from a SI engine. 1. Experimental findings. Fuel 2004, 83, 2301-2311.

Zhang, H. R.; Eddings, R.; Sarofim, A. F. Pollutant emissions from gasoline combustion. 1. Dependence on fuel structural functionalities. Environ. Sci. Technol. 2008, 42, 5615-5621.

Zhang, S.; McMahon, W. Particulate emissions for LEV II light-duty gasoline direct injection vehicles. SAE Int. J. Fuels Lubr. 2012, 5, 637-646.

Zhu, R.; Hu, J.; Bao, X.; He, L.; Zu, L. Effects of aromatics, olefins and distillation temperatures (T50 & T90) on particle mass and number emissions from gasoline direct injection (GDI) vehicles. Energy Policy 2017, 101, 185-193.

3.8. **Supporting Information**

3.8.1. **Emissions Analysis**

PM measurements were made on both a mass and number basis. PM mass samples were collected cumulatively over the entire length of the LA92 cycle, with one sample collected for each test. Total PM mass samples were coll0ected using 47-mm polytetrafluoroethylene (PTFE) filters (Whatman) and weighed with a 1065-compliant microbalance in a temperature and humidity controlled clean chamber meeting 1065 requirements. Buoyancy corrections for barometric pressure differences were also made for the PM filter weights as per CFR 1065.

Total particle number was measured using a TSI 3776 ultrafine-Condensation Particle Counter (CPC) with a 2.5 nm cut point. The instrument operated at a flowrate of 1.5 L/min. Solid particle number counts were measured with the use of a catalytic stripper. The catalytic stripper both vaporizes volatile species and oxidizes them, and hence more efficiently removes volatiles from the sample than thermal treatment alone. For this study, the catalytic stripper used was 40 mm long with a diameter of 17 mm and was based on a cordierite monolith with a 400 cpsi cell density and a 6 mils substrate thickness. It had both oxidation and sulfur storage capability, but its exact chemical composition was unknown. The particular unit was characterized according to the protocol outlined by Amanatidis et al. [1] and was deemed appropriate for the measurements of this study. The particles were counted downstream of the catalytic stripper with a TSI 3776 ultrafine CPC at a flow rate of 1.5 L/min. An ejector diluter was used to collect particle number samples from the CVS tunnel for the GDI vehicles.

Real-time particle size distributions were obtained using an Engine Exhaust Particle Sizer (EEPS) spectrometer. The EEPS (TSI 3090, firmware version 8.0.0) was used to obtain real-time second-by-second size distributions between 5.6 to 560 nm. Particles were sampled at a flow rate of 10 L/min, which is considered to be high enough to minimize diffusional losses. They were then charged with a corona charger and sized based on their electrical mobility in an electrical field. Concentrations were determined through the use of multiple electrometers. In this study, the measured electrometer currents over 22 electrometers were inverted to particle size distributions into 32 bins using two inversion matrices, known as Default Matrix or Soot Matrix.

Real-time soot or black carbon emissions were measured using an AVL Micro-Soot Sensor (MSS). The MSS is an instrument that measures soot mass concentration at a frequency of one Hertz basis using a photo acoustic detection technique, where the light-absorbing PM components (such as soot particles) are exposed to laser light that is periodically modulated at the acoustical resonant frequency [2]. The instrument is designed to measure soot concentrations down to ~5µg/m3, and operates at a flow rate of 2 L/min.

3.8.2. **Supplemental Tables**

Table S3-1 Monoaromatic and other VOCs emitted during the cold-start and hot-start LA92 cycles

	Cold-start LA92				Hot-start LA92			
	E10	E10HA	E30	E78	E10	E10HA	E30	E78
Ethylene	23290.3±142.6	22843±11	23093±22.3	22977.3±22.9	23218.7±32.5	22896.7±21.5	23125.3±26.7	22988±38.2
Acetylene	149.97±0.03	152±0.14	148.65±0.66	151.91±0.43	149.32±0.86	151.83±0.68	149.1±0.87	152.38±0.75
Ethane	11.06±0.018	11.037±0.09	11.09±0.023	11.082±0.009	11.085±0.014	11.092±0.014	11.055±0.03	11.092±0.013
Propylene	1.675±0.477	1.998±0.01	1.73±0.115	2.467±0.041	1.002±0.036	0.769±0.023	0.572±0.014	0.412±0.024
Propane	0.467±0.215	0.851±0.097	0.546±0.013	1.323±0.081	0.073±0.019	0.07±0.015	0.012±0.004	0.019±0.017
Isobutane	1.045±0.229	1.371±0.05	0.977±0.035	1.358±0.045	0.886±0.037	1.153±0.025	0.657±0.022	0.681±0.092
1-Butene	1.224±0.5	1.657±0.015	1±0.027	0.503±0.007	0.775±0.003	0.735±0.016	0.388±0.025	0.126±0.02
1,3 Butadiene	0.054±0.138	0.331±0.065	0.126±0.021	0.084±0.138	-0.025±0.032	0.192±0.106	0.038±0.007	0.639±0.778
n-Butane	-0.023±0.013	0.931±0.02	0.022±0.01	-0.003±0.006	-0.015±0.001	0.551±0.046	0.01±0.001	-0.004±0.017
trans-2-Butene	0.22±0.089	0.304±0.009	0.147±0.016	0.07±0.013	0.089±0.005	0.133±0.002	0.048±0.014	0.025±0.003
cis-2-Butene	0.2±0.115	0.254±0.074	0.171±0.007	0.07±0.003	0.125±0.03	0.13±0.003	0.061±0.002	0±0
Isopentane	0.968±0.244	0.562±0.008	0.775±0.083	0.101±0.02	0.755±0.146	0.383±0.019	0.432±0.029	0.074±0.047
1-Pentene	0.067±0.041	0.103±0.002	0.062±0.001	0.03±0.001	0.048±0.001	0.05±0.002	0.028±0	0±0
n-Pentane	0.049±0.028	0.075±0.002	0.046±0.002	0.029±0.004	0.036±0	0.037±0.002	0.021±0	0±0
Isoprene	0.991±0.507	0.938±0.031	1.024±0.074	0.14±0.008	0.678±0.005	0.586±0.028	0.558±0.002	0.091±0.004
trans-2-Pentene	0.055±0.022	0.065±0.001	0.056±0	0.026±0.001	0.036±0	0.037±0	0.03±0.006	0.014±0.001
cis-2-Pentene	2.331±0.473	2.854±0.172	1.953±0.159	0.669±0.084	1.251±0.02	1.321±0.057	0.983±0.023	0.327±0.028
2,2-Dimethylbutane	0.062±0.046	0.032±0.015	0.061±0	0.025±0.002	0.045±0.029	0.05±0	0.014±0	0±0
Cyclopentane	0.025±0.016	0.044±0	0.024±0.002	0.015±0.002	0.009±0.013	0.024±0.001	0±0	0±0
2,3-Dimethylbutane	0.012±0.017	0.026±0	0.017±0.001	0±0	0±0	0.014±0.001	0±0	0±0
2-Methylpentane	0.645±0.136	0.029±0.001	0.4±0.02	0.263±0.03	0.273±0.026	0.025±0	0.225±0.007	0.146±0.009
3-Methylpentane	0.888±0.137	0.021±0.001	0.553±0.044	0.353±0.047	0.334±0.036	0.007±0.01	0.242±0.002	0.142±0.009
1-Hexene	0.058±0.027	0.117±0.006	0.055±0.005	0.03±0	0.031±0.003	0.066±0.002	0.031±0.004	0.019±0.006
n-Hexane	0.305±0.106	0.643±0.038	0.276±0.013	0.128±0.009	0.156±0.015	0.317±0.01	0.137±0.006	0.066±0.015
Methylcyclopentane	0.3±0.077	0.635±0.045	0.276±0.03	0.114±0.008	0.158±0.014	0.288±0.015	0.138±0.002	0.065±0.008

2,4-Dimethylpentane	0.72±0.285	1.52±0.132	0.569±0.024	0.155±0.027	0.182±0.017	0.247±0.009	0.124±0	0.034±0.002
Benzene	0.581±0.075	1.107±0.076	0.467±0.021	0.206±0.02	0.26±0.014	0.491±0.018	0.219±0.004	0.099±0.015
Cyclohexane	0.224±0.019	0.417±0.035	0.168±0.007	0.071±0.003	0.093±0.006	0.186±0.002	0.077±0.006	0.036±0.01
2-Methylhexane	0.085±0.037	0.163±0.023	0.078±0.008	0.035±0.001	0.042±0.004	0.09±0.002	0.028±0.002	0.009±0.012
2,3-Dimethylpentane	1.092±0.451	1.824±0.025	0.986±0.07	0.599±0.001	0.899±0.008	0.972±0.031	0.471±0.05	0.151±0.02
3-Methylhexane	0.03±0.005	0.065±0.003	0.025±0.001	0.02±0	0.007±0.01	0.04±0	0.007±0.01	0.008±0.011
2,2,4-Trimethylpentane	0.133±0.051	0.371±0.026	0.13±0.007	0.052±0.003	0.065±0.007	0.175±0.007	0.054±0.004	0.023±0.007
n-Heptane	0.07±0.018	0.147±0.003	0.072±0.018	0.034±0.007	0.03±0.003	0.079±0.003	0.03±0.002	0.018±0.007
Methylcyclohexane	0.105±0.05	0.367±0.029	0.105±0.007	0.034±0.008	0.056±0.004	0.163±0.008	0.046±0.006	0.019±0.007
2,3,4-Trimethylpentane	2.829±0.585	1.264±0.096	2.404±0.004	1.128±0.128	1.411±0.177	0.613±0.029	1.201±0.009	0.536±0.029
Toluene	0.011±0.015	0.174±0.015	0.027±0.002	0.026±0.001	0.007±0.01	0.082±0.003	0.015±0.002	0.011±0.016
2-Methylheptane	0.054±0.042	0.08±0.003	0.063±0.002	0.028±0.003	0.031±0.004	0.042±0.001	0.027±0.003	0.008±0.012
3-Methylheptane	0.469±0.118	0.774±0.065	0.416±0.005	0.13±0.014	0.216±0.034	0.339±0.016	0.186±0.001	0.057±0.006
n-Octane	1.798±0.671	2.912±0.22	1.654±0.071	0.628±0.027	0.908±0.017	1.014±0.014	0.509±0.041	0.127±0.034
Ethylbenzene	0.071±0.049	0.075±0.006	0.081±0.001	0.023±0.002	0.044±0.007	0.035±0.002	0.035±0	0±0
m/p-Xylenes	0.049±0.033	0.052±0.004	0.058±0	0.017±0.002	0.03±0.005	0.026±0.001	0.025±0	0±0
Styrene	0.22±0.129	0.191±0.015	0.243±0.003	0.059±0.005	0.128±0.015	0.09±0.005	0.102±0.002	0.024±0.003
o-Xylene	0.311±0.132	0.519±0.055	0.281±0.026	0.104±0.008	0.152±0.001	0.187±0.006	0.092±0.002	0.027±0.003
Nonane	0.656±0.383	1.344±0.058	0.682±0.047	0.211±0.033	0.366±0.009	0.509±0.001	0.183±0.005	0.043±0.008
Isopropylbenzene	0.03±0.043	0.118±0.023	0.07±0.011	0.016±0.002	0.018±0.026	0.048±0.003	0±0	0±0
n-Propylbenzene	0.2±0.07	0.364±0.028	0.217±0.005	0.075±0.012	0.106±0.011	0.141±0	0.056±0.004	0.021±0.002
m-Ethyltoluene	0.153±0.024	0.119±0.022	0.138±0.004	0.051±0.004	0.075±0.007	0.065±0.001	0.058±0.001	0.022±0.001
1,3,5-Trimethylbenzene	0.035±0.017	0.073±0.01	0.037±0.002	0.018±0.002	0.018±0.002	0.027±0.001	0.006±0.009	0±0
o-Ethyltoluene	0.146±0.067	0.326±0.038	0.16±0.005	0.07±0.006	0.082±0.015	0.129±0.001	0.041±0.001	0.022±0.001
1,2,4-Trimethylbenzene	0.051±0.022	0.145±0.013	0.065±0.014	0.038±0.001	0.033±0.003	0.061±0.001	0.017±0.001	0.014±0.001
n-Decane	0.067±0.048	0.159±0.021	0.073±0.002	0.038±0.005	0.044±0.013	0.07±0.005	0.019±0.003	0.015±0.001
1,2,3-Trimethylbenzene	0.026±0.037	0.097±0.022	0.036±0.007	0.024±0.004	0.009±0.012	0.036±0.003	0±0	0±0
m-Diethylbenzene	0.126±0.085	0.271±0.072	0.129±0.001	0.064±0.006	0.084±0.043	0.121±0.002	0.035±0.004	0.021±0
p-Diethylbenzene	0.048±0.023	0.004±0.015	0.048±0.004	0.019±0.002	0.036±0.003	0±0.01	0.028±0.002	0.012±0

3.8.3. **Supplementary References**

Amanatidis, S.; Ntziachristos, L.; Giechaskiel, B.; Katsaounis, D.; Samaras, Z.; Bergmann, A. Evaluation of an Oxidation Catalyst ("Catalytic Stripper") in Eliminating Volatile Material from Combustion Aerosol. Journal of Aerosol Science, 2013, 57, 144-155.

Schindler, W.; Haisch, C.; Beck, H.A.; Niessner, R.; Jacob, E.; Rothe, D. A Photoacoustic Sensor System for the Time Resolved Quantification of Diesel Soot Emission. SAE Technical Paper 2004, 2004-01-0969.

4. Physical, Chemical, and Toxicological Characteristics of Particulate Emissions from Current Technology Gasoline Direct Injection Vehicles

4.1. Abstract

We assessed the physical, chemical and toxicological characteristics of particulate emissions from four light-duty gasoline direct injection vehicles when operated over the LA92 driving cycle. Our results showed that particle mass and number emissions increased markedly during accelerations. For three of the four vehicles tested, particle mass and number emissions were markedly higher during cold-start and the first few accelerations following the cold-start period than during the hot running and hot-start segments of the LA92 cycle. For one vehicle (which had the highest emissions overall) the hot-start and cold-start PM emissions were similar. Black carbon emissions were also much higher during the cold-start conditions, indicating severe fuel wetting leading to slow evaporation and pool burning, and subsequent soot formation. Particle number concentrations and black carbon emissions showed large reductions during the urban and hot-start phases of the test cycle. The oxidative potential of particulate matter (PM) was quantified with both a chemical and a biological assay, and the gene expression impacts of the PM in a macrophage model with PCR and ELISA analyses. Inter- and intra-vehicle variability in oxidative potential per milligram of PM emitted was relatively low for both oxidative assays, suggesting that real-world emissions and exposure can be estimated with distance-normalized emission factors. The PCR response from signaling markers for oxidative stress

(e.g., NOX1) was greater than from inflammatory, AhR, or MAPK signaling. Protein production associated with inflammation (TNFα) and oxidative stress (HMOX-1) were quantified and displayed relatively high inter-vehicle variability, suggesting that these pathways may be activated by different PM components. Correlation of trace metal concentrations and oxidative potential suggests a role for small, insoluble particles in inducing oxidative stress.

4.2. Introduction

Gasoline direct injection (GDI) vehicles are on the rise and are receiving increased attention by automotive manufacturers because of their improved fuel economy and hence lower greenhouse gas (GHG) emissions compared to their port-fuel injection (PFI) counterparts (Xu et al., 2011). GDI engines combined with turbocharging and light-weighting technologies are one of the very few viable engine platforms to meet the Corporate Average Fuel Economy (CAFE) standards that have specified fuel economy to exceed 55 miles/gallon (4.2 L/100km) in passenger cars by 2025. Though the fuel economy and GHG benefits from GDI engines are clear, several studies have reported higher particulate matter (PM) and particle number emissions compared to other engine technologies such as PFI engines and modern diesel vehicles equipped with diesel particle filters (Zinola et al., 2016; Sobotowski et al., 2015; Karavalakis et al., 2014). The higher particulate emissions from GDI engines are largely due to the presence of fuel-rich regimes (resulting from the insufficient preparation of air-fuel mixtures) where soot particles are formed. In addition, the direct contact of fuel onto cold piston and cylinder walls (fuel

wetting) leads to flame quenching, resulting in incomplete combustion and volatile organic compound (VOC) emissions (Attar and Xu, 2016; Piock et al., 2011).

The elevated particulate emissions from GDI vehicles are especially concerning given the context of increasingly strict PM emissions regulations in both the United States (US) and the European Union (EU). These regulations have been driven by the large and growing body of science implicating PM in a broad range of human health impacts. In the US, where PM regulations are expressed in terms of filter-collected mass emitted per mile, California implemented their LEV III light-duty PM standard of 3 mg/mile (1.9 mg/km) for model year 2017 vehicles and a 1 mg/mile (0.6 mg/km) target for model year 2025 vehicles over the Federal Test Procedure (FTP). In the EU, where PM regulations are in-place for both mass and particle number, the proposed Euro 6c solid particle number (i.e., the number of particles with diameters greater than 23 nm after heating to 300 °C) limit for spark-ignition engines is at 6.0x1011 particles/km with a PM mass limit of 4.5 mg/km over the New European Driving Cycle (NEDC).

The physiochemical and toxicological characteristics of the PM emissions are as, or more, relevant to potential human health impacts than the mass emission factors. However, toxicological impacts of PM emissions, especially from GDI engines, are poorly understood. Several studies have examined the nature of particulate emissions from GDI engines as a function of fuel type, fuel injection architecture, after-treatment control, and engine operating parameters (Chen et al., 2012; Chan et al., 2014; Barrientos et al., 2016). Particles from GDI engines are generally formed from fuel and lubricant oil and are complex agglomerates of volatile and non-volatile substances, both organic and inorganic

(sulfate, nitrate, metal species) in nature (Piock et al., 2011). Karavalakis and co-workers (2015) documented that greater aromatic hydrocarbon content in gasoline resulted in higher PM mass, particle number, and black carbon emissions from a fleet of GDI and PFI vehicles. Pirjola et al. (2015) showed a clear effect of lubricant oil on particle emissions from a modern GDI vehicle. Badshah et al. (2016) reported that under cold-start conditions the large majority of the total exhaust particles from GDI vehicles were solid soot and only a small fraction were semi-volatile.

A number of studies have shown that exposure to primary PM emissions from mobile sources is linked directly to adverse health implications (Bisig et al., 2018; Tzamkiozis et al., 2010; Seagrave et al., 2002). Epidemiologic and toxicological studies have reported that elevated levels of PM are associated with cardiopulmonary mortality and morbidity (Araujo and Nel, 2009; Bates et al., 2015; Reed et al., 2008). The underlying mechanisms via which PM exposure contributes to adverse human health outcomes are the subject of intense study and our understanding is incrementally expanding. Increasing evidence suggests that transition metals present in PM (e.g., iron, manganese, vanadium), as well as certain organic species (e.g., quinones) generate reactive oxygen species (ROS) that may be involved in producing respiratory symptoms (Rohr and Wyzga, 2012; Diaz et al., 2012; Charrier and Anastasio, 2012). Diaz et al. (2012) showed that primary particles emitted from a gasoline vehicle might be able to cause a change in the breathing patterns of male Sprague Dawley rats. Lund and co-workers (2007) showed that inhalational exposure to gasoline engine emissions resulted in increased aortic mRNA expression of several genes, including matrix metalloproteinase-3 (MMP-3), MMP-7, and MMP-9,

tissue inhibitor of metalloproteinases-2, endothelin-1 and heme oxygenase-1 (HO-1) in ApoE-/- mice (an animal model of atherosclerosis). The authors concluded that exposure to gasoline exhaust results in vascular remodeling, as well as increased expression of markers of oxidative stress, which may contribute to the progression of atherosclerosis. A recent study showed that exposure to GDI exhaust contributes to upregulation of genes related to the metabolism of polycyclic aromatic hydrocarbons (PAHs) and oxidative stress (Maikawa et al., 2016). There is significant body of evidence documenting that insoluble particulate matter can initiate inflammatory cascades in lung tissues with resulting morbidity, including carcinogenesis and endothelial dysfunction (Freire et al., 2013; Tamagawa et al., 2008).

The primary objectives of this study were to advance our understanding of the physical and chemical properties of particulate emissions from current technology GDI light-duty vehicles and provide a new primary assessment of the oxidative stress potential and inflammatory responses of the emitted PM. Dynamometer testing was conducted using model year 2015 and 2016 GDI passenger cars on California E10 gasoline fuel over the LA92 cycle. The physical, chemical, and toxicological properties of the particulate emissions are discussed in the context of the influences of the driving cycle and engine technology.

4.3. **Experimental**

4.3.1. **Vehicles, Driving Cycle, and Measurement Protocols**

Emissions from four 2015 and 2016 model year GDI passenger cars (as described in Table S4-1, in the Supplementary Material (SM)) were characterized in this study. They

are referred to as GDI_1, GDI_2, GDI_3, and GDI_4 throughout this manuscript. All vehicles were equipped with wall-guided fuel injection systems, operated with overall stoichiometric air-fuel ratios, and had three-way catalysts (TWCs). The vehicles were certified to meet either the Federal Tier 2, Bin 2 emission standards or the California LEV-II, SULEV emission standards (for PM mass, both are 10 mg/mile).

Each vehicle was exercised over the LA92 test cycle (also known as the California Unified Cycle, or UC), which is a dynamometer driving schedule for light-duty vehicles developed by the California Air Resources Board (CARB). The LA92 consists of three phases (i.e., cold-start, urban, and hot-start phases) and has a similar three-bag structure to the FTP cycle. The LA92 is characterized by higher speeds, higher accelerations, fewer stops per mile, and less idle time than the FTP. Testing included at least duplicate LA92s using a commercially available California E10 fuel. Emissions measurements were conducted in CE-CERT's Vehicle Emissions Research Laboratory (VERL), on a Burke E. Porter 48-inch single-roll electric dynamometer using a Pierburg Positive Displacement Pump-Constant Volume Sampling (PDP-CVS) system.

4.3.2. **PM Sampling and Extraction Protocols**

Particulate matter was sampled from the CVS dilution system and collected onto 47-mm polytetrafluoroethylene (PTFE) filters, following the procedures in 40 CFR 1065. Cumulative PM samples were collected over each LA92 cycle with flow-weighting mass flow controllers. Sample and control filters were frozen until analyzed. Emissions measurements of total and solid particle numbers, black carbon, and particle size

distributions were also made. The testing methods for the real-time particulate measurements are provided in the SM.

Filters were transported on ice to the University of Wisconsin, Madison, where they were extracted in ultra-pure MQ water and the unfiltered extracts (containing both insoluble and water-soluble species) subjected to a suite of chemical and toxicological analyses using the following protocols. Portions of the PM extract suspensions were digested and analyzed for 43 elements using magnetic-sector inductively-coupled plasma mass spectrometry (SF-ICPMS). The reactive oxygen species (ROS), generated by the water extracts were quantified with both a chemical method that measures the consumption rate of dithiothreitol (DTT), and an in vitro method that measures PM-induced production of ROS via a fluorescent probe in a rat alveolar macrophage (NR8383) cell line. Cells exposed to the PM sample extracts were also assessed for signs of overt cytotoxicity via two well-established approaches: (a) propidium iodide (PI; Invitrogen, ThermoFisher Scientific) nucleic acid staining using flow cytometry, (b) the MTT assay (Molecular Probes Vybrant MTT Cell Proliferation Assay Kit) using a 96-well plate format and the absorbance plate reader. In addition, the expression of 29 genes (Table S4-2) in NR8383 macrophages exposed for 4 hours to GDI PM water extract suspensions was also determined using Qiagen's Custom Rat RT2 Profiler™ PCR Array. Finally, expression of two specific proteins: tumor necrosis factor alpha (TNFα) and heme oxygenase 1 (HMOX-1), produced by the NR8383 cells exposed for 6h to the PM extracts, was quantified via ELISA methods. Detailed description of the methods utilized for the analyses are provided in the SM.

4.4. Results and Discussion

4.4.1. Particle Size Distribution

The transient nature of the particle size distributions for GDI_2 and GDI_4 vehicles are illustrated in Figure 4-1 and Figure 4-2, respectively. Figure 4-1a shows the particle size distribution for the cold-start and hot-running phases (phase 1 and 2), while Figure 4-1b shows the hot-start emissions (phase 3) for the GDI_2 vehicle. The cold-start phase dominated the overall particle size distribution, with the formation of particles occurring during the first 200 seconds. The particle peaks were centered in the nucleation mode at about 25 nm and the accumulation mode at about 60 nm in diameter. Overall, cold-start and hot-running particle size distributions were bimodal in nature, with higher proportions of accumulation mode particles at the cold-start and more nucleation mode particles present as the engine warmed up. Accumulation mode particles from GDI engines consist of carbonaceous chain agglomerates similar to those found in diesel engines (Badshah et al., 2016). The much higher concentrations of accumulation mode particles during cold-start could be related to poor fuel vaporization because of the lower combustion temperatures and pressures that can lead to very rich localized pockets of mixture and rapid formation and growth of soot particles (Cheng et al., 2001; Sakai et al., 2013). These observations are in agreement with other studies and a building consensus that the direct injection of fuel into the combustion chamber and the cold piston crown can lead to relatively slow evaporation and pool fires, contributing to the formation of soot (Badshah et al., 2016; Koczak et al., 2016; Peckham et al., 2011).

A

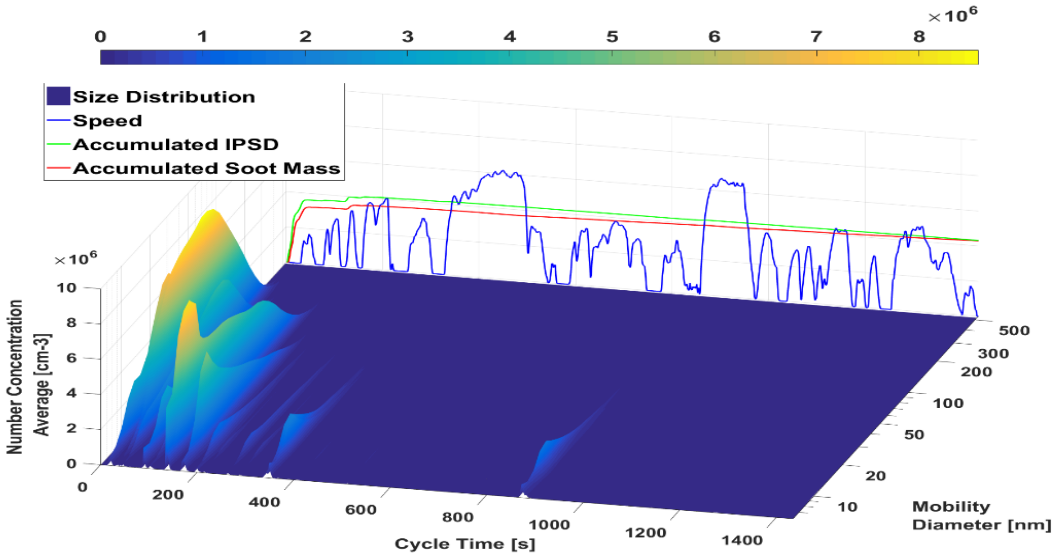

B

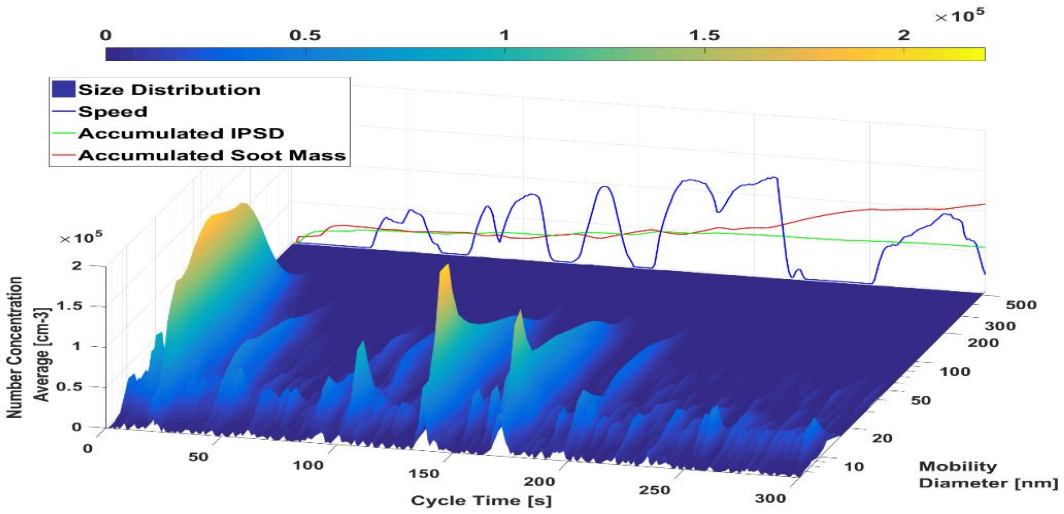

Figure 4-1 (a-b): Particle size distributions for GDI_2 for phases 1 and 2 (top panel, A) and phase 3 (bottom panel, B) of the LA92 cycle. The drive trace is included for visual reference, as well as the cumulative soot mass IPSD mass emissions. Note the factor of ten difference between the vertical scales of the top and bottom panels

A

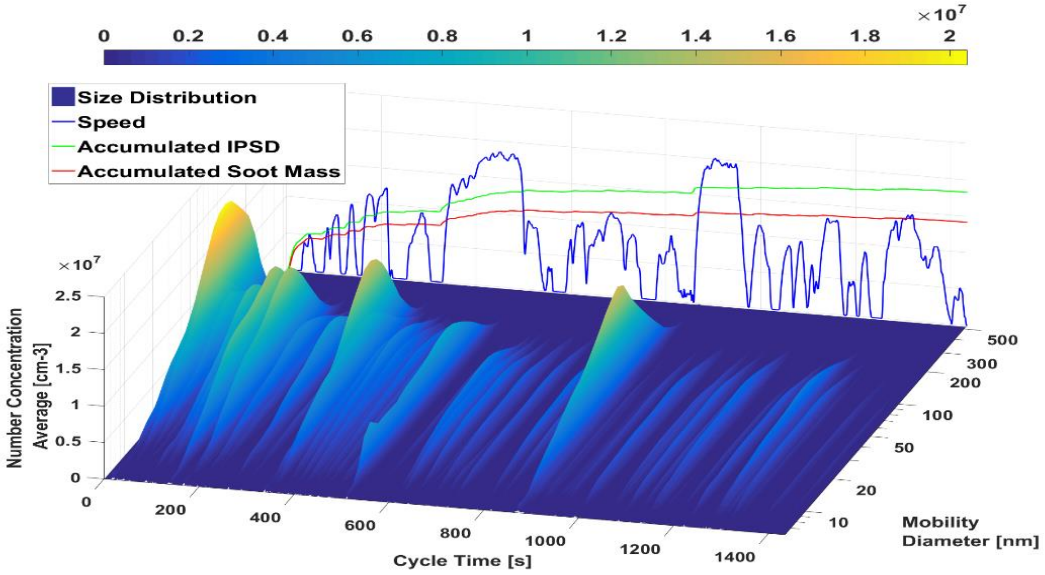

B

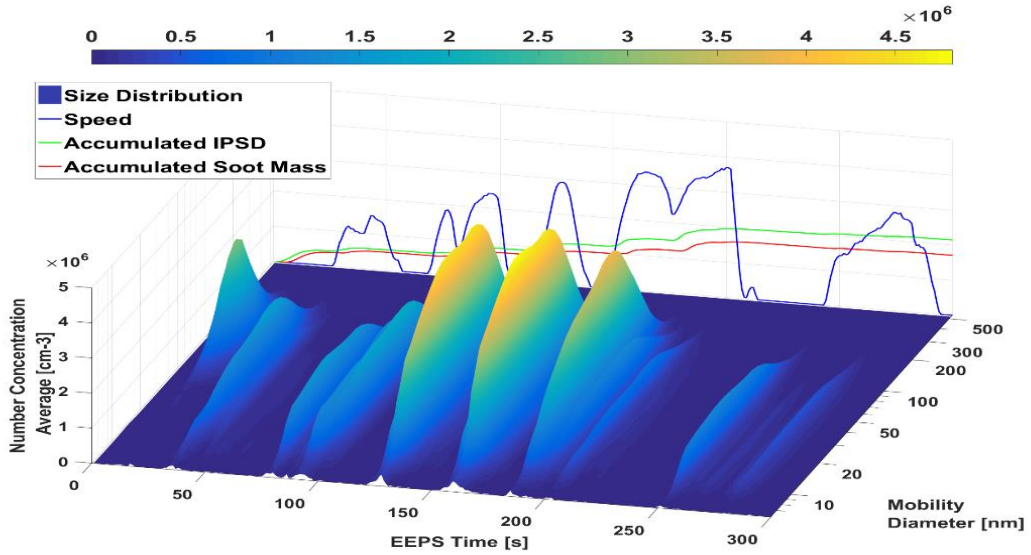

Figure 4-2 (a-b): Particle size distributions for GDI_4 for phases 1 and 2 (top panel, A) and phase 3 (bottom panel, B) of the LA92 cycle. The drive trace is included for visual reference, as well as the cumulative soot mass IPSD mass emissions. Note the factor of ten difference between the vertical scales of the top and bottom panels

After the cold-start period, in the warmed-up engine, the particle populations have significantly decreased in modal size, with nucleation mode particles centered at 10nm dominating the particle size distribution profile, as shown in Figure 4-1a. It is reasonable to assume that the population of accumulation mode particles dropped due to the warming of engine and exhaust surfaces, as well as the less rich fuel-air mixture and the improved fuel vaporization. After the first 200 seconds, both the nucleation and accumulation mode particles were virtually eliminated, suggesting that the warmed-up engine lessens fuel wetting and its effect on global and local air-fuel ratios. The disappearance of the nucleation mode particles suggests that the TWC achieved its light-off temperature and significantly reduced the hydrocarbon and semi-volatile species that contribute to the formation of nucleation mode particles via condensation.

The third phase of the LA92 is much shorter than the first two phases (Figure 4-1b). Analogous to the first two phases, particle size distributions were bimodal in nature; with higher levels of accumulation mode particles at the beginning of the hot-start followed by higher concentrations of nucleation mode particles. The nucleation mode was prominent during the majority of the hot-start phase. The large nucleation mode particle spikes were observed during accelerations as transients disrupt the control of global air-fuel ratios and exacerbate the heterogeneity of the cylinder charge (Sobotowski et al., 2015; Tan et al., 2014). It has been previously hypothesized that the origin of nucleation mode particles stems primarily from volatile hydrocarbons derived from unburned fuel and metallic particles contributed from the lubricant oil additive package (Pirjola et al., 2015). By the end of phase 3 the particles were very small in size with the mode at about 10-15 nm. It

should be noted that for phases 1 and 2, peak concentrations were on the order of 106 cm-3, whereas an order of magnitude reduction was observed after the hot-soak.

The particle size distribution profile for GDI_4 was different from GDI_2, as shown in Figure 4-2 (a-b). For both the cold-start and hot-running phases, particle size distributions were dominated by accumulation mode particles, with a much smaller mode in the nucleation regime. After 600 seconds, the populations of accumulation mode particles decreased due to the warming of the engine. A significant spike in the accumulation mode was seen during the steep accelerations of the second phase. It is plausible that some fuel films survived the higher combustion temperatures associated with accelerations, causing pool fires and fuel pyrolysis, and consequently enhancing soot formation. Similar to GDI_2, phase 3 showed an order of magnitude reduction of accumulation mode particles (Figure 4-2b). The distribution profile was decidedly unimodal, with a significant peak in the accumulation mode between 50nm to 100nm during the major hard accelerations of phase 3.

The particle size distributions for GDI_1 and GDI_3 vehicles are shown in Figures S4-1 and S4-2, respectively, in the SM. GDI_1 vehicle particle concentrations were overall lower than those of the GDI_4 vehicle, with higher particle concentrations in the nucleation mode at the start of ignition. This could be ascribed to the TWC being below its light-off temperature, allowing hydrocarbons from unburned fuel and other semi-volatile compounds to form nucleation mode particles. As the engine warmed-up, particle concentrations were considerably reduced, with the particle size distribution profile being predominantly in the accumulation mode. Similarly, the phase 3 particle size distributions

were dominated by accumulation mode particles, and the nucleation mode was practically absent. It can be assumed that the large surface area of the accumulation mode particles would favor the condensation of gas phase compounds onto pre-existing particles (heterogeneous nucleation) over new particles (homogeneous nucleation). Also, the TWC may have effectively removed semi-volatile gas-phase compounds, promoting evaporation of nucleation mode particles.

Particle size distributions for GDI_3 during phases 1 and 2 were dominated by nucleation mode particles, with the particle size distribution profile having a nearly unimodal distribution. Notably, large spikes in the nucleation regime were observed during the accelerations in phase 2. These phenomena were likely due to the higher exhaust gas temperature and the resulting enhanced formation of sulfuric acid with increasing engine load and engine speed, causing a stronger formation of nucleation mode particles (Herner et al., 2011). For the hot-start phase, the distribution was decidedly bimodal with the largest spikes being in the accumulation mode regime.

4.4.2. PM Mass, Black Carbon, and Particle Number Emissions

The gravimetric PM mass emissions are shown in Figure 4-3, and they ranged from 0.26 to 4.72 mg/mile. While testing was performed over the LA92 cycle and not the certification FTP, PM mass levels were close to or below the 2017 PM mass emissions standards of 3 mg/mile. One of the vehicles (GDI_2) exhibited very low PM mass emissions compared to the other vehicles, even below the 2025 PM standards of 1 mg/mile. Previous studies conducted with older technology GDI vehicles equipped with wall-guided fuel injection systems over the FTP and LA92 cycles showed higher PM mass emissions

than those reported here, ranging from 3 mg/mile to 8 mg/mile (Karavalakis et al., 2014; Zhang and McMahon, 2012). The low PM mass emissions from the GDI_2 vehicle is comparable to those reported in previous studies of older GDI vehicles with typically lower-emitting centrally-mounted injection systems, suggesting substantial progress in lowering PM mass emissions for some of the current technology GDI vehicles (Karavalakis et al., 2015b; Zhang and McMahon, 2012). These reductions in PM levels for the newer wall-guided GDI engines were likely a combination of improvements to the fuel injection system for controlling in-cylinder PM formation, such as increased fuel pressure, improved spray patterns, and reduced injector tip wetting.

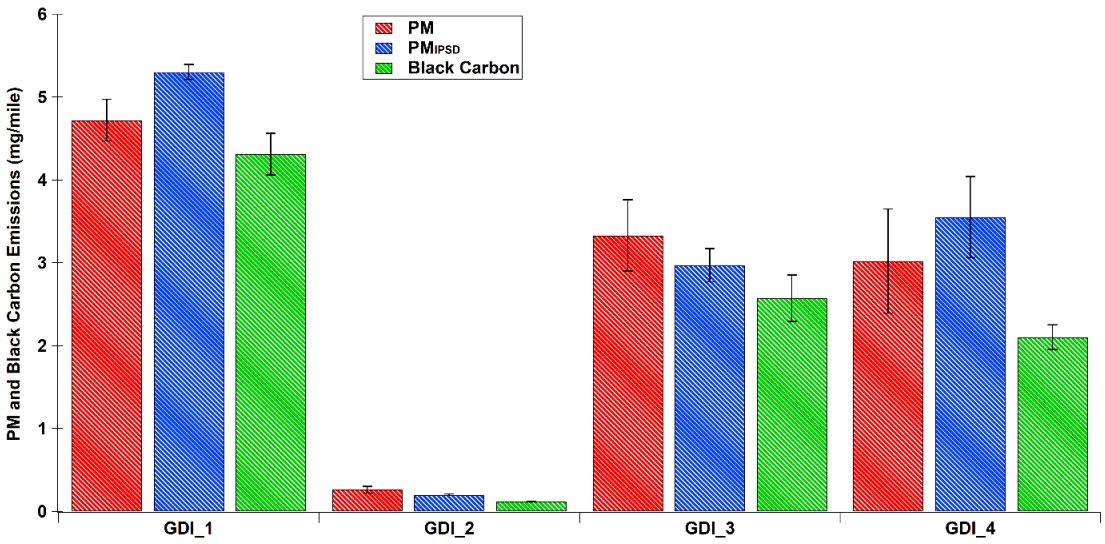

Figure 4-3 Gravimetric PM, PM derived from integrated particle size distribution method (PM_{IPSD}), and black carbon/soot emissions expressed in mg/mile over the LA92 cycle. Data presented as mean ± standard deviation, N=2

Figure 4-3 also shows the PM mass emissions calculated with the Integrated Particle Size Distribution (IPSD) method, which is an alternative for measuring PM mass at low emission levels (Quiros et al., 2015). This method evaluates real-time PM mass by

integrating the products of the particle volume concentration derived from the particle size distribution and size-dependent particle effective density for each size/volume increment (Xue et al., 2016; Quiros et al., 2015). The results reported here were determined using the IPSD method with the EEPS Soot Matrix for each test vehicle. As observed in the gravimetric PM mass findings, the emission rates with the IPSD method varied across the test vehicles, ranging from 0.20 mg/mile to 5.30 mg/mile. For GDI_2 and GDI_3 vehicles, the IPSD method underestimates the gravimetric filter-collected PM mass by 23% and 11%, respectively, suggesting that particulates from these vehicles were mostly organic in nature and closely resembled the PM emissions characteristics of PFI vehicles (Sonntag et al., 2014). This is probably due to the fact that the EEPS soot matrix underestimated the nucleation mode concentration where most of the organic compounds are sourced from (Wang et al., 2016). For GDI_1 and GDI_4 vehicles, the IPSD method overestimates the PM mass by 12% and 18%, respectively. Though this agreement is quite reasonable considering method uncertainties, the overestimation suggests that the composition of particulate emissions from these vehicles was primarily elemental carbon (EC)/soot.

These hypotheses about the chemical nature of the PM are supported by the data on particle number emissions, as shown in Figure 4-4, where for GDI_2 and GDI_3 vehicles EC/soot (solid particles) represented 41% and 35% of the particle number emissions respectively, leaving 59% and 65% that are either OC (non- or semi-volatile) or inorganic in nature (for GDI_1 and GDI_4, EC/soot represented 61% and 71% of the particle number emissions, respectively). This is also in agreement with the particle size distribution profiles for GDI_2 and GDI_3 vehicles, which were dominated by nucleation mode

particles (Figs. 1 & S2), suggesting an abundance of semi-volatile species, which could potentially result in filter sampling artifacts from organics and semi-volatile species condensing onto filters and detected by gravimetric analysis, but not being accounted for by the IPSD method.

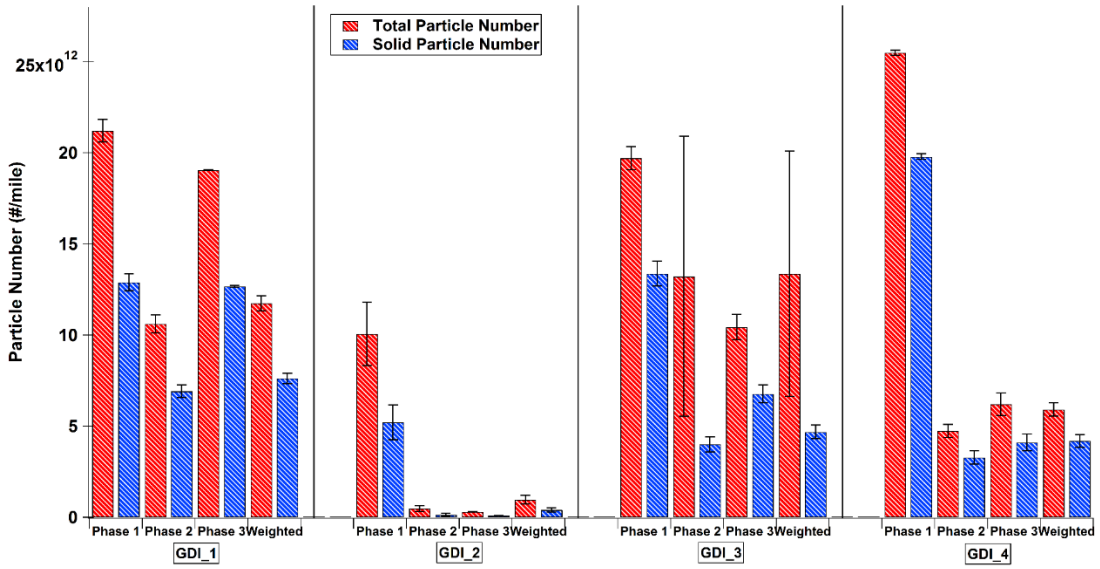

Figure 4-4 Total and solid particle number emissions for all test vehicles for the cold-start (Phase 1), hot-running (Phase 2), hot-start (Phase 3), and the weighted LA92 cycle

The black carbon emissions are shown in Figure 4-3. Consistent with the PM mass emissions, GDI_2 showed the lowest black carbon emissions of the four vehicles tested. For all vehicles, black carbon was systematically lower than the gravimetric filter-collected PM mass, but accounted for a large fraction of that mass (91%, 45%, 77%, and 69% of the total PM mass for GDI_1, GDI_2, GDI_3, and GDI_4, respectively). Similar findings were also seen in previous studies utilizing GDI vehicles (Karavalakis et al., 2014; Chan et al., 2014; Bahreini et al., 2015).

Figure 4-4 shows the total particle number and solid particle number emissions for all test vehicles. Both total and solid particle number emissions showed consistent trends with PM mass. The cold-start phase of the LA92 had the highest particle emission factors, followed by the hot-start phase, and then the lowest emission factors during hot-running phase. The higher particle number emissions during the cold-start phase can be attributed to the reduced evaporation of the fuel wall film and the limited turbulent mixing with air, which cause a high amount of engine-out particulates (Piock et al., 2011; He et al., 2010). Several investigations have shown that in GDI engines, PM mass and number emissions are higher than those in PFI engines (Karavalakis et al., 2014; Bahreini et al., 2015). The increase in particulate emissions for GDI engines is likely due to the increased liquid fuel impingement on the combustion chamber walls that can result in liquid fuel that is not totally vaporized and well mixed at the start of combustion. This is turn may cause fuel pool fires generating higher PM emissions (Su et al., 2014; Szybist et al., 2011).

4.4.3. **Oxidative Potential**

The oxidative potential of the PM emitted from the GDI vehicles was measured with both a biological (macrophage-mediated ROS production) and a chemical (dithiothreitol, or DTT oxidation) assay. Results are summarized on a per mile basis in Figure 4-5a and on a per PM mass basis in Figure 4-5b. On a per mile basis (Fig. 5a) the ROS data ranged over a factor of 70 and the DTT data by a factor of 20. However, inter- and intra- vehicle variability was substantially lower for both the ROS and DTT datasets when results were expressed on a per mass basis.

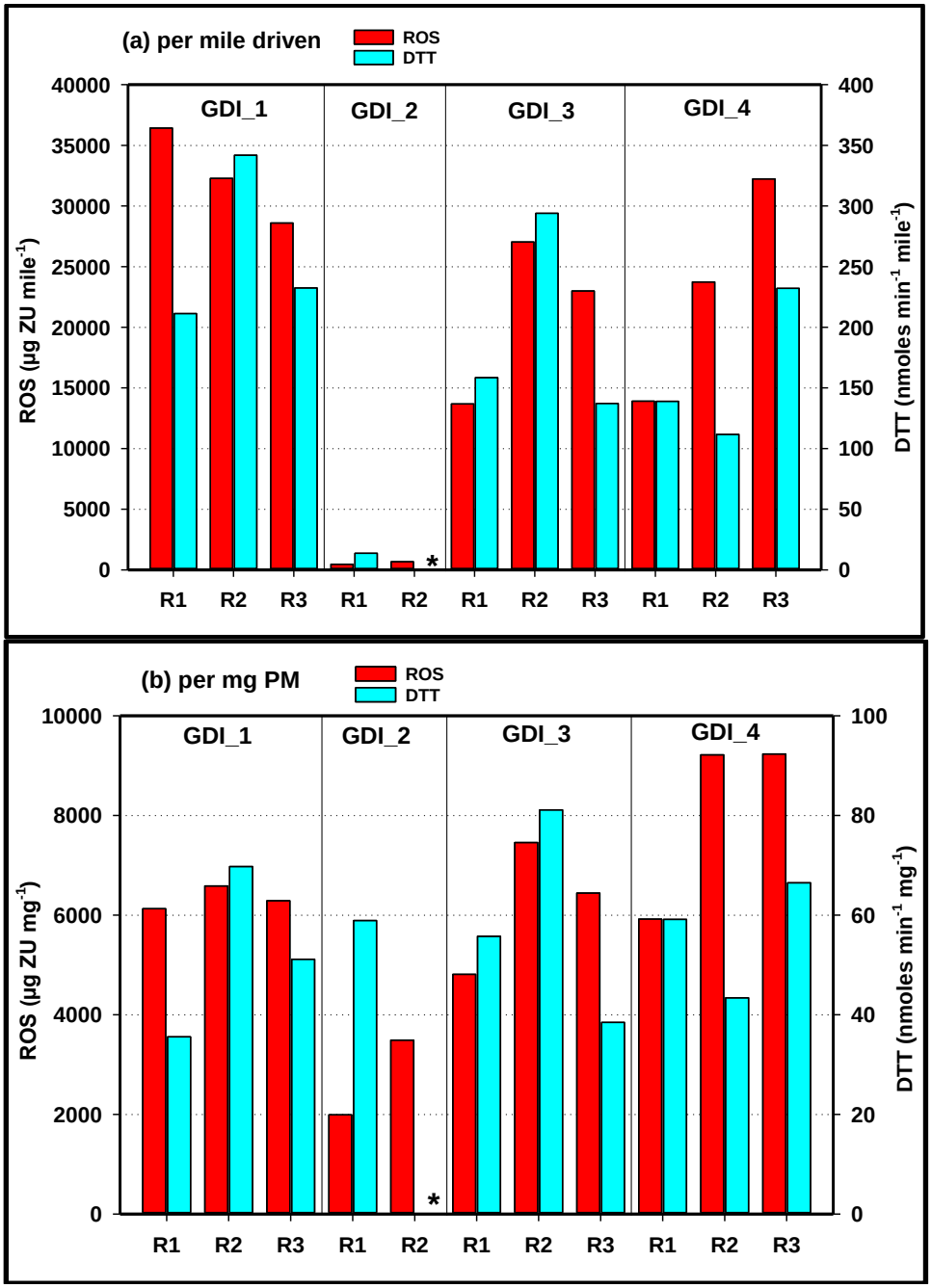

Figure 4-5 (a-b) Macrophage-based ROS and acellular DTT oxidation as two measures of oxidative potential of vehicular emissions. Data expressed on per mile basis (a) and per mg of PM mass (b), indicative of the intrinsic activity of the particles. R1 - R3 represent replicate samples collected for the same vehicle. Note that the asterisk (*) in the plot indicates that the assay was not performed due to insufficient PM mass

An approximately 3-fold range was observed for the macrophage-mediated ROS and 2-fold range for the DTT data (Fig. 5b), implying a general similarity and consistency of the intrinsic (per mass basis) oxidative activity of PM emissions from these GDI technology vehicles. Moreover, when data for the low PM emitter vehicle (GDI_2) is excluded, the data ranges for the other 3 vehicles substantially overlap and little to no correlation is apparent between these two independent metrics of oxidative potential (DTT and macrophage-ROS) for either per mile or per PM mass normalization method. This likely reflects differences in the inherent sensitivity of the DTT and macrophage-ROS assay to the suite of organic and inorganic drivers of ROS. As mentioned above, one of the four vehicles (GDI_2) exhibited significantly lower oxidative potential in both ROS assays, particularly for the per mile metric, due to its substantially lower PM emissions. It is clear, therefore, that the wide range in per mile oxidative potential emissions is driven by this low PM emitting vehicle - if excluded, oxidative potential emission factors are remarkably consistent across vehicles.

The PM mass-normalized ROS outcomes from these 4 light-duty vehicles can be put into context by comparing to previously-published results using the same assay for both ambient PM samples and PM emitted from heavy-duty vehicles (Saffari et al., 2014a). The macrophage-mediated ROS induced by the PM emitted from vehicles in this study averaged 6409 μg ZU mg-1, which is approximately mid-range of the values reported for a variety of urban ambient PM samples (Shafer et al., 2016), as well as for the ultrafine PM, the size range into which most vehicular emissions fall (Saffari et al., 2016; Daher et al., 2014). ROS ranged from 740 to 9200 μg ZU mg-1 in a large set of ambient urban

European PM samples (Shafer et al., 2016), a slightly wider, but overlapping range to that of the tailpipe samples from the current study. This finding is consistent with the hypothesis that, in urban centers dominated by vehicular-sourced PM, vehicular emissions likely contribute a significant fraction of the ROS activity of urban ambient PM due to the presence of relatively non-labile, redox active species. In contrast, the DTT results of the current study, with an average of 56 nmol min-1 mg-1, fall quite a bit higher than the reported activity of urban ambient PM from the above mentioned European study, which ranged from 5.2 to 20.0 nmol min-1 mg-1. Thus, the mass-normalized, i.e. intrinsic DTT activity of PM from these vehicles was 2-10-fold higher than the typical urban ambient sample, possibly due to the higher organic content of GDI tailpipe emissions in comparison to ambient aerosols, though PM age and particle-size contrasts are also important factors. Previous studies have shown that a large portion of DTT activity can be due to the presence of reactive organic compounds such as quinones and humic like substances (Ghio et al., 2012). A study of quasi-ultrafine particles ($dp < 0.25$ μm) representing source, urban, rural receptor and desert locations across the Los Angeles air basin concluded that water soluble organic carbon (WSOC), water insoluble organic carbon (WIOC), EC, and hopanes had a combined contribution that explained up to 88% of the DTT activity (Saffari et al., 2014b). It should be pointed out that the current study's data range for the mass-normalized DTT falls well within the range of DTT activities determined in other quasi-ultrafine particle studies, including a summer study characterizing diurnal trends in urban PM from downtown Los Angeles. This study also found a high correlation between DTT and WSOC (Verma et al., 2009) suggesting that organic components of vehicular emissions are likely

important drivers of their DTT activity. Therefore, as with the macrophage-ROS and metals, the current study's data is consistent with tailpipe emissions being a significant source, if not a dominant one, of DTT activity in urban ambient PM.

4.4.4. **Water Extractable Metals**

A total of 45 elements were characterized in the PM extracts, as shown in Table 4-1. Sulfur (S), which is sourced from both the fuel and lubricant oil (Pirjola et al., 2015) was the most abundant element, with an average emission factor of 29.9 µg/mile. The element with the second highest emission factor was iron (Fe) (averaging 12.4 µg/mile), followed by calcium (Ca), aluminum (Al), phosphorus (P), sodium (Na), potassium (K), and chromium (Cr) (averaging between 0.96 to 7.62 µg/mile). These elements can be emitted from several sources, including engine wear (abrasion from piston ring, cylinder liner, valves, etc.), combustion of fuel and lubricant oil, the lubricant oil additive package, and from tailpipe emission catalysts. Platinum-group element (PGE) emissions, primarily sourced from TWC, including those of platinum (Pt), palladium (Pd), and rhodium (Rh) were very low (averaging from 0.001 to 0.21 µg/mile). PGE emissions are released from the TWCs in PM form, primarily as the metal (oxidation state = 0) species, but oxides can represent a significant fraction (Hyde and Sankar, 2014).

Table 4-1 Emission factors (in ng per mile) for PM elements detected by ICPMS, ranked by the sum of the averages for each of the four vehicles. Quoted uncertainty is the standard deviation. Also included are correlation coefficients with the ROS and DTT methods for measuring generation of reactive oxygen species and ELISA protein expression. Correlation coefficients of >0.5 are highlighted in bold

	ng/mile				r^2			
	GDI_1	GDI_2	GDI_3	GDI_4	ROS	DTT	HMOX	TNF-α
S	56000±46000	1570±120	43700±21600	18500±17200	0.24	0.22	0.06	0.06
Fe	6800±4400	4500±1090	15900±11100	22400±24000	0.25	0.21	0.17	**0.51**
Ca	7210±920	5660±520	9410±900	8200±2260	0.19	0.18	0.03	0.13
Al	3550±640	3400±1660	2910±800	6960±4600	0.12	0.18	0.18	0.06
P	3570±1200	1140±50	3400±580	3310±1100	**0.59**	**0.61**	0	0.39
Na	2010±550	1790±0	2130±170	2040±1030	0.11	0.04	0.02	0.07
K	484±106	1720±43	1950±940	809±446	0.36	0.09	0.02	0.11
Zn	992±137	387±13	1670±600	869±535	0.33	0.41	0.01	**0.5**
Cr	1130±931	339±235	1420±850	966±731	**0.51**	0.4	0.01	0.41
Ti	891±153	354±22	848±645	395±172	0.24	**0.55**	0.18	0.39
Mg	744±130	585±158	578±269	545±252	0.15	0.46	0.1	0.49
Ni	441±256	168±119	667±411	823±716	0.39	0.32	0.1	**0.52**
Mo	627±85	101±26	571±154	141±75	0.41	0.43	**0.59**	0.14
Cu	162±28	101±6	359±117	326±212	0.24	0.2	0.12	0.39
Ce	259±61	23±2	297±171	285±235	**0.62**	**0.51**	0.01	**0.68**
Pd	123±12	13±2	395±94	327±193	0.26	0.16	0.17	0.29
Mn	96±30	59±21	227±99	212±214	0.23	0.24	0.08	0.48
Sr	254±41	22±9	26±8	46±20	0.44	0.32	0.44	0
Sn	87±51	44±1	129±43	66±2	0.16	0.28	0.01	0.22
La	91±23	7±4	40±27	106±85	**0.63**	0.4	0.03	0.35
Nd	41±10	4±1	43±25	22±20	**0.61**	**0.61**	0.15	0.49
W	12±5	17±3	30±15	25±20	0.04	0.14	0.12	**0.63**
Co	16±8	15±4	27±12	15±9	0.04	0.05	0.01	0.23
Li	16±1	8±6	9±0	38±10	0.22	0.08	0.47	0.01
Pb	17±7	8±5	21±7	24±11	0.14	0.08	0.13	0.04
Y	43±10	2±0	9±2	5±3	0.47	0.29	**0.54**	0
Pr	1±0	1±1	24±11	26±20	0.13	0.09	0.32	0.3
As	9±1	5±3	13±7	15±4	0.16	0.02	0.13	0.03
V	10±6	4±0	10±3	9±4	**0.54**	0.29	0.04	0.18
Ag	4±1	3±2	9±8	10±13	0.18	0.26	0.09	**0.62**
Sb	8±5	2±0	7±2	5±2	0.49	0.68	0.02	0.47
Rh	2±0	0±0	1±1	8±5	0.29	0.12	0.36	0.14
Rb	2±1	3±1	3±1	3±1	0	0.01	0.17	0.35

Redox-active transition metals, such as vanadium (V), chromium (Cr), manganese (Mn), iron (Fe), nickel (Ni), and copper (Cu) were measured at relatively high concentrations in all vehicles, with their emission factor sum averaging from 5.2 µg/mile to 24.7 µg/mile (a range comparable to that of measured variation in ROS activity). Redox-active transition metals are known to facilitate the generation of ROS that can damage cellular membrane lipids, proteins or enzymes, and DNA (Jomova et al., 2012), and importantly result in initiation of a pro-inflammatory cascade. The six redox-active transition metals listed above were weakly to moderately correlate with both the DTT and the ROS assay activities (r2 of 0.25 to 0.46 for DTT and r2 of 0.18 to 0.50 for ROS (Table 4-1). These results, though the sample number is small, contrast in-part to some previously reported chassis dynamometer data where both ROS and DTT assays showed good correlations with the redox-active transition metals (Karavalakis et al., 2017; Verma et al., 2010). Strong correlations were seen between the total sum of water-soluble metals and ROS (r2 of 0.85) and DTT (r2 of 0.92). Interestingly, molybdenum (Mo) was detected in relatively high levels compared to other metals (averaging at 0.36 µg/mile), with GDI_1 and GDI_3 having the highest emission concentrations, which were also the vehicles with the highest black carbon emissions. Mo-nanoparticles have been reported to induce significant cytotoxicity and generate ROS (Siddiqui et al., 2015). Under the present test conditions, it is possible that Mo also played some role in the generation of ROS both in the DTT and macrophage-ROS assays.

Several rare earth elements (Ce, La, Nd), as well as Cr and Ti, exhibited moderate correlations with both ROS and DTT activity. The similar reactivity profiles of ROS and

DTT lend support to the robustness of these correlations. These correlations may suggest a role for small insoluble particles in inducing oxidative stress, either directly, or by providing a catalytic particle surface.

4.4.5. Gene Market Expression Analysis

mRNA from the NR8383 macrophages exposed to the PM emitted by three of the four GDI vehicles (insufficient mass was available from the lowest-emitting vehicle – GDI_2) was analyzed for expression of 29 genes, including 2 housekeeping genes (Table S4-2). The genes selected for this study include those associated with oxidative stress and inflammatory signaling including asthma, as well as AhR and MAPK signaling markers. Overall, the vehicular emission-induced gene expression changes (i.e., fold regulation relative to the untreated controls) were quite low (with only 3 genes exhibiting regulation over 2-fold change), likely due in-part to the relatively low masses of PM available for the macrophage exposures and the relatively short, single-dose, exposure duration (one time-point at 4 hours). Collection of adequate PM mass from traditional chassis dynamometer is a serious problem in all toxicologically directed studies, particularly from modern low PM emitting vehicles. Though we extended collection periods as long as feasible and performed multiple experiments on a given vehicle, the mass available for chemical and toxicological characterization was typically less than 200 µg.

Of the gene categories listed above, the greatest regulation was observed within the oxidative stress signaling markers (Tables S4-3 & S4-4). The upregulation of NADPH oxidase 1 (Nox1) expression in 2 out of 3 vehicles, as well as quite consistent downregulation (2- to 3-fold in 5 out of 9 samples) of myeloperoxidase (MPO), both of

which play an important role in the respiratory burst signaling, confirm that the vehicular exhaust can lead to oxidative stress in macrophages (Hideki, 2008; Odobasic et al., 2016). The downregulation of MPO measured at 4 hours exposure likely reflects regulatory feedback signaling initiated after the induction of ROS production (as measured at 2.5h of exposure via the cellular ROS assay). The mRNA gene expression patterns in this very same exposure system can change within 1 hour (Sijan et al., 2015). In addition, a small upregulation of the anti-inflammatory cytokine IL-10 was observed in our data set, which could also suggest activation of protective mechanisms in response to the aerosol exposure. While the overall fold regulation range for a given marker in the current study was quite small, the gene expression data can be used to look for signaling patterns and/or sample relationships using tools like hierarchical clustering. Figure 4-6 presents such an analysis of the gene expression data. Replicate samples from the GDI_1 exhibit a very similar pattern of gene regulation, however, the replicates for the other two vehicles, especially GDI_3 exhibit more differentiated gene expression, which may be in part due to the small overall differences in gene expression between samples. Importantly, however, clustering confirmed that both MPO and NOX1 genes are co-regulated, in addition to several anti-oxidant (Gstp1, SOD2) and pro-inflammatory genes (Tnf, Il1b, Bcl6) that also appear co-regulated in these samples (Figure 4-6).

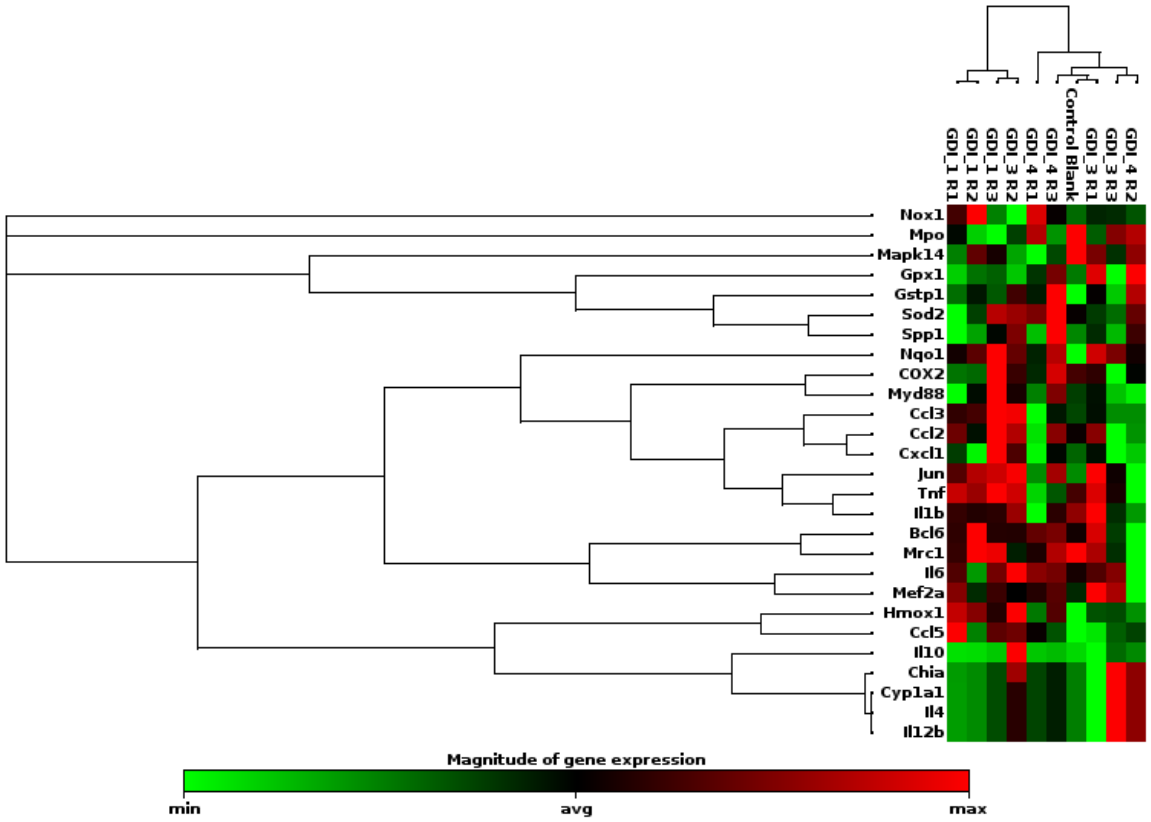

Figure 4-6 Non-supervised hierarchical clustering of gene regulation (mRNA level fold change relative to untreated control) upon 4h exposure to vehicular exhaust extracts of 3 vehicles. Dendrograms indicate co-regulated genes as well as similarities of gene expression patterns between individual samples

While the PCR-array analysis provides a robust and a relatively high throughput method for assessing the transcript regulation of multiple target genes at once, it is also quite sensitive to the timing of exposure, since, as noted earlier, gene expression changes on mRNA level can occur quite rapidly (Li et al., 2015). In addition, even a substantial increase at the mRNA level of a gene does not guarantee that an upregulation of a gene protein will also be observed, e.g. due to potential post-transcriptional regulatory steps. Therefore, it is useful to couple the PCR screening approach of identifying larger regulatory patterns (e.g., cluster analysis as presented above) with targeted protein measurements. To that end we employed ELISA technology, though its limitations include

relatively low sensitivity (high detection limit), which can often be prohibitively poor for protein targets with a low expression level. This problem was exacerbated by the low masses available from the chassis dynamometer trials.

Based on the PCR results and taking under consideration the character of protein targets, two of the genes discussed above were quantified via ELISA: the pro-inflammatory cytokine TNFα (Figure 4-7a) and a cytoprotective, anti-inflammatory and an antioxidant-response gene HMOX-1 (Figure 4-7b). Their expression was assessed in the NR8383 alveolar macrophages exposed for 6h to PM extracts from three of the four GDIs (GDI_2 samples had insufficient mass). The results presented (Fig. 7a and 7b) are corrected for the basal expression of these proteins measured in a corresponding untreated (buffer only) control. Since the low-emitting vehicle was excluded, the overall range for both the TNFα and HMOX-1 protein data was much smaller and more comparable across the vehicles than the ROS and DTT ranges that included the GDI_2. The TNFα protein level expressed as an emission factor (i.e., per mile) varied less than 3-fold across all samples (Fig. 7a) and the per car average results varied less than 2-fold. The 3-car average PM mass-normalized induction of TNFα protein secretion (274 pg/mg PM) is low in comparison to ambient PM studies that ranged from 100 to 300,000 pg/mg PM (Shafer et al., 2016; Heo et al., 2015).

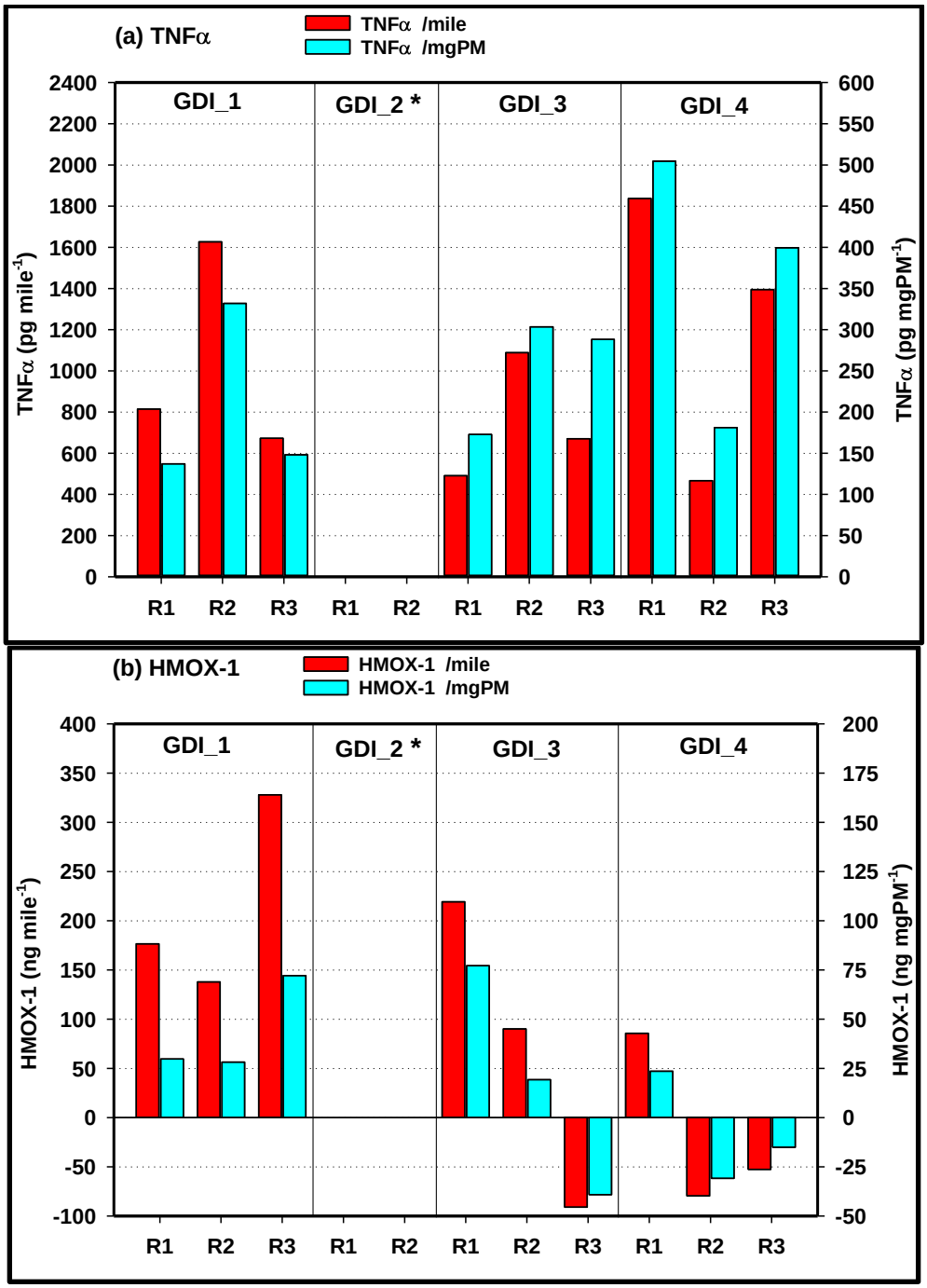

Figure 4-7 (a-b) Protein expression response (ELISA) corrected for the baseline expression of untreated control cells for tumor necrosis factor alpha (TNFα, a) and heme oxygenase 1 (HMOX-1, b) following 6h exposure to vehicular exhaust extracts. Note that the asterisk (*) in the plot indicates that the assay was not performed due to insufficient PM mass

The data range of HMOX-1 expression measured in our study was very similar to TNFα, with the exception of the per-car averages, where the range was slightly larger (due primarily to the negative, though not significantly different than zero, values resulting from a higher expression level of HMOX-1 in the untreated control (Fig. 7b). Relative to control, GDI_4 induced the lowest levels of HMOX-1 (-15 ng/mi), followed by GDI_3 (73 ng/mi) and GDI_1 (214 ng/mi). It is difficult to directly compare the protein levels of HMOX-1 expressed in this study to these induced by other aerosol materials due to the paucity of published information. However, several studies of diesel particulates, black carbon and crystalline silica reported an increase in expression of HMOX-1 in various exposure systems (Van Berlo et al., 2010; Koike et al., 2006; Fukui et al., 2016). In contrast, multiple studies have reported the effects of aerosols on both inflammatory cytokines and antioxidant response genes at the mRNA level (PCR analysis). Interestingly, a differential expression profile of pro-inflammatory TNFα and the oxidative stress-related HMOX-1 has been reported for both ambient PM, as well as gasoline vehicular exhaust and diesel exhaust particles (DEP) suggesting that the expression of oxidative stress markers is potentially driven by different components of PM than the pro-inflammatory markers (Heo et al., 2015; Hamad et al., 2016; Bisig et al., 2015; Totlandsdal et al., 2015).

Two redox active metals (Fe and Ni) were moderately correlated with TNFα expression (Table 4-1). Two rare earth (REE) elements (Ce with TNFα; and Y with HMOX-1) exhibit correlations with the measured proteins. Molybdenum was correlated with HMOX-1 expression, and as noted in the water extractable metals discussion, was present in the PM at relatively high concentrations. As noted previously, the REE findings

are consistent with those found with the oxidative activity metrics (ROS and DTT) and likely suggest a role for small insoluble particles in inducing oxidative stress, either directly or by providing a catalytic particle surface.

4.5. **Conclusions**

This work examined the physical and toxicological properties of particulate emissions from current technology GDI light-duty vehicles while operating over the LA92 driving cycle. Our results showed that three of the four GDI vehicles tested had PM emissions from 3 to 5 mg/mile, while one emitted about 0.2 mg/mile, thus showing the technical possibility for significant reductions. From an environmental standpoint, GDI vehicles are still an important source of ultrafine particles, especially in densely populated areas. Our findings showed that PM mass, particle number, and black carbon emissions during the cold-start phase of the LA92 cycle were higher than in the hot running or hot-start phases. In the case of the cleanest vehicle, the difference between cold-start and hot-start emissions was more than 10-fold. Under both hot and cold conditions, PM emission rates were highest at engine start and during the hard accelerations in the test cycle.

The toxicology metrics employed in this study indicate that at least for acute exposure, toxicity is relatively low in comparison to many ambient PM samples, both for ROS generation and for inflammatory potential. DTT and ROS follow a different activity profile across the samples which is likely due to contrasts in PM composition, but additional studies with larger statistical power will be needed to better resolve those relationships. Our transcript analysis suggests that by 4h of exposure protective mechanisms are at work trying to restore homeostasis: HMOX-1 is cyto-protective, an anti-

oxidant response battery gene, and also upregulates IL-10 (an anti-inflammatory cytokine, which we saw in one sample). The overall suite of toxicology measurements suggests a likely role for small insoluble particles in inducing oxidative stress, either directly or by providing a catalytic particle surface. Ultrafine particles can partition into the blood stream from the lungs and can travel to other organs including the brain – whole animal studies will be needed to address these systemic effects; effects on macrophages can be especially important since the microglia in the brain share some responses are key players in some neurodegenerative diseases.

4.6. **Acknowledgements**

The authors thank the following organizations and individuals for their valuable contributions to this study. We acknowledge funding from the South Coast Air Quality Management District (SCAQMD) under contract 15625. The authors thank Mr. Mark Villela and Daniel Gomez of the University of California, Riverside for their contribution in conducting the emissions testing for this program. We also wish to acknowledge Dr. Jocelyn Hemming of the UW-WSLH Environmental Toxicology Program for conducting the DTT analyses and assisting with the macrophage ROS and other assays; and Joel Overdier of the UW-WSLH Trace Element Research Group for performing the SF-ICPMS measurements.

4.7. **References**

Attar MA, Xu H. Correlations between particulate matter emissions and gasoline direct injection spray characteristics. Journal of Aerosol Science 2016;102:128-141.

Araujo JA, Nel AE. Particulate matter and atherosclerosis: role of particle size, composition and oxidative stress. Part Fibre Toxicol 2009;24.

Badshah H, Kittelson D, Northrop W. Particle emissions from light-duty vehicles during cold-cold start. SAE Technical Paper, 2016; 2016-01-0997.

Bahreini R, Xue J, Johnson K, Durbin T, Quiros D, Hu S, Huai T, Ayala A, Jung H. Characterizing emissions and optical properties of particulate matter from PFI and GDI light-duty gasoline vehicles. Journal of Aerosol Science 2015;90:144-153.

Bates JT, Weber RJ, Abrams J, Verma V, Fang T, Klein M, Tolbert PE. Reactive oxygen species generation linked to sources of atmospheric particulate matter and cardiorespiratory effects. Environ. Sci. Technol. 2015;49:13605-13612.

Barrientos, E.J.; Anderson, J.E.; Maricq, M.M.; Boehman, A.L. Particulate matter indices using smoke point for vehicle emissions with gasoline, ethanol blends, and butanol blends. Combustion and Flame 2016, 167, 308-319.

Bisig C, Steiner S, Comte P, Czerwinski J, Mayer A, , Petri-Fink A, Rothen-Rutishauser B. Biological effects in lung cells in vitro of exhaust aerosols from a gasoline passenger car with and without particle filter. Emission Control Science and Technology 2015;1:237-246.

Bisig C, Comte P, Gudel M, Czerwinski J, Mayer A, Muller L, Petri-Fink A, Rothen-Rutishauser B. Assessment of lung cell toxicity of various gasoline engine exhaust using a versalite in vitro exposure system. Environmental Pollution 2018;235:263-271.

Chan TW, Meloche E, Kubsh J, Brezny R. Black carbon emissions in gasoline exhaust and a reduction alternative with a gasoline particulate filter. Environ. Sci. Technol. 2014;48:6027-6034.

Charrier JG, Anastasio C. On dithiothreitol (DTT) as a measure of oxidative potential for ambient particles: evidence for the importance of soluble transition metals, Atmos. Chem. Phys. 2012;12:9321-9333.

Che W, Qiu H, Liu G, Ran Y, Zhang H, Zhang L, Wen W. Oxidative damage of the extracts of condensate particulate and semivolatile organic compounds from gasoline engine

exhausts on testicles of rats. Bulletin of Environmental Contamination and Toxicology 2009;83:42-47.

Chen L, Stone R, Richardson D. A study of mixture preparation and PM emissions using a direct injection engine fueled with stoichiometric gasoline/ethanol blends. Fuel 2012;96:120-130.

Cheng Y, Wang J, Zhuang R, Wu N. Analysis of combustion behavior during cold-start and warm-up process of SI gasoline engine. SAE Technical Paper 2001;2001-01-3557.

Daher N, Saliba NA, Shihadeh AL, Jaafar M, Baalbaki R, Shafer MM, Schauer JJ, Sioutas C. Oxidative potential and chemical speciation of size-resolved particulate matter (PM) at nearfreeway and urban background sites in the greater Beirut area. Science of the Total Environment 2014;470−471:417−426.

Diaz EA, Chung Y, Papapostolou V, Lawrence J, Long MS, Hatakeyama V, Gomes B, Calil Y, Sato R, Koutrakis P, Godleski JJ. Effects of fresh and aged vehicular exhaust emissions on breathing pattern and cellular responses-pilot single vehicle study. Inhalation Toxicology 2012;25:288-295.

Freire J, Ajona D, De Biurrun G, Agorreta J, Segura V, Guruceaga E, Bleau AM, Pio R, Blanco D, Montuega LM. Silica-induced chronic inflammation promotes lung carcinogenesis in the context of an immunosuppressive microenvironment. Neoplasia 2013;15:913-924.

Fukui H, Endoh S, Shichiri M, Ishida N, Hagihara Y, Yoshida Y, Iwahashi H, Horie M. The induction of lipid peroxidation during the acute oxidative stress response induced by intratracheal instillation of fine crystalline silica particles in rats. Toxicol Ind Health 2016;32:1430-1437.

Ghio AJ, Carraway MS, Madden MC. Composition of air pollution particles and oxidative stress in cells, tissues, and living systems. J Toxicol Environ Health B Crit Rev 2012;1:1-21.

Hamad SH, Schauer JJ, Antkiewicz DS, Shafer MM, Kadhim AKh. ROS production and gene expression in alveolar macrophages exposed to PM(2.5) from Baghdad, Iraq: Seasonal trends and impact of chemical composition. Science of the Total Environment 2016;543:739-745.

He X, Ratcliff MA, Zigler BT. Effects of gasoline direct injection engine operating parameters on particle number emissions. Energy and Fuels 2010;26:2014-2027.

Heo J, Antkiewicz DS, Shafer MM, Perkins DAK, Sioutas C, Schauer JJ. Assessing the role of chemical components in cellular responses to atmospheric particle matter (PM)

through chemical fractionation of PM extracts. Analytical and Bioanalytical Chemistry 2015; 405:5953-5963.

Herner JD, Hu S, Robertson WH, Huai T, Oliver Chang MC, Rieger P, Ayala A. Effect of advanced aftertreatment for PM and NOx reduction on heavy-duty diesel engine ultrafine particle emissions. Environ. Sci. Technol. 2011;45:2413-2419.

Hideki S. Structure, regulation and evolution of Nox-family NADPH oxidases that produce reactive oxygen species. FEBS Journal 2008;275:3249-3277.

Hyde TL, Sankar G. Solid state platinum speciation from x-ray absorption spectroscopic studies of fresh and road aged three way and diesel vehicle emission control catalysts. In: Platinum Metals in the Environment, Environmental Science and Engineering (ESE) book series, Springer. pp 289-308.

Jomova K, Baros S, Valko M. Redox active metal-induced oxidative stress in biological systems. Transition Met Chem 2012;37:127-134.

Karavalakis G, Short D, Vu D, Villela M, Asa-Awuku A, Durbin TD. Evaluating the regulated emissions, air toxics, ultrafine particles, and black carbon from SI-PFI and SI-DI vehicles operating on different ethanol and iso-butanol blends. Fuel 2014, 128, 410-421.

Karavalakis G, Short D., Vu D, Russell R, Hajbabaei M, Asa-Awuku A, Durbin TD. Evaluating the effects of aromatics content in gasoline on gaseous and particulate matter emissions from SI-PFI and SI-DI vehicles. Environ. Sci. Technol. 2015a;49:7021-7031.

Karavalakis G, Short D, Vu D, Russell R,L, Asa-Awuku A, Jung H., Johnson KC, Durbin TD. The impact of ethanol and iso-butanol blends on gaseous and particulate emissions from two passenger cars equipped with spray-guided and wall-guided direct injection SI (spark ignition) engines. Energy 2015b;82:168-179.

Karavalakis K, Gysel N, Schmitz DA, Cho AK, Sioutas C, Schauer JJ,; Cocker DR, Durbin TD. Impact of biodiesel on regulated and unregulated emissions, and redox and proinflammatory properties of PM emitted from heavy-duty vehicles. Science of the Total Environment 2017;584-585:1230-1238.

Koczak, J.; Boehman, A.; Brusstar, M. Particulate emissions in GDI vehicle transients: An examination of FTP, HWFET, and US06 measurements. SAE Technical Paper, 2016, 2016-01-0992.

Koike E, Kobayashi T. Chemical and biological oxidative effects of carbon black nanoparticles. Chemosphere 2006;65:946-951.

Li Y, Varala K, Coruzzi GM. From milliseconds to lifetimes: tracking the dynamic behavior of transcription factors in gene networks. Trends Genet. 2015;31:509-515.

Lund, A.K.; Knuckles, T.L.; Akata, C.O.; Shohet, R.; McDonald, J.D.; Gigliotti, A.; Seagrave J.C.; Campen, M.J. Gasoline exhaust emissions induce vascular remodeling pathways involved in atherosclerosis. Toxicological Sciences 2007, 95, 485-494.

Maikawa CL, Zimmerman N, Rais K, Shah M, Hawley B, Pant P, Jeong CH, Delgado-Saborit JM, Volkens J, Evans G, Wallace JS, Godri Pollitt KJ. Murine precision-cut lung slices exhibit acute responses following exposure to gasoline direct injection engine emissions. Science of the Total Environment 2016;568:1102-1109.

Odobasic D, Kitching AR, Holdsworth SR. Neutrophil-Mediated Regulation of Innate and Adaptive Immunity: The Role of Myeloperoxidase. Journal of Immunology Research 2016, Article ID 2349817, 11 pages, 2016. doi:10.1155/2016/2349817

Peckham M, Finch A, Campell B, Price P, Davies MT. Study of particle number emissions from a turbocharged gasoline direct injection (GDI) engine including data from a fast-response particle size spectrometer. SAE Technical Paper, 2011;2011-01-1224.

Piock, W.; Hoffmann, G.; Berndorfer, A.; Salemi, P.; Fusshoeller, B. Strategies towards meeting future particulate matter emission requirements in homogeneous gasoline direct injection engines. SAE Int. J. Engines 2011, 4, 1455-1468.

Pirjola, L.; Karjalainen, P.; Heikkila, J.; Saari, S.; Tzamkiozis, T.; Ntziachristos, L.; Kulmala, K.; Keskinen, J.; Ronkko, T. Effects of fresh lubricant oils on particle emissions emitted by a modern gasoline direct injection passenger car. Environ. Sci. Technol. 2015, 49, 3644-3652.

Quiros DC, Zhang S, Sardar S, Kamboures MA, Eiges D, Zhang M, Jung HS, Mcarthy MJ, Chang MCO, Ayala A, Zhu Y, Huai T, Hu S. Measuring particulate emissions of light duty passenger vehicles using integrated particle size distribution (IPSD). Environ. Sci. Technol. 2015;49:5618-5627.

Reed MD, Barret EG., Campen MJ, Divine KK, Gigliotti AP, McDonald JD, Seagrave JC, Mauderly JL, Seilkop SK, Swenberg JA. Health effects of subchronic inhalation exposure to gasoline engine exhaust. Inhalation Toxicology 2008;20:1125-1143.

Rohr AC, Wyzga RE. Attributing health effects to individual particulate matter constituents. Atmospheric Environment 2012;62:130-152.

Saffari A, Daher N, Shafer MM, Schauer JJ, Sioutas C. Global Perspective on the Oxidative Potential of Airborne Particulate Matter: A Synthesis of Research Findings. Environ. Sci. Technol. 2014a;48:7576−7583.

Saffari A, Daher N, Shafer MM, Schauer JJ, Sioutas C. Seasonal and spatial variation in dithiothreitol (DTT) activity of quasi-ultrafine particles (PM0.25) in the Los Angeles Basin and its association with chemical species. Journal of Environmental Science and Health, Part A 2014b;49:441−451.

Saffari A, Hasheminassab S, Shafer MM, Schauer JJ, Chatila, TA, Sioutas C. Nighttime aqueous-phase secondary organic aerosols in Los Angeles and its implication for fine particulate matter composition and oxidative potential. Atmospheric Environment 2016;113:112-122.

Sakai S, Hageman M, Rothamer D. Effect of equivalence ratio on the particulate emissions from a spark-ignited, direct-injected gasoline engine. SAE Technical Paper, 2013;2013-01-1560.

Seagrave JC., McDonald JD, Gigliotti AP, Nikula KJ, Seilkop SK Curevich M, Mauderly JL. Mutagenicity and in vivo toxicity of combined particulate and semivolatile organic fractions of gasoline and diesel engine emissions. Toxicological Sciences 2002;70:212-226.

Shafer MM, Hemming JDC, Antkiewicz DS, Schauer JJ. Oxidative potential of size-fractionated atmospheric aerosol in urban and rural sites across Europe. Faraday Discuss. 2016;189:381.

Siddiqui MA, Saquib Q, Ahamed M, Farshori NN, Ahmad J, Wahab R, Khan ST, Alhadlaq HA, Musarrat J, Al-Khedhairy AA. Molybdenum nanoparticles-induced cytotoxicity, oxidative stress, G2/M arrest, and DNA damage in mouse skin fibroblast cells (L929). Colloids and Surfaces B: Biointerfaces 2015;125:73-81.

Sijan Z, Antkiewicz DS, Heo J, Kado NY, Schauer JJ, Sioutas C. and Shafer MM. An In Vitro alveolar macrophage assay for the assessment of inflammatory cytokine expression induced by atmospheric particulate matter. Environ. Toxicol. 2015;30:836–851.

Sobotowski RA, Butler AD, Guerra Z. A pilot study of fuel impacts on PM emissions from light-duty gasoline vehicles. SAE Technical Paper, 2015;2015-01-9071.

Sonntag DB, Baldauf RW, Yanca CA, Fulper CR. Particulate matter speciation profiles for light-duty gasoline vehicles in the United States. Journal of the Air & Management Association 2014;64:529-545.

Su J, Lin W, Sterniak J, Xu M, Bohac SV. Particulate matter emission comparison of spark ignition direct injection (SIDI) and port fuel injection (PFI) operation of a boosted gasoline engine. J. Eng. Gas Turbines Power 2014;136:091513-1-091513-6.

Szybist JP, Youngquist AD, Barone TL, Storey JM, Moore WR,; Foster M, Confer K. Ethanol blends and engine operating strategy effects on light-duty spark ignition engine particle emissions. Energy and Fuels 2011;25:4977-4985.

Tamagawa E, Bai N, Morimota K, Gray C, Mui T, Yatera K, Zhang X, Xing L, Li Y, Laher I, Sin DD, Man SFP, van Eeden SF. Particulate matter exposure induces persistent lung inflammation and endothelial dysfunction. American Journal of Physiology: Lung Cellular and Molecular Physiology, 2008;295:L79-L85.

Tan C, Xu H,; Ma H, Ghafourian A. Investigation of VVT and spark timing on combustion and particle emission from a GDI engine during transient operation. SAE Technical Paper, 2014;2014-01-1370.

Tzamkiozis T, Stoeger T, Cheung K, Ntziachristos L, Sioutas C, Samaras Z. Monitoring the inflammatory potential of exhaust particles from passenger cars in mice. Inhalation Toxicology 2010;22:59-69.

Totlandsdal AI, Låg M, Lilleaas E, Cassee F, Schwarze P. Differential proinflammatory responses induced by diesel exhaust particles with contrasting PAH and metal content. Environ Toxicol. 2015;30:188-196.

Van Berlo D, Albrecht C, Knaapen AM, Cassee FR, Gerlofs ME, Kooter IM, Palomero-Gallagher N, Bidmon HJ, van Schooten FJ, Krutmann J, Schins RPF. Comparative evaluation of the effects of short-term inhalation exposure to diesel engine exhaust on rat lung and brain. Archives of Toxicology 2010;84:553-562.

Verma V, Ning Z, Cho AK, Schauer JJ, Shafer MM, Sioutas C. Redox activity of urban quashi-ultrafine particles from primary and secondary sources. Atmospheric Environment 2009;43:6360-6368.

Verma V, Shafer MM, Schauer JJ, Sioutas C. Contribution of transition metals in the reative oxygen species activity of PM emissions from retrofitted heavy-duty vehicles. Atmospheric Environment 2010;44:5165-5173.

Wang X, Grose MA, Caldow R, Osmondson BL, Swanson JJ, Chow JC, Watson JG, Kittelson DB, Li Y, Xue J, Jung H, Hu S, Improvement of Engine Exhaust Particle Sizer (EEPS) size distribution measurement – II. Engine exhaust particles. Journal of Aerosol Science 2016;92:83-94.

Xu F, Chen L, Stone R. Effects of a catalytic volatile particle remover (VPR) on the particulate matter emissions from a direct injection spark ignition engine. Environ. Sci. Technol. 2011;45:9036-9043.

Xue J.; Quiros D, Wang X,; Durbin TD, Johnson KC, Karavalakis G, Hu S, Huai T, Ayala A.; Jung HS. Using a new inversion matrix for a fast-sizing spectrometer and a photo-acoustic instrument to determine suspended particulate mass over a transient cycle for light-duty vehicles. Aerosol Science and Technology 2016;50:1227-1238.

Zinola S, Raux S, Leblanc M. Persistent particle number emissions sources at the tailpipe of combustion engines. SAE Technical Paper 2016;2016-01-2283.

Zhang S, McMahon W. Particulate emissions for LEV II light-duty gasoline direct injection vehicles. SAE Int. J. Fuels Lubr. 2012;5:637-646.

4.8. **Supporting Information**

4.8.1. **Emissions Analysis**

PM measurements were made on both a mass and number basis. PM mass samples were collected cumulatively over the entire length of the LA92 cycle, with one sample collected for each test. Total PM mass samples were coll0ected using 47-mm polytetrafluoroethylene (PTFE) filters (Whatman) and weighed with a 1065-compliant microbalance in a temperature and humidity controlled clean chamber meeting 1065 requirements. Buoyancy corrections for barometric pressure differences were also made for the PM filter weights as per CFR 1065.

Total particle number was measured using a TSI 3776 ultrafine-Condensation Particle Counter (CPC) with a 2.5 nm cut point. The instrument operated at a flowrate of 1.5 L/min. Solid particle number counts were measured with the use of a catalytic stripper. The catalytic stripper both vaporizes volatile species and oxidizes them, and hence more efficiently removes volatiles from the sample than thermal treatment alone. For this study, the catalytic stripper used was 40 mm long with a diameter of 17 mm and was based on a cordierite monolith with a 400 cpsi cell density and a 6 mils substrate thickness. It had both oxidation and sulfur storage capability, but its exact chemical composition was unknown. The particular unit was characterized according to the protocol outlined by Amanatidis et al. (2013) and was deemed appropriate for the measurements of this study. The particles were counted downstream of the catalytic stripper with a TSI 3776 ultrafine CPC at a flow rate of 1.5 L/min. An ejector diluter was used to collect particle number samples from the CVS tunnel for the GDI vehicles.

Real-time particle size distributions were obtained using an Engine Exhaust Particle Sizer (EEPS) spectrometer. The EEPS (TSI 3090, firmware version 8.0.0) was used to obtain real-time second-by-second size distributions between 5.6 to 560 nm. Particles were sampled at a flow rate of 10 L/min, which is considered to be high enough to minimize diffusional losses. They were then charged with a corona charger and sized based on their electrical mobility in an electrical field. Concentrations were determined through the use of multiple electrometers. In this study, the measured electrometer currents over 22 electrometers were inverted to particle size distributions into 32 bins using two inversion matrices, known as Default Matrix or Soot Matrix (Xue et al., 2015). A detailed mathematical description of how the inversion matrix converts electrometer signals to size distributions is given elsewhere (Wang et al., 2016). PM mass measurements based on the integrated particle size distribution (IPSD) method were made according to Xue et al. (2016).

Real-time soot or black carbon emissions were measured using an AVL Micro-Soot Sensor (MSS). The MSS is an instrument that measures soot mass concentration at a frequency of one Hertz basis using a photo acoustic detection technique, where the light-absorbing PM components (such as soot particles) are exposed to laser light that is periodically modulated at the acoustical resonant frequency (Schindler et al., 2004). The instrument is designed to measure soot concentrations down to ~5µg/m3, and operates at a flow rate of 2 L/min.

4.8.2. **PM Sampling and Extraction Protocol**

Filters were transported on ice to the University of Wisconsin, Madison, where they were extracted in ultra-pure MQ water using the following protocol. After a short mix on a vortexer and a 15 min sonication period, the filter/PM-suspensions were agitated overnight on a platform table shaker isolated from light. The filter-suspensions were sonicated again post-leaching and the unfiltered PM suspensions were then sub-sampled for the targeted analyses. Portions of the PM extracts were digested and analyzed for 43 elements using magnetic-sector inductively-coupled plasma mass spectrometry (SF-ICPMS) (Okuda et al., 2014). The reactive oxygen species (ROS) generated by these extracts were quantified with both a chemical method that measures the consumption rate of dithiothreitol, or DTT, and an in vitro method that measures PM-induced production of ROS via a fluorescent probe in a rat alveolar macrophage (NR8383) cell line. More details on the ROS and DTT protocols can be found in Shafer et al. (2016).

In addition to the oxidative potential measurements, the cells exposed to the PM sample extracts were assessed for signs of overt cytotoxicity via two well-established approaches: (a) propidium iodide (PI; Invitrogen, ThermoFisher Scientific) nucleic acid staining using flow cytometry, (b) the MTT assay (Molecular Probes Vybrant MTT Cell Proliferation Assay Kit) using a 96-well plate format and the absorbance plate reader. Manufacturer's instructions were followed for both methods and efforts were made to match the handling and sample incubation conditions that the cells undergo during the ROS assay. Both methods showed only minimal increase in cytotoxicity from the PM sample exposure (compared with the untreated control cells) ranging from 0 to 15% (data not shown).

The expression (quantified as fold regulation relative to buffer control) of 29 genes (Table S4-2) in NR8383 macrophages exposed for 4 hours to engine PM extracts was determined using Qiagen's Custom Rat RT2 Profiler™ PCR Array (SABiosciences/Qiagen, Alameda,CA, USA Cat#: CAPR13658) method according to the manufacturer's protocol. The expression of 25 of these genes was deemed quantifiable and included genes associated with NRF-2-mediated anti-oxidant response, inflammation/immune response, AhR signaling, asthma, and MAPK signaling. Fold regulation indicates the difference in the amount of mRNA produced by the macrophages relative to the buffer-exposed control cells. Values greater than one indicate enhanced response ("up-regulation") relative to the control, and values less than one indicate a diminished response ("down-regulation"). Fold changes are reported all as positive numbers where a fraction of one is down-regulation. Finally, expression of two specific proteins, tumor necrosis factor alpha (TNFα) and heme oxygenase 1 (HMOX-1), produced by the NR8383 cells exposed for 6h to the PM extracts was quantified via ELISA methods (BD OptEIATM, Cat# C560479, and LifeSpan Biosciences, Inc. Cat# LS-F11649, respectively). The ELISA analyses were performed according to the manufacturer's instructions on PM samples from three of the four GDI vehicles, as insufficient PM mass was collected from the lowest-emitting vehicle (GDI_2).

4.8.3. **Quantitative RT-PCR Gene Expression Analysis**

Macrophages (NR8383 cells) were exposed to PM suspensions and collected as described previously (Sijan et al., 2015). Briefly, cells were plated into a 24-well plate at a density of 1 × 106 cells well -1 and exposed to 500 μL of PM extract or control solution

for 4h. Afterwards supernatants were aspirated and the adherent cells were collected using cell scrapers (Leap Biosciences, Palo Alto, CA, USA). The contents of two replicate wells were combined in a nuclease-free microfuge tube and flash-frozen in liquid nitrogen.

Total RNA was then extracted and purified using the RNeasy Mini Kit (Qiagen, Alameda, CA, USA) following the manufacturer's instructions. The concentration of the diluted RNA subsample was spectrophotometrically quantified at 260 nm, after which RNA was reverse-transcribed to the first strand cDNA using the RT2 First Strand Kit as instructed by the manufacturer (Qiagen, Alameda, CA, USA).

We then applied carefully designed Qiagen's RT2 ProfilerTM custom PCR Array to quantify the expression of 27 genes targeting several potential toxicity pathways (SABiosciences/Qiagen, Alameda,CA, USA Cat#: CAPR13658) including Nrf2-mediated oxidative stress (HMOX-1, GPX1- GSTP-1 and NQO-1), endogenous ROS production (NOX-1 and MPO), immune response (TNF- α, IL1β, IL-4, IL-6, COX-2, MCP-1 (CCL2), MIP-1 α (CCL3), MyD88, IL-10, IL-12β and Spp1), Ahr (CYP1A1, Bcl6, RANTES (CCl5), GRO α (CXCl1)), MAPK (c-Jun, MEF-2 and p38), and alternative macrophage activation (Mrc1, Chia). Two housekeeping genes (Rplp1 and Ldha), as well as internal quality controls for genomic contamination, reverse transcription efficiency control and PCR reproducibility were included with each array.

Quantitative Real Time-Polymerase Chain Reaction (qRT-PCR) was performed with the RT2 SYBR Green/ROX Master mix using an Applied Biosystems Instrument (7500 Fast). The threshold and baseline values were chosen based on the results of all the arrays run for the study and manually fixed across all the samples, ensuring that the 2(-

Delta Delta C(T)) method (Livak and Schmittgen, 2001) can be applied for quantification. The Ct values obtained in this manner were used for the fold change analysis and the average of two housekeeping genes was used for normalization of the Ct values of all target genes on the same array plate according to the following equation:

$2^{-\Delta Ct} = 2 - [Ct\ (GOI) - Avg\ Ct\ (HKG)]$ where Ct (GOI) represents the raw Ct value of the gene of interest and the Avg Ct (HKG) represents the average Ct value for housekeeping genes. The gene expression of the field blank was chosen as the control to which all of the sample gene expression was compared (as fold changes relative to control).

4.8.4. **Supplemental Tables**

Table S4-1 Main technical specifications of the test vehicles

	Hyundai Accent (GDI_1)	Honda Accord (GDI_2)	Kia Soul (GDI_3)	Chevrolet Impala (GDI_4)
Model Year	2012	2012	2012	2012
Displacement, L	1.8	3.6	2.0	3.5
Cylinders/configuration	4, inline	V6	4, inline	V6
Injection system	DI, wall-guided	DI, wall-guided	DI, wall-guided	DI, wall-guided
Horsepower, hp	140 at 6500 rpm	300 at 6500 rpm	148 at 6500 rpm	365 at 5000 rpm
Torque, Nm	173 at 4300 rpm	355 at 5300 rpm	183 at 4500 rpm	569 at 2500 rpm
Mileage	4,524	24,315	11,046	9,560
Emission Standards	Tier 2, Bin 2	LEVII, SULEV	LEVII, SULEV	Tier 2, Bin 4

Table S4-2 Comprehensive list of the gene targets of the custom PCR array from Qiagen (CAPR 13658)

Gene Symbol	Alias	Refseq #	Official Full Name	Qiagen RT2 Catalog Number
Hmox1	HEOXG/Heox/Hmox/Ho-1/Ho1/hsp32	NM_012580	Heme oxygenase (decycling) 1	PPR57718
Sod2	-	NM_017051	Superoxide dismutase 2, mitochondrial	PPR57578
Gpx1	GSHPx/GSHPx-1	NM_030826	Glutathione peroxidase 1	PPR45366
Gstp1	GST-P/Gst3/Gstp/Gstp2	NM_012577	Glutathione S-transferase pi 1	PPR52644
Nqo1	Dia4	NM_017000	NAD(P)H dehydrogenase, quinone 1	PPR45314
Nox1	-	NM_053683	NADPH oxidase 1	PPR50029
Mpo	-	NM_001107036	Myeloperoxidase	PPR50140
Tnf	RATTNF/TNF-alpha/Tnfa	NM_012675	Tumor necrosis factor (TNF superfamily, member 2)	PPR06411
Il1b	-	NM_031512	Interleukin 1 beta	PPR06480
Il6	ILg6/Ifnb2	NM_012589	Interleukin 6	PPR06483
COX2	COII	AW141241	COXII	PPR60011
Ccl2	MCP-1/Scya2/Sigje	NM_031530	Chemokine (C-C motif) ligand 2	PPR06714
Ccl3	MIP-1a/Scya3	NM_013025	Chemokine (C-C motif) ligand 3	PPR06717
Myd88	-	NM_198130	Myeloid differentiation primary response gene 88	PPR48967
Cyp1a1	AHH/AHRR/CP11/CYP1/Cyp 45c/Cypc45c/P-450MC/P1-450/P450-C/P450DX	NM_012540	Cytochrome P450, family 1, subfamily a, polypeptide 1	PPR57580
Bcl6	-	NM_001107084	B-cell CLL/lymphoma 6	PPR51800
Ccl5	Rantes/Scya5	NM_031116	Chemokine (C-C motif) ligand 5	PPR06854
Cxcl1	CINC-1/Gro1	NM_030845	Chemokine (C-X-C motif) ligand 1 (melanoma growth stimulating activity, alpha)	PPR06663
Il4	Il4e12	NM_201270	Interleukin 4	PPR56680
Mrc1	-	NM_001106123	Mannose receptor, C type 1	PPR44294
Chia	-	NM_207586	Chitinase, acidic	PPR49637
Rplp1	-	NM_001007604	Ribosomal protein, large, P1	PPR42363
Ldha	Ldh1	NM_017025	Lactate dehydrogenase A	PPR56603
Jun	-	NM_021835	Jun oncogene	PPR53221
Il10	IL10X	NM_012854	Interleukin 10	PPR06479
Il12b	Il12	NM_022611	Interleukin 12b	PPR06446
Spp1	OSP	NM_012881	Secreted phosphoprotein 1	PPR44222
Mef2a	-	NM_001014035	Myocyte enhancer factor 2a	PPR62504
Mapk14	CRK1/CSBP/CSPB1/Csbp1/Csbp2/Exip/Hog/Mxi2/Prkm14/Prkm15/RK/Sapk2A/p38	NM_031020	Mitogen activated protein kinase 14	PPR52703

Table S4-3 Fold regulation of gene expression in NR8383 macrophages following a 4h exposure to vehicular exhaust extracts from 3 different GDI vehicles (excluding genes whose expression was not altered by the exposure). Red highlights mark gene expression that is up-regulated more than 1.7-fold and green highlights mark the downregulation of over 1.7 fold

	GDI_1			GDI_3			GDI_4		
Gene	**ID#1**	**ID#2**	**ID#3**	**ID#1**	**ID#2**	**ID#3**	**ID#1**	**ID#2**	**ID#3**
TNF a	1.0849	1.0561	1.1199	1.0923	-1.2289	1.0893	-1.0324	-1.2735	-1.1165
cxcl1	1.0331	-1.1361	1.2922	1.0655	-1.1421	1.1442	-1.1485	-1.0958	1.0752
MPO	-1.5752	-2.7846	-3.4004	-1.9353	-1.1171	-1.792	-1.2057	-1.1182	-2.2646
IL-10	-1.028	-1.0113	1.0405	-1.1256	1.0466	**2.3308**	1.3128	1.2176	1.0764
Hmox1	1.4118	1.3582	1.2643	1.1512	1.1235	1.4659	1.1645	1.0958	1.3049
Nox1	1.4914	**2.0392**	-1.0735	1.1931	1.9335	-1.7542	1.1798	1.0580	1.3185

Table S4-4 Functional categories of the genes assessed via PCR Array, though many genes belong to multiple categories

Nrf2-Response/Antioxidant Response Genes	HMOX-1, SOD-2, GPX1, GSTP-1, NQO-1
Endogenous ROS Production	NOX-1, MPO
Inflammation/Immune Response	TNFα, IL1β, IL-6, COX-2, MCP-1 (CCl2), MIP-1α (CCL3), MyD88 IL-10, IL-12β, Spp1
AhR Pathway (Th2 & Metabolism)	CYP1A1, Bcl6, RANTES (CCL5), GROα (CXCl1), IL-4,
MAPK Pathway	c-Jun, MEF-2a, p38
Alternative Macrophage Activation/Asthma	Mrc1, Chia

4.8.5. **Supplemental Figures**

A

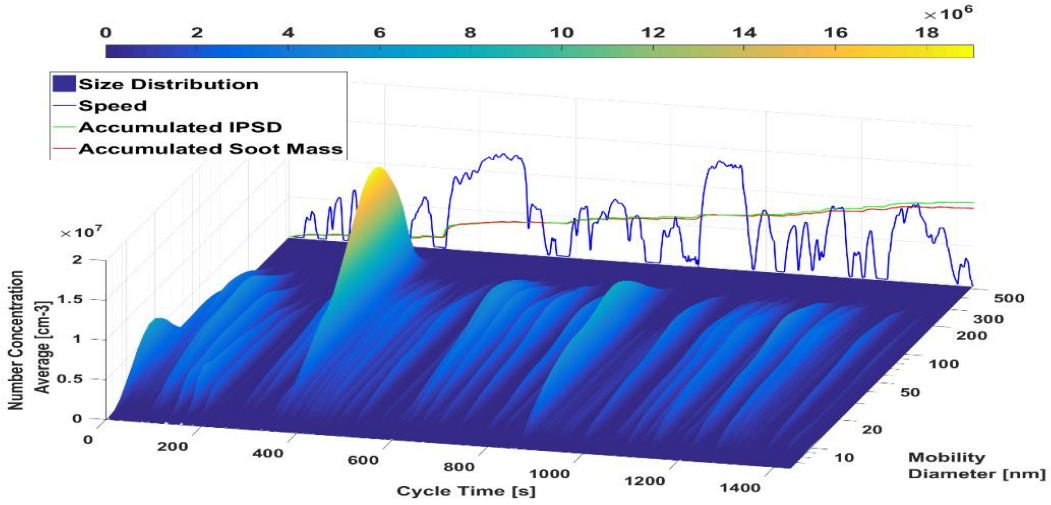

B

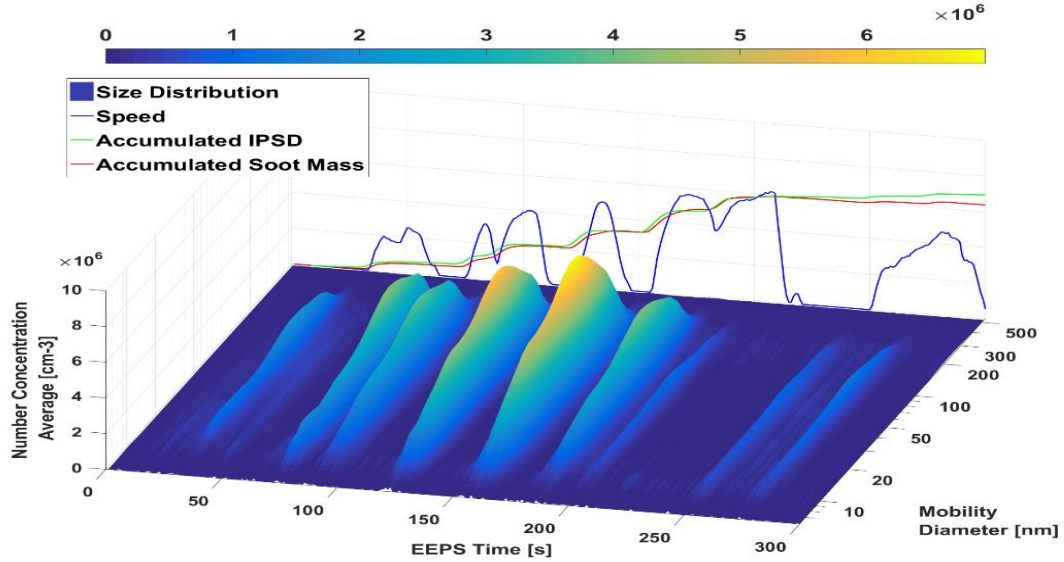

Figure S4-1 (a-b) Particle size distributions for GDI_1 for phases 1 and 2 (top panel, A) and phase 3 (bottom panel, B) of the LA92 cycle. The drive trace is included for visual reference, as well as the cumulative soot mass and IPSD mass emissions. Note the factor of ten difference between the vertical scales of the top and bottom panels

A

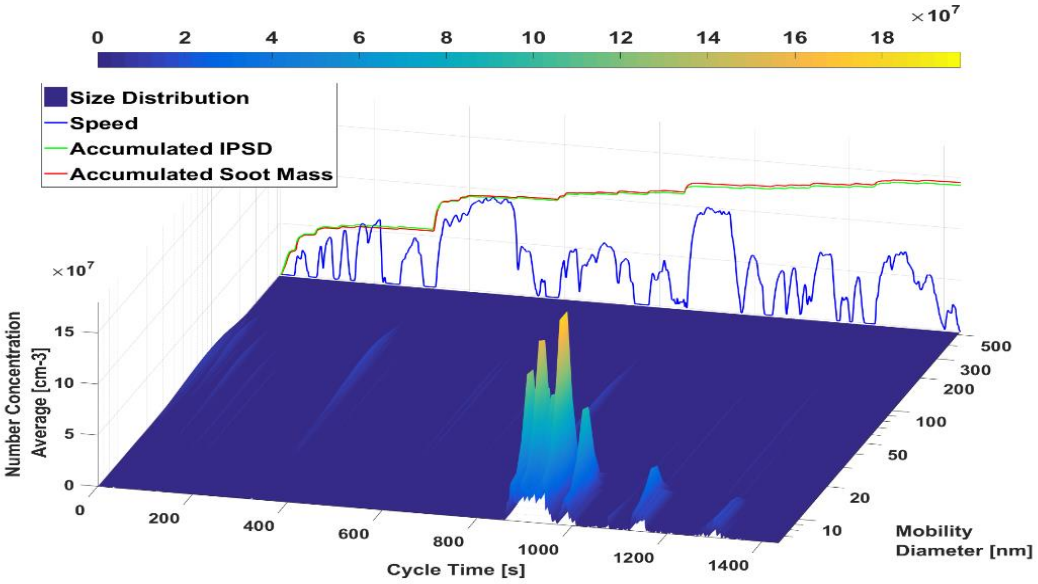

B

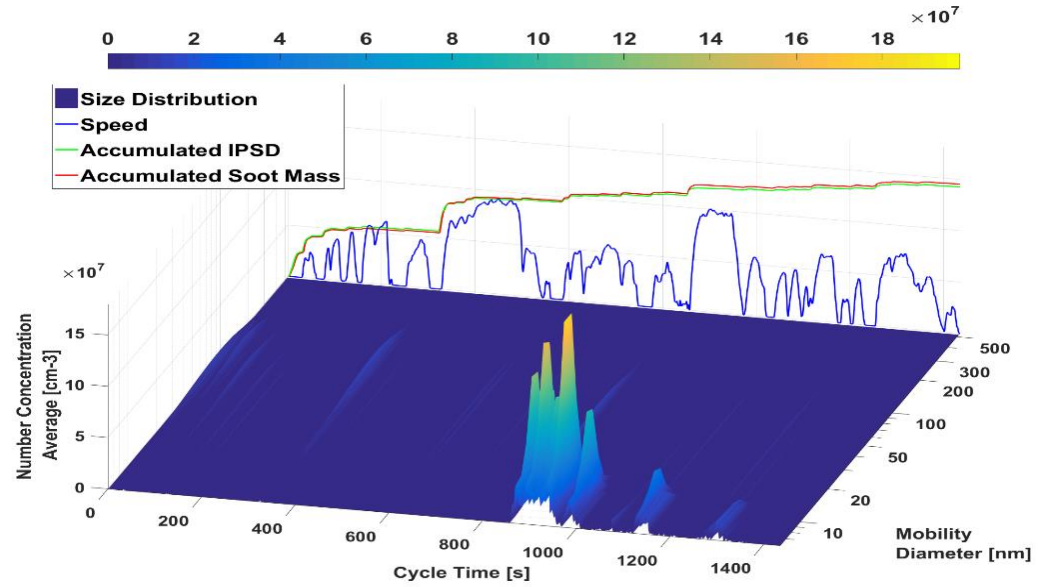

Figure S4-2 (a-b) Particle size distributions for GDI_3 for phases 1 and 2 (top panel, A) and phase 3 (bottom panel, B) of the LA92 cycle. The drive trace is included for visual reference, as well as the cumulative soot mass and IPSD mass emissions. Note the factor of ten difference between the vertical scales of the top and bottom panels

4.8.6. **Supplemental References**

Amanatidis S, Ntziachristos L, Giechaskiel B, Katsaounis D,; Samaras Z, Bergmann A. Evaluation of an Oxidation Catalyst ("Catalytic Stripper") in Eliminating Volatile Material from Combustion Aerosol. Journal of Aerosol Science 2013;57:144-155.

Livak KJ, Schmittgen TD. Analysis of relative gene expression data using real-time quantitative PCR and the 2(-Delta Delta C(T)) Method. Methods 2001;25:402-408.

Okuda T, Schauer JJ, and Shafer MM. Improved methods for elemental analysis of atmospheric aerosols for evaluating human health impacts of aerosols in East Asia. Atmospheric Environment 2014;97:552-555.

Schindler W, Haisch C, Beck HA, Niessner R, Jacob E, Rothe D. A Photoacoustic Sensor System for the Time Resolved Quantification of Diesel Soot Emission. SAE Technical Paper 2004;2004-01-0969.

Shafer MM, Hemming JDC, Antkiewicz DS, Schauer JJ. Oxidative potential of size-fractionated atmospheric aerosol in urban and rural sites across Europe. Faraday Discuss. 2016;189:381.

Sijan Z, Antkiewicz DS, Heo J, Schauer JJ, Sioutas C, Shafer MM. An in vitro alveolar macrophage assay for the assessment of inflammatory cytokine expression induced by atmospheric particulate matter. Environ Toxicol 2015;30:836-850.

Wang XL, Grose M, Avenido A, Stolzenburg MR, Caldow R, Osmondson BL, Chow JC, Watson JG. Improvement of Engine Exhaust Particle Sizer (EEPS) Size Distribution Measurement - I. Algorithm and Applications to Compact Aerosols. J. Aerosol Sci. 2016;92:95-108.

Xue J, Li Y, Wang, XL, Durbin TD, Johnson KC, Karavalakis G, Awuku A, Villela M, Quiros D, Hu, SH, Huai T, Ayala A, Jung, HJ. Comparison of Vehicle Exhaust Particle Size Distributions Measured by SMPS and EEPS During Steady-state Conditions. Aerosol Sci. Technol. 2015;49:984-996.

Xue J, Quiros D, Wang X, Durbin TD, Johnson KC, Karavalakis G, Hu S, Huai T, Ayala A, Jung HS. Using a new inversion matrix for a fast-sizing spectrometer and a photo-acoustic instrument to determine suspended particulate mass over a transient cycle for light-duty vehicles. Aerosol Sci. Technol., 2016, 50, 1227-1238.

5. A Comparison of a Mini-PEMS and a 1065 Compliant PEMS for On-road Gaseous and Particulate Emissions from a Light Duty Diesel Truck

5.1. Abstract

The primary goal of this study was to compare emissions measurements between a 1065 compliant PEMS, and the NTK Compact Emissions Meter (NCEM) capable of measuring NOx, PM, and solid PN. Both units were equipped on a light-duty diesel truck and tested over local, highway, and downtown driving routes. The results indicate that the NOx measurements for the NCEM were within approximately ±10% of those the 1065 compliant PEMS, which suggests that the NCEM could be used as a screening tool for NOx emissions. The NCEM showed larger differences for PM emissions on an absolute level, but this was at PM levels well below the 1 mg/mi level. The NCEM differences ranged from -2% to +26% if the comparisons are based on a percentage of the 1.0 mg/mi standard. Larger differences were also seen for PN emissions, with the NCEM measuring higher PN emissions, which can primarily be attributed to a zero current offset that we observed for the NCEM, which has been subsequently improved in the latest generation of the NCEM system. The comparisons between the 1065 compliant PEMS and the NCEM suggest that there could be applications for the NCEM or other mini-PEMS for applications such as identification of potential issues by regulatory agencies, manufacturer evaluation and validation of emissions under in-use conditions, and potential use in inspection and maintenance (I/M) programs, especially for heavy-duty vehicles.

Figure: Graphic Abstract

5.2. **Introduction**

Portable Emissions Measurement Systems (PEMS) are tools that are designed to measure vehicle/truck emissions while operating on the road. The application and technology of PEMS has evolved considerably over the past 20 years. PEMS serve an important role in helping to better understand and characterize the differences between laboratory certification and other testing and real-world emissions. PEMS were incorporated into the regulatory process as part of the 1998 consent decree in the United States (U.S.) and the regulations for in-use compliance testing of heavy-duty vehicles within the Not-to-Exceed (NTE) areas of operation that were created as part of these proceedings (Federal Register 2003, 2005; US EPA, 2008). This provided an impetus for the development of more commercial PEMS. PEMS have also been used extensively for measurements of emissions from heavy-duty trucks, light-duty vehicles, and construction

equipment (Johnson, 2002; Gautam et al. 2001; Kishan et al., 2011; Frey et al. 2010; Cao et al., 2016). More recently, PEMS have been incorporated into regulations for Real Driving Emissions (RDE) testing in Europe (Vlachos et al., 2014).

In the development of specifications for in-use compliance testing, there has been an emphasis on PEMS that can replicate the performance of laboratory grade equipment to the greatest extent possible. In the U.S., the Code of Federal Regulations (CFR) under Title 40 Part 1065 has regulated the design and measurement techniques that can be used for such instrumentation, as well as the methods and verification processes to determine the PEMS unit is valid for the in-use compliance purposes, such as linearity verification, dew point calibration, etc. (40 CFR 1065). An extensive Measurement Allowance program was also conducted to evaluate the potential variance of such PEMS in comparison to more traditional laboratory equipment, and to provide an allowance for such deviations in the regulations (Fiest et al., 2008; Johnson et al., 2008, 2009, 2011a, 2011b; Khalek et al., 2010; Khan et al., 2012; Miller et al., 2006). PEMS that are 1065 compliant and have been verified include systems by such major manufacturers as AVL, Horiba, and Sensors Inc. While such PEMS provide a traceable level of accuracy for regulatory purposes, 1065 compliant PEMS units are still somewhat large in size, relatively expensive, and can be complex to use in terms of setup and operation.

As in-use emissions testing has advanced, emissions data has continued to show the importance of measuring emissions in-use to fully understand the range of emissions emitted by vehicles under different operating conditions. The complexity of in-use emissions has been put in the spotlight with some high profile cases where excess

emissions have been identified for vehicles operating differently under in-use vs. laboratory conditions (Federal Register 2003; Thompson et al., 2014). It is also known that it is difficult to fully characterize and control emissions under all conditions as part of laboratory based certification testing, given the expense of laboratory testing. These issues have put greater emphasis on the need to collect in-use emissions measurements from a wider range of vehicles and operating conditions.

Given the complexity and cost of 1065 compliant PEMS, there is a growing interest in the development of mini-PEMS that are not targeted at compliance with 1065 specifications, but still provide reliable emissions measurements, and are easy to deploy and less expensive. Mini-PEMS are simplified versions of the 1065 compliant PEMS discussed above. Such PEMS could have a number of applications in that they could be used to screen larger numbers of vehicles to identify and characterize potential emissions issues. This could be of use to both engine and vehicle manufacturers to identify potential issues under real-world, or to government agencies looking for issues that might require more extensive investigation as part of enforcement programs. Such PEMS could also be used for enforcement in applications such as Inspection and Maintenance (I/M) programs. Some simpler instruments designed to target only a single emissions component are already being applied in I/M type of applications. Opacity has been used extensively as a surrogate for particulate matter (PM) emissions in a number of different areas. More recently, the Swiss SR941.242 Regulation in Europe is requiring biannual testing of off-road diesel machinery equipped with DPFs for compliance with a particle number (PN) mini-PEMS.

The development of non1065 compliant mini-PEMS type of systems that can provide measurements of multiple pollutants has also expanded recently. Maha has developed a PEMS that can measure NOx, CO_2, and PM. The company 3DATX has developed their 2nd generation parSYNC PEMS that includes the real-time measurement of NOx, CO_2, and PM mass (Ropkins et al., 2016). Pegasor (Saukko et al., 2016), TSI (2016), Testo, and Emisense (Stepphan et al., 2011) have also developed small measurement systems or sensors for PEMS for PM/PN. NGK Spark Plug has also developed a mini-PEMS called the NTK Compact Emissions Meter (NCEM) (Jiang et al., 2016). The system can be used to measure particulate matter (PM) and particle number (PN), nitrogen oxides (NOx), oxygen (O_2), and air/fuel ratio. While such low cost mini-PEMS could provide considerably utility in measuring a large number of vehicles under many different operating conditions, it is important to better characterize the accuracy, repeatability, and robustness of such systems.

The goal of this study was to compare emissions measurements between a 1065 compliant PEMS, and one of the current generation mini-PEMS. This included a 1065 compliant AVL M.O.V.E system and a NTK NCEM system. Both PEMS units were equipped on a light-duty truck over local, highway, and downtown driving over 2 days. The results indicate that the NOx measurements between a 1065 compliant PEMS and the mini-PEMS were within approximately ±10%, suggesting the NTK PEMS could be used as a screening tool for NOx emissions. Larger differences were found for PM and solid PN measurements that suggest that additional development of these measurement methods could be beneficial.

5.3. Materials and Methods

5.3.1. Test Vehicle, Engine, and Fuel

The test vehicle is a model year 2012 Chevrolet Silverado 2500HD Duramax light duty diesel pickup truck, which is widely available and used in the U.S. market. This vehicle has 43,140 miles at the start of the test and GVWR is in the range of 8501-10000 lbs. The vehicle is equipped with advanced aftertreatment technologies that have been implemented in the diesel fleet, such as DOC, DPF, and SCR. The vehicle is certified to U.S. EPA Tier 2 HDV/HD8510 (NOx at 0.8 g/mi and PM at 0.06 g/mi [U.S. EPA, 2016]) and CARB MDV/ULEV (NOx at 0.2 g/mi and PM at 0.06 g/mi [CARB, 2016]) emissions standards.

This vehicle is equipped with an engine family CGMXD06.6355 diesel engine. The engine is 6.6-liter, eight cylinders, turbocharged, direct injection, and common-rail engine configuration with a six-speed automatic transmission. The engine can deliver 397 horsepower at 3,000 rpm and 765 lb-ft torque at 1,600 rpm and has a compression ratio of 16.8:1.

The test fuel of this study was commercially available No. 2 diesel fuel from a local retail fueling station. It should be noted that the vehicle was filled up several times at the same retail fueling station. Since the properties of in-use California ultralow-sulfur diesel are tightly controlled to provide comparable emissions, the use of diesel fuel from different fill ups is expected to have minimal impact on the emissions results.

5.3.2. **Test Cycles**

The vehicle was tested over a period of two days using three different driving routes designed to represent local, highway, and LA downtown driving conditions. The characteristics of these three different cycles are shown in Table 5-1, along with the details for the FTP test for comparison.

The local route started and ended at the UCR CE-CERT facility in Riverside, and covered a distance of 6.8 miles. The local route was performed triplicate in order to get repeatable results. The local route is used to simulate the local driving and has a similar driving pattern to FTP driving cycle.

The highway route started at UCR and went to the main campus of the University of Southern California. The total distance of this route was 63.6 miles. The highway route includes over 95% highway driving along Highways I-60, I-10, I-710, and I-110. This route was conducted as a round trip, going first from UCR to USC and then back to UCR.

The LA downtown route started and ended at USC main campus on Jefferson Boulevard. It covered a distance of 15.7 miles. This route is used to simulate urban driving conditions in downtown LA. This route essentially represents the route that was used to develop the original FTP cycle. Additional idle and creep driving was also incorporated into this route. This route was performed twice.

Table 5-1 Summary of Trips Statistics for Different Routes and Cycles

Test Routes/Cycles	Distance (mi)	Average Speed (mph)	Maximum Speed (mph)	Number of Stops	Cycle Duration (s)
FTP	11.04	21.2	56.7	23	1874
LA4	7.50	19.6	56.7	18	1372
Local	6.80	16.3	53.6	11	1402
Highway	63.10	34.8	81.4	22	6545
LA Downtown	15.80	15.8	65.6	45	3617
Idle and Creep	1.80	2.5	32.9	18	2624

5.3.3. **Instruments**

For this study, a commercial available 1065 compliant AVL M.O.V.E system was utilized (Cao et al., 2016b). The AVL M.O.V.E system includes gas-phase analyzers for nitrogen oxide (NO) and nitrogen dioxide (NO2), carbon monoxide (CO), carbon dioxide (CO_2), total hydrocarbon (THC), nonmethane hydrocarbon (NMHC), and methane (CH4) and also particulate phase emissions of PM mass, solid PM mass, and also solid particle number (PN). The AVL M.O.V.E system measures oxides of nitrogen (NO and NO2) by non-dispersive ultraviolet radiation (NDUV), and then calculates the NOx value based on the reported NO and NO2 emissions. The AVL PM PEMS measurement system selected is AVL's 483 micro soot sensor (MSS) in conjunction with their gravimetric filter module (GFM) option. The combined system is called the AVL 494 PM system. The MSS instrument measures the modulated laser light absorbed by particles from an acoustical microphone. Since the MSS only detects elemental carbon, the GFM is included along with a post processor to allow the soluble organic fraction (SOF) and sulfate fraction to be estimated, based on a comparison of the MSS and GFM measurements. The combined

MSS+GFM system recently received type approval by EPA as a total PM measurement solution for in-use testing, thus making it one of the few 1065 compliant PM PEMS. For this study, both total PM using the MSS+GFM and soot PM using only the MSS are reported. In additional to the AVL 494 PM system, an AVL PN PEMS iS was also utilized. The PN PEMS measures solid particle number concentrations using diffusion charger principles consistent with the European RDE compliant program.

The mini-PEMS evaluated in this study was an NTK NCEM. The system can be used to measure PM mass, PN, NOx, and oxygen (O_2). Air/fuel ratio is also available on the latest generation NCEM, but this feature was not available for the version utilized for this study. The NCEM uses direct measurement sensors rather than dilution sampling. As the result, there is no delay time and measurements can be performed with good responsiveness in real-time. The system weights about 12 kg and measures 340 mm by 280 mm by 270 mm. It can be set up in approximately 10 minutes. It can be powered by a DC12/24V vehicle battery and draws less than 10 Amp to operate.

The NOx sensor is based on an original equipment manufacturer (OEM) product used for engine control and on-board diagnostic (OBD) of SCR systems The NOx sensor detects NOx by measuring O_2 ions created by the dissociation of NOx into N_2 and O_2 in the detection chamber, as shown in Figure 5-1. The design used for this specific sensor dissociates NO_2 to NO and O_2 in a trap layer before the gases reach the detection portion of the element. Therefore, the sensitivity to NO and NO_2 is essentially the same. Only under conditions where there is a very high gas flow rate or very cold gas that the element

heater cannot overcome, would the ratio start to diverge from 1:1. In these cases the sensitivity to NO_2 could be slightly lower than the sensitivity to NO.

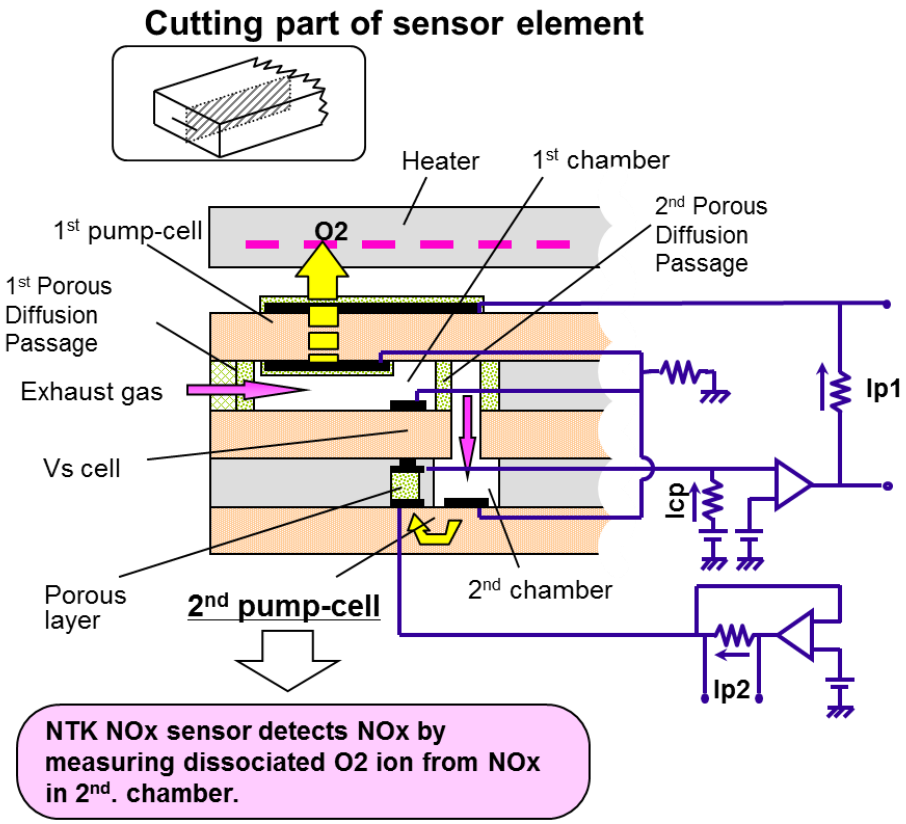

Figure 5-1 NCEM NOx Measurement Design Schematic

The PM/PN sensor is based on the Pegasor PPS-M technology, where particles are charged in a corona discharge, such that the total measured charge is proportional to the particle surface area, as shown in Figure 5-2 (Lanki et al., 2011; Ntziachristos et al., 2011; Ntziachristos et al., 2013; Rostedt et al. 2017). PM/PN can then be determined via calibrations that are used to establish calibration constants (Ntziachristos et al., 2013; Rostedt et al., 2014). To determine PM mass, the signal is calibrated against an AVL MSS 483, which is in turn calibrated against a gravimetric filter where the filter face temperature is not controlled to the 47°C±5°C specifications in 40 CFR 1065.

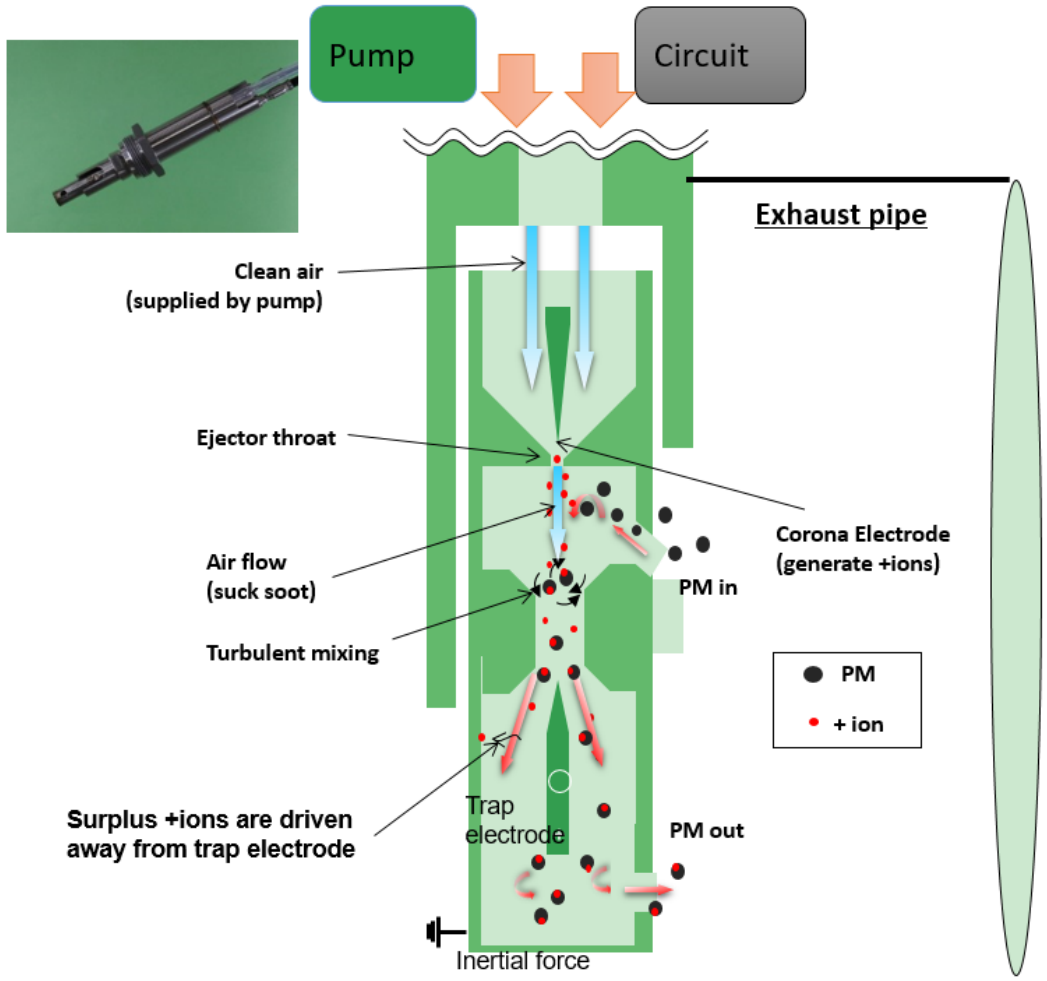

Figure 5-2 NCEM PM and PN Measurement Design Schematic

To determine PN, the sensor is calibrated against a TSI scanning mobility particle sizer (SMPS). Both the PM and PN calibrations are performed with a soot generator that provides soot particles with a unimodal distribution with peak concentration around 75 nm. The calibration does have some sensitivity to the particle size distribution, which has been discussed in detail elsewhere (Ntziachristos et al., 2011; Rostedt et al., 2014; Rostedt et al., 2017). Simulations using a range of possible diesel particle size distributions, however, have shown that the maximum theoretical error is 23% when using surface area as a proxy for number and 39% when using surface area as a proxy for soot mass, although the actual

error is expected to be much less than these values (Ntziachristos et al., 2012). For the test vehicle itself, our own internal data indicates that its size distribution is bimodal with a minor peak at 15 nm and a larger peak at 75 nm, which should be relatively well represented by the distribution used for the calibration. Also, since the sensor measures PM in the raw exhaust, with only a small amount of dilution, the total PM and total PN measured by the NCEM is primarily solid PM. A Semtech 4 inch Exhaust Flow Measurement (EFM) system was used by both systems for the measurement of the exhaust flow to provide integrated mass emissions as well as second by second data for each pollutant.

5.3.4. **Measurement Protocols**

The experimental set up for study is shown in the Figure 5-3. This includes the NCEM, AVL gaseous M.O.V.E. system, AVL PM System, and the AVL PN PEMS iS. The power system for the set up included a Yamaha gasoline generator model EF2800i, which has two 120V AC plugs with 20A maximum current each, a CHARGEMASTER 12V power converter to power the AVL Gas M.O.V.E system, and a Xantrex sine wave inverter powered through a twin 12V battery pack to power the EFM and the computers. The purpose of the 12V batteries were to support as a backup power source, which was necessary when switching from building power to the generator power, or when powering down the generator to add more fuel.

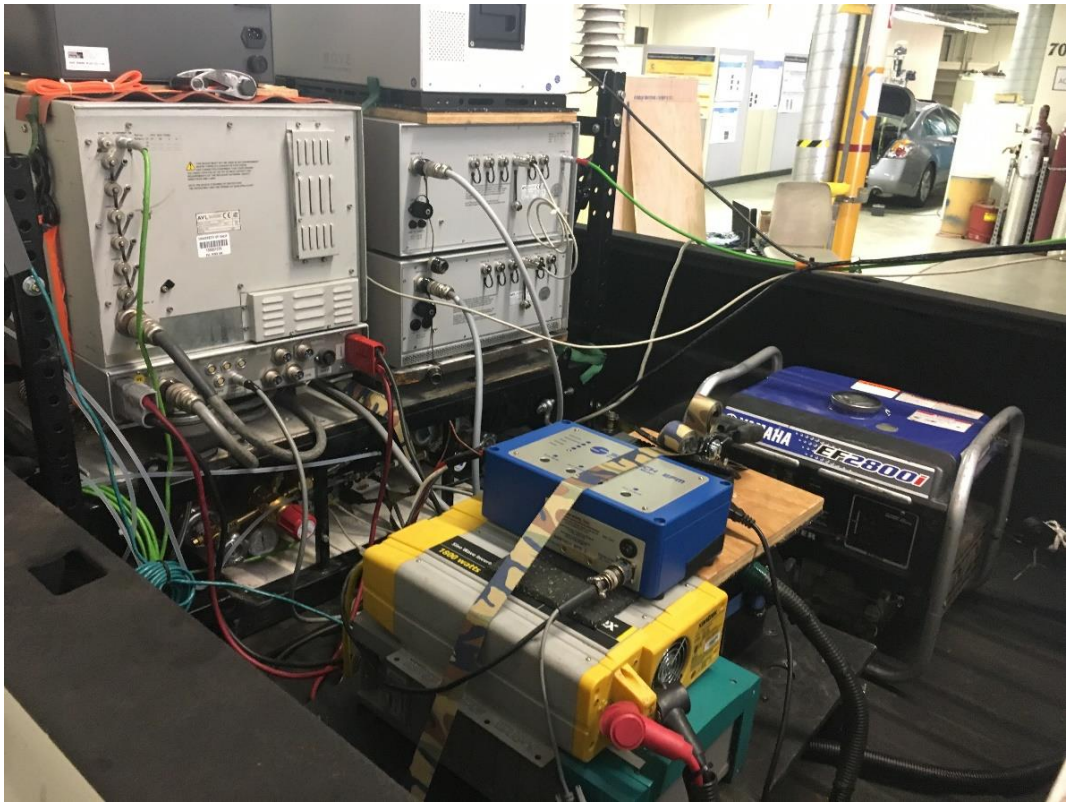

Figure 5-3 Instrument Setup and Power Supply for On-road PEMS Testing

For the AVL Gas M.O.V.E system, the tests were performed using the certification test protocol provided with Concerto software (1065 compliant), including pre- and post-test calibrations and drift corrections of the gaseous data. The NCEM was controlled through the screen of the unit with the data logged to a flash drive.

5.4. Results and Discussion

5.4.1. NOx Emissions

The NOx emissions results for all the testing routes are shown below in Table 5-2. The range of NOx emissions are in the range of 2.76 to 5.76 g/mi for NCEM unit and in the range 2.26 to 6.36 g/mi for AVL M.O.V.E. system, as shown in Table 5-2 below. Overall, the NOx emissions shown reasonably good agreement between NCEM unit and

AVL M.O.V.E system. The average NCEM emissions were within 3% of those for the AVL M.O.V.E for both the highway and the LA downtown routes. The average differences for the local routes and the idle and creep were somewhat higher, but were still within 10% for both cycles. The NCEM did not show a consistent bias compared to the AVL M.O.V.E system, with the NCEM reading higher for some test routes and lower for others. In fact, the total grams of NOx emissions measured over two days of testing with variety of routes, resulting in 457.84 grams for NECM and 457.68 grams for AVL M.O.V.E system. This represents a difference of only 0.03% for total emissions, indicating that the NCEM read higher or lower than the AVL M.O.V.E with roughly equal frequency. The potential impacts of different NO/NO2 ratios in the exhaust were also examined, as shown in Table 5-2. Although larger differences between the NTK and AVL were found for the idle/creep conditions, where the NO/NO_2 ratios were higher, and smaller differences were seen for the LA Downtown route where the NO/NO_2 were lower, the local and highway cycles also showed higher and lower differences, respectively, even though the NO/NO_2 ratios were fairly similar for these routes. As such, there were no definitive trends in terms of analyzer performance as a function of NO/NO_2 ratios.

Table 5-2 Summary of NOx Emissions

Results	Start Location	End Location	Mini-PEMS	1065 Compliance PEMS			Mini-PEMS	1065 Compliance PEMS			
			NOx	NOx	NO	NO_2	NOx	NOx	NO	NO_2	NO/NO_2
			g/cycle				g/mi				
Local_1	UCR CECERT	UCR CECERT	23.26	25.14	13.39	4.63	3.44	3.72	1.98	0.69	2.89
Local_2	UCR CECERT	UCR CECERT	33.19	31.06	14.64	8.64	4.82	4.51	2.12	1.25	1.7
Local_3	UCR CECERT	UCR CECERT	34.22	26.85	12.79	7.25	5.06	3.97	1.89	1.07	1.76
average							4.44	4.07			
% difference							9.20%				
Highway_1	UCR CECERT	USC main campus	137.21	142.99	68.51	38.06	2.17	2.26	1.08	0.6	1.8
Highway_2	USC main campus	UCR CECERT	144.14	146.72	69.4	40.43	2.29	2.33	1.1	0.64	1.72
average							2.23	2.3			
% difference							-2.90%				
LA Downtown_1	USC main campus	USC main campus	36.39	35.75	15.39	12.18	2.3	2.26	0.97	0.77	1.26
LA Downtown_2	USC main campus	USC main campus	39.03	37.71	16.07	13.1	2.47	2.39	1.02	0.83	1.23
average							2.39	2.32			
% difference							2.70%				
Idle and Creep	USC main campus	USC main campus	10.38	11.45	6.23	1.91	5.76	6.36	3.46	1.06	3.26
% difference							-9.40%				
Total			457.84	457.68	216.42	126.2	3.54	3.47	1.7	0.86	1.97

*These values are the average of all the NOx emissions over all different cycles in g/mi basis

Some additional analyses were also conducted to evaluate the NOx data in different ways. Comparisons between NOx emissions for different speed bins are provided in Figure 5-4 for one day of testing that included two highway routes, two LA downtown routes, and an idle and creep route. The data showed relatively good comparisons throughout the full range of vehicle operation, with the exception of some bigger discrepancies seen at speeds between 80 and 90 mph. The data also show a general trend of increasing NOx emissions as a function of speed, with the exception of the 80 to 90 mph measurements with the AVL M.O.V.E. It should be noted that only 19 data points were found in the 80 to 90 mph category, considerably smaller than the number of data points in the other speed. While the NCEM measurements were higher than those for the AVL M.O.V.E. for most of these data points, this represents a relatively small data set in comparison with the data available for the other speeds.

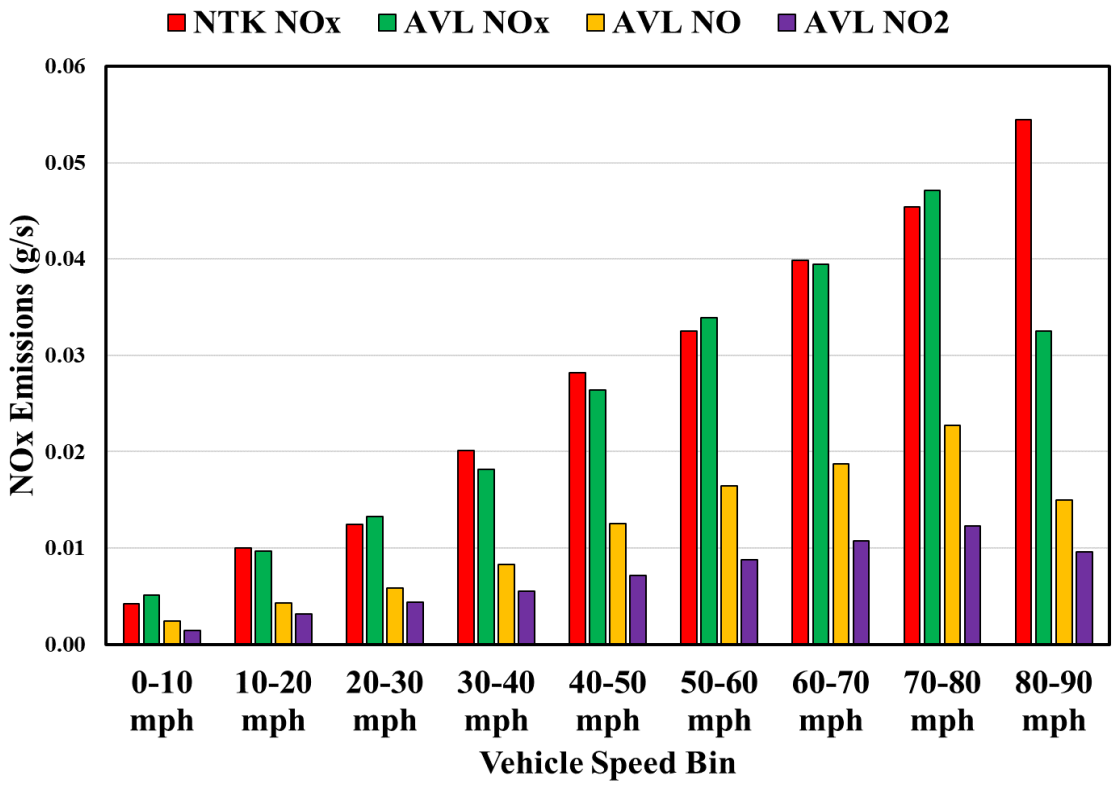

Figure 5-4 Vehicle speed based comparisons for NOx emissions for one day of testing

Additional analyses were also conducted using quantile-quantile (Q-Q) plots for 1 second, 3 second, 10 second, and 100 second averaged data, as shown in Figure 5-5 for the same routes used for the speed bin plot. For this analysis, the data are sorted from the lowest to highest value for each instrument. Overall, the Q-Q plots showed relatively good agreement between the instruments, with the lines being only slightly higher than the 1:1 line. The 25 and 75 percentile points are provided in Table 5-3, which are the points below which 25% and 75% of the measurements fall for both instruments. These points define the highest and lowest quantiles for the Q-Q plots.

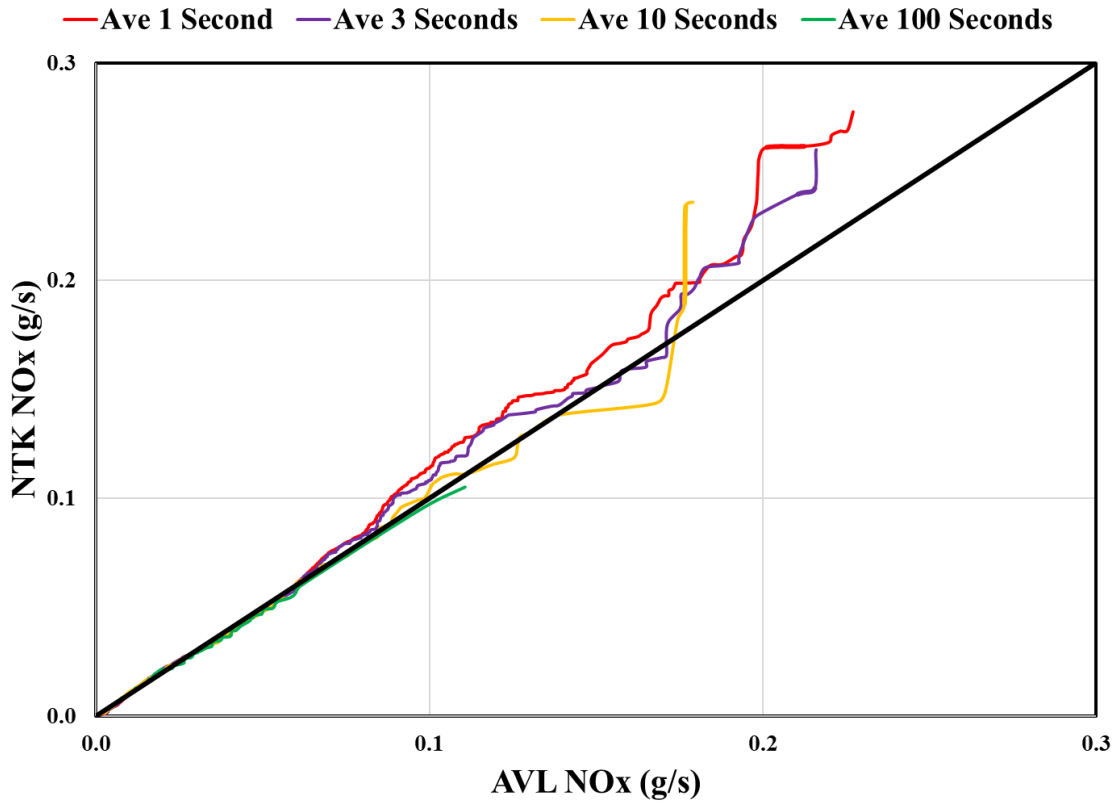

Figure 5-5 Q-Q Plot Analysis on NOx Emissions for one day of testing

Regression analyses were also performed for the real-time data for 1 second, 3 second, 10 second, and 100 second averaged data. A range of different averaging intervals were used since such a comparison could be very sensitive to time alignment in addition to the actual precision of the measurement itself. The results of these analyses are presented in Table 5-4 for total NOx. The results show that the correlation R^2 improves and the slope gets closer to 1 as the time interval for the averaging increases, which is a measure of how this comparison can be impacted by time alignment. The local cycle showed a slope near 1 for the NTK vs. AVL NOx, but the correlation for the local cycle was relatively poor, even for the 100 second average.

Table 5-3 Summary of 25th and 75th Percentile Q-Q Plot Values for NOx, PM, and PN Emissions

Routes	Percentile	NOx (g/s)		PM and Soot (mg/s)			PN (#/s)	
		NTK	AVL	NTK	AVL MSS	AVL PM	NTK	AVL
Local_1	25%	0.0035	0.0081	0.0000	0.0002	0.0005	0.00E+00	0.00E+00
	75%	0.0087	0.0190	0.0000	0.0008	0.0012	0.00E+00	1.47E+08
Local_2	25%	0.0043	0.0075	0.0000	0.0002	0.0005	0.00E+00	1.67E+07
	75%	0.0166	0.0223	0.0000	0.0009	0.0013	0.00E+00	1.82E+08
Local_3	25%	0.0043	0.0074	0.0000	0.0002	0.0005	0.00E+00	1.78E+03
	75%	0.0184	0.0182	0.0002	0.0009	0.0014	8.24E+08	1.80E+08
Local_Average	25%	0.0040	0.0077	0.0000	0.0002	0.0005	0.00E+00	5.58E+06
	75%	0.0146	0.0198	0.0001	0.0009	0.0013	2.75E+08	1.70E+08
Highway_1	25%	0.0042	0.0046	0.0000	0.0004	0.0005	0.00E+00	0.00E+00
	75%	0.0312	0.0339	0.0000	0.0015	0.0015	0.00E+00	2.14E+08
Highway_2	25%	0.0040	0.0056	0.0000	0.0004	0.0006	0.00E+00	2.77E+07
	75%	0.0200	0.0192	0.0001	0.0012	0.0014	3.87E+08	2.49E+08
Highway_Average	25%	0.0041	0.0051	0.0000	0.0004	0.0006	0.00E+00	1.39E+07
	75%	0.0256	0.0265	0.0000	0.0014	0.0015	1.93E+08	2.31E+08
LA Downtown_1	25%	0.0037	0.0046	0.0004	0.0003	0.0004	1.83E+09	0.00E+00
	75%	0.0083	0.0082	0.0013	0.0007	0.0010	6.28E+09	8.93E+07
LA Downtown_2	25%	0.0035	0.0047	0.0008	0.0003	0.0005	3.64E+09	1.91E+07
	75%	0.0089	0.0089	0.0019	0.0008	0.0011	9.25E+09	1.48E+08
LA Downtown_Average	25%	0.0036	0.0047	0.0006	0.0003	0.0004	2.74E+09	9.56E+06
	75%	0.0086	0.0085	0.0016	0.0008	0.0010	7.77E+09	1.19E+08
Idle and Creep	25%	0.0030	0.0036	0.0002	0.0002	0.0006	9.68E+08	0.00E+00
	75%	0.0034	0.0040	0.0003	0.0002	0.0006	1.64E+09	4.23E+07

Table 5-4 Summary of Correlation Slope and Regression Statistics for NOx Emissions NOx (g/s)

Routes		Ave 1 second			Ave 3 seconds		
		NTK vs AVL NOx	NTK vs AVL NO	NTK vs AVL NO2	NTK vs AVL NOx	NTK vs AVL NO	NTK vs AVL NO2
Local_1	Slope	1.137	2.142	3.468	1.135	2.147	3.409
	R2	0.450	0.421	0.328	0.491	0.461	0.354
Local_2	Slope	1.089	2.190	4.195	1.131	2.284	4.310
	R2	0.534	0.509	0.563	0.586	0.562	0.610
Local_3	Slope	0.884	1.634	3.825	0.917	1.719	3.880
	R2	0.335	0.287	0.421	0.372	0.324	0.455
Local_Average	Slope	1.037	1.988	3.829	1.061	2.050	3.866
	R2	0.440	0.406	0.438	0.483	0.449	0.473
Highway_1	Slope	0.790	1.528	3.012	0.805	1.562	3.055
	R2	0.573	0.542	0.549	0.622	0.591	0.593
Highway_2	Slope	0.799	1.540	3.204	0.818	1.584	3.267
	R2	0.535	0.501	0.548	0.594	0.561	0.601
Highway_Average	Slope	0.795	1.534	3.108	0.811	1.573	3.161
	R2	0.554	0.522	0.549	0.608	0.576	0.597
LA Downtown_1	Slope	0.776	1.491	2.687	0.812	1.582	2.767
	R2	0.340	0.279	0.406	0.402	0.337	0.465
LA Downtown_2	Slope	0.749	1.494	2.611	0.769	1.540	2.662
	R2	0.373	0.327	0.423	0.436	0.384	0.491
LA Downtown_Average	Slope	0.763	1.492	2.649	0.790	1.561	2.714
	R2	0.356	0.303	0.414	0.419	0.361	0.478
Idle and Creep	Slope	0.724	1.124	1.599	0.767	1.198	1.553
	R2	0.202	0.128	0.168	0.257	0.160	0.202
		Ave 10 seconds			**Ave 100 seconds**		
		NTK vs AVL NOx	NTK vs AVL NO	NTK vs AVL NO2	NTK vs AVL NOx	NTK vs AVL NO	NTK vs AVL NO2
Local_1	Slope	1.090	2.051	3.083	0.942	1.921	1.864
	R2	0.529	0.489	0.371	0.435	0.416	0.242
Local_2	Slope	1.203	2.475	4.387	0.988	1.994	3.747
	R2	0.684	0.666	0.685	0.646	0.621	0.663
Local_3	Slope	0.921	1.718	3.982	0.896	1.756	3.481
	R2	0.395	0.342	0.489	0.346	0.294	0.454
Local_Average	Slope	1.072	2.081	3.817	0.942	1.890	3.030
	R2	0.536	0.499	0.515	0.476	0.444	0.453
Highway_1	Slope	0.869	1.712	3.202	0.914	1.869	3.315
	R2	0.801	0.774	0.730	0.988	0.979	0.925
Highway_2	Slope	0.898	1.772	3.423	0.948	1.918	3.609
	R2	0.785	0.761	0.741	0.979	0.973	0.925
Highway_Average	Slope	0.884	1.742	3.312	0.931	1.893	3.462
	R2	0.793	0.767	0.736	0.984	0.976	0.925
LA Downtown_1	Slope	0.948	1.949	2.920	1.020	2.139	2.838
	R2	0.635	0.581	0.623	0.924	0.885	0.771
LA Downtown_2	Slope	0.893	1.830	2.971	1.025	2.212	2.837
	R2	0.665	0.614	0.687	0.936	0.894	0.835
LA Downtown_Average	Slope	0.920	1.889	2.946	1.023	2.175	2.838
	R2	0.650	0.597	0.655	0.930	0.889	0.803
Idle and Creep	Slope	0.974	1.680	1.494	1.206	2.193	1.234
	R2	0.513	0.356	0.302	0.950	0.504	0.538

The differences in integrated NOx emissions between the NTK and the AVL PEMS over various routes are comparable to those found in previous studies. In a previous study, comparisons were made between an earlier version of NTK's NCEM system, a AVL 1065 compliant gaseous portable emission measurement system (PEMS), and UCR's 1065 compliant mobile emissions laboratory (MEL) for engine dynamometer tests under transient and steady state conditions (Jiang et al., 2016) and for chassis dynamometer measurements for a truck equipped with a 2014 on-highway engine equipped with a properly functioning DPF/SCR system (Johnson and Jiang, 2015). For this previous study, the NTK NOx measurements were lower than the MEL reference method and ranged from -16.3% for the FTP to -4.7% for an engine dynamometer version of the UDDS (Jiang et al., 2016). The AVL PEMS, on the other hand, was higher than the MEL reference method by +7.9% for the FTP and +16.7% for the UDDS. For the chassis dynamometer testing for the DPF/SCR equipped vehicle, the NTK NOx measurements were lower than the MEL reference method for the UDDS, Creep, and Transient cycles, ranging from -13% for the UDDS to -30% for the Creep, while they were higher than those for the MEL reference method for two cruise cycles with lower NOx emissions rates, with differences of +120% or greater.

The NOx emissions can also be compared back to early comparisons between 1065 compliant PEMS and CVS reference methods conducted as part of the Measurement Allowance program (Johnson et al., 2009, 2011a). For the on-road comparisons done as part of the Measurement Allowance program, bsNOx emissions for the PEMS measurements were consistently higher than those for the MEL. The deviations were 8%

± 4%, 4% ± 5%, and 3% ± 5%, for different calculation methods, relative to the NTE NOx standard 2.68 g kW^{-1} h^{-1} (2.0 g hp^{-1} h^{-1}). In another study that was done as part of the initial validation tests for the AVL's M.O.V.E GAS PEMS 493 system testing included in-lab and on-road emission comparisons between the AVL PEMS and the UCR MEL for three different heavy-duty engines with NOx emission certification levels ranging from 0.27 g/kWh (0.2 g/hp-hr) to 5.4 g/kWh (4.0 g/hp-hr) (Cao et al., 2016b). The relative error for the AVL PEMS brake-specific NOx (bsNOx) measurements was within +5 to -10% relative error over the 1.0 to 7.0-g/kWh range, ranged from a +15 to -15% over the lower 0.1 to 1 g/kWh range, and increased sharply below 0.1 g/kWh from 15% to more than 50% at 0.02 g/kWh. The larger relative error below 0.10 g/kWh was due to the very low NOx emission rates that approached the detection limits of both the raw PEMS and dilute MEL measurement methods. It is worth adding that in all of these previous studies the PEMS measured exhaust flow independently of the MEL, which represents an important source of error that was not characterized in the current study, as the AVL PEMS and NCEM used exhaust flow measurements from the same EFM.

Overall, the differences between the instruments seem reasonable given the measurement methodologies, and are well within the ranges that would be acceptable for screening tests or tests designed to identify high emitting vehicles or off-cycle emissions events. It is worth noting that the NCEM did show a higher coefficient of variation (COV) for the local tests.

It is also worth noting that the NOx emission levels of this vehicle were considerably higher than what might be expected based on its certification level. The

vehicle's FTP certification level (CARB MDV/ULEV) is 0.2 g/mi, and previous laboratory chassis dynamometer test results for this same vehicle have shown NOx emission levels below 0.2 g/mi. However, the average on-road NOx emissions results for this study were 3.5 g/mi, which suggests a potential malfunction of the SCR system. Although the malfunction indicator light (MIL) was not on during testing, subsequent to testing, the MIL did turn on with several codes indicative of a DEF coolant, DPF, and reduced power issues. The dealership performed three regenerations for the DPF, replaced the reductant temperature sensor/reservoir, and replaced the coolant reservoir/low coolant assembly. Following the repairs, the vehicle was tested again over the FTP cycle on a chassis dynamometer, and NOx emission levels were found to be below the 0.2 g/mi NOx emission standard. It should be noted that the primary purpose of this testing was a comparison between the NTK and AVL system, as such the vehicle only served as an emissions source, so the results still provide a valid comparison between the two systems independent of the condition of the vehicle.

5.4.2. **PM Emissions**

The test vehicle was equipped with a DPF, so the PM emissions levels were generally low. The PM emissions results for all the testing routes are shown below in Table 5-5. PM emissions were in the range of 0.09 to 0.80 mg/mi for the total PM for the NCEM unit, in the range 0.11 to 1.06 mg/mi for the total PM for the AVL MSS+GFM measurements, and in the range of 0.11 to 0.37 mg/mi for soot PM for the AVL MSS. For the AVL MSS+GFM measurements, the PM emission rates were typically around 25% of the 2025 ARB 1.0 mg/mi standard or less, with the exception of the idle and creep cycle.

To get PM mass, the AVL MSS+GFM system multiplies the measured PM-soot by the calculated filter correction factor. The PM filter correction factor averaged from 1.02 to 1.38 for the non-idle tests, which suggests a fairly low organic carbon (OC) fraction of less than 38% of the total PM mass. It should be noted that since the AVL measures dilute PM, its PM value would include any PM that may have been formed in the dilution system, which would not be measured by the NCEM system since NCEM primarily measures solid PM in the hot raw exhaust.

In general, the PM NCEM system behaved well and showed a reasonable comparison to a 1065 compliant MSS+GFM PM measurements and the AVL MSS soot measurements given the low levels of the PM emissions. The relative differences between the NCEM and AVL MSS+GFM PM mass [RelDif_% = (NCEM-[MSS+GFM])/NCEM] ranged from -31% to +109%. The relative differences between the NCEM and the AVL MSS soot measurements ranged from -8.1% to +177%. The NCEM total PM measurements showed a better comparison with AVL MSS soot measurements than the AVL total PM measurements for the local and highway driving, which is consistent with the fact that the NCEM and AVL MSS characterize primarily solid/soot PM. However, the NCEM showed greater differences for the AVL MSS than the AVL total PM for the LA downtown route and the idle and creep testing. In comparison with previous studies, Nziachristos et al. (2013) found that the PPS measured 8% lower PM than a MSS for a diesel vehicle and approximately 40% lower PM than an MSS for a lower emitting direct injection spark ignition engine-equipped vehicle. It should be noted that NTK has improved the offset current variation for its PM measurement by 81% in its more recent version of

the system, which is expected to improve the accuracy of the system at lower PM levels (Tange, 2017).

It is also worthwhile to evaluate the PM differences in the context of the future 2025 California LEVIII PM emissions standard of 1 mg/mi, as there is considerable interest in how effective gravimetric and other methodologies are in quantifying PM emissions at levels below 1 mg/mi (Xue et al., 2017; Sardar et al., 2015; Swanson et al., 2018). If the comparisons were based on the future 1.0 mg/mi PM standard, the average differences reduce to -2% to +26% for the AVL total PM mass measurements [StdDif_% = (NCEM-[MSS+GFM])/1.0] and to -1% to 43% for the AVL MSS soot measurements. The lower difference relative to the emission standard suggests the NCEM system is capable of quantifying PM at and below the 1 mg/mi standard with fairly good confidence. The NCEM system showed a lower PM emission level for the FTP-like and highway routes, but a higher emission level for the LA downtown routes compared to both the MSS+GFM and MSS alone systems. This suggests a possible PM physical characteristic change between in-town driving and cruise conditions that may have caused the NCEM to report differently. Overall, the total PM emissions showed good agreement between NCEM unit and AVL MSS+GFM and MSS alone systems. The total mass of PM emissions measured over the two days of testing over a variety of routes was 31.36 milligrams for NECM and 28.87 milligrams for AVL MSS+GFM system. The difference between the NCEM and the 1065 compliant PEMS is 8.62%.

Additional analyses of the PM data included speed bin plots, Q-Q plots, and regression analyses. Comparisons between PM emissions for different speed bins are

provided in Figure 5-6 for day of testing that included two highway routes, two LA downtown routes, and an idle and creep route. The results showed that the largest PM discrepancies were seen in the 10 to 30 mph range, and for speed from 80 to 90 mph. For the 80 to 90 mph speed bin, it should be noted that only 19 data points are available, so this is a very small data set for comparison. For these 19 data points, the NCEM measured no PM emissions for all but two points, which appear to be outliers, that lead to the higher average emissions for the NCEM. The Q-Q plots for the same day of testing for the different data averaging times show the NCEM PM measurements are biased high relative to the AVL PM, particularly for the 1 second averaging. The 25 and 75 percentile values from the Q-Q plots for the NCEM, AVL MSS, and AVL PM are provided in Table 5-3. Regression analyses were performed for the PM real-time data for 1 second, 3 second, 10 second, and 100 second averaged data, as shown in Table 5-6. The results show a relatively poor correlation for the regression analyses between the NTK and AVL PM measurements for most of the test cycles and averaging intervals.

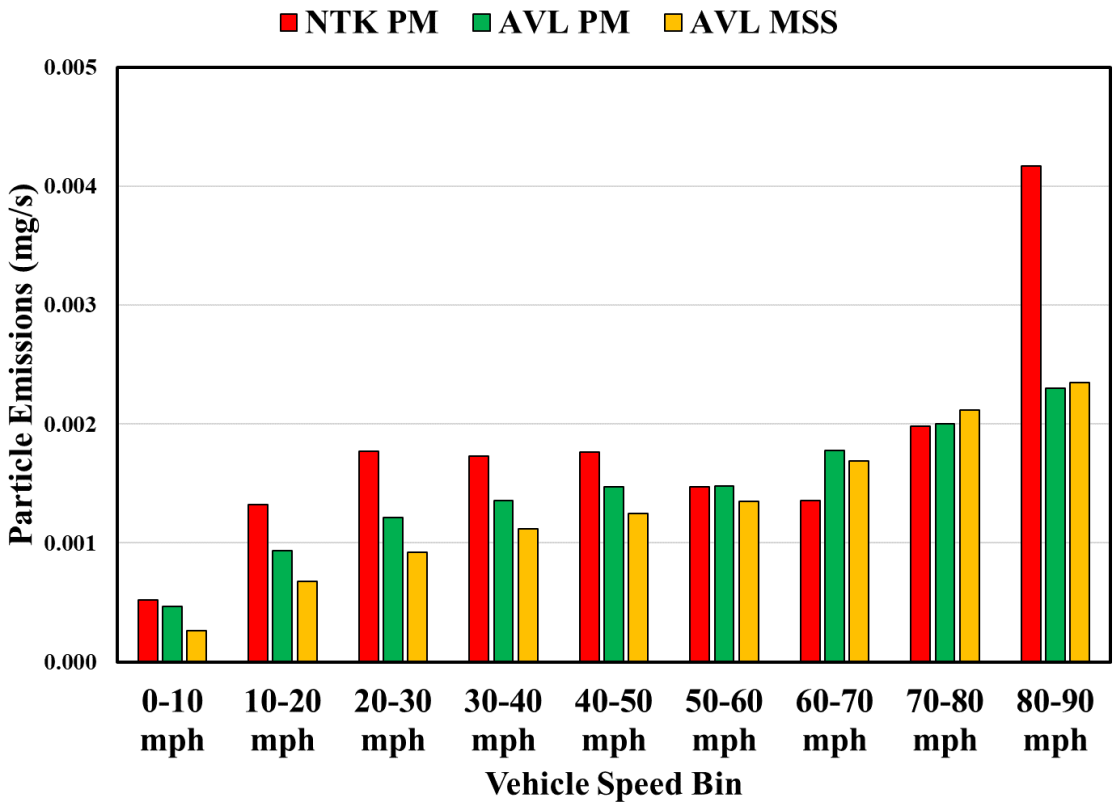

Figure 5-6 Vehicle speed based comparisons for particle emissions for one day of testing

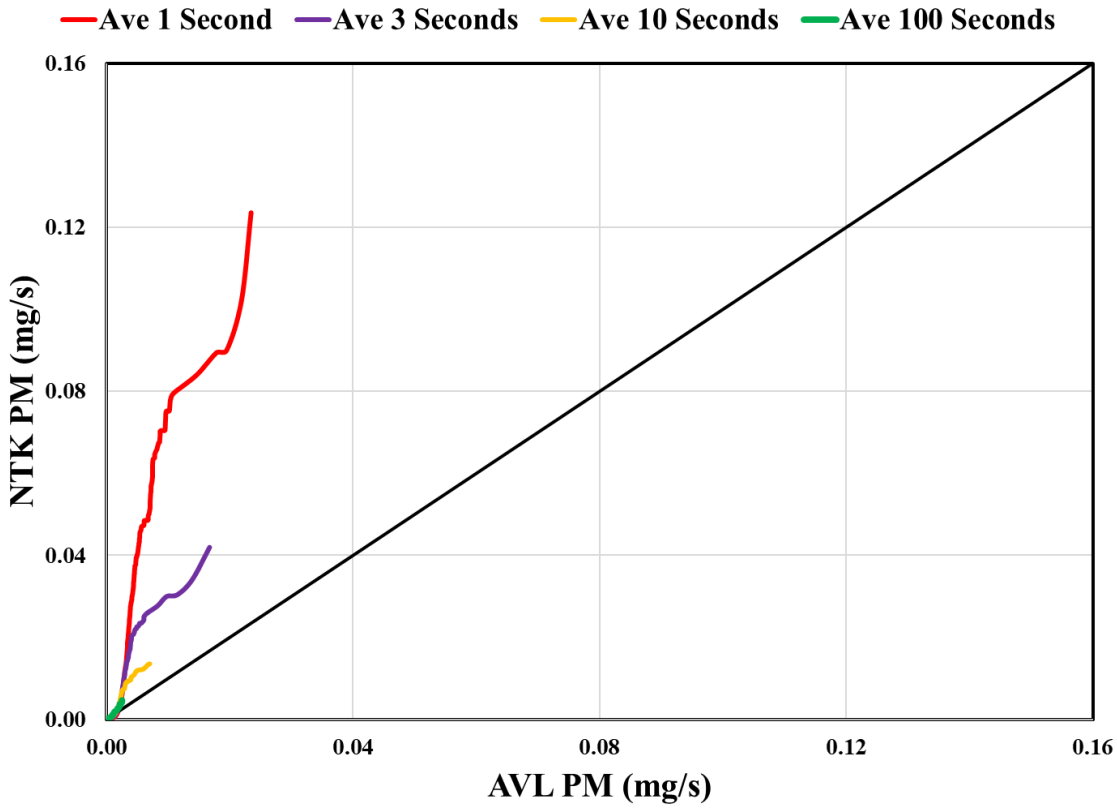

Figure 5-7 Q-Q Plot Analysis on PM Emissions for one day of testing

These results can be compared to a previous engine dynamometer study with an older NTK NCEM PM instrument compared against a 1065 compliant AVL PM PEMS and the MEL reference laboratory (Jiang et al., 2016). In this previous study, the NCEM PM emissions were lower compared to the MEL PM method for all the cycles except for an engine dynamometer version of the UDDS cycle, with differences ranging from -60% for the FTP to -23% for two steady state supplementary emission test (SET) cycles to +50% for the UDDS cycle. The soot emissions for the 1065 compliant AVL PM PEMS were also lower than the MEL PM values, and varied from -23% to -83% for the FTP and UDDS cycles and from -50% to -87% for the two steady state ramp modal cycles. Some of the higher differences for the AVL PM PEMS were attributed to PM with a higher fraction of

organic carbon for the more lightly loaded cycles. Earlier testing of the photoacoustic part of the AVL PM PEMS without a filter, as part of the measurement allowance program, also showed a good correlation for a truck with high soot emissions (R2=0.91, slope=0.95), but much lower PM mass levels than the MEL PM filters for trucks with little soot emissions (R2=0.18 to 0.75, slope=0.04 to 0.11) (Johnson et al., 2011). A second study as part of this measurement allowance work that included tests on a DPF equipped truck with an AVL PM PEMS with and without a prototype gravimetric filter system showed good slopes and correlations for both systems for tests where there were no regenerations (R2=0.87 to 0.88, slope=0.90 to 1.1), but essentially no correlation for tests under regeneration conditions (Khan et al., 2012).

Another point of consideration is that it is unclear how the sensor accuracy might change over long term usage. The AVL PM system has a more robust principle that includes a reference to the NIOSH thermal optical calibration method and a gravimetric filter correction. This suggests PM from the AVL PM system can be managed over time with some level of confidence. Additional studies are needed to understand the long term accuracy of the NCEM PM system.

Table 5-5 Summary of PM Emissions

Results	Start Location	End Location	Mini- PEMS	1065 Compliance PEMS		Mini- PEMS	1065 Compliance PEMS	
			Total PM	Total PM	Soot PM	Total PM	Total PM	Soot PM
			mg/cycle			mg/mi		
Local_1	UCR CECERT	UCR CECERT	0.98	1.67	1.15	0.14	0.25	0.17
Local_2	UCR CECERT	UCR CECERT	1	1.77	1.43	0.15	0.26	0.21
Local_3	UCR CECERT	UCR CECERT	1.61	1.76	1.39	0.24	0.26	0.21
Average			1.19	1.73	1.32	0.18	0.25	0.19
% difference NCEM Total PM to AVL Total PM						-31.10%		
% difference NCEM Total PM to AVL Soot PM						-9.70%		
Highway_1	UCR CECERT	USC main campus	5.42	6.94	6.82	0.09	0.11	0.11
Highway_2	USC main campus	UCR CECERT	7.15	8.24	6.87	0.11	0.13	0.11
Average			6.29	7.59	6.85	0.1	0.12	0.11
% difference NCEM Total PM to AVL Total PM						-17.20%		
% difference NCEM Total PM to AVL Soot PM						-8.10%		
LA Downtown_1	USC main campus	USC main campus	6.34	3.23	2.34	0.4	0.2	0.15
LA Downtown_2	USC main campus	USC main campus	7.43	3.36	2.63	0.47	0.21	0.17
Average			6.88	3.29	2.49	0.44	0.21	0.16
% difference NCEM Total PM to AVL Total PM						109.00%		
% difference NCEM Total PM to AVL Soot PM						177.00%		
Idle and Creep	USC main campus	USC main campus	1.44	1.9	0.66	0.8	1.06	0.37
% difference NCEM Total PM to AVL Total PM						-24.30%		
% difference NCEM Total PM to AVL Soot PM						117.70%		
Total			31.36	28.87	23.29	0.3	0.31	0.19

*These values are the average of all the PM emissions over all different cycles in g/mi basis

Table 5-6 Summary of Correlation Slope and Regression Statistics for PM and Soot Emissions

PM and MSS (mg/s)		Ave 1 second			Ave 3 seconds		
		NTK vs AVL MSS	NTK vs AVL PM	AVL MSS vs AVL PM	NTK vs AVL MSS	NTK vs AVL PM	AVL MSS vs AVL PM
Local_1	Slope	0.729	0.841	0.926	0.781	0.876	0.931
	R2	0.017	0.024	0.920	0.052	0.071	0.931
Local_2	Slope	0.401	0.522	1.100	0.428	0.565	1.105
	R2	0.024	0.031	0.940	0.067	0.091	0.947
Local_3	Slope	1.170	1.261	1.041	1.199	1.291	1.046
	R2	0.083	0.083	0.937	0.220	0.220	0.945
Local_Average	Slope	0.767	0.875	1.022	0.803	0.911	1.027
	R2	0.041	0.046	0.932	0.113	0.127	0.941
Highway_1	Slope	0.697	0.806	1.126	0.700	0.812	1.132
	R2	0.017	0.016	0.926	0.048	0.047	0.937
Highway_2	Slope	0.833	0.454	0.578	0.830	0.513	0.630
	R2	0.019	0.009	0.548	0.053	0.030	0.590
Highway_Average	Slope	0.765	0.630	0.852	0.765	0.663	0.881
	R2	0.018	0.013	0.737	0.050	0.039	0.763
LA Downtown_1	Slope	2.177	2.038	0.862	2.175	2.081	0.892
	R2	0.113	0.117	0.874	0.242	0.249	0.896
LA Downtown_2	Slope	2.269	2.043	0.874	2.294	2.133	0.892
	R2	0.155	0.153	0.933	0.337	0.346	0.946
LA Downtown_Average	Slope	2.223	2.040	0.868	2.235	2.107	0.892
	R2	0.134	0.135	0.904	0.290	0.298	0.921
Idle and Creep	Slope	2.154	0.935	0.430	2.208	1.011	0.447
	R2	0.102	0.095	0.917	0.262	0.260	0.948
		Ave 10 seconds			**Ave 100 seconds**		
		NTK vs AVL MSS	NTK vs AVL PM	AVL MSS vs AVL PM	NTK vs AVL MSS	NTK vs AVL PM	AVL MSS vs AVL PM
Local_1	Slope	0.716	0.787	0.938	0.358	0.380	0.894
	R2	0.112	0.144	0.940	0.110	0.148	0.952
Local_2	Slope	0.353	0.471	1.102	0.281	0.502	1.029
	R2	0.094	0.131	0.953	0.076	0.215	0.936
Local_3	Slope	1.213	1.256	1.034	1.174	1.197	0.941
	R2	0.319	0.303	0.946	0.433	0.480	0.944
Local_Average	Slope	0.760	0.838	1.024	0.604	0.693	0.955
	R2	0.175	0.193	0.946	0.206	0.281	0.944
Highway_1	Slope	0.716	0.821	1.139	0.713	0.831	1.154
	R2	0.142	0.136	0.946	0.607	0.596	0.964
Highway_2	Slope	0.763	0.597	0.784	0.946	0.973	0.951
	R2	0.112	0.077	0.688	0.460	0.431	0.802
Highway_Average	Slope	0.739	0.709	0.962	0.830	0.902	1.052
	R2	0.127	0.106	0.817	0.533	0.514	0.883
LA Downtown_1	Slope	2.104	2.096	0.904	2.927	2.838	0.809
	R2	0.340	0.374	0.905	0.426	0.537	0.877
LA Downtown_2	Slope	2.283	2.155	0.907	1.975	2.085	0.940
	R2	0.504	0.519	0.950	0.503	0.597	0.940
LA Downtown_Average	Slope	2.194	2.126	0.905	2.451	2.461	0.874
	R2	0.422	0.446	0.927	0.465	0.567	0.909
Idle and Creep	Slope	2.098	1.005	0.464	1.853	0.936	0.494
	R2	0.487	0.496	0.957	0.874	0.877	0.957

5.4.3. **PN Emissions**

PN emissions varied from 2.6x1010 #/mi to 5.4x1010 #/mi for the AVL PN PEMS system and from 5.0x1011 and 2.7x1012 #/mi for the NCEM system, as shown in Table 5-7. AVL PN PEMS emissions can be compared to the European standard on PN emissions for light-duty trucks of 6.0x1011. For the AVL PN PEMS, the PN emissions were typically 93% below the PN standard. The NCEM system, on the other hand, showed the vehicle's PN emissions were 142% higher than the standard. The differences between the NCEM and the PN PEMS ranged from 16 times higher (down town LA route) to ~35 times higher (freeway and FTP-like routes).

The high bias for the NTK PN measurements relative to the AVL PN PEMS measurements is also seen in both the speed bin and the Q-Q plots in Figure 5-8 and Figure 5-9, respectively, for one day of testing that included two highway routes, two LA downtown routes, and a idle and creep route, and the 25 and 75 percentile results from the Q-Q plots for PN in Table 5-3. Regression analyses for the real-time data for 1 second, 3 second, 10 second, and 100 second averaged data also showed a relatively poor correlation between the NTK PN and AVL PN PEMS results for almost all of the test cycles and averaging intervals, as shown in Table 5-8.

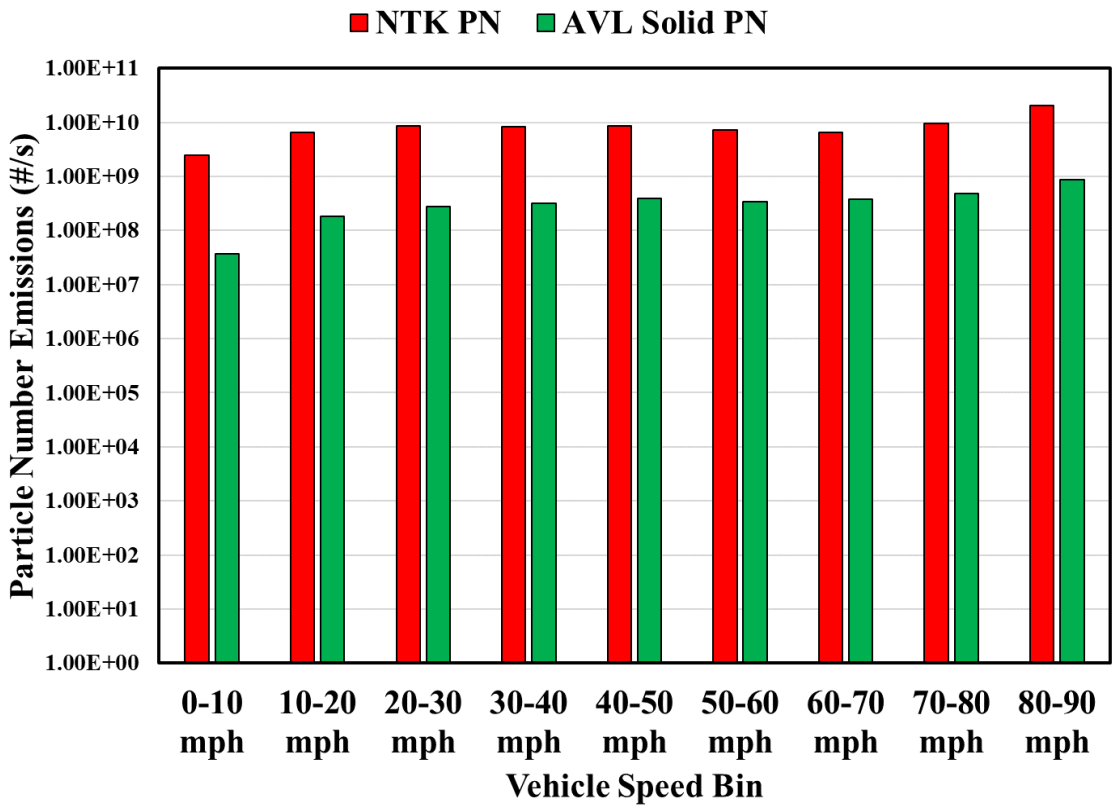

Figure 5-8 Vehicle speed based comparisons for particle number emissions for one day of testing

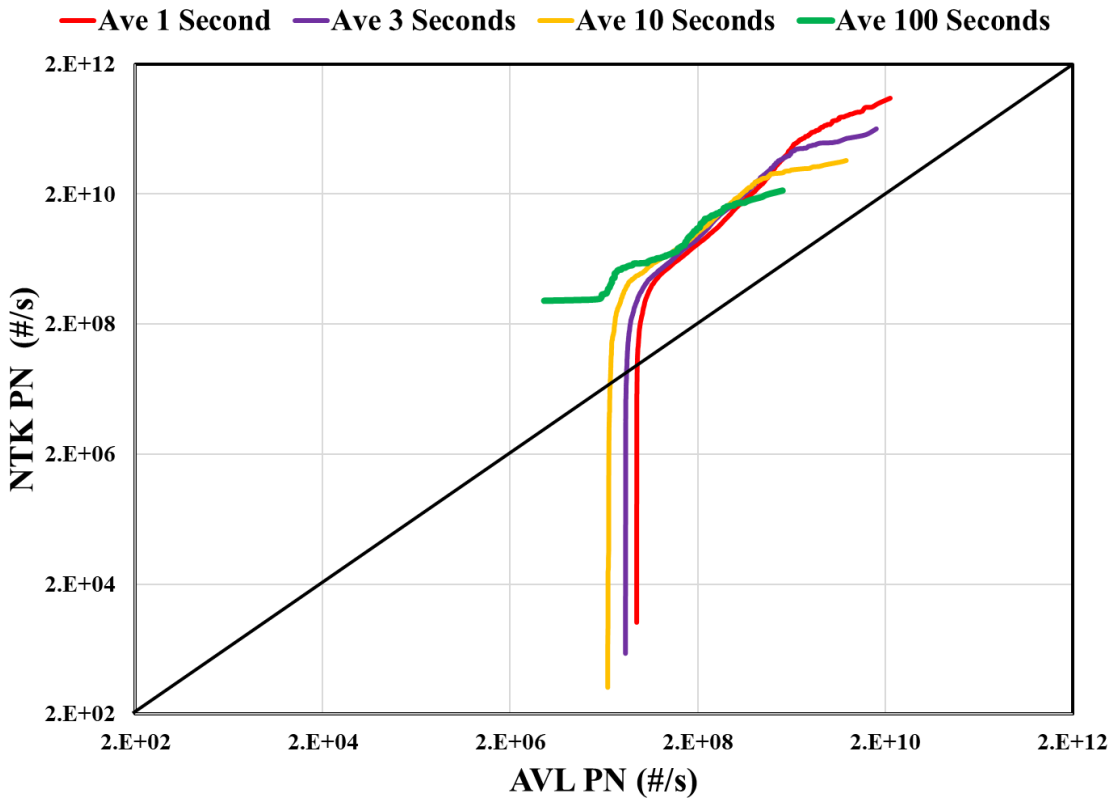

Figure 5-9 Q-Q Plot Analysis for PN Emissions for one day of testing

The discrepancy between the NCEM and PN PEMS measurements can be attributed to a zero current offset. This has been seen in other tests conducted by NTK. NTK has subsequently improved the PM/PN circuit and has shown a reduction of 81% in the zero offset variation, which should reduce these PN discrepancies (Tange, 2017). Other factors that could contribute to PN differences between the PN measurements include the nature of the particles. Both the PN PEMS and NCEM PN sensor measuring in the raw exhaust would be measuring particles that are primarily solid in nature, so discrepancies due to the nature of the particles should not be significant. The NCEM also measures particles down to ~10 nm (Amanatidis et al., 2017), as opposed to the PN PEMS that has a 23 nm size cut off, which could contribute to higher PN measurements for the NCEM.

Our internal particle size distribution data for this vehicle shows a primary peak at ~75 nm, however, with only a minor peak at ~15 nm, so this would only represent a small portion of the differences seen between the instruments. It should be noted that it is possible to adjust the trap voltage on the NCEM PN sensor in order to simulate higher particle cut-points (such as particles >23 nm), which could allow for a more direct comparison with a PMP compliant PEMS.

In comparison with previous studies, an older NTK PM instrument was compared to dilution tunnel PN measurements using the UCR MEL for engine dynamometer emissions measurements (Jiang et al., 2016). In this study, the NTK PM was measured raw, while the MEL PN measurements were measured dilute (>100 – 1) without a catalytic stripper. In this previous study, the NTK PN measurements were 45% and 69% lower than the CPC PN for the FTP and UDDS, respectively. The steady state SET cycles showed a larger bias, where the NTK PN system was about -90% of the EEPS measurement. In other work, Tikkanen et al. (2013) found the PPS reported 80% higher PN than an APC for a heavy-duty engine and somewhat higher PN emissions for a passenger car, but lower PN emissions than an APC during a regeneration due to desorption from the CVS and for a Euro 4 diesel vehicle during high speed portions of the testing.

Table 5-7 Summary of Total and Solid PN Emissions

Results	Start Location	End Location	Mini-PEMS	PN PEMS	Mini-PEMS	PN PEMS
			Total PN	Solid PN	Total PN	Solid PN
			#/cycle		#/mi	
Local_1	UCR CECERT	UCR CECERT	4.72E+12	2.96E+11	6.98E+11	4.38E+10
Local_2	UCR CECERT	UCR CECERT	4.83E+12	3.48E+11	7.02E+11	5.05E+10
Local_3	UCR CECERT	UCR CECERT	7.76E+12	3.38E+11	1.15E+12	4.99E+10
average					8.49E+11	4.81E+10
Highway_1	UCR CECERT	USC main campus	2.62E+13	1.40E+12	4.15E+11	2.22E+10
Highway_2	USC main campus	UCR CECERT	3.46E+13	2.09E+12	5.49E+11	3.32E+10
average					4.82E+11	2.77E+10
LA Downtown_1	USC main campus	USC main campus	3.07E+13	4.84E+11	1.94E+12	3.07E+10
LA Downtown_2	USC main campus	USC main campus	3.59E+13	7.05E+11	2.27E+12	4.46E+10
average					2.11E+12	3.76E+10
Idle and Creep	USC main campus	USC main campus	6.97E+12	1.37E+11	3.87E+12	7.62E+10
Total			1.52E+14	5.80E+12	1.45E+12	4.22E+10

*These values are the average of all total or solid PN emissions over all different cycles in g/mi basis

Table 5-8 Summary of Correlation Slope and Regression Statistics for PN Emissions

PN (#/s)		Ave 1 second	Ave 3 seconds	Ave 10 seconds	Ave 100 seconds
		NCEM vs PN PEMS	NCEM vs PN PEMS	NCEM vs PN PEMS	NCEM vs PN PEMS
Local_1	Slope	2.323	6.279	6.730	3.036
	R2	0.002	0.018	0.040	0.027
Local_2	Slope	3.041	6.447	7.802	7.153
	R2	0.008	0.056	0.130	0.138
Local_3	Slope	7.551	17.830	21.131	23.144
	R2	0.024	0.199	0.290	0.390
Local_Average	Slope	4.305	10.185	11.888	11.111
	R2	0.011	0.091	0.154	0.185
Highway_1	Slope	2.320	3.040	5.926	13.913
	R2	0.002	0.007	0.049	0.535
Highway_2	Slope	3.152	3.975	4.090	6.929
	R2	0.009	0.032	0.061	0.212
Highway_Average	Slope	2.736	3.507	5.008	10.421
	R2	0.006	0.019	0.055	0.373
LA Downtown_1	Slope	13.573	21.184	28.236	41.409
	R2	0.037	0.114	0.217	0.260
LA Downtown_2	Slope	10.555	16.472	21.769	23.304
	R2	0.053	0.171	0.342	0.399
LA Downtown_Average	Slope	12.064	18.828	25.003	32.357
	R2	0.045	0.143	0.279	0.329
Idle and Creep	Slope	9.366	12.399	18.542	19.197
	R2	0.051	0.125	0.405	0.716

5.5. **Conclusion**

The primary goal of this study was to compare emissions measurements between a 1065 compliant AVL M.O.V.E.S. PEMS, and a current generation mini-PEMS capable of measuring NOx, PM, and solid PN. Both PEMS units were equipped on a light-duty diesel truck and tested over local, highway, and downtown driving routes over 2 days. The results indicate that the NOx measurements for the mini-PEMS were within approximately ±10% of those the 1065 compliance PEMS, which suggests that the mini-PEMS could be used as a screening tool for NOx emissions. The NCEM showed larger differences for PM emissions on an absolute level, but this was at PM levels well below the 1 mg/mi level. The NCEM differences ranged from -2% to +26% if the comparisons are based on a percentage of the 1.0 mg/mi standard. Larger differences were also seen for PN emissions, with the NCEM measuring higher PN emissions. This can be attributed to a zero current offset that was found for the NCEM system, which has been subsequently improved in the latest generation of the NCEM system. One other important consideration is that an external EFM was utilized to obtain the exhaust flow for these measurements, which is a part of the AVL PEMS set-up but is not typically utilized in conjunction with the NCEM. While the ECM data was not collected with the NCEM used in this study, the current version of the NCEM does collect ECM data that could be utilized for determining the exhaust flow rate. This would represent an additional source of differences between the NCEM and the AVL PEMS that was not quantified in this study.

The comparisons between the 1065 compliant PEMS and the NCEM suggest that there could be applications for the NCEM or other mini-PEMS in areas where larger data

sets of emissions data, or where the cost of full laboratory or 1065 compliant PEMS testing is prohibitive. As recent findings have suggested that it is important to monitor vehicle emissions under a much wider range of conditions than can be duplicated in the laboratory, the NCEM could play a role in allowing for the testing of more vehicles under a broader range of conditions. As in-use testing becomes increasing more prevalent as part of regulatory compliance procedures, this might also suggest potential uses for the NCEM. This could include testing by government agencies to identify potential emissions issues that could subsequently be more extensively investigated in the laboratory or with 1065 compliant PEMS. Similarly, the NCEM could be utilized by vehicle/engine manufacturers to ensure are not specific environmental or operational regimes that could trigger emissions issues with their products. Finally, there is increased interest in the regulatory community to expand inspection and maintenance programs to heavy-duty vehicles, which to data have only been subject to testing with opacity or other methods that do not capture a full breadth of emissions. For the NCEM in particular, the good comparison for NOx emissions suggests that the NCEM could be applied in all of these areas where characterization of NOx is considered to be important, which could include in-use or I/M testing of light-duty or heavy-duty diesel vehicles. The PM emissions comparisons with the NCEM suggest that the NCEM could be effective in identifying potential situations where high PM emissions might be found for either gasoline direct injection vehicles or diesel vehicles with DPFs in various stages of failure. Additional testing of PM emissions over a wider range of PM emissions levels would be needed to better understand this possibility.

5.6. **Acknowledgements**

The authors thank the following organizations and individuals for their valuable contributions to this study. We acknowledge funding from the NGK Spark Plugs Co., LTD. The authors thank Mr. Eddie O'Neal and Mr. Mark Villela of the University of California, Riverside for their contribution in contacting this research program.

5.7. **References**

Amanatidis, S., Maricq, M.M, Ntziachristos, L., Samaras, Z., 2017. Application of the dual Pegasor Particle Sensor to real-time measurement of motor vehicle exhaust PM. Journal of Aerosol Science. 103, 93–104.

California Air Resource Board (CARB), 2016. The California Low-Emission Vehicle Regulation: The LEV II (Criteria Pollutant) Regulation. California Air Resource Board, Sacramento, US.

Cao, T., Johnson, K.C., Durbin, T.D., Russell, R.L., Cocker III, D.R., Maldonado, H., 2016a. Evaluations of In-Use Emission Factors from Off-Road Construction Equipment, Atmos. Environ. 147, 234-245.

Cao, T., Durbin, T.D., Cocker III, D.R., Wanker, R., Schimpl, T., Pointner, V., Oberguggenberger, K., Johnson, K.C., 2016b. A Comprehensive Evaluation of a Gaseous Portable Emissions Measurement System with a Mobile Reference Laboratory, Emissions Control Sci. & Technol. 2, 173-180.

Code of Federal Regulations, Title 40, Part 1065, Engine Testing Procedures.

40 CFR 86.1370-2007, Not-To-Exceed test procedures, 65 Federal Register 59958, (2000)

Boucher, T.L., Khalek, I.A., Laroo, C.A., Bishnu, D.K., 2012. Determination of the PEMS measurement allowance for PM emissions regulated under the heavy-duty diesel engine in-use testing program. SAE Int. J Engines 5, 1371–1386.

Durbin, T.D., Johnson, K., Cocker, D.R., Miller, J.W., Maldonado, H., Shah, A., Ensfield, C., Weaver, C., Akkard, M., Harvey, N., Symon, J., T. Lanni, T., Bachalo, W.D., Payne, G., Smallwood, G., Linke, M., 2007. Evaluation and Comparison of Portable Emissions Measurement Systems and Federal Reference Methods for Emissions from a Back-up Generator and a Diesel Truck Operated on a Chassis Dynamometer. Environ. Sci. & Technol. 41, 6199-6204.

Federal Register, 2003. Proposed Settlement Agreement, Federal Register 68:113, June 12 2003, pp. 35211–35212.

Federal Register, 2005. Control of Emissions of Air Pollution From New Motor Vehicles: In-use Testing for Heavy-duty Diesel Engines and Vehicles, Federal Register, June 14, 2005, vol. 70 No. 113.

Fiest, M.D., Sharp, C.A., Mason, R.L., Buckingham, J.P., 2008. Determination of PEMS Measurement Allowance for Gaseous Emissions Regulated under the Heavy-duty Diesel Engine In-use Testing Program. Final Report Prepared by Southwest Research

Institute, San Antonio, TX, EPA. Contract No. EP-C-05e018, February. http://www.epa.gov/otaq/regs/hd-hwy/inuse/420r08005.pdf.

Frey, H.C., Rasdorf, W., Lewis, P., 2010b. Comprehensive field study of fuel use and emissions of nonroad diesel construction equipment. Transp. Res. Rec. 2158, 69e76.

Gautam, M., Clark, N.N., Riddle, W., Nine, R., Wayne, W.S., Maldonado, H., Agrawal, A., Carlock, M., 2002. Development and initial use of a heavy-duty diesel truck test schedule for emissions characterization. In Proceedings of Society of Automotive Engineers (SAE) Fuels and Lubricants Meeting; SAE Paper 2002-01-1753. SAE: Warrendale, PA.

Jiang, Y., Johnson, K.C., Durbin, T.D., Yang, J., 2016. Evaluation of NTK Compact Emission Meter (NCEM), PEMS Workshop 2016, UC Riverside, Riverside, CA, March.

Johnson, D., 2002. ROVER – Real-time On-road Vehicle Emissions Reporter. Presentation for the Mobile Source Technical Review Committee, February.

Johnson, K.C., Durbin, T.D., Cocker III, D.R., Miller, J.W., Agama, R.J., Moynahan, N., Nayak, G., 2008. On-Road Evaluation of a PEMS for Measuring Gaseous In-Use Emissions from a Heavy-Duty Diesel Vehicle. SAE Int. J. Commer. Veh. 1, 200-209.

Johnson, K.C., Durbin, T.D., Cocker III, D.R., Miller, J.W., Bishnu D.K., Maldonado H., Moynahan N., Ensfield C., Laroo C.A., 2009. On-Road Comparison of a Portable Emission Measurement System with a Mobile Reference Laboratory for a Heavy Duty Diesel Vehicle. Atmospheric Environment. 43, 2877-2883.

Johnson, K.C., Durbin, T.D., Jung, H., Cocker III, D.R., Giannelli, R., Bishnu, D., 2011a. Quantifying In-Use PM Measurements for Heavy Duty Diesel Vehicles. Environ. Sci. Technol. 45, 6073-6079.

Johnson, K., Durbin, T.D., Jung, H., Cocker, D.R., Kahn, M.Y., 2011b. Supplemental Testing of PPMD at CE-CERT to Resolve Issues with the PPMD Observed during the HDIUT PM MA Program, Prepared for Mr. Andrew Redding. Sensors Inc.

Khalek, I.A., Bougher, T.L., Mason, R.L., Buckingham, J.P., 2010. PM-PEMS Measurement Allowance Determination, Final Report by Southwest Research Institute for the Heavy Duty In-use Testing Steering Committee. SwRI Project 03.14956.12, June.

Khan, M.Y., Johnson, K.C., Durbin, T.D., Jung, H., Cocker III, D., Bishnu, D., Giannelli, R. 2012. Characterization of PM-PEMS for In-Use Measurements – Validation Testing

for the PM-PEMS Measurement Allowance Program. Atmospheric Environment, 55, 311-318.

Kishan, S., Fincher, S., Sabisch, M., 2011. Populations, Activity and Emissions of Diesel Nonroad Equipment in EPA Region 7, Final Report for the US EPA and the CRC E-70 Program by Eastern Research Group. EPA Contract No. EP-C-06e080.

Lanki, T., Tikkanen, J., Janka, K., Taimisto, P., and Lehtim€aki, M. 2011. An electrical sensor for long-term monitoring of ultrafine particles in workplaces. J. Phys.: Conf. Ser., 304:012013. Available at http://iopscience. iop.org/1742-6596/304/1/012013.

Miller, J.W., Durbin, T.D., Johnson, K.J., Cocker III, D.R., 2006. Evaluation of Portable Emissions Measurement Systems (PEMS) for Inventory Purposes and the Not-to-exceed Heavy-duty Diesel Engine Regulations; Final Report for the California Air Resources Board, July.

Ntziachristos, L., Fragkiadoulakis, P., Samaras, Z, Janka, K., and Tikkanen, J., 2011. Exhaust Particle Sensor for OBD Application. SAE Technical Paper 2011-01-0626.

Ntziachristos, L., Amanatidis, S., Rostedt, A., Keskinen, J., Janka, K., Tikkanen, J., 2012, Calibration and performance of a novel particle sensor for automotive application, EAC - 2012, European Aerosol Conference, Granada, Spain, 2-7 Sept.

Ntziachristos, L., Amanatidis, S., Samaras, Z., Janka, K., and Tikkanen, J., 2013. Application of the Pegasor Particle Sensor for the Measurement of Mass and Particle Number Emissions. SAE Int. J. Fuels Lubr. 6(2), 521–531.

Ropkins, K., Li, H., Burnette, A., 2016. Next Generation (Smaller, Lower Cost, Lower Energy Consumption) Portable Emissions Measurement Systems, PEMS Workshop 2016, UC Riverside, Riverside, CA, March.

Rostedt, A., Arffman, A., Janka, K., Yli-Ojanperä, J., & Keskinen, J., 2014. Characterization and Response Model of the PPS-M Aerosol Sensor. Aerosol Science and Technology. 48(10), 1022-1030, DOI: 10.1080/02786826.2014.951023.

Rostedt, A., Ntziachristos, L., Simonen, P., Rönkkö, T. Samaras, Z.C., Hillamo, R., Janka, K., and Keskinen, J., 2017. A New Miniaturized Sensor for Ultra-Fast On-Board Soot Concentration Measurements. SAE Int. J. Engines. 10(4), doi:10.4271/2017-01-1008.

Sardar, S., Zhang, S., Larsen, L., Frodin, B., McMahon, M., Huang, S.M., et al., 2015. Evaluation of PM Measurement Precision and the Equivalency of the Single and Three Filter Sampling Methods for LEV III FTP Standards. SAE Int. J. Engines. doi:10.4271/2015-01-9045.

Saukko, E., Järvinen, A., Wihersaari, H., Rönkkö, T., Janka, K., Keskinen, J., 2016. Expanded Capabilities of Dual Pegasor PPS-M Sensor in PEMS Measurements Beyond PN, PM and Particle Size, PEMS Workshop 2016, UC Riverside, Riverside, CA, March.

Steppan, J., Henderson, B., Johnson, K., Khan, M.Y., Diller, T., Hall, M., Lourdhusamy, A., Allmendinger, K., Matthews, R., 2011, 2017, Comparison of an On-Board, Real-Time Electronic PM Sensor with Laboratory Instruments Using a 2009 Heavy-Duty Diesel Vehicle, SAE Technical Paper No. 2011-01-0627.

Swanson, J., et al., 2018, Uncertainty in Gravimetric Analysis Required for LEV III Light-Duty Vehicle PM Emission Measurements, submitted to the Society of Automotive Eningeers International Journal of Engines.

Tange, T., 2017, Development of Compact Multi Gas Measurement System (NCEM©), 7th International PEMS Conference and Workshop, Riverside, CA, March.

Thompson, G.J., Carder, D.K., Besch, M.C., Thiruvengadam, A., Kappanna, H.K., 2014. In-use emissions testing of light-duty diesel vehicles in the United States, Center for Alternative Fuels, Engines and Emissions, West Virginia University.

Tikkanen, J., Janka, K., Rostedt, A., Röbel, M., Amanatidis, S., Ntziachristos, L., 2013. Dilution Artifacts. A Significant Source of Error from Absolute Concentration and Possibly Difficult to Reproduce. PMP vs. Raw Exhaust. 17th ETH-Conference on Combustion Generated Nanoparticles. Zürich, Switzerland, June 23th – 26th.

TSI Incorporated, 2015, Nanoparticle Emissions Tester Model 3795 brochure and website, www.tsi.com/NPET.

U.S. Environmental Protection Agency, 2008. Determination of PEMS measurement allowances for gaseous emissions regulated under the heavy-duty diesel engine in-use testing program. Revised Final Report EPA420-R-08-005. United States Environmental Protection Agency, Arlington, US.

U.S. Environmental Protection Agency, 2016. Light-Duty Vehicles and Light-Duty Trucks: Clean Fuel Fleet Exhaust Emission Standard. Revised Final Report EPA420-B-16-006. United States Environmental Protection Agency, Arlington, US.

Vlachos, T., Bonnel, P., Perujo, A., Weiss, M. et al., 2014. In-Use Emissions Testing with Portable Emissions Measurement Systems (PEMS) in the Current and Future European Vehicle Emissions Legislation: Overview, Underlying Principles and Expected Benefits, SAE Int. J. Commer. Veh. 7(1), 2014-01-1549, doi:10.4271/2014-01-1549.

Xue, J., Johnson, K.C., Durbin, T.D., Russell, R.L., Pham, L., Miller, W., et al., 2017, Very Low Particle Matter Mass Measurements from Light-Duty Vehicles. J Aerosol Sci., Under review.

6. Impacts of dimethyl carbonate blends on gaseous and particulate emissions from a heavy duty diesel engine

6.1. Abstract

The reduction of emissions from diesel engines has been one of the primary elements in obtaining improvements in air quality and greenhouse gas reduction goal. Dimethyl carbonate (DMC) is an oxygenate fuel that can be used in petroleum diesel that is been lightly studied, but could provide significant reductions in particulate matter (PM) emissions from internal combustion engines. This study evaluated the emissions impacts of 5%, 12.5%, 20%, and 30% blends of DMC in a California diesel fuel. DMC showed PM reductions increased with increasing DMC blend levels, ranging from 30% to 78% for the DMC5 to DMC30 blends. In contrast, particle number emissions increased with increasing DMC levels, which could be attributed to the enhanced formation of small nucleation particles as the levels of larger accumulation particles were reduced. NO_x emissions showed increases of 3.2% and 3.1%, respectively, for the higher 20% and 30% blends, but no statistically significant differences for the 5% and 12.5% blends. Carbon monoxide (CO) emissions showed strong reductions from 26.3% to 60.9% with DMC blending, while total hydrocarbons (THC) emissions showed increases from 32.5% to 137% with DMC. Most of the hydrocarbon species showed increases with increasing DMC blend levels, including benzene and most mono-aromatic hydrocarbons. Similarly, formaldehyde and acetaldehyde showed statistically significant increases with DMC blending relative to

diesel fuel. The carbon dioxide (CO_2) emissions and brake specific fuel consumption (BSFC) increased with increasing DMC blend levels compared to diesel fuel.

6.2. **Introduction**

Diesel exhaust and specific components within that exhaust continue to receive attention because of their adverse health effects and environmental impacts [Mills et al., 2005; Nel et al., 1998]. In California, diesel particulate matter (PM) has been classified as a toxic air pollutant since 1998 [CARB, 1998]. On a federal level, the United States Environmental Protection Agency (USEPA) enacted stringent 2007 emission standards for heavy-duty diesel engines to reduce PM on-road to 0.0134 g/kWh [Johnson, 2016]. In addition to diesel PM, USEPA has been regulating nitrogen oxides (NOx) emissions, a known pollutant that promotes secondary organic aerosol formation and enhances ozone in the presence of sunlight [Wofsy et al., 1990], from heavy-duty diesel engines with the aim to achieve a 95% reduction in NOx emissions, effective as of 2010 [Johnson, 2016]. To meet the USEPA standards, common approaches for PM and NOx emissions reductions include the use of diesel particulate filters (DPFs) and selective catalytic reduction (SCR), respectively [Johnson, 2016; Herner et al., 2009]. In addition to the implementation of sophisticated aftertreatment systems in automotive engines, new alternative fuel formulations are being introduced into the fuel market that are required to reach targets for renewable fuel use.

There is a growing interest in the use of renewable oxygenated fuels either as replacements of, or additives to, petroleum-based transportation fuels in internal combustion engines. Oxygenated biofuels, such as ethanol and fatty acid methyl esters, are

attractive because they offer greenhouse gas (GHG) emission benefits, reduce the tendency to form soot and black carbon emissions, help address climate change, and reduce the dependence on fossil fuel resources [Karavalakis et al., 2014; Hajbabaei et al., 2014; Ratcliff et al., 2016]. Carbonate esters (which consist of a carbonyl group connecting two alkyl groups) are promising fuels for use in compression ignition engines [Kumar and Sarayanan, 2016; Sivalakshmi and Balusamy, 2012]. Dimethyl carbonate [$CH_3OC(=O)OCH_3$, DMC] is a fuel that generates interest primarily due to its high oxygen content (53% by weight) [Pacheco and Marshall, 1997]. DMC is non-toxic, biodegradable, and highly miscible with diesel fuel. An additional benefit is that DMC can be produced from methanol and carbon dioxide (CO_2) in the presence of a catalyst (usually potassium chloride) providing a sink for the GHG, CO_2 [Souza et al., 2014]. The molecular structure of DMC includes oxygen atoms paired up with carbon atoms to form CO. Hence, the absence of carbon-carbon bonds in the fuel moiety will contribute to hydrocarbon oxidation rather than participation in soot growth reactions [Glaude et al., 2005].

There have been studies of the combustion performance and emissions of diesel engines operating on DMC blends with petroleum diesel fuel [Sun et al., 2016; Kocis et al., 2000; Kozak et al., 2009]. Fundamental chemical kinetic studies have shown that when DMC is tested in a flame much of the oxygen in the dimethyl carbonate goes directly to CO2, which reduces the effectiveness of DMC for soot reduction in diesel engines [Glaude et al., 2005; Sun et al., 2016]. Rubino and Thomson [1999] observed a marked reduction of soot precursors, such as acetylene and benzene, when using a counter-flow propene/air diffusion flame to study the inhibition of soot formation with DMC. This systematic

tendency of DMC to reduce soot was also confirmed in older studies, where soot and smoke emissions declined almost linearly with increasing DMC content [Miyamoto et al., 1998; Murayama et al., 1995]. Cheung et al. [2011] investigated DMC-diesel blends in a direct injection diesel engine and found small differences in gaseous emissions, with some increases in carbon monoxide (CO) total hydrocarbons (THC) especially at lighter engine loads. They also found significant reductions in PM mass and particle number emissions with higher DMC concentrations, especially at higher engine loads. Huang et al. [2003] studied the combustion and emissions characteristics of a diesel engine fueled with DMC-diesel blends and found that the engine's thermal efficiency increases and the emissions of PM, THC, and CO decrease. Similar reductions in PM emission were also seen in other studies with DMC-diesel blends, as well as the potential of reducing benzene and 1,3-butadiene emissions [Rounce et al., 2010].

Motivated by previous studies published in the open literature as well as by the concerns regarding global climate change caused by GHG emissions and the contribution of heavy-duty diesel engines to PM emissions, the present work investigates the impact of DMC blending on the regulated emissions, mobile source air toxics (MSATs) that include some aromatics and carbonyl compounds, and particulate emissions. For this study, emission measurements were performed on 5%, 12.5%, 20%, and 30% DMC blends by volume. Testing was conducted on a 1991 Detroit Diesel Corporation (DDC) Series 60 engine over the standard Federal Test Procedure (FTP) cycle. The results of this work are discussed in the context of different DMC-diesel concentration and the influence of DMC properties on pollutant formation.

6.3. Experimental

6.3.1. Test Fuels

A total of six fuels were employed in this study. The baseline fuel was a typical on-road CARB ultra-low sulfur diesel (ULSD). The DMC was provided by Yashentech Corporation of China. The DMC was produced using carbon dioxide and methanol as the only feedstock. Typical properties of DMC include a cetane number of 35.5, a viscosity (at 40 °C) of 0.6 mm^2/s, and calorific value of 15.8 MJ/kg [Rounce et al., 2010]. The CARB ULSD was used to prepare blends with the DMC at proportions of 5% (denoted as DMC5), 12.5% (denoted as DMC12.5), 20% (denoted as DMC20), and 30% (denoted as DMC30) by volume. The blends were tested over two testing periods. The initial tests included a CARB ULSD and DMC20 blend. A second set of tests was then conducted on a CARB ULSD and a wider range of blends, including DMC5, DMC12.5, and DMC30. Although a different CARB ULSD was obtained for each of the two test periods, CARB diesel fuels are all certified to have emissions comparable to those of a 10% aromatic reference fuel, so it is expected that the two CARB ULSDs would have similar emissions characteristics.

6.3.2. Test Engines, Cycles, and Test Sequence

Testing was conducted on a 1991 model year Detroit Diesel Corporation (DDC) Series 60 engine. The engine had a displacement of 11.1 L, 6 cylinders in-line, and a rated horsepower of 360 hp at 1800 rpm, equipped with electronically controlled unit fuel injectors, and a turbocharger with an aftercooler. The 1991 DDC Series 60 engine is the engine that has traditionally been used for the emissions equivalent diesel certification

procedure in California, so it is one of the most widely tested engines in terms of studying CARB diesel fuels.

Emissions testing were conducted over the Federal Test Procedure (FTP) cycle for heavy-duty engines. The test matrix included 3 FTPs on each test fuel for each of the test periods. For each test period, an engine map was obtained for the CARB ULSD that was used for the testing on all fuels to provide a consistent basis for comparing the fuels.

6.3.3. Emissions Testing

All tests were conducted in CE-CERT's heavy-duty engine dynamometer laboratory. This laboratory is equipped with a 600-hp General Electric DC electric engine dynamometer. Emissions measurements were obtained using the CE-CERT Mobile Emissions Laboratory (MEL). The facility and sampling setup have been described in detail previously and are only discussed briefly here [Cocker et al., 2004]. For all tests, standard emissions measurements of THC, CO, NOx, carbon dioxide (CO_2), and PM, were measured. CO and CO_2 emissions were measured with a 602P nondispersive infrared (NDIR) analyzer from California Analytical Instruments (CAI). THC emissions was measured with a 600HFID flame ionization detector (FID) from CAI. NOx emissions were measured with a 600HPLC chemiluminescence analyzer from CAI. Fuel consumption was determined from these emissions measurements via carbon balance using the densities and carbon weight fractions from the fuel analysis. The mass concentrations of PM were obtained by analysis of particulates collected on 47 mm diameter 2 μm pore Teflon filters (Whatman brand). The filters were measured for net gains using a UMX2 ultra precision

microbalance with buoyancy correction following the weighing procedure guidelines of the Code of Federal Regulations (CFR).

Particle number measurements were made with a TSI model 3776 ultrafine condensation particle counter (CPC), with a cut point of 2.5 nm. Particle size distributions were obtained using an Engine Exhaust Particle Sizer (EEPS) spectrometer. The EEPS (TSI 3090, MCU firmware version 3.05) was used to obtain real-time second-by-second size distributions between 5.6 to 560 nm. Particles were sampled at a flow rate of 10 L/min, which is considered to be high enough to minimize diffusional losses. The sample flow first went through a cyclone, which removes particles larger than 1μm in diameter. Then, they were then charged with a corona charger and sized based on their electrical mobility in an electrical field. Concentrations were determined through the use of 22 ring-shaped electrometers. All the data were post-processed under the newly released 'soot' matrix from TSI.

Samples for carbonyl analysis were collected onto 2,4-dinitrophenylhydrazine (DNPH) coated silica cartridges (Waters Corp., Milford, MA). A critical flow orifice controlled the flow to 1.0 L/min through the cartridge. Sampled cartridges were extracted using 5 mL of acetonitrile and injected into an Agilent 1200 series high performance liquid chromatograph (HPLC) equipped with a variable wavelength detector. The column used was a 5 μm Deltabond AK resolution (200cm x 4.6mm ID) with an upstream guard column. The HPLC sample injection and operating conditions were set up according to the specifications of the SAE 930142HP protocol. Samples from the dilution air were collected for background corrections.

Hydrocarbon species were collected using a 6 L specially-prepared SUMMA passivated canister, which was connected to the CVS system. Analysis of the hydrocarbon species was conducted using a Gas Chromatography/Mass Spectrometry/Flame Ionization Detector (GC/MS/FID) analytical system with the standard PAMS Protocol Compendium Method TO-15.

6.4. **Results and Discussion**

The following figures/tables present the results of this study. The results shown in the figures/tables represent the average of all test runs performed on that fuel for the specific test segment. The error bars represent one standard deviation on the average value. Statistical analyses were performed using a 2-tailed, 2-sample, equal-variance *t*-test. The statistical analyses provide information on the statistical significance of the different individual findings. The following discussion focuses predominantly on results that were found to be either statistically significant or marginally statistically significant. Results are considered to be statistically significant for p values ≤ 0.05. Results are considered marginally statistically significant for $0.05 \leq p < 0.1$. It should be noted that the CARB ULSD results are presented separately for the different test periods, and are shown with different bars in the figures, denoted as CARB #1 and CARB #2.

6.4.1. **PM Mass, Particle Number, and Particle Size Distribution**

Emissions of PM mass, expressed on a gram per brake horsepower hour (g/bhp-hr) basis, for the different DMC blends tested over the two periods are shown in Figure 6-1. Overall, PM mass emissions showed substantial reductions with DMC application compared to CARB ULSD ranging from 30% to 78%, with these reductions being

statistically significant. The results reported here are in good agreement with previous studies showing strong reductions in PM and soot emissions with DMC-diesel blends [Kocis et al., 2000; Kozak et al., 2009; Zhang and Balasubramanian et al., 2014; Kitagawa et al., 2001], as well as studies of other oxygenates such as biodiesel [USEPA, 2002; Hajbabaei et al., 2013; Giakoumis et al., 2012; Robbins et al., 2011]. In comparison with biodiesel, however, the percentage reductions for the DMC are much larger than those seen for biodiesel for a comparable blend level.

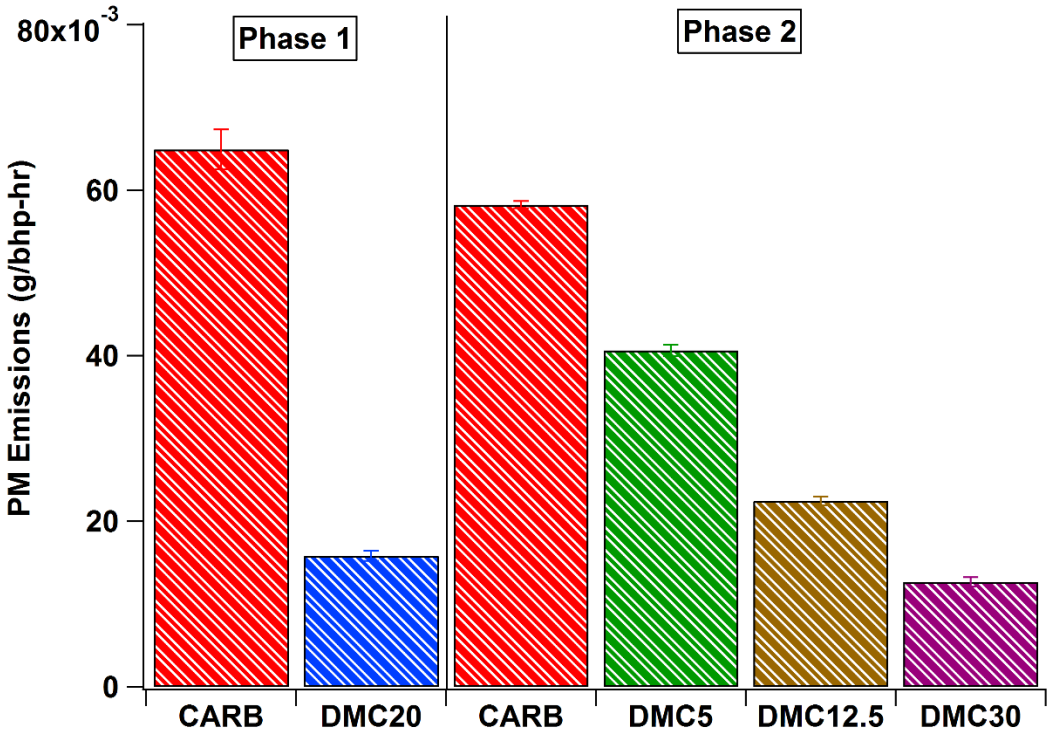

Figure 6-1 Average PM mass emission results for the DMC blends and CARB ULSD. The error bars represent one standard deviation of the average values

There are several contributing factors that could be affecting the formation of PM with oxygenated fuels. The presence of oxygen in the fuel can lead to PM reductions due to its impact on reducing excessively rich zones during combustion. A comparison between the PM reductions as a function of oxygen content is provided in Figure 6-2. This comparison shows that at lower blend levels the PM reductions for DMC and biodiesel both seem to be driven by the impact of oxygen on PM formation during combustion. For oxygen contents above 10%, however, the DMC shows slightly greater reductions on a per oxygen basis. This indicates that synergistic effects of DMC's chemical structure and physical properties may also be of importance at the higher oxygen levels. The absent of C-C bonds in DMC could reduce the formation of the precursor soot species, such as acetylene (C_2H_2) and benzene (C_6H_6) [Rubino and Thomson, 1999]. On the other hand, the production of free radicals (•O, •OH, etc.) with DMC combustion would promote the carbon oxidation to CO and CO_2 within the premixed flame zone, thus limiting the carbon available and modifying the path for the formation of soot [Zhang and Balasubramanian et al., 2014, Cheng et al., 2002]. DMC also has a lower viscosity and boiling point and a lower cetane number compared to diesel fuel. This may also lead to an increase in ignition delay together with an increase in the amount of fuel burned in the premixed combustion phase, since it was expected that the fuel atomized in smaller fuel droplets and at faster rates of vaporization and thus increasing the efficiency of fuel and air mixing prior to the start of combustion [Kocis et al., 2000; Miyamoto et al., 1998; Zhang and Balasubramanian et al., 2014, Wu et al., 2006; Zhu et al., 2011; Hellier et al., 2013]. These phenomena would

reduce the amount of fuel burned in the diffusion mode and hence suppress the formation of soot and subsequently PM emissions.

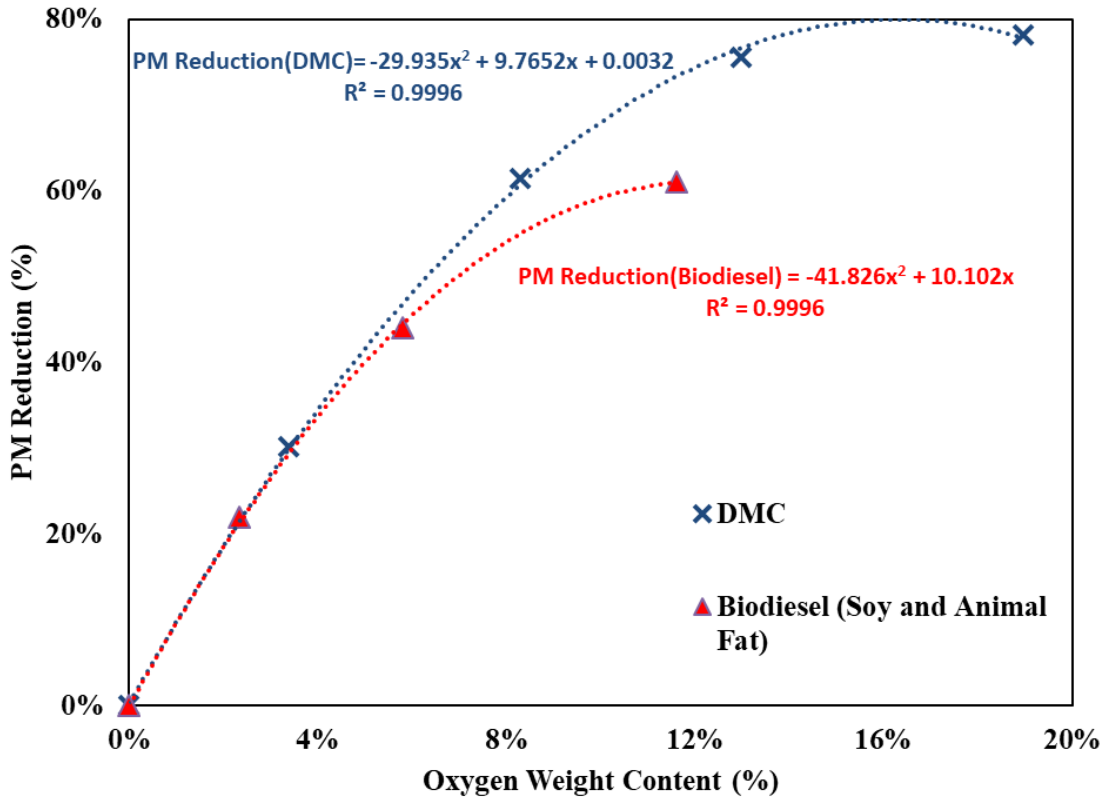

Figure 6-2 Relationship between PM mass reduction (%) and oxygen content by weight (%)

Particle number emissions are shown in Figure 6-3. The use of DMC resulted in statistically significant increases in particle number emissions compared to CARB ULSD, ranging from 66% to 141%. Our results are in contrast with those seen in previous studies of DMC where particle number emissions showed reductions with higher concentrations of DMC in diesel fuel [Cheung et al., 2011; Zhang and Balasubramanian, 2014; Zhu et al., 2011]. Zhang and Balasubramanian [2014] found reductions in particle number emissions of 25.1% and 36.1% for 5% and 10% DMC blends, respectively, based on measurements

with a fast mobility particle sizer (FMPS), while Cheung et al. [2011] also showed reductions in particle number on average of 21% and 37%, for 9.1% to 18.6% DMC blends, respectively. On the other hand, similar increases in PN have also been seen in studies of DME [Kwak et al., 2014]. Under the present test conditions, the increase in particle number emissions could be associated with the fuel's oxygen atoms through the formation of hydroxyl radicals that can consume the soot precursors, thus yielding a reduction in soot formation [Song et al., 2002]. The corresponding decreased surface area of soot particles, available for condensation of volatile and semi-volatile species would promote the formation of nanoparticles by homogenous nucleation. This phenomenon results in an increase in the total particle number population [Fontaras et al., 2009].

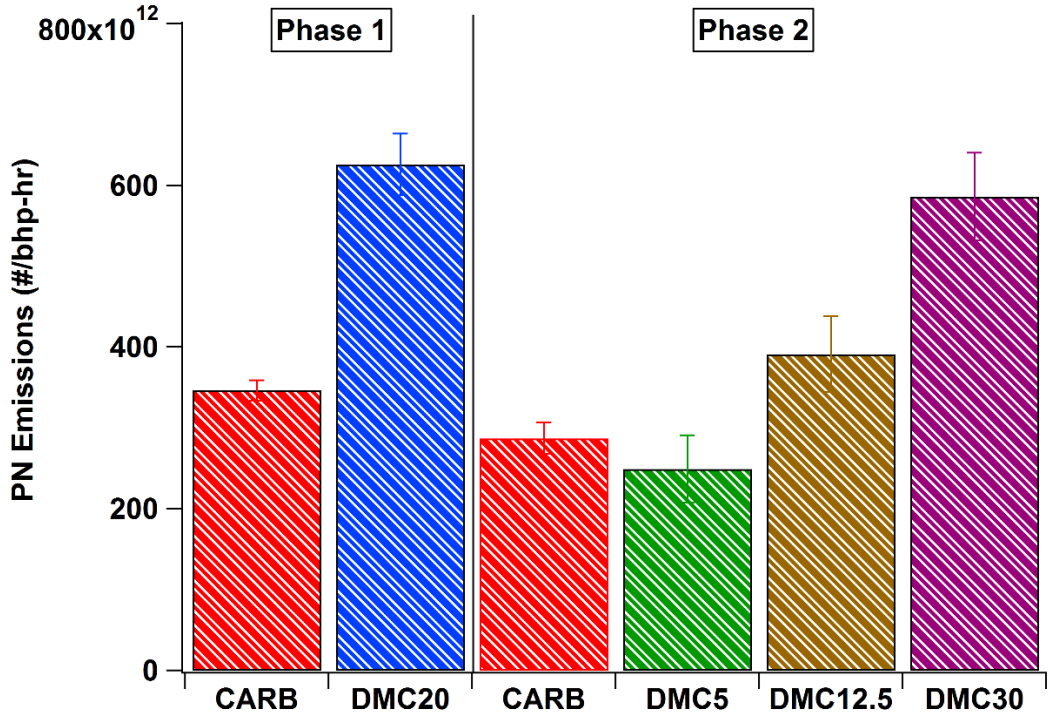

Figure 6-3 Average particle number emission results for the DMC blends and CARB ULSD. The error bars represent one standard deviation of the average values

The average particle size distributions for all test fuels are displayed in Figure 6-4 (a-b). The results show, that for each DMC blend, there is a shift towards lower concentrations of accumulation mode particles and substantially higher concentrations of nucleation mode particles. The results reported here are consistent with those of the total particle number emissions. In particular, with a suppression of soot nuclei growth at the core of fuel droplets, homogeneous nucleation can be enhanced. It was also possible that condensed droplets of unburned and partially burned fuel account for a significant proportion of nucleation mode particles observed for the DMC blends. This could be a plausible explanation for the higher concentrations of nucleation mode particles with the

DMC blends, since DMC possesses a lower boiling point than typical diesel fuel and emits higher levels of nucleation mode particles. Previous studies have shown a shift of the geometric mean diameter of particles towards smaller sizes in comparison to diesel fuel, primarily due to the fuel-borne oxygen [Rounce et al., 2010; Zhu et al., 2011]. Increases in nucleation particles have also been seen in studies of DME [Kwak et al., 2014]. In a recent investigation, Zhang and Balasubramanian [2014] found that particle size distributions consisted of only an accumulation mode at the 50% and 75% loads. At the 25% load, the particle size distribution was bimodal, but the accumulation mode particles were considerably higher in concentration compared to the nucleation mode particles. The nature of these differences could be due to differences in the testing conditions, as the testing in our study was done over a transient cycle while the testing in the other study was conducted at steady-state conditions.

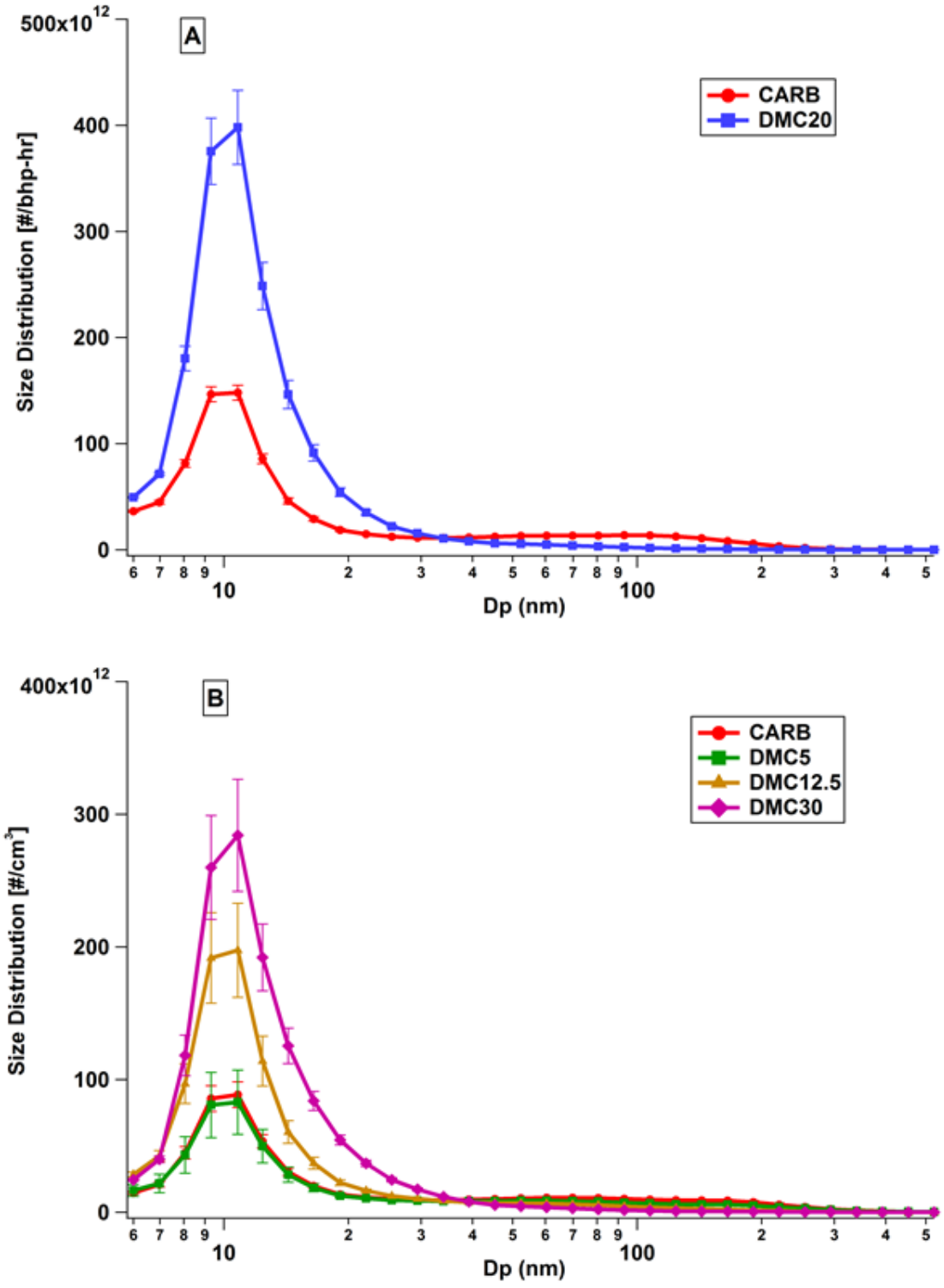

Figure 6-4 (a, b) Particle size distributions for CARB ULSD and the DMC blends

6.4.2. **NOx Emissions**

The effect of DMC on NOx emissions is shown in Figure 6-5. NOx emissions showed increases of 3.2% and 3.1%, respectively, for the higher DMC20 and DMC30 blends compared to CARB ULSD at a statistically significant level, but no statistically significant differences for DMC5 and DMC12.5 blends. The higher NOx emissions for the higher concentration DMC blends could be attributed to the increased oxygen content in the fuel blend, and NOx increases have been seen with other oxygenated fuels, such as biodiesel [Hajbabaei et al., 2014, USEPA, 2002; Hajbabaei et al., 2013; Giakoumis et al., 2012; Robbins et al., 2011; Hajbabaei et al., 2012; Mueller et al., 2009]. For biodiesel, Mueller et al. [2009] showed that more oxygenated charge air mixtures that are closer to stoichiometric at ignition and in the standing premixed autoignition tend to produce higher local and average in-cylinder temperatures, lower radiative heat losses, and a shorter more advanced combustion, all factors that would be expected to increase thermal NOx emissions. For DMC blends, the lower cetane number also leads to longer ignition delay and higher fraction of the premixed combustion phase, and hence higher NOx emissions. A similar PM/NOx emissions trade-off was observed in a previous investigation [Kozak et al., 2009]. Previous studies have also shown that the application of DMC can increase NOx emissions [Sivalakshmi and Balusamy, 2012; Rounce et al., 2010], whereas other studies have reported minimal changes in NOx emissions with DMC [Kocis et al., 2000, Cheung et al., 2011]. Murayama et al. [1995] have shown that NOx increases were very significant with oxygen addition. However, they have also demonstrated the possibility of simultaneous reduction of PM and NOx emissions when they applied a high EGR ratio in

conjunction with oxygenated fuel combustion. Mei et al. [2014] reported some increases for a 10% DMC blend at a higher engine load, but no significant changes at a lower engine load. On the contrary, Ren et al. [2008] found slight decreases in NOx emissions with increasing oxygen content for DMC and other oxygenates.

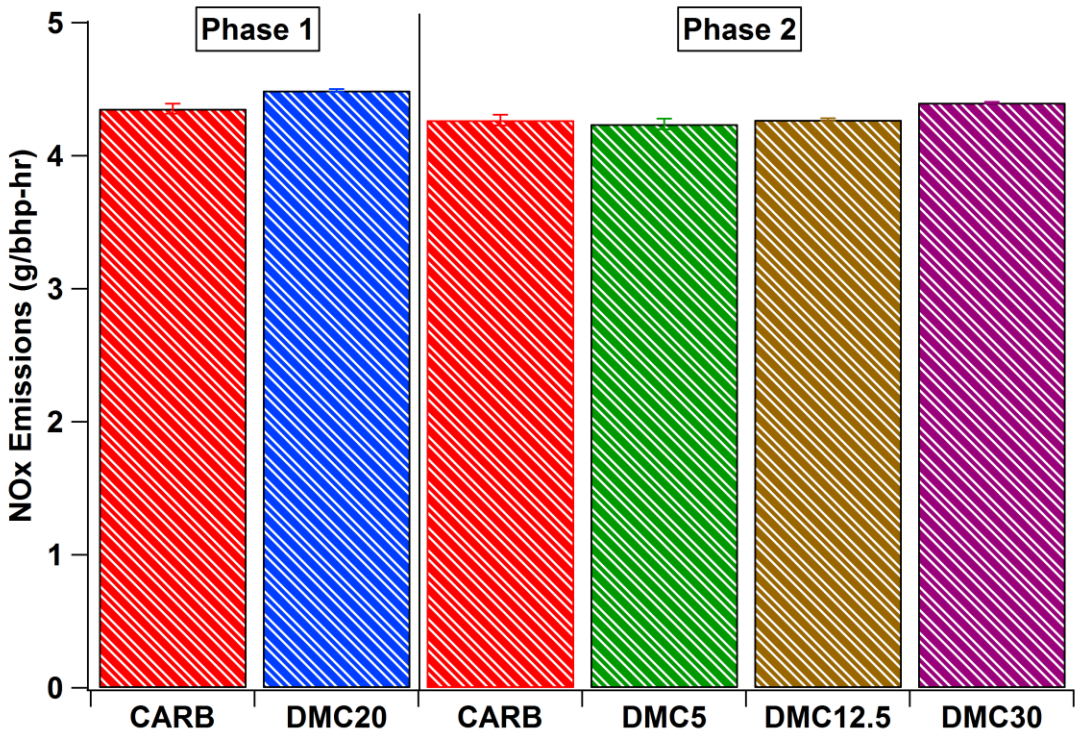

Figure 6-5 Average NO_x emission results for the DMC blends and CARB ULSD. The error bars represent one standard deviation of the average values

6.4.3. CO and THC Emissions

The CO emission results for the different DMC blends are shown in Figure 6-6 on a g/bhp-hr basis. CO emissions showed consistent, statistically significant reductions for all DMC blends compared to CARB ULSD, ranging from 26.3% to 61%. CO is a known product of incomplete combustion, arising under fuel rich conditions. Consistent with

previous studies, our results attribute the reductions in CO emissions of DMC blends relative to CARB ULSD to the provision of oxygen in fuel rich zones and to more complete combustion [Kocis et al., 2000; Cheung et al., 2011; Ren et al., 2008].

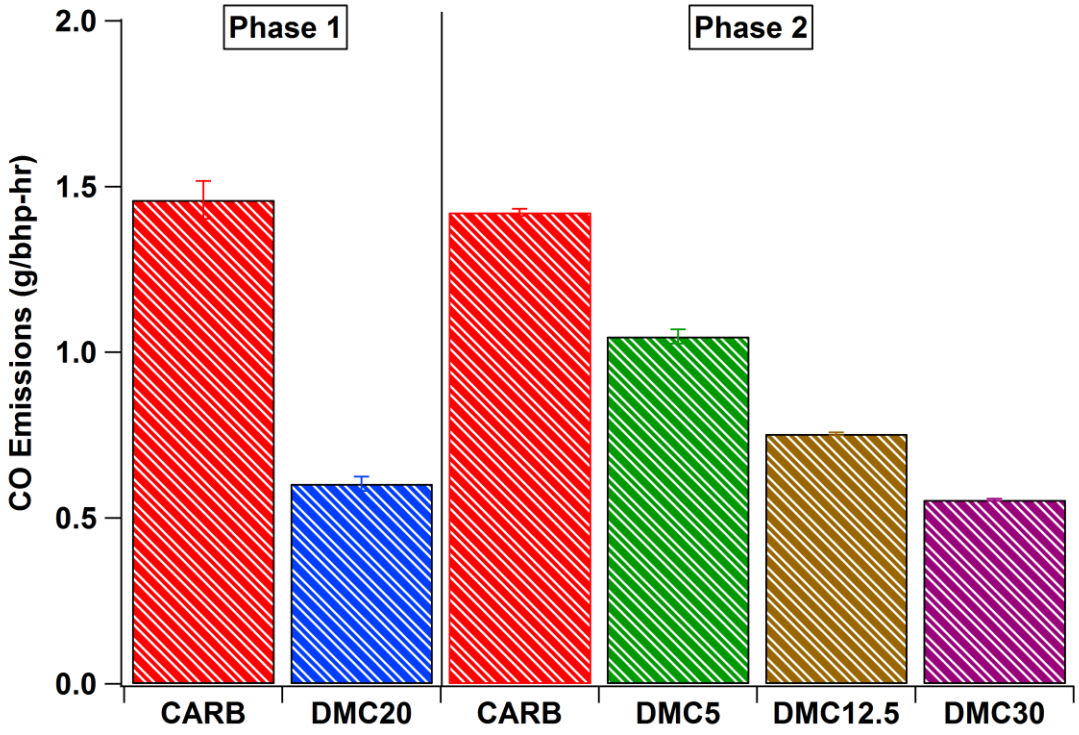

Figure 6-6 Average CO emission results for the DMC blends and CARB ULSD. The error bars represent one standard deviation of the average values

THC emissions showed systematic increases with the use of DMC blends, at a statistically significant level (Figure 6-7). The increases in THC emissions ranged from 33% to 137% for DMC5 to DMC30 relative to CARB ULSD. The findings of this study are in line with those of Lu et al. [Lu et al., 2005], but generally in contrast with the majority of studies where they reported lower THC emissions with the application of DMC-diesel blends as a consequence of the fuel-borne oxygen [Sivalakshmi and Balusamy, 2012,

Rounce et al., 2010, Mei et al., 2014; Ren et al., 2008]. A trend of increasing THC emissions has also been seen with other oxygenates in diesel fuel, such as ethanol-diesel blends [Li et al., 2005, Merritt et al., 2005]. THC, a product of incomplete combustion, is formed where combustion is quenched [Cheung et al., 2011]. It is theorized that the higher THC emissions for the DMC blends were likely produced due to quenching at the cylinder walls during the mixture formation as a result of the higher latent heat of evaporation of DMC relative to diesel fuel, which caused the oxygenated fuel in the blend to disperse to the crevice volumes of the combustion chamber and then discharge from the cylinder during the expanding stroke [Lu et al., 2005].

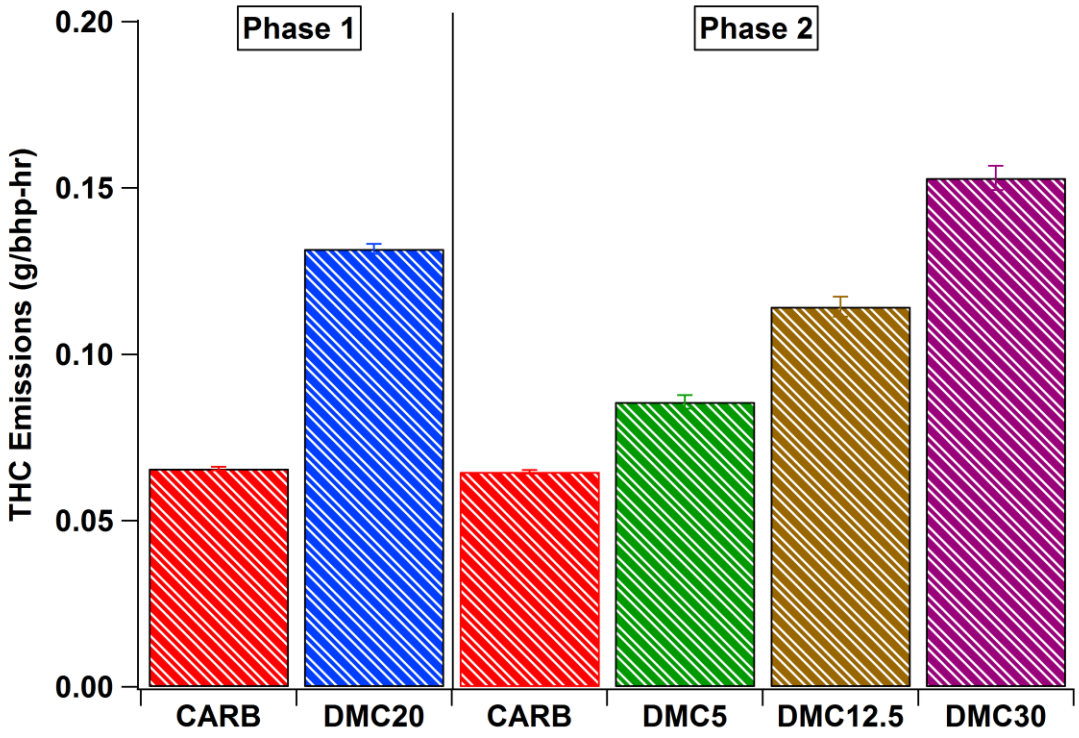

Figure 6-7 Average THC emission results for the DMC blends and CARB ULSD. The error bars represent one standard deviation of the average values

6.4.4. CO_2 Emissions and Brake Specific Fuel Consumption

The CO_2 emission results are presented in Figure 6-8. CO_2 emissions showed statistically significant increases for the DMC blends compared to CARB ULSD, with the exception of DMC5. The increases in CO_2 emissions were in the range of 1.1%, 3.8%, and 4.7%, respectively, for DMC12.5, DMC20, and DMC30. The CO_2 increases were as expected and could be related to the generally higher carbon content per unit of energy for DMC compared to typical diesel fuel. The increases in the grams of carbon per unit of energy are approximately 0.5%, 1.3%, 2.2%, and 3.5%, respectively, for DMC5, DMC12.5, DMC20, and DMC30 compared to diesel fuel. These values are comparable to the percentage increases in CO_2 emissions that were observed in this study. Chemical kinetic modelling studies have also suggested that the DMC decomposition results in production of CO_2, an alkyl radical, and an alkyoxy radical [Glaude et al., 2005; Sun et al., 2016].

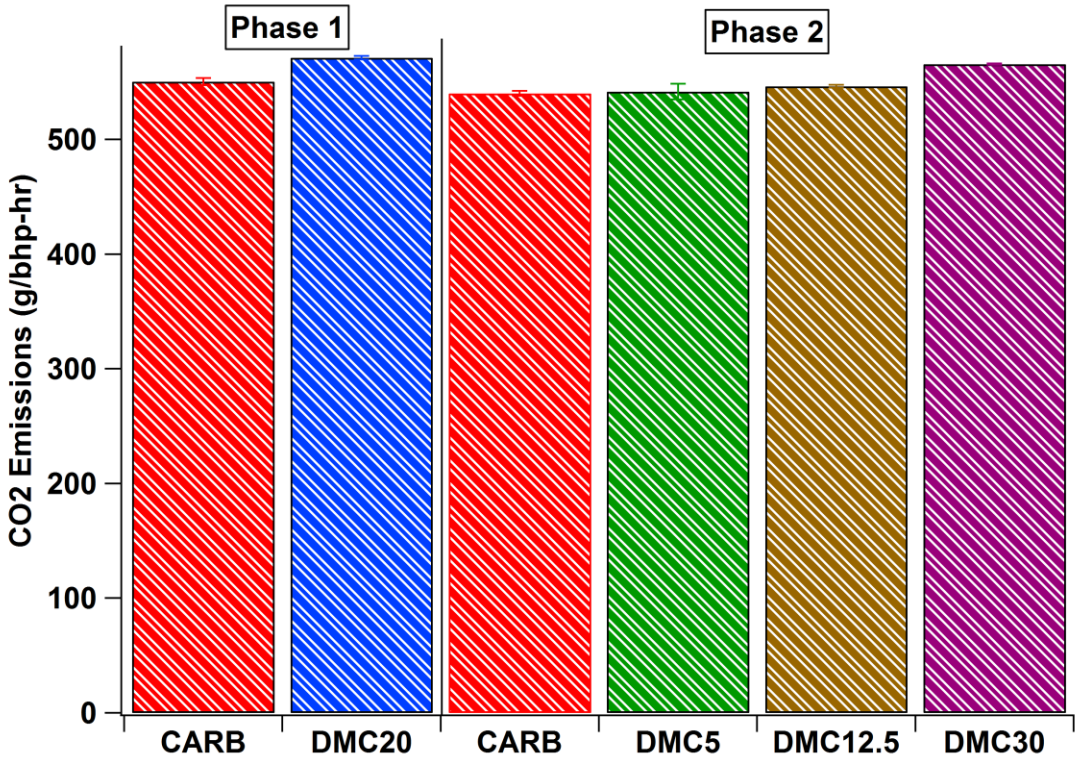

Figure 6-8 Average CO_2 emission results for the DMC blends and CARB ULSD. The error bars represent one standard deviation of the average values

Figure 6-9 shows the brake specific fuel consumption (BSFC) for the DMC blends on a gal/bhp-hr basis. BSFC showed statistically significant increases for all of the DMC blends relative to CARB ULSD, with the exception of DMC5. BSFC increased with increasing DMC levels in diesel fuel, with increases on the range of 4.5%, 9.7%, and 14.6%, respectively, for DMC12.5, DMC20, and DMC30. The higher BSFC with the application of DMC blends were as expected and can be attributed to the lower energy content of DMC compared to CARB ULSD. The heat value of DMC, at 15.78 MJ/kg, is considerably lower than that of diesel fuel, which is around 42.5 MJ/kg [Mei et al., 2014]. The reductions in the energy density per gallon are approximately 1.8%, 4.7%, 7.8%, and 12.2%, respectively,

for DMC5, DMC12.5, DMC20, and DMC30 compared to diesel fuel. These values are comparable to the percentage increases in BSFC that were observed in this study. Thus, the addition of DMC leads to a drop in the volumetric energy density in the blended fuel, which leads to an increase in the fuel consumed per unit or work for the DMC blended fuel.

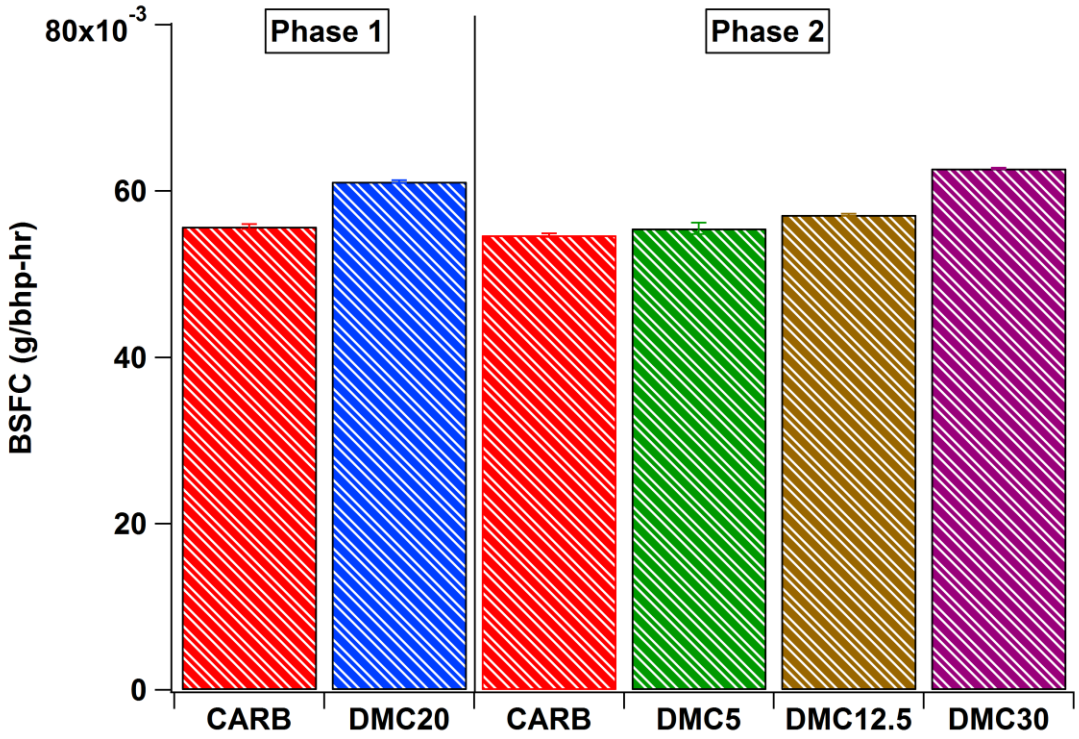

Figure 6-9 Average BSFC results for the DMC blends and CARB ULSD. The error bars represent one standard deviation of the average values

6.4.5. Volatile organic compounds (VOCs) and carbonyl emissions

Figure 6-10 presents the benzene, toluene, ethylbenzene, m/p-xylene, and o-xylene compounds, collectively known as BTEX, and the sum of VOCs for each test fuel, while Table 6-1 shows all the VOC species quantified in the tailpipe. Benzene, a known carcinogen, was the dominant mono-aromatic hydrocarbon in the exhaust followed by

toluene and xylenes. Overall, the polyunsaturated hydrocarbons (i.e., mono-aromatics and alkynes) increased with the use of DMC blends relative to CARB ULSD. Particularly, the increases for benzene and toluene emissions were statistically significant for DMC12.5 and DMC30 blends. For the DMC blends relative to CARB ULSD, increases for benzene emissions ranged from 4.4% to 13.6%, for toluene ranged from 19.5% to 35%, for ethylbenzene ranged from 126% to 399%, for m/p-xylene ranged from 35% to 94%, and for o-xylene ranged from 50% to 102%. Further increases for the DMC blends were also seen with the saturated hydrocarbons, including ethane and propane. Interestingly, the results reported here contradict those published in previous studies showing that the oxygen in DMC is the main driver for the reduction in the formation of soot precursors, such as benzene, acetylene, and other cyclization components [Glaude et al., 2005; Sun et al., 2016; Rubino and Thomson, 1999; Kitagawa et al., 2001]. In addition to BTEX species, ethylene, acetylene, propylene, butane, etc. were also found to increase with DMC blending. The higher emission levels of these compounds is consistent with the higher THC emissions observed for the DMC blends compared to CARB ULSD. The higher concentrations of these compounds could be due to quenching of the combustion flame, which could play a role in the early stages of particle formation and particularly semi-volatile material, may also contribute to the enhancement of nucleation mode particles, as seen in the particle size distributions above.

Table 6-1 Hydrocarbon emissions results for CARB ULSD and the DMC blends

Hydrocarbon Species (g/bhp-hr)	CARB ULSD	DMC5	DMC12.5	DMC30
Ethylene	0.0067 ± 0.0003	0.0072 ± 0.0002	0.0076 ± 0.0004	0.0091 ± 0.0002
Acetylene	0.0012 ± 0.0000	0.0013 ± 0.0000	0.0013 ± 0.0001	0.0015 ± 0.0000
Ethane	0.0003 ± 0.0000	0.0006 ± 0.0001	0.0006 ± 0.0005	0.0005 ± 0.0000
Propylene	0.0024 ± 0.0001	0.0027 ± 0.0001	0.0029 ± 0.0001	0.0034 ± 0.0000
Propane	0.0002 ± 0.0000	0.0005 ± 0.0002	0.0004 ± 0.0003	0.0004 ± 0.0000
Isobutane	0.0000 ± 0.0000	0.0001 ± 0.0000	0.0001 ± 0.0001	0.0001 ± 0.0000
1-Butene	0.0007 ± 0.0000	0.0007 ± 0.0000	0.0008 ± 0.0000	0.0010 ± 0.0000
n-Butane	0.0001 ± 0.0000	0.0002 ± 0.0000	0.0002 ± 0.0001	0.0001 ± 0.0000
trans-2-Butene	0.0001 ± 0.0000	0.0001 ± 0.0000	0.0002 ± 0.0000	0.0002 ± 0.0000
cis-2-Butene	0.0000 ± 0.0000	0.0000 ± 0.0000	0.0002 ± 0.0002	0.0001 ± 0.0000
Isopentane	0.0001 ± 0.0000	0.0002 ± 0.0001	0.0002 ± 0.0001	0.0002 ± 0.0000
1-Pentene	0.0003 ± 0.0000	0.0003 ± 0.0000	0.0004 ± 0.0000	0.0004 ± 0.0000
n-Pentene	0.0001 ± 0.0000	0.0001 ± 0.0000	0.0001 ± 0.0001	0.0001 ± 0.0000
Isoprene	0.0001 ± 0.0000	0.0002 ± 0.0000	0.0001 ± 0.0001	0.0000 ± 0.0000
trans-2-Pentene	0.0000 ± 0.0000	0.0001 ± 0.0000	0.0001 ± 0.0000	0.0001 ± 0.0000
1-Hexene	0.0002 ± 0.0000	0.0003 ± 0.0000	0.0003 ± 0.0000	0.0003 ± 0.0000
n-Hexene	0.0000 ± 0.0000	0.0001 ± 0.0000	0.0001 ± 0.0000	0.0001 ± 0.0000
Benzene	0.0006 ± 0.0000	0.0007 ± 0.0000	0.0007 ± 0.0000	0.0007 ± 0.0000
n-Heptane	0.0001 ± 0.0000	0.0001 ± 0.0000	0.0001 ± 0.0000	0.0001 ± 0.0000
Methylcyclohexane	0.0001 ± 0.0000	0.0001 ± 0.0000	0.0001 ± 0.0000	0.0001 ± 0.0000
Toluene	0.0003 ± 0.0000	0.0004 ± 0.0000	0.0005 ± 0.0001	0.0005 ± 0.0000
2-Methylheptane	0.0000 ± 0.0001	0.0000 ± 0.0001	0.0001 ± 0.0000	0.0001 ± 0.0000
n-Octane	0.0001 ± 0.0000	0.0002 ± 0.0000	0.0003 ± 0.0000	0.0003 ± 0.0000
Ethylbenzene	0.0000 ± 0.0000	0.0001 ± 0.0000	0.0001 ± 0.0000	0.0001 ± 0.0000
m/p-Xylenes	0.0002 ± 0.0000	0.0002 ± 0.0000	0.0003 ± 0.0001	0.0003 ± 0.0000
o-Xylene	0.0001 ± 0.0000	0.0001 ± 0.0000	0.0001 ± 0.0000	0.0002 ± 0.0000
Nonane	0.0002 ± 0.0000	0.0003 ± 0.0000	0.0004 ± 0.0000	0.0004 ± 0.0000
Isopropylbenzene	0.0007 ± 0.0009	0.0000 ± 0.0000	0.0000 ± 0.0000	0.0000 ± 0.0000
m-Ethyltoluene	0.0000 ± 0.0000	0.0001 ± 0.0000	0.0001 ± 0.0000	0.0001 ± 0.0000
1,3,5-Trimethylbenzene	0.0000 ± 0.0000	0.0000 ± 0.0000	0.0001 ± 0.0000	0.0001 ± 0.0000
o-Ethyltoluene	0.0000 ± 0.0000	0.0001 ± 0.0000	0.0001 ± 0.0000	0.0001 ± 0.0000
1,2,4-Trimethylbenzene	0.0001 ± 0.0000	0.0002 ± 0.0000	0.0003 ± 0.0000	0.0003 ± 0.0000
n-Decane	0.0004 ± 0.0000	0.0006 ± 0.0000	0.0007 ± 0.0001	0.0008 ± 0.0000
1,2,3-Trimethylbenzene	0.0000 ± 0.0000	0.0001 ± 0.0000	0.0001 ± 0.0000	0.0001 ± 0.0000
m-Diethylbenzene	0.0001 ± 0.0001	0.0001 ± 0.0000	0.0001 ± 0.0001	0.0000 ± 0.0000
p-Diethylbenzene	0.0001 ± 0.0000	0.0002 ± 0.0000	0.0001 ± 0.0001	0.0000 ± 0.0000
n-Undecane	0.0005 ± 0.0000	0.0007 ± 0.0000	0.0008 ± 0.0000	0.0009 ± 0.0000
n-Dodecane	0.0006 ± 0.0000	0.0009 ± 0.0000	0.0009 ± 0.0000	0.0011 ± 0.0000

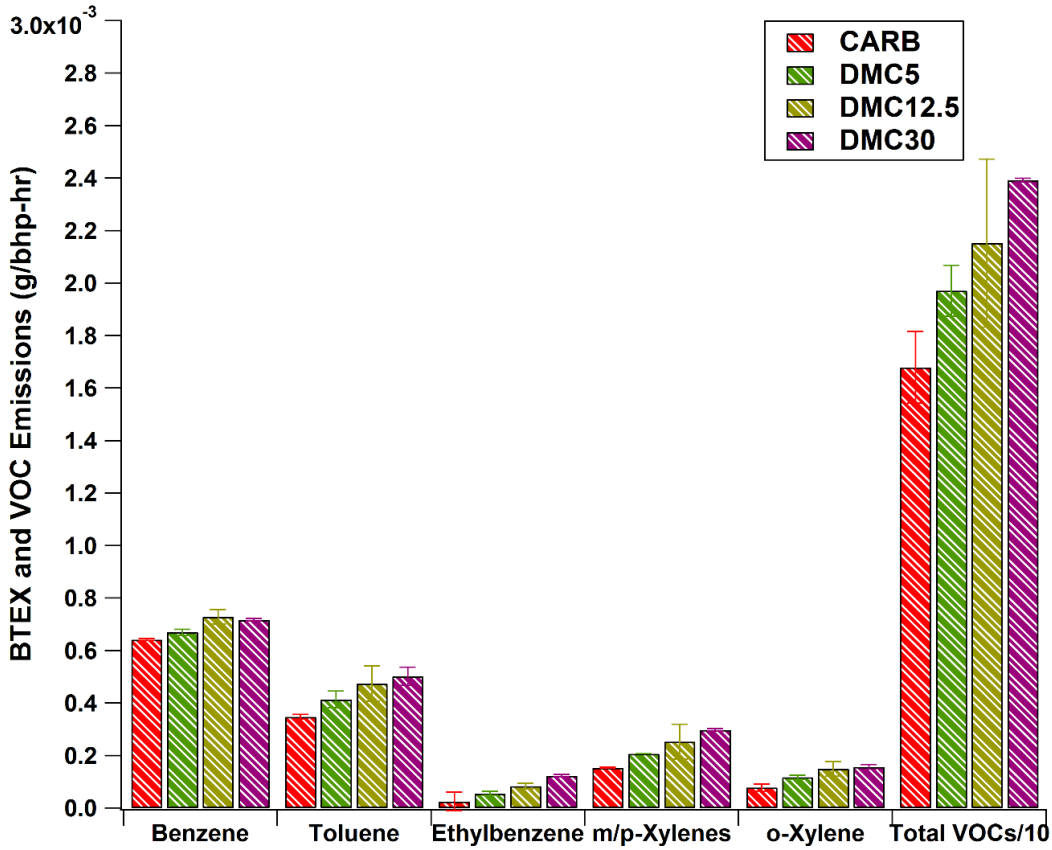

Figure 6-10 Average BTEX emissions and total VOCs for the DMC blends and CARB ULSD. The error bars represent one standard deviation of the average values

The carbonyl emissions, expressed in mg/bhp-hr, are shown in Figure 6-11. Formaldehyde and acetaldehyde were the dominant aldehydes in the exhaust followed by benzaldehyde and propionaldehyde. Heavier aldehydes were also present, but in lesser amounts. These results are in reasonable agreement with other studies showing the predominance of low molecular aldehydes in the exhaust from oxygenated fuels [Karavalakis et al., 2014, Fontaras et al., 2009, Correa and Arbilla, 2008; Nord and Haupt, 2005]. The application of DMC blends led to statistically significant higher formaldehyde and acetaldehyde emissions relative to CARB ULSD, which could be a consequence of the

oxygen content in the fuel molecule. For formaldehyde and acetaldehyde emissions, the increases for DMC blends relative to CARB ULSD ranged from 117% to 171% and from 115% to 154%, respectively. It should be noted that carbonyls are oxygenated hydrocarbons, and as such would have a reduced response for THC FID measurements, so in terms of overall organic material hydrocarbons, the increases with the DMC would be even greater than those found for the THC FID measurements. Previous studies have shown that formaldehyde is an important intermediate species in the DMC combustion, with H-atom abstraction from DMC leading to the formation of formaldehyde and methoxyl radical (CH3OC=O) [Glaude et al., 2005, Chen et al., 2012; Sinha and Thomson, 2004]. Acetaldehyde is primarily formed from reactions involving the C2 species [Sun et al., 2016].

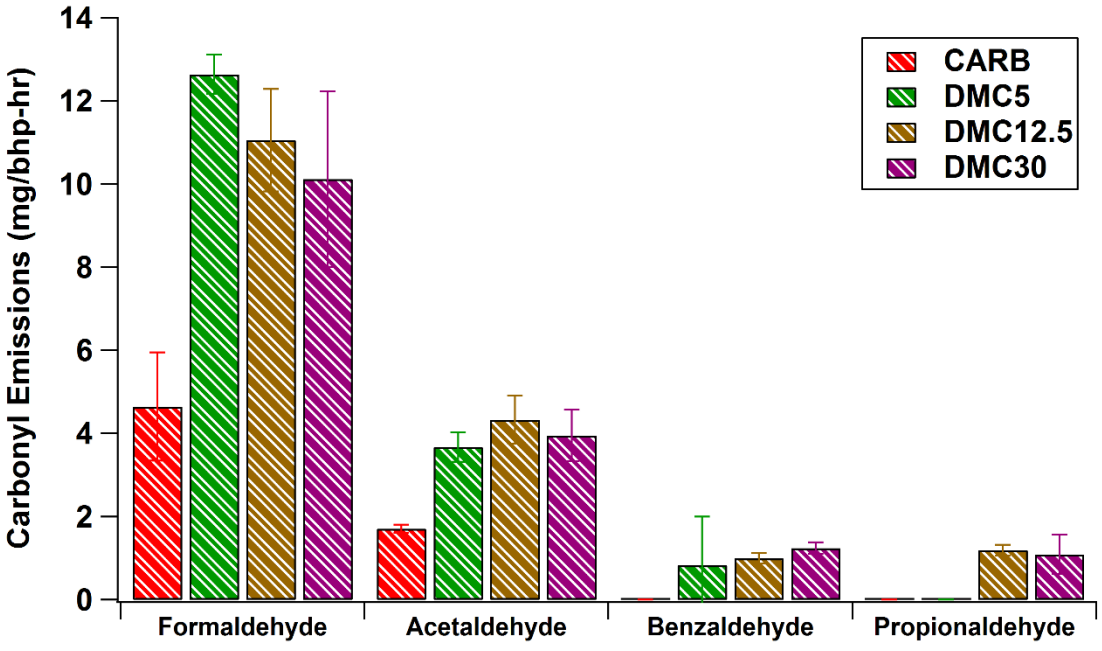

Figure 6-11 Average carbonyl emission results for the DMC blends and CARB ULSD. The error bars represent one standard deviation of the average values

6.5. **Conclusion**

As the use of renewable fuels continues to expand in the transportation sector, it is important to continue to evaluate their overall impact on ambient air quality. Oxygenated fuels, and in particular DMC, has been shown to reduce soot emissions when blended with petroleum diesel fuel. The main goal of this study was to assess the emissions performance of DMC when blended with typical on-road CARB ULSD on a 1991 DDC Series 60 engine over the FTP test cycle. PM emissions showed consistent, statistically significant reductions for all of the DMC blends. PM emissions decreased with increasing DMC blend levels, ranging from 30 to 78% for the DMC5 to DMC30 blends. These reductions were significantly higher than those typically seen for biodiesel at a comparable blend level. This can be attributed to the higher oxygen content in the DMC molecule, with DMC's chemical structure and physical properties potentially also being of importance at the higher oxygen levels. Particle number emissions followed opposite trends to the PM mass and showed increases with increasing DMC blending. The increases in particle number emissions for the DMC blends were statistically significant, with the exception of DMC5. Consistent with the particle number emission results, the application of DMC resulted in higher concentrations of nucleation mode particles compared to CARB ULSD, suggesting a suppression of soot particles available for condensation of semi-volatile species and a promotion of nucleation mode particles.

Emissions of NOx were generally increased, especially for the higher DMC blends. The same observation holds for the THC emissions, where the increases for the DMC blends relative to CARB ULSD were at a statistically significant level. As expected, BSFC

showed increases with the DMC blends as a result to the lower energy content of DMC compared to diesel fuel. On the other hand, CO emissions showed clear reduction with the use of DMC blends at a statistically significant level. Overall, the use of DMC led to increases in BTEX emissions and most VOCs relative to CARB ULSD, including the carcinogenic benzene. It was observed that mono-aromatic and polyunsaturated hydrocarbons that are known soot precursors showed increases with increasing DMC blending. Formaldehyde and acetaldehyde were the predominant aldehydes in the exhaust, and the use of DMC resulted in higher aldehyde levels compared to CARB ULSD.

6.6. **Acknowledgements**

The authors thank the following organizations and individuals for their valuable contributions to this study. We acknowledge funding from the National Center for Sustainable Transportation and from Yashentech LLC. The authors thank Mr. Don Pacocha, Mr. Mark Villela and Mr. Eddie O'Neal of the University of California, Riverside for their contribution in conducting the emissions testing for this program.

6.7. **References**

California Air Resources Board: Resolution 98-35: Identification of particulate emissions from diesel-fueled engines as a toxic air contaminant; http://www.arb.ca.gov/regact/diesltac/res98-35. California Air Resources Board, 1998.

Chen G, Yu W, Fu J, Mo J, Huang Z, Yang J, Wang Z, Jin H, Qi F. Experimental and modeling study of the effects of adding oxygenated fuels to premixed n-heptane flames. Combustion and Flame 2012;159:2324-2335.

Cheng AS, Dibble RW, Buchholz BA. The effect of oxygenates on diesel engine particulate matter. SAE Technical Paper 2002;2002-01-1705.

Cheung CS, Zhu R, Huang Z. Investigation on the gaseous and particulate emissions of a compression ignition engine fueled with diesel-dimethyl carbonate blends. Science of the Total Environment 2011;409:523-529.

Cocker DR, Shah S, Johnson K, Miller JW, Norbeck J. Development and application of a mobile laboratory for measuring emissions from diesel engines. I regulated gaseous emissions. Environ. Sci. Technol. 2004;38: 2182-2189.

Correa SM, Arbilla G. Carbonyl emissions in diesel and biodiesel exhaust. Atmospheric Environment 2008;42: 769-775.

Fontaras G, Karavalakis G, Kousoulidou M, Tzamkiozis T, Ntziachristos L, Bakeas E, Stournas S, Samaras Z. Effects of biodiesel on passenger car fuel consumption, regulated and non-regulateed pollutant emissions over legislated and real-world driving cycles. Fuel 2009;88:1608-1617.

Giakoumis EG, Rakopoulos CD, Dimaratos AM, Rakopoulos DC. Exhaust emissions of diesel engines operating under transient conditions with biodiesel fuel blends. Progress in Energy and Combustion Science 2012;38: 691-715.

Glaude PA, Pitz WI, Thomson MJ. Chemical kinetic modeling of dimethyl carbonate in an opposed-flow diffusion flame. Proceedings of the Combustion Institute 2005;30:1111-1118.

Hajbabaei M, Johnson K, Okomoto R, Durbin TD. Evaluation of the impacts of biodiesel and second generation biofuels on NOx emissions for clean diesel fuels. Environ. Sci. Technol. 2012;46:9163-9173.

Hajbabaei M, Johnson KC, Okamoto R, Durbin TD. Evaluation of the impacts of Biofuels on Emissions for a California-Certified Diesel Fuel from Heavy-Duty Engines. SAE Technical Paper 2013;2013-01-1138.

Hajbabaei, M, Karavalakis G, Johnson KC, Guthrie J, Mitchell A, Durbin TD. Impacts of biodiesel feedstock and additives on criteria emissions from a heavy-duty engine. Fuel Processing Technology 2014;126:402-414.

Hellier P, Ladommatos N, Allan R, Rogerson J. Influence of carbonate ester molecular structure on compression ignition combustion and emissions. Energy and Fuels 2013;27:5222-5245.

Herner JD, Hu S, Robertson WH, Huai T, Collins JF, Dwyer H, Ayala A. Effect of advanced aftertreatment for PM and NOx control on heavy-duty diesel truck emissions. Environ. Sci. Technol. 2009;43:5928-5933.

Huang ZH, Jiang DM, Zeng K, Liu B, Yang ZL. Combustion characteristics and heat release analysis of a direct injection compression ignition engine fuelled with diesel-dimethyl carbonate blends. Proc. Instn. Mech. Engrs. Part D: J. Automobile Engineering 2003;217:595-605.

Johnson T. Vehicular emissions in review. SAE Int. J. Engines 2016;9:doi:10.4271/2016-01-0919.

Karavalakis G, Short D, Vu D, Villela M, Asa-Awuku A, Durbin TD. Evaluating the regulated emissions, air toxics, ultrafine particles, and black carbon from SI-PFI and SI-DI vehicles operating on different ethanol and iso-butanol blends. Fuel 2014;128:410-421.

Kitagawa H, Murayama T, Tosaka S, Fujiwara Y. The effect of oxygenated fueel additive on the reduction of diesel exhaust particulates. SAE Technical Paper 2001; 2001-01-2020.

Kocis D, Song K, Lee H, Litzinger T. Effects of dimethoxymethane and dimethylcarbonate on soot production in an optically-accessible DI diesel engine. SAE Technical Paper 2000;2000-01-2795.

Kozak M, Merkisz J, Bielaczyc P, Szczotka A. The influence of oxygenated diesel fuels on a diesel vehicle PM/NOx emission trade-off. SAE Technical Paper 2009;2009-01-2996.

Kumar BR, Saravanan S. Partially premixed low temperature combustion using dimethyl carbonate (DMC) in a DI diesel engine for favorable smoke/NOx emissions. Fuel 2016;180:396-406.

Kwak JH, Kim HS, Lee JH, Lee SH. On-road chasing measurement of exhaust particle emissions from diesel, CNG, LPG, and DME-fueled vehicles using a mobile emission laboratory. International Journal of Automotive Technology 2014;15:543-551.

Li DG, Zhen H, Xingcai L, Wu-Gao Z, Jian-Guang Y. Physico-chemical properties of ethanol–diesel blend fuel and its effect on performance and emissions of diesel engines. Renewable Energy 2005;30:967-976.

Lu XC, Yang JG, Zhang WG, Huang Z. Improving the combustion and emissions of direct injection compression ignition engines using oxygenated fuel additives combined with a cetane number improver. Energy and Fuels 2005;19:1879-1888.

Mei D, Hielscher K, Baar R. Study on combustion process and emissions of a single-cylinder diesel engine fueled with DMC/diesel blend. Journal of Energy Engineering 2014;140:04013004.

Merritt PM, Ulmet V, McCormick R. Regulated and unregulated exhaust emissions comparison for three tier II non-road diesel engines operating on ethanol-diesel blends. SAE Technical Paper 2005; 2005-01-2193.

Mills NL, Torngvist H, Robinson SD, Gonzalez M,Darnley K, MacNee W, Boon NA, Donaldson K, Blomberg A, Sandstorm T, Newby DE. Diesel exhaust inhalation causes vascular dysfunction and impaired endogenous fibrinolysis. Circulation 2005;112:3930-3936.

Miyamoto N, Ogawa H, Nurun NM, Obata K, Arima T. Smokeless, low NOx, high thermal efficiency, and low noise diesel combustion with oxygenated agents as main fuel. SAE Technical Paper 1998;980506.

Mueller C, Boehman A, Martin G. An experimental investigation of the origin of increased NOx emissions when fueling a heavy-duty compression-ignition engine with soy biodiesel. SAE Technical Paper 2009;2009–01–1792.

Murayama T, Zheng M, Chikahisa T, Oh Y-T, Fujiwara Y, Tosaka S, Yamashita M, Yoshitake H. Simultaneous reductions of smoke and NOx from a DI diesel engine with EGR and dimethyl carbonate. SAE Technical Paper 1995;952518.

Nel AE, Diaz-Sanchez D, Ng D, Hiura T, Saxon A, Enhancement off allergic inflammation by the interaction between diesel exhaust particles and the immune system. J. Allergy Clin. Immunol. 1998;102:539-554.

Nord KE, Haupt D. Reducing the emission of particles from diesel engine by adding an oxygenate to the fuel. Environ. Sci. Technol. 2005;39:6260-6265.

Pacheco MA Marshall CL. Review of dimethyl carbonate (DMC) manufacture and its characteristics as fuel additive. Energy and Fuels 1997;11:2-29.

Ratcliff MA, Burton J, Sindler P, Christensen E, Fouts L, Chupka GM, McCormick RL. Knock resistance and fine particle emissions for several biomass-derived oxygenates in a direct-injection spark-ignition engine. SAE Technical Paper 2016;2016-01-0705.

Ren Y, Huang ZH, Miao HY, Di YG, Jiang DM, Zeng K, Liu B, Wang XB. Combustion and emissions of a DI diesel engine fueled with diesel-oxygenate blends. Fuel 2008;87:2691-2697.

Robbins C, Hoekman SK, Ceniceros E, Natarajan M. Effects of Biodiesel Fuels Upon Criteria Emissions. SAE Technical Paper 2011;2011–01–1943.

Rounce P, Tsolakis A, Leung P, York APE. A comparison of diesel and biodiesel emissions using dimethyl carbonate as an oxygenated additive. Energy and Fuels 2010;24:4812-4819.

Rubino L, Thomson MJ. The effect of oxygenated additives on soot precursor formation in a couterflow diffusion flame. SAE Technical Paper 1999;1999-01-3589.

Sinha A, Thomson MJ. The chemical structures of opposed flow diffusion flames of C3 oxygenated hydrocarbons (isopropanol, dimethoxy methane, and dimethyl carbonate) and their mixtures. Combustion and Flame 2004;136:548-556.

Sivalakshmi S, Balusamy T. Effects of Dimethylcarbonate-biodiesel blends on the combustion, performance and exhaust emissions of a DI diesel engine. SAE Technical Paper 2012;2012-01-0870.

Song J, Cheenkachorn K, Wang J, Perez J, Boehman AL. Effect of oxygenated fuel on combustion and emissions in a light-duty turbo diesel engine. Energy and Fuels 2002;16:294-301.

Souza LFS, Ferreira PRR, de Medeiros JL, Aves RMB, Araujo OQF. Production of DMC from CO_2 via indirect route: Technical-economical-environmental assessment and analysis. ACS Sustainable Chem. Eng. 2014;2:62-69.

Sun W, Yang B, Hansen N, Westbrook CK, Zhang F, Wang G, Moshammer K, Law CK. An experimental and kinetic modeling study on dimethyl carbonate (DMC) pyrolysis and combustion. Combustion and Flame 2016;164:224-238.

U.S Environmental Protection Agency. A Comprehensive Analysis of Biodiesel Impacts on Exhaust Emissions. EPA Draft Final Report; 2002.

Wofsy SC, Logan JA, Sillman S. The sensitivity of ozone to nitrogen oxides and hydrocarbons in regional ozone episodes. Journal of Geophysical Research 1990;95:1837-1851.

Wu ZJ, Zhu ZY, Huang Z. An experimental study on the spray structure of oxygenated fuel using laser-based visualization and particle image velocimetry. Fuel 2006;85:1458-1464.

Zhang ZH, Balasubramanian R. Effect of oxygenated fuels on physicochemical and toxicological characteristics of diesel particulate emissions. Environ. Sci. Technol. 2014;48:14805-14813.

Zhu R, Cheung CS, Huang Z. Particulate emission characteristics of a compression ignition engine fueled with diesel-DMC blends. Aerosol Science and Technology 2011;45:137-147.

7. Evaluation of the feasibility and emissions benefits of equipping small off-road diesel engines with advanced PM and/or NOx aftertreatment

7.1. Abstract

Off-road emissions represent one of the most important categories for emissions inventories. The existing standard for tier 4 off-road engines were developed based on a Regulatory Impact Analysis (RIA) conducted back in 2004, and do not require aftertreatment for NOx below 75 hp or PM below 25 hp. Since aftertreatment control devices for diesel vehicles and equipment are considerably more common now, the use of these strategies for <37kW engines may be considerably more viable than at the time of the previous RIA, which could warrant renewed consideration for adopting more stringent exhaust standards for the <37kW sector.

The objective of this study is to evaluate the feasibility and emissions benefits of implementing regulations on mobile off-road diesel engines with rated powers of less than 37 kilowatts (kW) that will require the use of advanced emission control strategies, such as DPFs and SCR. This project includes a comprehensive review of available aftertreatment and other technologies, demonstration of selected aftertreatment technologies on four actual engines and verification of the emissions performance of these devices through a series of emissions and durability tests, evaluation of the cost implications of the added emissions control strategies, evaluation of the potential impacts of additional emissions controls on the emissions inventory, and evaluation of the potential

impact on the small engine marketplace and consumer choice in that area. The aftertreatment demonstrations include the use of a DPF on a TRU engine, the addition of an SCR to an already DPF equipped ride mower, the use of a DPF on a miniexcavator engine, and the addition of a DPF and SCR on a skid steer engine. This chapter will provide an overview of the different elements of the program, and preliminary results to the extent that they are available.

7.2. **Introduction**

Diesel engines represent one of the most critical components of the emissions inventory, and have been the subject of increasingly more stringent regulations for the past few decades. Diesel emissions are a primary source of diesel particulate matter (PM), which is a known carcinogen, and oxides of nitrogen (NOx), which contribute to the formation of secondary PM and are also a precursor for the formation of ozone. On-highway diesel engines have been the subject of increasing more stringent emissions regulations since 1974. The latest round of emissions standards for on-highway diesel engines have essentially required the implementation of diesel particulate filter, as of 2007, and selective catalytic reduction (SCR), as of 2010, for the reduction of particulate matter (PM) and oxides of nitrogen (NOx).

The implementation of emissions standards for off-road diesel engines has generally lagged that for on-highway diesel engines. Tier 1-3 Standards for new nonroad diesel engines were adopted in 1994 for engines over 37 kW (50 hp) and were phased-in from 1996 to 2000 (Dieselnet, 2018). The EPA introduced Tier 1 standards for equipment under 37 kW (50 hp) in 1998, and increasingly more stringent Tier 2 and Tier 3 standards

for all equipment with phase-in schedules from 2000 to 2008. Tier 1-3 standards were met through advanced engine designs, with no/limited use of exhaust gas aftertreatment. Tier 3 standards for NOx+HC were similar to the 2004 standards for highway engines; however, Tier 3 standards for PM were never adopted.

Tier 4 emission standards for nonroad engines were adopted in 2004, with a phase-in over the period of 2008-2015. The Tier 4 emissions standards were developed based on a Regulatory Impact Analysis (RIA) of adopting advanced aftertreatment standards that was conducted in support of the federal rulemaking in 2004. The Tier 4 standards that were developed on the basis of this RIA require that emissions of PM and NOx be further reduced by about 90% for nonroad engine categories above 37 kW. Such emission reductions can be achieved through the use of control technologies, including engine modifications and advanced exhaust gas aftertreatment, similar to those used by those meeting the 2007-2010 standards for on-highway engines. As such, the majority of mobile source off road diesel engines sold as new since 2011 have also been subject to federal and State regulations that have pushed the implementation of DPFs and SCR. Off-road diesel engines less than 37 kW are allowed to certify to less stringent standards as part of the Tier 4 regulations, largely due to the belief that advanced aftertreatment would severely impact the cost of these smaller engines. This is because the RIA found that on a cost percentage basis the technological cost component forms a greater proportion of the total product cost for lower-power engines in comparison to average and higher power engines in the category. As such, the Tier 4 off-road standards do not require aftertreatment for NOx below 75 hp or PM below 25 hp.

Currently, small off-road diesel engines comprise approximately 20-40% of the population of all off-road diesel engines within the State, and are responsible for a roughly equivalent portion of those emissions. As aftertreatment systems (DPFs and SCR) have been implemented for large off-road diesel engines; however, the impact of emissions from small off-road engines with less controls on the emissions inventory is expected to increase. While the RIA is an important part of the regulatory process, the RIA for the Tier 4 off-road standards estimated the costs of anticipated emission control technologies that were not in wide production at the time. However, some of the technologies anticipated in the RIA are now common today in both the off-road and on road diesel sectors. Thus, the "economies of scale" of today's market, as well as the availability of additional exhaust control strategies and techniques not evaluated originally in the RIA, may warrant renewed consideration for adopting more stringent exhaust standards for the under 37 kW sector.

The objective of this study was to evaluate the potential effectiveness and feasibility of implementing regulations on mobile off-road diesel engines with rated powers of less than 37 kilowatts (kW) that will require the use of advanced emission control strategies, such as DPFs and SCR. This study includes a demonstration of selected aftertreatment technologies on actual engines and verification of the emissions performance of these devices through a series of emissions and durability tests. This study included the application of DPFs for a transportation refrigeration unit and an excavator engine, and the application of an SCR with a DPF for a ride mower and a skid steer engine. This study was part of a larger project that included a comprehensive review of available aftertreatment and other technologies, an evaluation of the cost implications of the added emissions

control strategies, an evaluation the potential impacts of additional emissions controls on the emissions inventory, and an evaluation of the potential impact of such regulations on the small engine marketplace and consumer choice in that area.

7.3. **Experimental**

7.3.1. **Engines and Test Fuels**

Testing was conducted on a total of 4 engines, including a Transportation Refrigeration Unit (TRU) engine, a ride mower engine, an excavator engine, and a skid steer engine. The characteristics of each of the engines are provided in Table 7-1.

Table 7-1 Description of Test Engines

System	Transportation Refrigeration Unit	Ride Mower	Excavator	Skid Steer
Engine vendor	Yanmar	John Deere	Kubota	Doosan
Engine family	8YDXL1.11W3N	FYDXL1.64NDA	GKBXL01.5BCB	FDICL02.4LEA
Engine model	3TNV76	3TNV88C-DJMZ	V1505	DL02-LEL03
Engine power (hp/kW)	20.25/15.10	37.4/27.9	24.80/18.50	49/37
AT vendor	Proventia	BASF, Donaldson, Continental	DCL	Johnson Matthey & Tenneco
AT type	DPF	SCR	DPF	DPF + SCR

The test fuel used was a California No. 2 diesel fuel with equal portion taken from an Arco, Shell, and Chevron station. This fuel was obtained in a single batch of six drums, which should be sufficient for the pre- and post-testing and degreening on all 4 test engines. A mixture of 15 gallons of each fuel blend was mixed into separate 55 gallon drums, and then it was mixed with an air-driven stirrer for 15 minutes each drum. A fuel sample from this batch of fuel was sent to ARB staff in El Monte for analysis using ARB methods for

the following properties: density (ASTM D4052), sulfur (ASTM D5453), distillation (ASTM D86), aromatics and polycyclic hydrocarbons (ASTM D5186), and cetane index derived from a density and distillation properties. The results of the fuel analyses are shown below in Table 7-2.

Table 7-2 Fuel Properties of Test Fuel

Fuel Analysis & Methods Evaluation Section (FAME) Monitoring and Laboratory Division, CARB							
Analytical Method	**ASTM D5186 - modified SFC/FID**				**ASTM D86 Automatic**		
Analysis Date	**10/31/2016**				**10/28/2016**		
Sample I.D.	***Total Aromatics (vol %)***	***Total Aromatics (mass%)***	***Polycyclic Aromatics (mass%)***	***Biodiesel (mass%)***	***T10 (deg C)***	***T50 (deg C)***	***T90 (deg C)***
2R1604	20.1	20.5	2.2	4	216	272	335
Analytical Method	**ASTM D5453 Antek**	**ASTM D4052 Density Mtr**	**ASTM D3343 Calculation**				
Analysis Date	**10/31/2016**	**10/31/2016**	**NR**				
Sample I.D.	***Sulfur (ppm)***	***Density (g/mL)***	***Carbon / Hydrogen (mass%)***				
2R1604	7.8	0.8348	*				

7.3.1.1. TRU Engines

The TRU engine was purchased directly from a dealer. This engine will only be used for the engine dynamometer test with and without the DPF. In the field, the DPF will be equipped directly to an engine that is already in an existing TRU that will be used for the 1,000 hour demonstration.

In conjunction with the installation of the DPF, an electric heating element was utilized for the DPF regenerations. This heating element essentially heats the intake air. For the DPF dynamometer set up, a separate power supply was set up to power the heating element for the intake air. A Hioki meter was used to measure the power used during

regenerations. This system was triggered by the measured back pressure in the DPF and regenerates the DPF by increasing the exhaust temperature to a level where the catalyzed DPF substrate is activated for regeneration. The DPF regenerations were mostly associated with engine loads above 75%. When the TRU engine operates in use, it generally running at a 50% load. A picture and schematic of the TRU engine with the DPF and heating element installed is provided in Figure 7-1 and Figure 7-2.

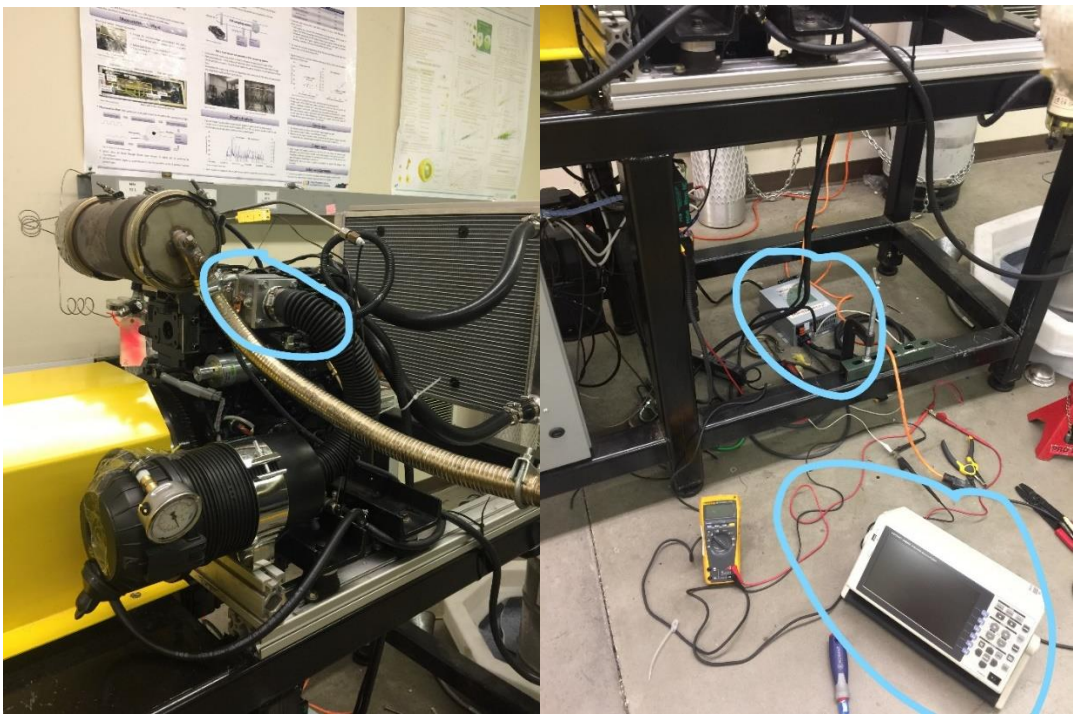

Figure 7-1 TRU Engine on the Engine Dynamometer with the DPF and the Regeneration Heating Unit

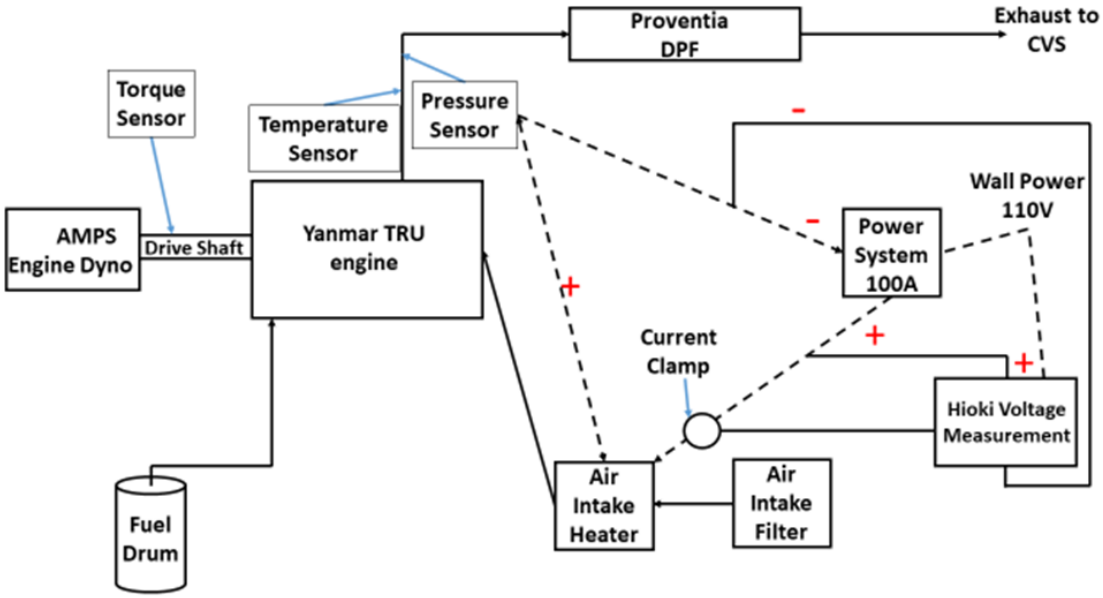

Figure 7-2 Schematic of TRU Engine with the DPF System

7.3.1.2. Ride Mover Engines

The ride mower engine in its original equipment manufacturer (OEM) configuration was equipped with a DPF. Prior to testing, it was operated for about 173 hours in the field in its original configuration. After the break in period in the field, the SCR system was installed on the ride mower engine while it was still housed in the ride mower. This allowed the functionality of the SCR to be verified prior to its installation on the engine dynamometer.

The SCR for this engine was provided in-kind by a collaboration between BASF, Donaldson, and Continental. The component provided by BASF, Donaldson, and Continental included a substrate, a mixer, and the dosing hardware, respectively. The SCR system was added to the system immediately after the OEM DPF. A picture of the ride mower engine with the SCR installed on the engine dynamometer is provided in Figure 7-3.

Figure 7-3 Ride Mover Engine on the Engine Dynamometer with the SCR

7.3.1.3. Excavator Engine

For excavator, the engine in its original configuration did not have any aftertreatment in its original configuration. Prior to testing, it was operated for about 25 hours in the field in its original configuration. After the break in period in the field, the DPF system was installed on the excavator engine while it was still housed in the excavator. This allowed the functionality of the DPF to be verified prior to its installation on the engine dynamometer.

The DPF for this engine was provided by DCL. This system utilizes an active regeneration system where diesel fuel is injected upstream of diesel oxidation catalyst (DOC). The combustion or reaction of the diesel across the DOC creates heat that is used

to raise the temperature of the exhaust gas to a level that is sufficient to regenerate the PM on the DPF. The DPF regeneration is triggered based on back pressure, which was set at a default value of 60 in H_2O. A picture of the excavator engine with the DPF installed on the engine dynamometer is provided in Figure 7-4.

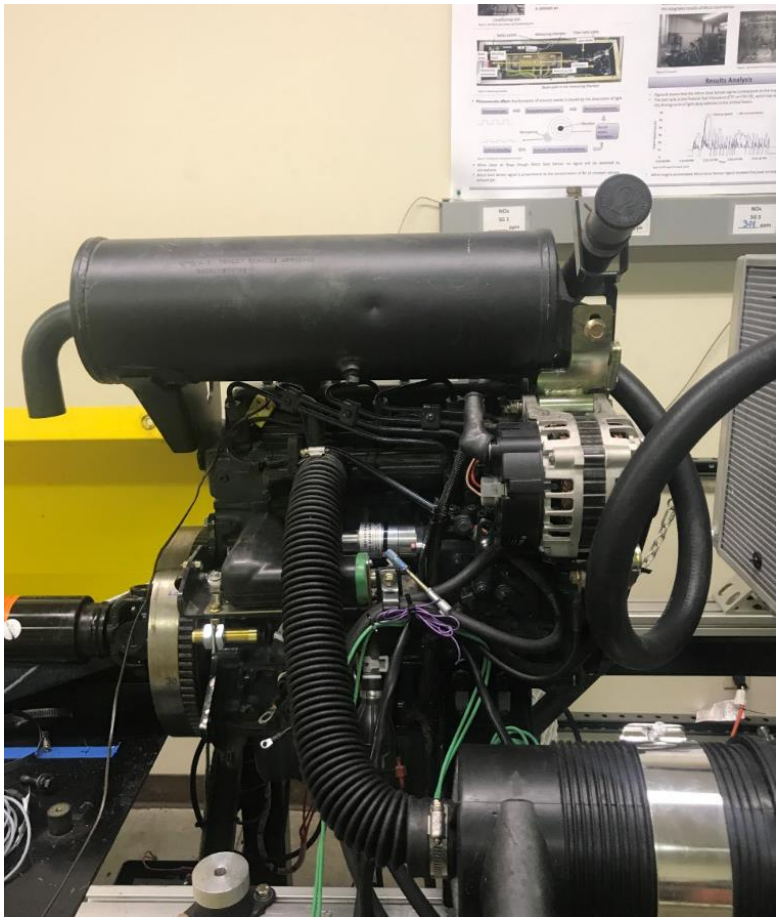

Figure 7-4 Mini-Excavator Engine on the Engine Dynamometer with the DPF

7.3.1.4. Skid Steer Engine

For skid steer engine, the engine is equipped with a DOC in its original configuration. The SCRT system was installed on the skid steer engine while it was still

housed in the skid steer. This allowed the functionality of the SCRT and urea dosing to be verified prior to its installation on the engine dynamometer.

The SCRT for this engine was provided by Johnson Matthey and Tenneco, where the substrate was provided by Johnson Matthey and the dosing system was provided by Tenneco. The SCRT system uses a DOC/DPF/SCR combined to allow control of both PM and NOx. CO/HC/PM emissions are controlled using the DOC/DPF combination. The regeneration principle for the DPF uses NO2 produced by the DOC to burn soot collected by the filter at typical operating temperatures. SCR catalyst is vanadium based on corderite substrate. A platinum group metal (PGM) catalyst on corderite substrate is used to prevent NH3 slip. A picture of the skid steer engine with the SCRT installed on the engine dynamometer is provided in Figure 7-5.

Figure 7-5 Mini-Excavator Engine on the Engine Dynamometer with the DPF

7.3.2. Engine Dynamometer Testing

7.3.2.1. Engine Dynamometer

Engine testing was conducted on a 50 horsepower (hp) dynamometer from Alternative Motive Power Systems (AMPS). The engine dynamometer uses a Baldor / Reliance IDBRPM25504 motor. The motor provides 50 hp at 1770 rpm at a torque of 150 ft-lbs. The motor can absorb 50 hp of power from 1770 up to 3540 rpm. At the higher speeds, the motor can provide constant hp up to 3540 rpm at 75 ft-lbs or torque (torque reduces to maintain hp). The maximum continuous torque for the motor is 150 ft-lbs at an engine speed of 1770 rpm or less. The motor provides a short term peak (60 seconds) overloading rating of 75 hp (150%) 1770 rpm with 225ft-lbs. A picture of the full engine dynamometer set-up with a typical engine in the lab is provided in Figure 7-6.

Figure 7-6 Engine Dynamometer used for Testing

7.3.2.2. General Test Sequence

Two different general test sequences were used throughout the testing. These sequences are shown in Table 7-3 and Table 7-4. For these tables, the main elements of the test sequence numbered, with the testing shaded in green and the durability demonstration shaded in orange. The main difference in the test sequences is the order of testing between the baseline testing and the degreened testing. The engines were initially uninstalled from the associated OEM equipment where it is originally installed. After the installation of the engine and aftertreatment system on the dynamometer, the primary test sequence in Table 7-3 proceeded with testing the engine in its baseline or original condition. The aftertreatment system was then installed and the engine with aftertreatment was then degreened for a period of 25 hours. Testing was then conducted on the degreened system with the aftertreatment installed. It should also be noted that for the TRU application, only the DPF was common to both the engine testing and the durability demonstration. The engine used for the engine dynamometer testing for the TRU engine was of the same make and engine family as the TRU engine that the DPF was installed on in the field.

Since some of the aftertreatment systems were installed in the equipment before the engines were pulled out of the equipment, it was decided to test some engines with the aftertreatment installed first, and then subsequently to do the baseline testing without the aftertreatment system. This would provide as much consistency as possible between how the aftertreatment is installed in the field compared with the dynamometer set up. The sequence for these engines is provided in Table 7-4. Following the testing with the degreened aftertreatment installed, the aftertreatment was uninstalled and such that the

engine was returned to its original OEM configuration, with only the DPF installed. This was done for the ride mower and mini-excavator applications. It should be noted that the 25 hours of degree was done for the aftertreatment configuration irregardless of whether then baseline or the degreened aftertreatment test was conducted first. This test sequence was used for the ride mower and mini-excavator engines.

Table 7-3. Summary of the Test Sequence for the Engine Dynamometer Testing

Description
1. Engine Mounting
Testing Preparation/pretesting/development testing
2. Baseline Testing (no aftertreatment)
Aftertreatment Installation
3. Aftertreatment Degreening (25 hours)
4. Degreened Aftertreatment Testing
Engine Removal

Table 7-4. Summary of the Test Sequence for the Engine Dynamometer Testing

Description
1. Engine Installation with Aftertreatment
Testing Preparation/pretesting/development testing
2. Aftertreatment Degreening (25 hours)
3. Baseline Degreened Aftertreatment Testing
Aftertreatment Removal
4. Baseline Testing (no aftertreatment)
Engine Removal

Following the completion of the initial baseline and degreened testing, the engine was then removed from the engine dynamometer and replace in the equipment that it was originally installed in for the 1,000 hour durability demonstration. Following completion of at least 1,000 hours of operation in the field, the engine/aftertreatment system will be returned to UCR, reinstalled on the engine dynamometer, and the final emissions test will be conducted. The data obtained from the baseline and 1,000 hour durability testing will

be used to extrapolate emissions performance out to the useful life periods of 3,000 hours or 5,000 hours, as applicable.

The degreening was done on the test cycle or cycles that were used for the actual emissions testing. These cycles were repeated back to back until 25 hours of operation was accumulated on the engine + aftertreatment combinations. Some of the hour accumulation may have also included other types of operation, such as engine maps or steady state operation at different load conditions that might be used to investigate the operation of the engine under different conditions to verify that it was ready for the actual emissions testing. For the TRU, the 25 hours of degreening was conducted over the 46 G2 test cycles and 2 hours steady state 70% load

7.3.2.3. **Engine Mapping**

For each engine, an engine map was conducted both in its original conditions and with the aftertreatment installed. The engine maps were used to determine the load points for the steady state C1 and G2 tests, and the engine rpm and torque values for the associated NRTC cycle.

For the TRU engine, the engine maps in the “baseline” and “degreened baseline” tests are shown in in Figure 7-7, along with the backpressure for both conditions. These engine maps were used to determine the load points for the G2 cycle for the corresponding “Baseline” and “Degreened Baseline” tests. The engine maps show that the maximum achievable power with the DPF installed was less than that for the engine without the DPF, so this had to be accounted for in the setting of the load points. The maximum engine rpm

was set at 2450 rpm based on the engine maps, since the dyno torque value drops off significantly after 2450 rpm, as shown in Figure 7-7.

Figure 7-7 shows that the back pressure increases with the addition of the DPF from approximately 7 in H_2O without a DPF up to 52 in H_2O when the DPF is installed. This could affect the performance of this 20 hp small diesel engine since the engine needs to work harder at the same load than without a DPF. Therefore, the engine was not able to meet the same maximum dyno torque with the addition of DPF, especially in the higher rpm range. One engine map has been performed every test day after a 20 minutes max power warm up at 2450 rpm. Based on the engine maps, the maximum torque for the baseline and degreened baseline tests were selected to be 480 in_lbs and 450 in_lbs, respectively, for to setup the G2 cycle test points.

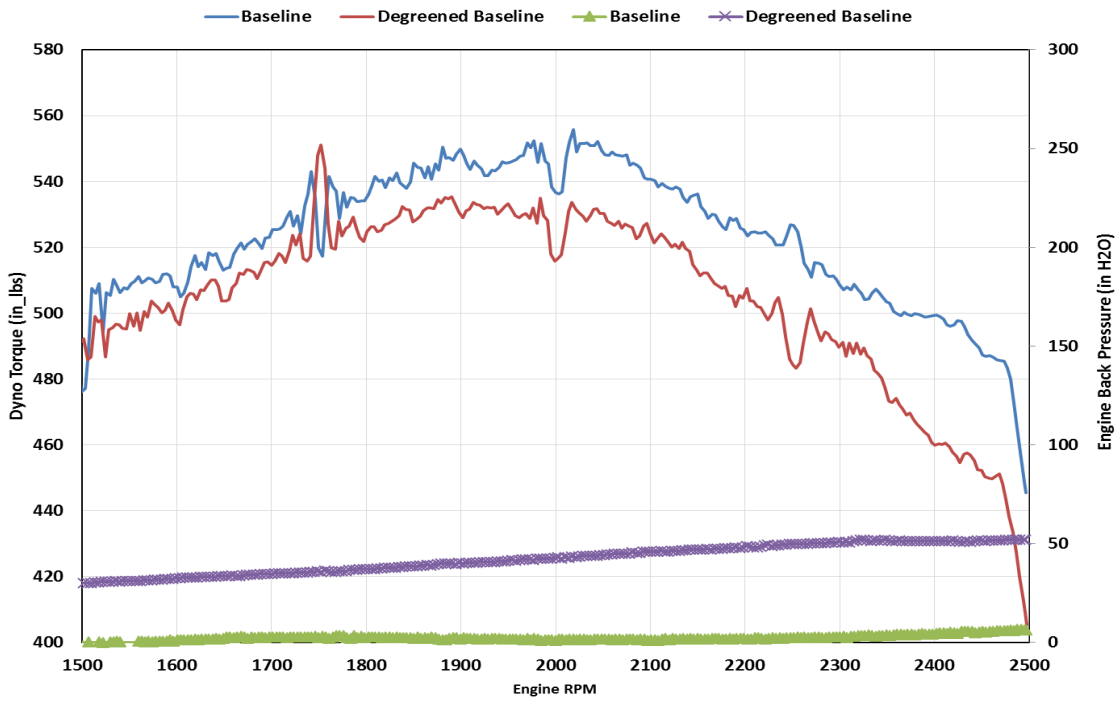

Figure 7-7 Engine Map and Corresponding Engine Back Pressure

The engine maps for the ride mower in both the “Baseline” and “Degreened Baseline” conditions are shown in Figure 7-8. These engine maps were used to determine the load points for the C1 cycles and Non-Road Transient cycles (NRTC) for the corresponding “Baseline” and “Degreened Baseline” tests. Since we are evaluating a SCR aftertreatment performance, we have selected the same load points for both “Baseline” and ‘Degreened Baseline” test. The idle and maximum engine rpm were set at 1525 rpm and 3030 rpm based on information on the engine label and discussions with the engine manufacturer.

The engine maps on “Baseline” and “Degreened Baseline” are relative close to each other. The difference between the two engine maps on maximum dyno achievable torque would be primarily contributed by the additional back pressure from the added SCR aftertreatment. However, this study was focus on the SCR removal efficiency on the NOx emissions, so the tests were run at the same rpm and torque settings for both “Baseline” and “Degreened Baseline” tests.

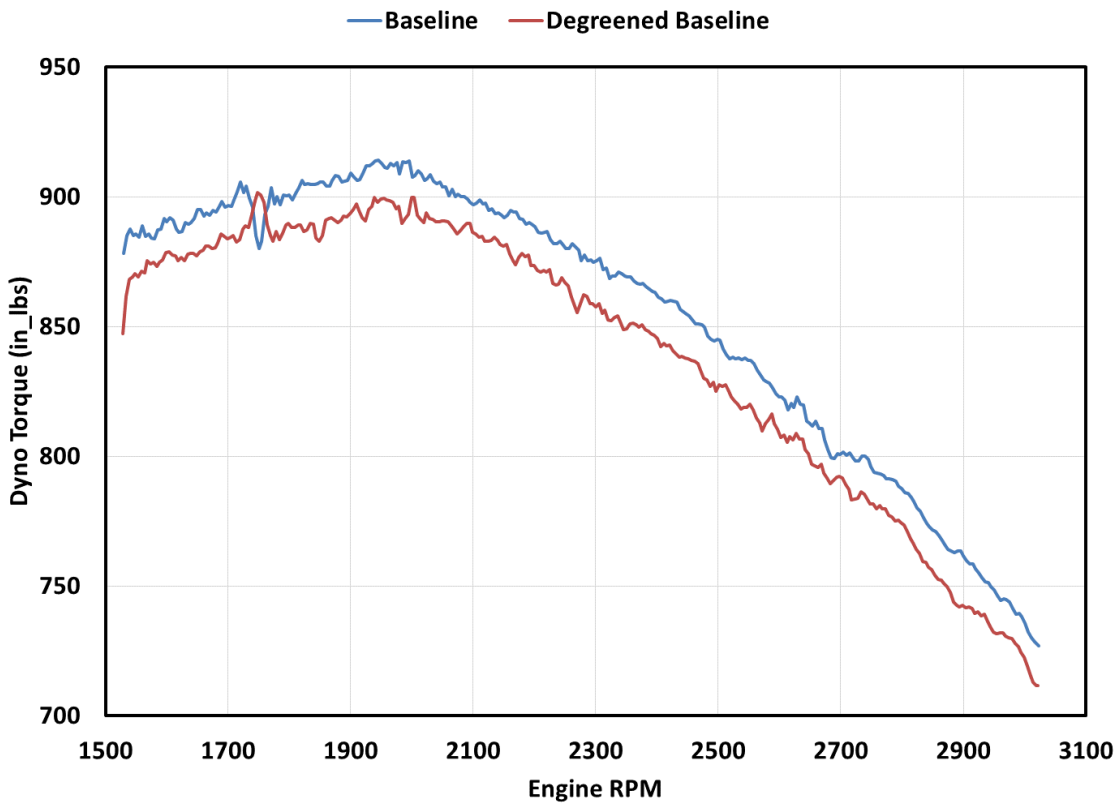

Figure 7-8 Engine Maps for Ride Mower Engine

The engine maps the mini-excavator for the "Baseline" and "Degreened Baseline" conditions are shown in Figure 7-9, along with the backpressure for both conditions. These engine maps were used to determine the load points for the C1 cycles and Non-Road Transient cycles (NRTC) for the corresponding "Baseline" and "Degreened Baseline" tests. The maximum engine rpm was set at 2300 rpm based on the engine maps based on information on the engine label and discussions with the engine manufacturer.

The back pressure level for this engine was about 35 in H_2O with the addition of DPF during the Degreened Baseline testing, while the back pressure for the Baseline testing was not measured. The testing rpm range for this engine was 1200-2300 rpm. The engine maps suggested that the torque did not change much between the DPF configuration and the

original muffler at the higher rpms above 1500, but the torque output at the rpms less than 1500 was lower when the DPF was equipped. The engine maps were performed prior to the main testing after a 20 minute warm up at 2200 rpm at the maximum load at that speed. The warm up was conducted at a speed 100 rpm less than the maximum rpm due to the observation that the drive shaft would overheat when the engine was run for extended periods of time at the maximum rpm. Based on the engine maps, the maximum torque for both baseline and degreened baseline tests was selected to be 725 in_lbs for intermediate speed and 600 in_lbs for maximum speed for to setup the C1 and NRTC test points. The 725 in_lbs was slightly below the maximum available torque, to provide a margin of safety in running the engine, and also to utilize a torque level that could safely be utilized for both the baseline and degreeened baseline tests.

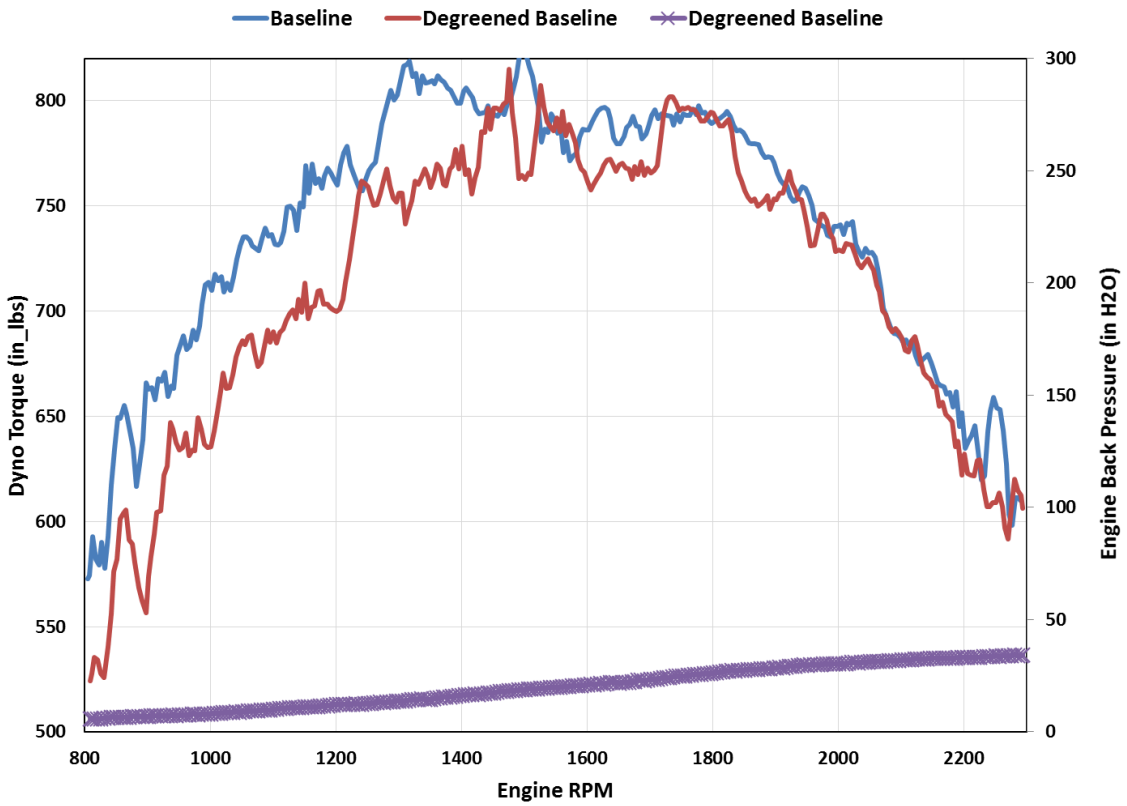

Figure 7-9 Engine Maps and Corresponding Engine Back Pressure for Mini-Excavator

The engine maps the skid steer for the "Baseline" and "Degreened Baseline" conditions are shown in Figure 7-10, along with the backpressure for both conditions. These engine maps were used to determine the load points for the C1 cycles and Non-Road Transient cycles (NRTC) for the corresponding "Baseline" and "Degreened Baseline" tests. The maximum engine rpm was set at 2600 rpm on the engine maps based on information on the engine label and discussions with the engine manufacturer.

Figure 7-10 shows that the back pressure increases with the addition of the SCRT from approximately 20 in H_2O without a SCRT up to 75 in H_2O when the SCRT is installed. This could affect the performance of this 49 hp small diesel engine since the engine needs

to work harder at the same load than without a SCRT. Therefore, the engine was not able to meet the same maximum dyno torque with the addition of SCRT, especially in the intermediate rpm range. The testing rpm range for this engine was 1200-2600 rpm. One engine map was performed each test day after a 20 minutes max power warm up at 2600 rpm. Based on the engine maps, the maximum torque for the baseline and degreened baseline tests were selected to be 1129 in_lbs and 1100 in_lbs, respectively, for to setup the C1 and NRTC test points. The 1100 in_lbs was slightly below the maximum available torque, to provide a margin of safety in running the engine, and also to utilize a torque level that could safely be utilized for both the baseline and degreeened baseline tests.

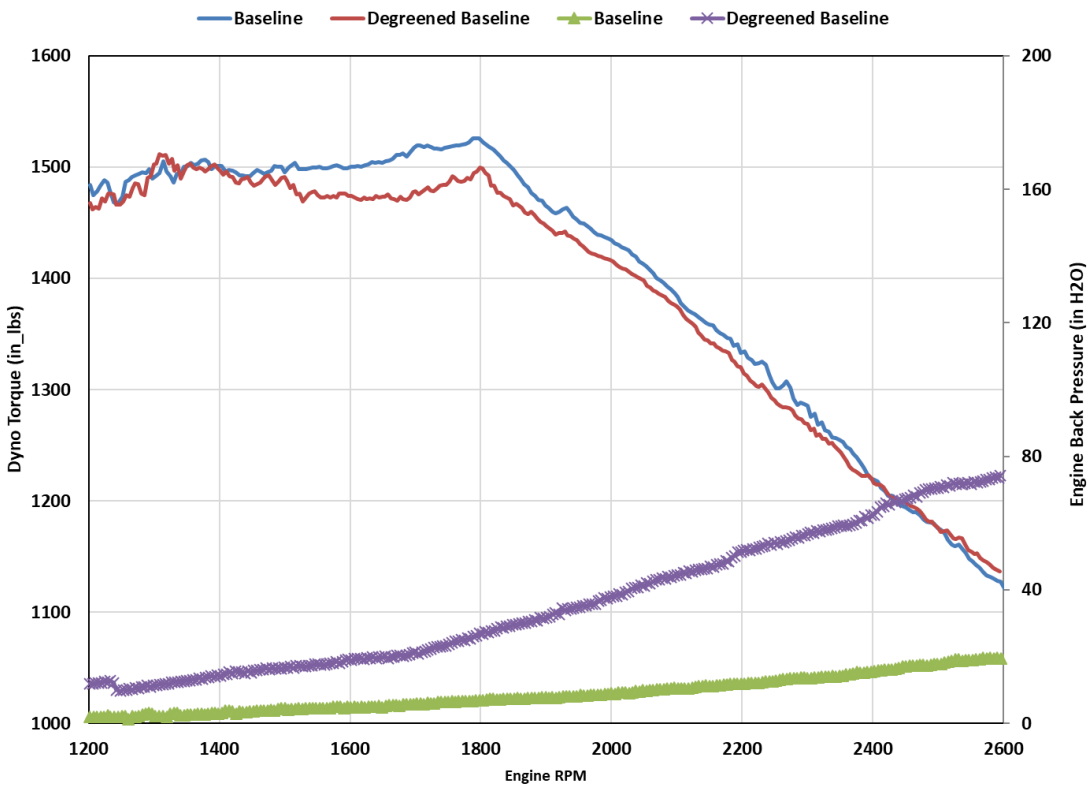

Figure 7-10 Engine Maps and Corresponding Engine Back Pressure for Skid Steer

7.3.2.4. **Test Cycle**

The emissions testing for the TRU engine was conducted in triplicate over the G2 test cycles. G2 test cycle is a 6-mode ramped modal test cycle (described in 40 CFR 1039 Appendix II (b)(2)). The ramped modal tests were run as hot stabilized tests, with the engine warmed up prior to the start of each emissions test. At the beginning of each test day, the engine was at maximum speed and power at 2450 rpm for 20 minutes to warm up, and then an engine map was run. Prior to each test, the engine was warmed up for 5 minutes at the maximum load at the maximum rpm where the max load was determined by an engine map run in the morning of each test day. This warm up procedure provided a stabilized engine temperature, such that the engine coolant/block/or head temperature was within ±2% of its mean value for at least 2 minutes, as per 40 CFR 1065.530. A description of the G2 test cycle is provided in Figure 7-11. A summary of the daily sequence for testing is given in Table 7-5 for the TRU engine. During the course of the engine installation and preparation, the engine was run over variety of engine maps, where the engine was run from the base idle to maximum engine speed while measuring the maximum power and torque at each speed. The engine map was used to determine the speed and torque test points for the G2 test cycles.

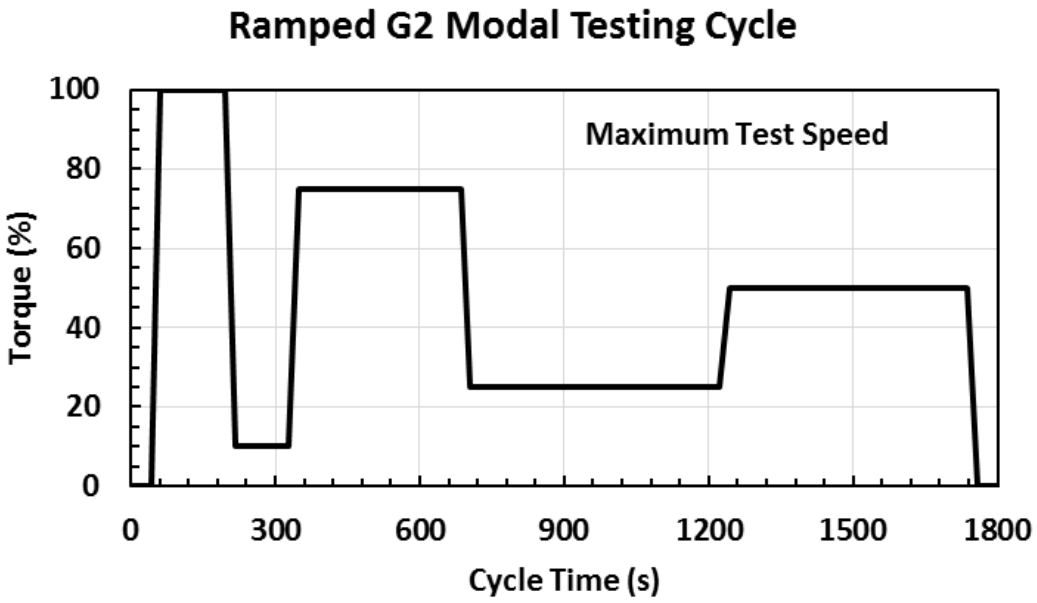

Figure 7-11 Graphical Presentation of the G2 Modal Test Cycle. Note that the entire test was run at a constant speed equal to 100% of maximum speed

Table 7-5 Summary of the Test Sequence for the Yanmar TRU

Testing Activity for TRU Engine	Test Number	Blue is full testing
VERL warm up		
20 Minutes Engine Warmup		Yellow is soak
Engine Map		
Soak		Green Is break
5 Minutes Engine Warmup		
Ramped-modal G2 testing	1	Red is prep/Conditioning
Soak		
5 Minutes Engine Warmup		Warm up/ Shutdown
Ramped-modal G2 testing	2	
Soak		
5 Minutes Engine Warmup		
Ramped-modal G2 testing	3	
VERL shut down and Data process		

Regeneration events were observed periodically over the course of the emissions testing. These regeneration events were representative of typical operation of the DPF, so

they were not eliminated from the emissions results. The regeneration results are shown in Figure 7-12 below, which shows the voltage across the Hioki meter related to when the heating circuit is triggered on. The DPF is considered to be regenerating when there is voltage being sent to the heating circuit. The fraction of the test when regenerations occurred seemed to increase with subsequent tests, as shown in Figure 7-12. The regenerations mostly happened during the maximum load and 75% load period during the test. For the first test with the DPF, there was only one regeneration event for 122 seconds, accounting for 6.8% of the test time of a G2 test cycle. For the second and third tests with the DPF, there were two regeneration events for a total of 437 seconds and 559 seconds, respectively, which accounted for 24.3% and 31.1% of the test time for the G2 test cycle. Note that the voltage did show some instability during portions of the regeneration. This can be attributed to hysteresis in the heating circuit. This stability should improve with a more responsive circuit. Although regenerations were not specifically recorded during the degreening process, it was observed that regenerations occurred at roughly the same frequency during the degreening as was observed during the emission testing.

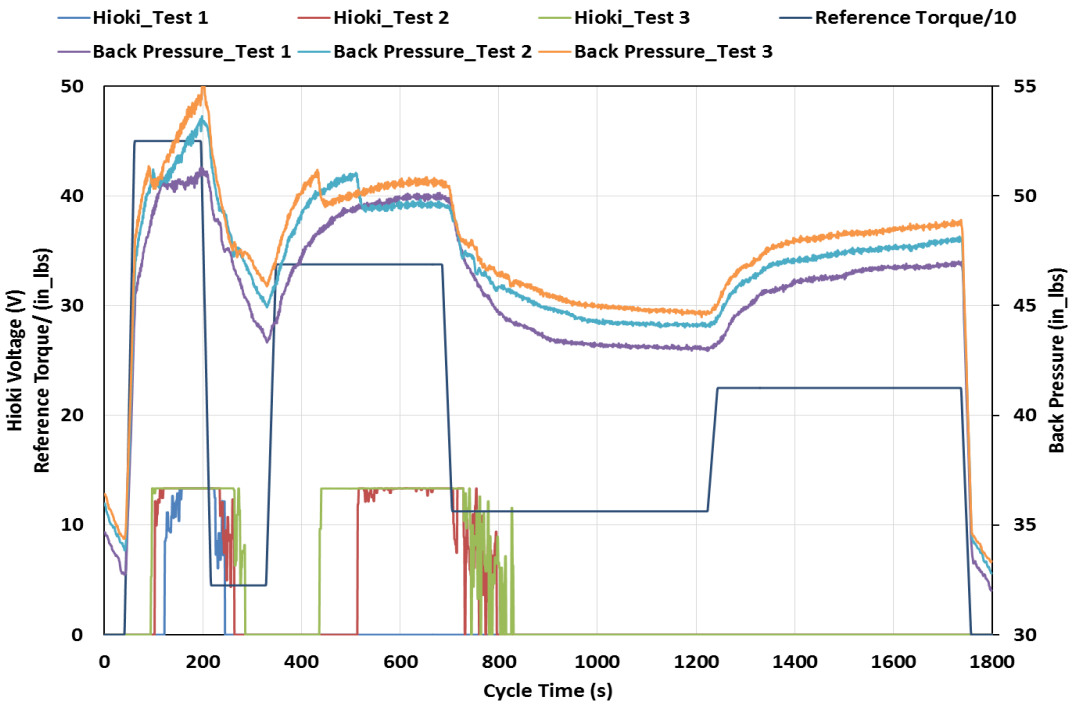

Figure 7-12 Regeneration Results for TRU DPF

The emissions testing for the ride mower mini-excavator, and skid steer engines were conducted in triplicate over the C1 test cycle. The C1 test is a 8-mode ramped modal test cycle (described in 40 CFR 1039 Appendix II (c)(2)). The ramped modal tests were run as hot stabilized tests, with the engine warmed up prior to the start of each emissions test. Prior to each C1 test, the engine was warmed up for 5 minutes at the maximum load at the maximum rpm. This warm up procedure provided a stabilized engine temperature, such that the engine coolant/block/or head temperature was within ±2% of its mean value for at least 2 minutes, as per 40 CFR 1065.530. A description of the C1 test cycle is provided in Figure 7-13.

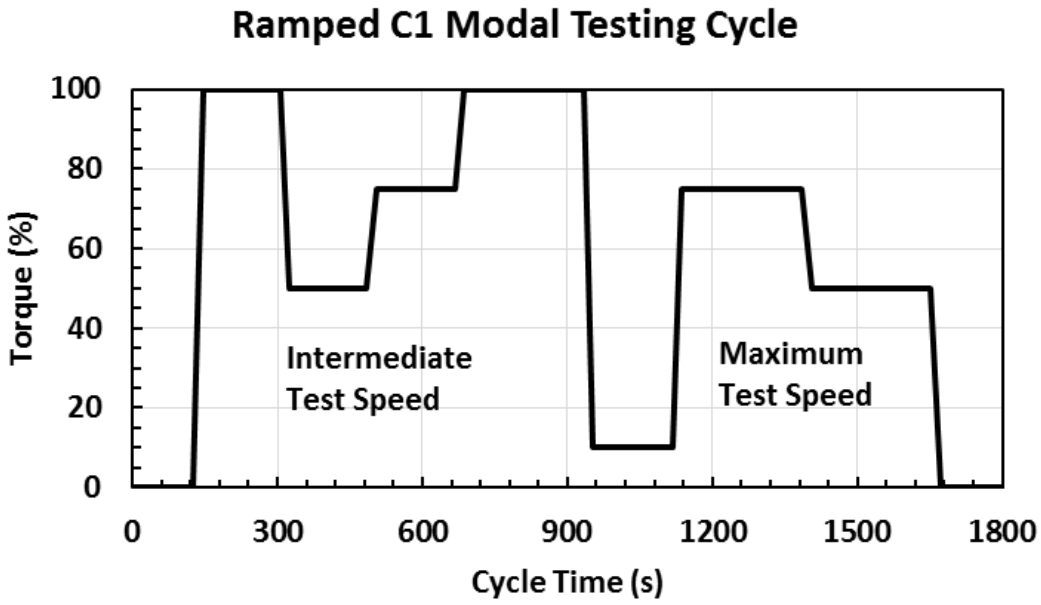

Figure 7-13 Graphical Presentation of the C1 Modal Test Cycle

These engines were also tested over both a cold start and a hot start NRTC. The hot start test was conducted in such a manner that the soak time between the end of the cold start test and the start of the hot start test will be as close as possible to 20 minutes. A description of the NRTC test cycle is provided in Figure 7-14.

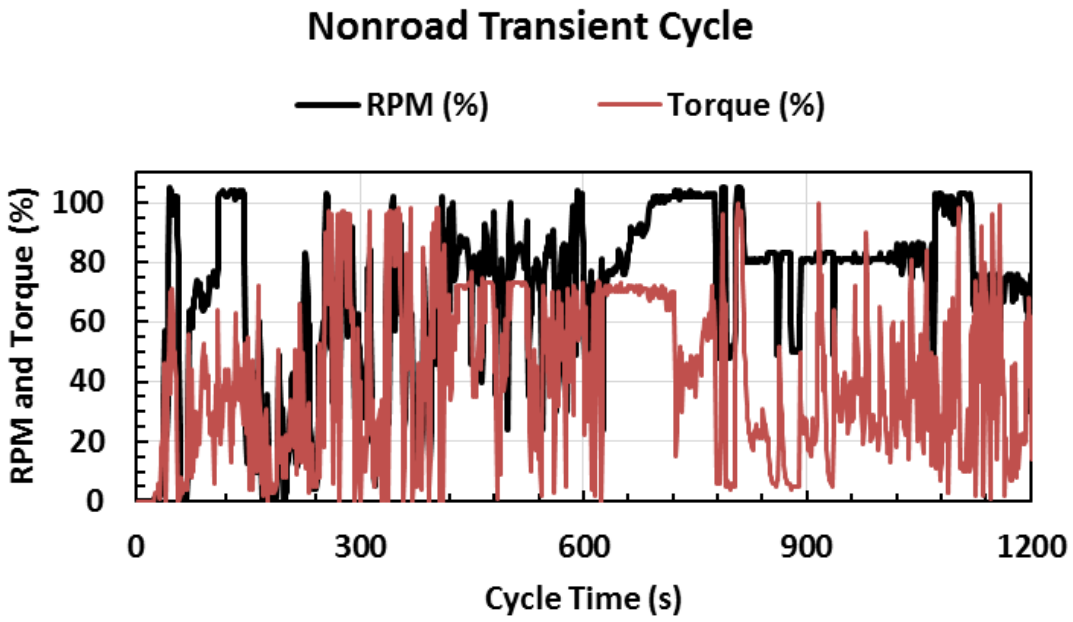

Figure 7-14 Graphical Presentation of the Nonroad Transient Cycle (Target)

A summary of the general test sequence is given in Table 7-6 for the ride mower, mini-excavator, and skid steer engine. It should be noted that the sequence in Table 7-6 represents the target test matrix. The sequence of the tests for the actual testing was determined at the time of testing depending on logistical and other considerations.

Table 7-6 Summary of the Test Sequence for the Ride Mower, Mini-excavator, and Skid Steer Engines

Testing Activity for Ride Mower Engine	Test Number		
Day 1		Blue is full testing	
VERL warm up			
Engine Warmup		Yellow is soak	
Ramped-Mode C1 testing	1		
Soak		Green Is break	
Engine Warmup			
Ramped-Mode C1 testing	2	Red is prep/Conditioning	
Soak			
Engine Warmup		Warm up/ Shutdown	
Ramped-Mode C1 testing	3		
Soak			
NRTC Prep			
VERL shut down and Data process			
Day 2			
VERL warm up			
Cold start NRTC	4		
Soak			
Hot start NRTC	5		
VERL shut down and Data process			

It should be noted that for the SCR configuration, the SCR urea injection needs to verify its functional during the test period. As such, the urea injection were both verified through the NOx concentration during the warm up period before each cycle, as well as the urea level in the urea tank before and after each test.

It should be noted that for this particular DPF configuration, the DPF regenerates on a relatively infrequent basis. As such, no regenerations were observed over the course of testing, and it was determined that the amount of time that would have been needed to prepare the engine such that it would trigger a regeneration during a C1 or NRTC was beyond the scope of the project. Provisions for not making adjustments to measured

emissions results for aftertreatment devices that regenerate infrequently are covered under Title 40 Code of Federal Regulations 1039.525.

7.3.3. Emissions Testing

Emissions tests was conducted to evaluate the effectiveness of the aftertreatment in terms of PM and NOx performance. The emissions tests were conducted in CE-CERT's Vehicle Emissions Research laboratory (VERL). This facility is our primary facility for testing of light-duty vehicles, but is also the facility that we have utilized in the past for conducting emissions tests of small engines. The VERL is equipped with a CVS dilution tunnel with a bag sampling system and a Pierburg AMA-4000 emissions bench. This includes a flame ionization detector (FID) for THC emissions, a chemiluminescence analyzer for NOx emissions and a non-dispersive infrared (NDIR) analyzer for CO and CO2. The analyzer bench is capable of providing both modal and integrated bag measurements of dilute tailpipe gas-phase emissions. The VERL is also equipped with a particulate sampling system that is 1065/1066 compliant for measuring PM mass via gravimetric analysis. For each test, gas-phase and PM emissions were reported in g/kW-hr for the integrated results. In addition, modal files for the gas-phase pollutants can be provided in g/second units. Emissions measurements was evaluated to determine the reduction efficiency of the aftertreatment by comparing the baseline and the degreened aftertreatment testing.

7.4. Results and Discussion

7.4.1. TRU Emissions Testing Results

The regulated gaseous and PM emissions results are shown below in Table 7-7 and Figure 7-15 in g/kw-hr units.

Table 7-7 Gaseous and PM results for TRU engine

Baseline	THC (g/kW-hr)	NMHC (g/kW-hr)	CH4 (g/kW-hr)	CO (g/kW-hr)	NOx (g/kW-hr)	CO_2 (g/kW-hr)	PM (g/kW-hr)	Power (kW-hr)
Test 1	0.172	0.174	0.000	0.937	5.526	931.532	0.1486	3.1940
Test 2	0.164	0.168	0.000	0.980	5.559	958.411	0.1416	3.1931
Test 3	0.174	0.178	0.000	0.954	5.520	951.236	0.1574	3.1934
Degreened Baseline	**THC (g/kW-hr)**	**NMHC (g/kW-hr)**	**CH4 (g/kW-hr)**	**CO (g/kW-hr)**	**NOx (g/kW-hr)**	**CO_2 (g/kW-hr)**	**PM (g/kW-hr)**	**Power (kW-hr)**
Test 1	0.024	0.024	0.000	0.002	5.799	1030.181	0.0025	2.9951
Test 2	0.017	0.017	0.000	0.000	6.121	1052.406	0.0030	2.9958
Test 3	0.009	0.009	0.000	0.000	6.240	1059.935	0.0028	2.9959
Ave	**THC (g/kW-hr)**	**NMHC (g/kW-hr)**	**CH4 (g/kW-hr)**	**CO (g/kW-hr)**	**NOx (g/kW-hr)**	**CO_2 (g/kW-hr)**	**PM (g/kW-hr)**	**Power (kW-hr)**
Baseline	0.170	0.174	0.000	0.957	5.53	947.1	0.1492	3.1935
Degreened Baseline	0.017	0.017	0.000	0.001	6.05	1047.5	0.0028	2.9956
Stdev	**THC (g/kW-hr)**	**NMHC (g/kW-hr)**	**CH4 (g/kW-hr)**	**CO (g/kW-hr)**	**NOx (g/kW-hr)**	**CO_2 (g/kW-hr)**	**PM (g/kW-hr)**	**Power (kW-hr)**
Baseline	0.006	0.005	0.000	0.022	0.02	13.9	0.0079	0.0005
Degreened Baseline	0.008	0.008	0.000	0.001	0.23	15.5	0.0002	0.0004
% Change Degreened Baseline to Baseline	-90.30%	-90.49%	0.00%	-99.95%	9.37%	10.61%	-98.14%	-6.20%

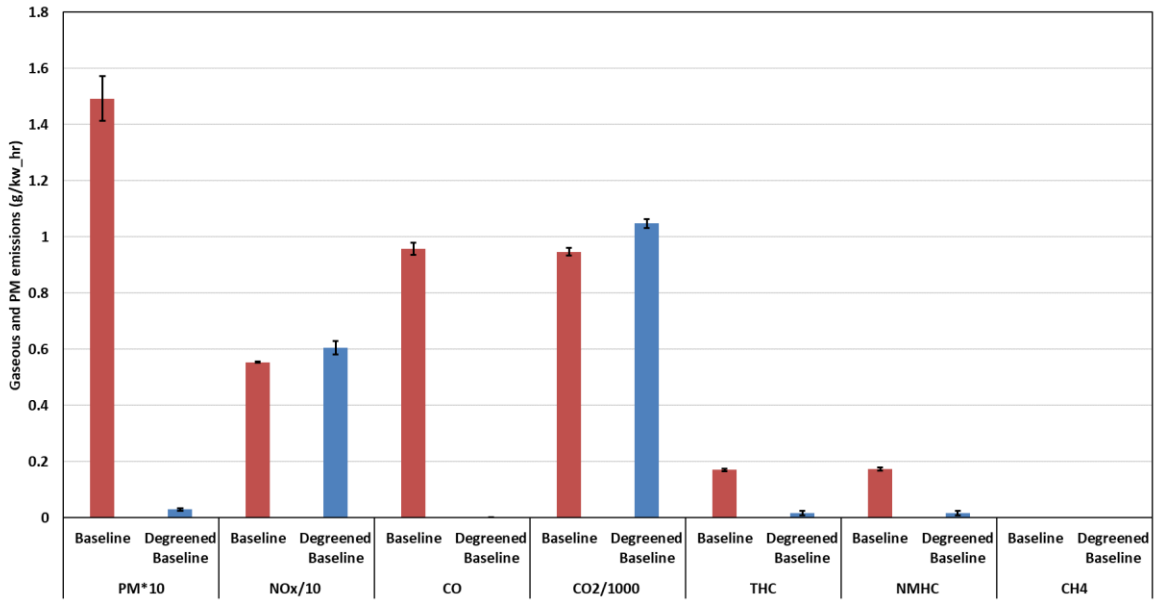

Figure 7-15 Gaseous and PM results for TRU engine

PM emissions are the primary pollutant of interest in terms of emissions reductions for this DPF. For the baseline testing, the PM emissions level was at 0.149 g/kw-hr, which is comparable to the certification value of 0.17 g/kw-hr for this engine. After installing the DPF and degreening it for 25 hours, the PM emissions were reduced to 0.003 g/kw-hr. Thus, the PM emission reductions with the DPF were about 98.1%.

The average NOx emissions were 5.33 g/kw-hr for the baseline testing and 6.05 g/kw-hr for the degreened DPF testing. This represents a 9.4% increase of NOx emissions with the addition of the DPF. The increase in NOx emissions can be attributed to slightly higher NOx concentrations coupled with lower work for the DPF tests. NOx emissions on a g/test basis were higher for the tests conducted with the DPF, as opposed to the tests conducted without the DPF. The g/test results are provided in Appendix A. The NOx g/test results show a general trend of higher average emission rates, but also higher emissions rates specifically for tests #2 and #3, where regeneration was more frequent. As discussed

above, regenerations are performed by heating the intake air. The higher temperature for the intake air leads to higher combustion temperatures, which would lead to higher NOx emissions, and also higher levels of NO2. Additionally, the engine equipped with the DPF was also not able to achieve the same power levels as the engine without the DPF, as discussed above. As such, the average engine work for the baseline tests was 3.19 kw-hr compared to 3.00 kw-hr for the DPF equipped test, a reduction of 6.2%. So both of these factors contributed to the overall higher NOx emissions for the DPF tests. The total NOx increases of about 9% are consistent with the increases seen by Proventia during their preliminary testing in Finland.

The DPF also provided reductions in THC, NMHC, and CO emissions. The DPF substrate is catalyzed and also include a diesel oxidation catalyst (DOC) component, both of which contribute to the observed THC, NMHC, and CO reductions. The emissions for these pollutants were reduced 90.30% for THC, 90.49% for NMHC, and 99.95% for CO. The CH4 emissions for these tests were at/below the background levels detection limit.

CO2 emissions showed an increase from 13.9 g/kw-hr for the baseline testing to 15.5 g/kw-hr for the degreened DPF baseline testing. This represents a 10.6% increase in CO2 emissions per unit work with the addition of the DPF. This result could be associated the impact of the back pressure and the reduction in the work over the cycle, although the highest CO2 emissions were found for the tests where higher levels of regeneration were found.

7.4.2. **Ride Mower Emissions Testing Results**

The regulated gaseous and PM emissions results are shown below in g/kw-hr units in Table 7-8 and Figure 7-16 for the C1 cycle, and in Table 7-9 and Figure 7-17 for the NRTC. Note that in the Figure the NOx and CO2 emissions were divided by 10 and 2000, while the PM results were multiplied by 10, respectively, to allow all the pollutants to be shown in the same graph.

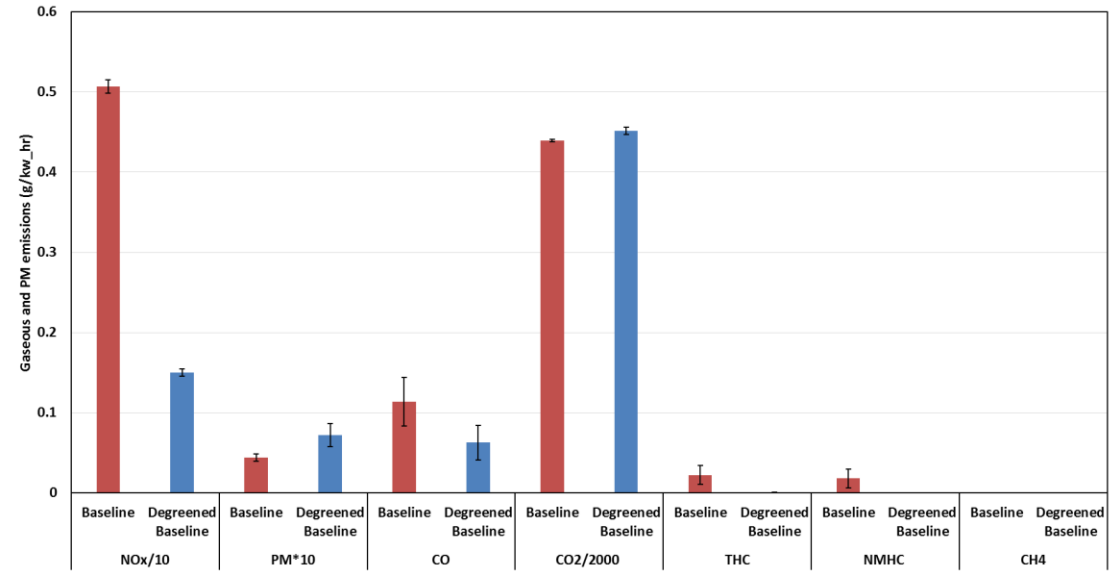

Figure 7-16 Gaseous and PM results for Ride Mower engine C1 cycle

Table 7-8 Gaseous and PM results for Ride Mower engine C1 cycle

Baseline	THC (g/kw-hr)	NMHC (g/kw-hr)	CH_4 (g/kw-hr)	CO (g/kw-hr)	NOx (g/kw-hr)	CO_2 (g/kw-hr)	PM (g/kw-hr)	Energy Consumption (kw-hr)
Test 1	0.009	0.004	0.000	0.079	5.151	875.281	0.0047	7.0154
Test 2	0.030	0.025	0.000	0.128	4.987	881.142	0.0039	7.0164
Test 3	0.028	0.025	0.000	0.134	5.067	879.744	0.0046	7.0177
Degreened Baseline	**THC (g/kw-hr)**	**NMHC (g/kw-hr)**	**CH_4 (g/kw-hr)**	**CO (g/kw-hr)**	**NOx (g/kw-hr)**	**CO_2 (g/kw-hr)**	**PM (g/kw-hr)**	**Energy Consumption (kw-hr)**
Test 1	0.001	0.000	0.000	0.073	1.501	892.744	0.0081	7.0163
Test 2	0.001	0.000	0.000	0.077	1.542	905.756	0.0081	7.0186
Test 3	0.001	0.000	0.000	0.037	1.455	911.091	0.0056	7.0175
Ave	**THC (g/kw-hr)**	**NMHC (g/kw-hr)**	**CH_4 (g/kw-hr)**	**CO (g/kw-hr)**	**NOx (g/kw-hr)**	**CO_2 (g/kw-hr)**	**PM (g/kw-hr)**	**Energy Consumption (kw-hr)**
Baseline	0.022	0.018	0.000	0.114	5.07	878.7	0.0044	7.0165
Degreened Baseline	0.001	0.000	0.000	0.063	1.50	903.2	0.0072	7.0175
Stdev	**THC (g/kw-hr)**	**NMHC (g/kw-hr)**	**CH_4 (g/kw-hr)**	**CO (g/kw-hr)**	**NOx (g/kw-hr)**	**CO_2 (g/kw-hr)**	**PM (g/kw-hr)**	**Energy Consumption (kw-hr)**
Baseline	0.012	0.012	0.000	0.030	0.08	3.1	0.0004	0.0011
Degreened Baseline	0.000	0.000	0.000	0.022	0.04	9.4	0.0014	0.0012
% Change Degreened Baseline to Baseline	-96.45%	-100.00%	0.00%	-45.04%	-70.42%	2.79%	64.44%	0.01%

Table 7-9 Gaseous and PM results for Ride Mower engine NRTC cycle

Baseline	THC (g/kW_hr)	NMHC (g/kW_hr)	CH_4 (g/kW_hr)	CO (g/kW_hr)	NOx (g/kW_hr)	CO_2 (g/kW_hr)	PM (g/kW_hr)	Energy Consumption (kW_hr)
Cold	0.062	0.051	0.000	0.232	4.445	1020.879	0.0036	3.2197
Hot	0.049	0.040	0.000	0.076	3.928	1009.147	-0.0001	3.2187
Degreened Baseline	**THC (g/kW_hr)**	**NMHC (g/kW_hr)**	**CH_4 (g/kW_hr)**	**CO (g/kW_hr)**	**NOx (g/kW_hr)**	**CO_2 (g/kW_hr)**	**PM (g/kW_hr)**	**Energy Consumption (kW_hr)**
Cold	0.057	0.049	0.000	0.230	2.337	1030.097	0.0025	3.2180
Hot	0.043	0.033	0.000	0.094	1.689	1011.484	0.0025	3.2209
Cold	**THC (g/kW_hr)**	**NMHC (g/kW_hr)**	**CH_4 (g/kW_hr)**	**CO (g/kW_hr)**	**NOx (g/kW_hr)**	**CO_2 (g/kW_hr)**	**PM (g/kW_hr)**	**Energy Consumption (kW_hr)**
% Change Degreened Baseline to Baseline	-8.09%	-5.48%	0.00%	-0.60%	-47.43%	0.90%	-30.79%	-0.05%
Hot	**THC (g/kW_hr)**	**NMHC (g/kW_hr)**	**CH_4 (g/kW_hr)**	**CO (g/kW_hr)**	**NOx (g/kW_hr)**	**CO_2 (g/kW_hr)**	**PM (g/kW_hr)**	**Energy Consumption (kW_hr)**
% Change Degreened Baseline to Baseline	-11.56%	-17.18%	0.00%	23.73%	-57.01%	0.23%	N.A.	0.07%

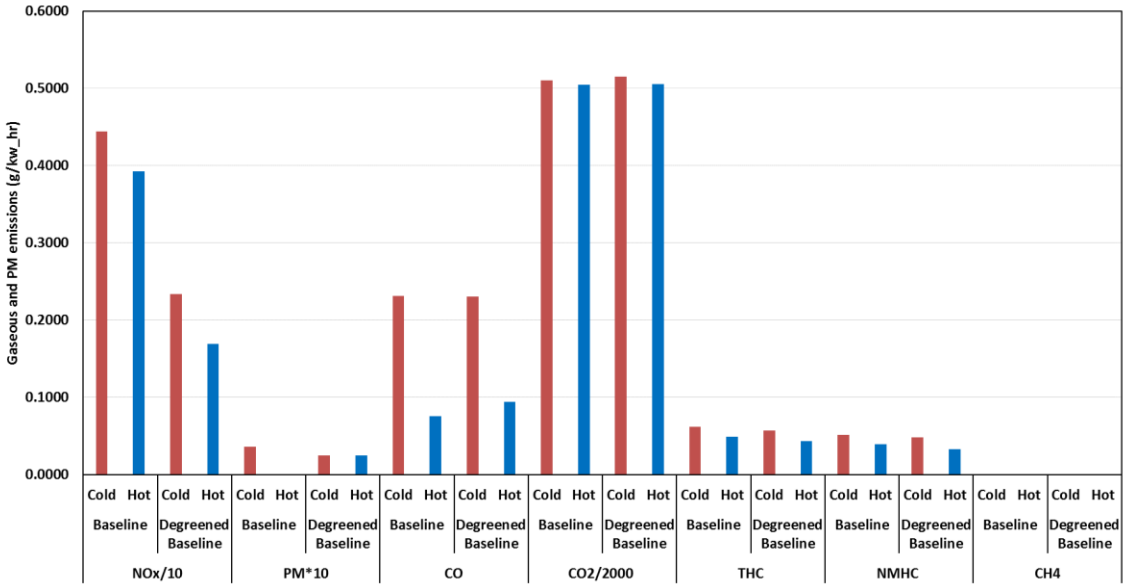

Figure 7-17 Gaseous and PM results for Ride Mower engine NRTC cycle

NOx emissions are the primary pollutant of interest in terms of emissions reductions for this SCR. For the baseline testing, the average NOx emissions levels were 5.07, 4.445, and 3.928 g/kw-hr, respectively, for the C1, NRTC cold start, and NRTC hot start tests. For the tests with the degreened SCR, the average NOx emissions were 1.50, 2.337, and 1.689 g/kw-hr, respectively, for the C1, NRTC cold start, and NRTC hot start tests. Thus, the NOx emission reductions with the SCR were 70.4%, 47.4%, and 57.0%, respectively, for the C1, NRTC cold start, and NRTC hot start tests. Real-time NOx emissions plots for the baseline and SCR-equipped tests are shown in Figure 7-18, Figure 7-19, and Figure 7-20, respectively, for the C1, NRTC cold start, and NRTC hot start tests.

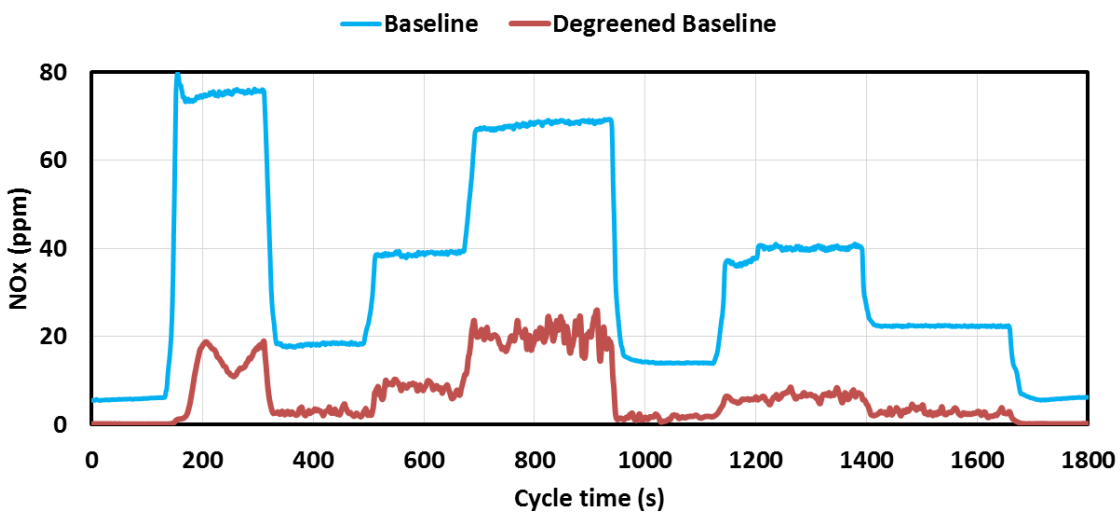

Figure 7-18 Real time NOx result for Ride Mower engine C1 cycle

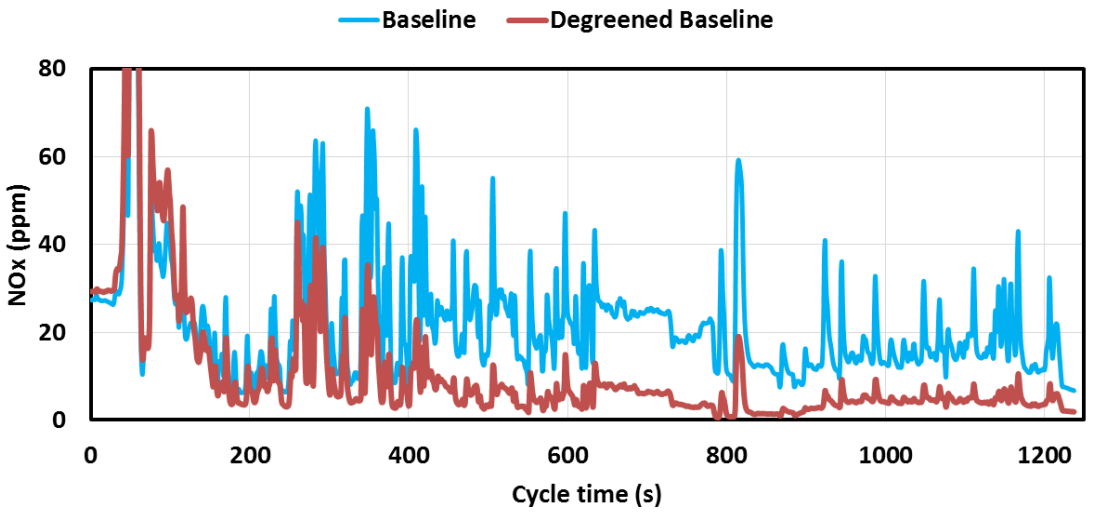

Figure 7-19 Real time NOx result for Ride Mower engine NRTC cycle cold start

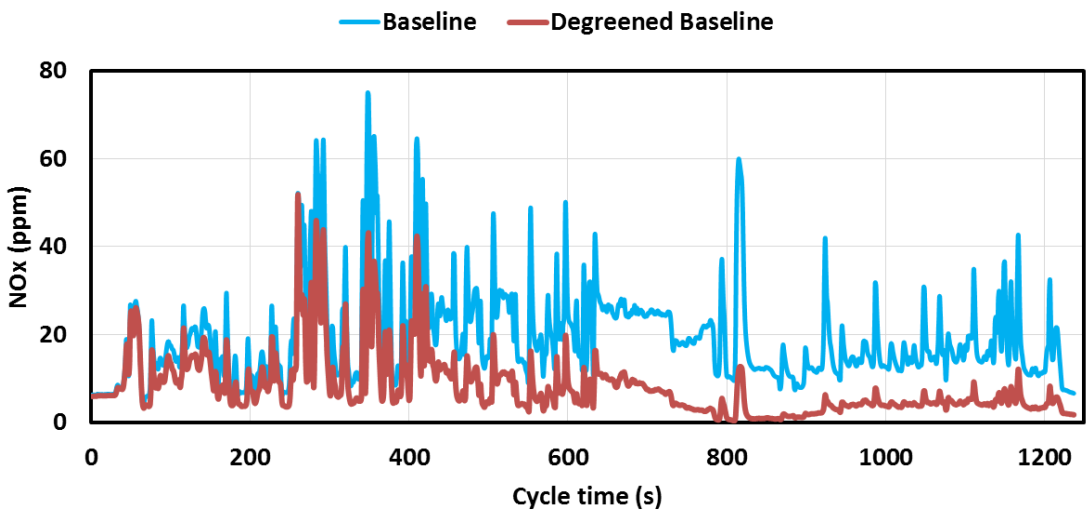

Figure 7-20 Real time NOx result for Ride Mower engine NRTC cycle hot start

The average PM emissions were low for both the C1 and NRTC cycles, since this engine was originally equipped with an OEM DOC and DPF. The PM emissions were somewhat higher on an absolute level for the tests with the SCR, but still within the certification limits. For the regulated gaseous emissions, THC, NMHC, and CO emissions were also relatively low for the baseline testing, due to the OEM DOC and DPF, but showed some additional reductions for the SCR tests. For THC, the emissions were reduced by 96.5%, 8.1%, and 11.6%, respectively, for the C1, NRTC cold start, and NRTC hot start SCR-equipped tests. For NMHC, the emissions were reduced by 100.0%, 5.5%, and 17.2%, respectively, for the C1, NRTC cold start, and NRTC hot start SCR-equipped tests. For CO, the emissions were reduced by 45.0%, 0.6%, and 23.7%, respectively, for the C1, NRTC cold start, and NRTC hot start tests. The CH4 emissions for these tests were at/below the background levels detection limit.

CO_2 emissions were comparable with and without SCR tests. CO_2 emissions rates for the C1 tests were within 3% for with and without SCR tests. CO_2 emissions rates for

the hot start and cold start NRTC tests with and without the SCR were within 1%. It should be noted that CO_2 emissions might be expected to increase slightly due to the additional back pressure from SCR catalyst unit. Given the results, it is expected that the use of this SCR configuration will not have a significant impact on fuel consumption over extended periods of use.

7.4.3. Excavator Emissions Testing Results

The regulated gaseous and PM emissions results are shown below in g/kw-hr units in Table 7-10 and Figure 7-21 for the C1 cycle, and in Table 7-11 and Figure 7-22 for the NRTC. Note that in the Figure 7-21 and Figure 7-22 the PM results were multiplied by 10, while the NOx and CO_2 emissions were divided by 10 and 2000, respectively, to allow all the pollutants to be shown in the same graph.

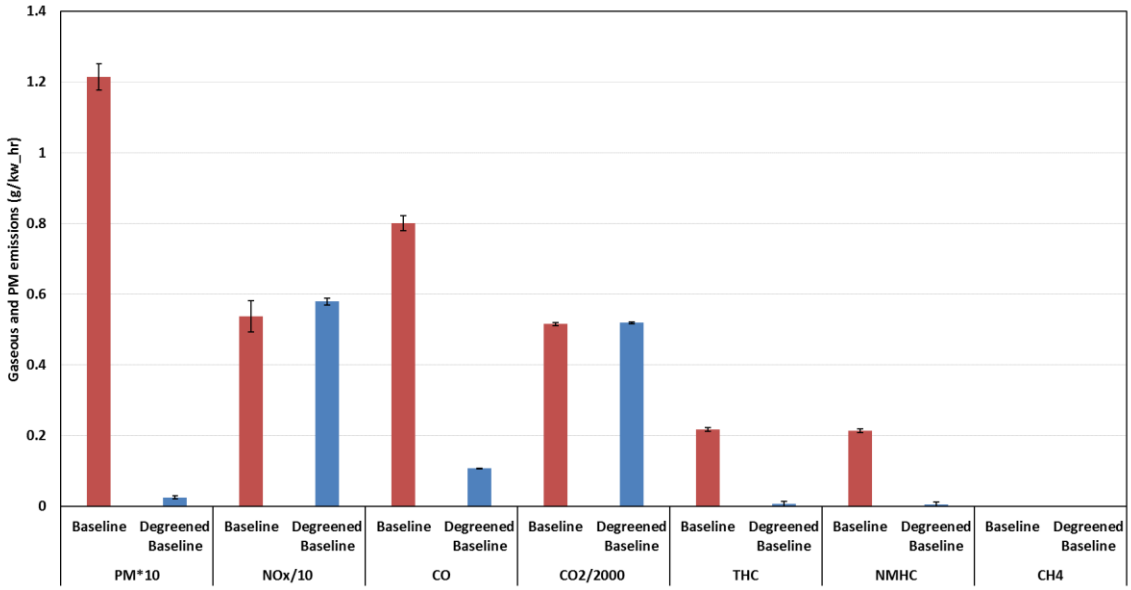

Figure 7-21 Gaseous and PM results for excavator engine C1 cycle

Table 7-10 Gaseous and PM results for excavator engine C1 cycle Baseline

	THC (g/kW-hr)	NMHC (g/kW-hr)	CH_4 (g/kW-hr)	CO (g/kW-hr)	NOx (g/kW-hr)	CO_2 (g/kW-hr)	PM (g/kW-hr)	Energy Consumption (kW-hr)
Test 1	0.212	0.212	0.000	0.785	4.917	1020.588	0.1180	4.4762
Test 2	0.220	0.216	0.000	0.786	5.386	1031.011	0.1254	4.4747
Test 3	0.222	0.213	0.000	0.831	5.808	1041.187	0.1210	4.4746
Degreened Baseline	**THC (g/kW-hr)**	**NMHC (g/kW-hr)**	**CH_4 (g/kW-hr)**	**CO (g/kW-hr)**	**NOx (g/kW-hr)**	**CO_2 (g/kW-hr)**	**PM (g/kW-hr)**	**Energy Consumption (kW-hr)**
Test 1	0.009	0.009	0.000	0.071	5.684	1032.482	0.0023	4.4744
Test 2	0.006	0.004	0.000	0.126	5.865	1042.770	0.0023	4.4746
Test 3	0.005	0.003	0.000	0.126	5.823	1040.763	0.0030	4.4775
Ave	**THC (g/kW-hr)**	**NMHC (g/kW-hr)**	**CH_4 (g/kW-hr)**	**CO (g/kW-hr)**	**NOx (g/kW-hr)**	**CO_2 (g/kW-hr)**	**PM (g/kW-hr)**	**Energy Consumption (kW-hr)**
Baseline	0.218	0.214	0.000	0.801	5.37	1030.9	0.1215	4.4752
Degreened Baseline	0.007	0.005	0.000	0.108	5.79	1038.7	0.0026	4.4755
Stdev	**THC (g/kW-hr)**	**NMHC (g/kW-hr)**	**CH_4 (g/kW-hr)**	**CO (g/kW-hr)**	**NOx (g/kW-hr)**	**CO_2 (g/kW-hr)**	**PM (g/kW-hr)**	**Energy Consumption (kW-hr)**
Baseline	0.005	0.002	0.000	0.026	0.45	10.3	0.0037	0.0009
Degreened Baseline	0.002	0.003	0.000	0.032	0.09	5.5	0.0004	0.0017
% Change Degreened Baseline to Baseline	-97.00%	-97.61%	0.00%	-86.56%	7.83%	0.75%	-97.89%	0.01%

Table 7-11 Gaseous and PM results for excavator engine NRTC cycle

Baseline	THC (g/kW-hr)	NMHC (g/kW-hr)	CH_4 (g/kW-hr)	CO (g/kW-hr)	NOx (g/kW-hr)	CO_2 (g/kW-hr)	PM (g/kW-hr)	Energy Consumption (kW-hr)
Cold	0.309	0.306	0.000	1.294	7.204	1254.274	0.1283	3.1940
Hot	0.321	0.319	0.000	1.247	7.016	1223.393	0.1251	3.1931
Degreened Baseline	**THC (g/kW-hr)**	**NMHC (g/kW-hr)**	**CH_4 (g/kW-hr)**	**CO (g/kW-hr)**	**NOx (g/kW-hr)**	**CO_2 (g/kW-hr)**	**PM (g/kW-hr)**	**Energy Consumption (kW-hr)**
Cold	0.041	0.045	0.000	0.174	5.956	1206.684	0.0017	2.9952
Hot	0.064	0.066	0.000	0.165	6.081	1202.031	0.0004	2.9958
Cold	**THC (g/kW-hr)**	**NMHC (g/kW-hr)**	**CH_4 (g/kW-hr)**	**CO (g/kW-hr)**	**NOx (g/kW-hr)**	**CO_2 (g/kW-hr)**	**PM (g/kW-hr)**	**Energy Consumption (kW-hr)**
% Change Degreened Baseline to Baseline	-86.78%	-85.40%	0.00%	-86.53%	-17.31%	-3.79%	-98.67%	-6.23%
Hot	**THC (g/kW-hr)**	**NMHC (g/kW-hr)**	**CH_4 (g/kW-hr)**	**CO (g/kW-hr)**	**NOx (g/kW-hr)**	**CO_2 (g/kW-hr)**	**PM (g/kW-hr)**	**Energy Consumption (kW-hr)**
% Change Degreened Baseline to Baseline	-80.09%	-79.26%	0.00%	-86.77%	-13.33%	-1.75%	-99.69%	-6.18%

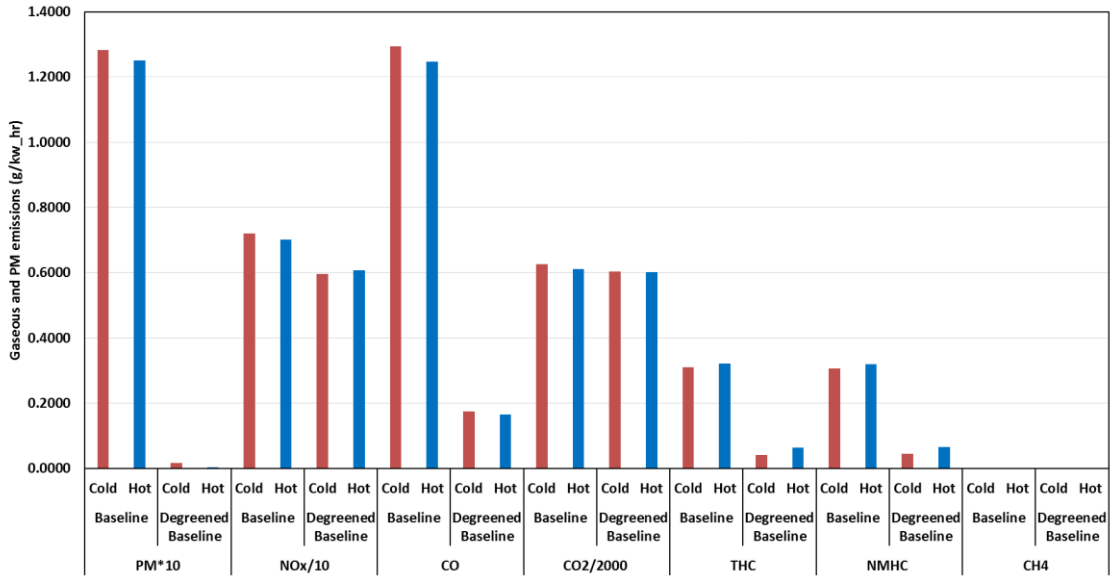

Figure 7-22 Gaseous and PM results for excavator engine NRTC cycle

PM emissions are the primary pollutant of interest in terms of emissions reductions for this DPF. For the baseline testing, the average PM emissions levels were 0.122, 0.128, and 0.125 g/kw-hr, respectively, for the C1, NRTC cold start, and NRTC hot start tests. For the tests with the degreened DPF, the average PM emissions were 0.003, 0.002, and 0.0004 g/kw_hr, respectively, for the C1, NRTC cold start, and NRTC hot start tests. Thus, the PM emission reductions with the DPF were 97.9%, 98.7%, and 99.7%, respectively, for the C1, NRTC cold start, and NRTC hot start tests.

The DPF also provided reductions in THC, NMHC, and CO emissions. The DPF substrate is catalyzed and also include a DOC component, both of which contribute to the observed THC, NMHC, and CO reductions. For THC, the emissions were reduced by 97.0%, 86.8%, and 80.1%, respectively, for the C1, NRTC cold start, and NRTC hot start tests. For NMHC, the emissions were reduced by 97.6%, 85.4%, and 79.3%, respectively, for the C1, NRTC cold start, and NRTC hot start tests. For CO, the emissions were reduced

by 86.6%, 86.5%, and 86.8%, respectively, for the C1, NRTC cold start, and NRTC hot start tests. The CH4 emissions for these tests were at/below the background levels detection limit.

The average NOx emissions showed mixed trends between the different test cycles, with NOx emissions slightly higher over the C1 cycle with the DPF, while being slightly lower with the DPF for the cold start and hot start NRTCs. The NOx increase with the DPF was 7.8% for the C1 test cycle, while the reductions were 13.3% to 17.3% for the hot start and cold start NRTC cycles.

CO2 emissions were comparable with and without DPF tests. CO2 emissions rates for the C1 tests were within 1% with and without DPF tests. CO2 emissions rates for the hot start and cold start NRTC were about 3.8% and 1.8% lower, respectively, for the DPF tests. It should be noted that CO2 emissions might be expected to increase slightly during a regeneration event, which was not observed during the course of this testing. Given the infrequency of the regeneration events, it is expected that the use of this DPF configuration will not have a significant impact on fuel consumption over extended periods of use.

7.4.4. **Skid Steer Emissions Testing Results**

The regulated gaseous emissions results are shown below in g/kw-hr units in Table 7-12 and Figure 7-23 for the C1 cycle, and in Table 7-13 and Figure 7-24 for the NRTC. Note that in the Figure 7-23 and Figure 7-24, the NOx and CO2 emissions were divided by 10 and 2000, respectively, to allow all the pollutants to be shown in the same graph.

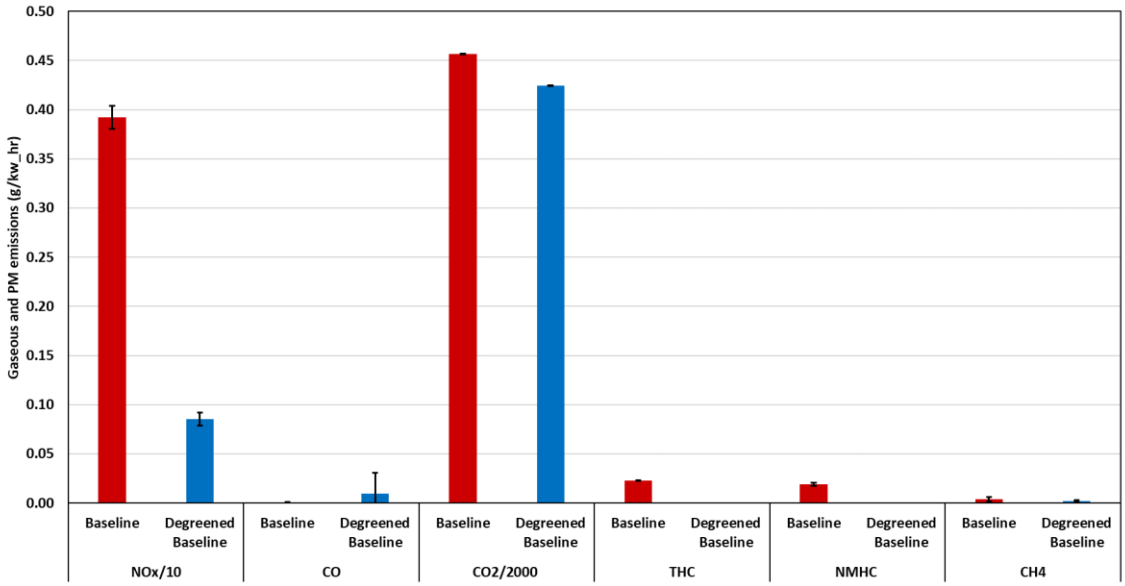

Figure 7-23 Gaseous results for skid steer engine C1 cycle

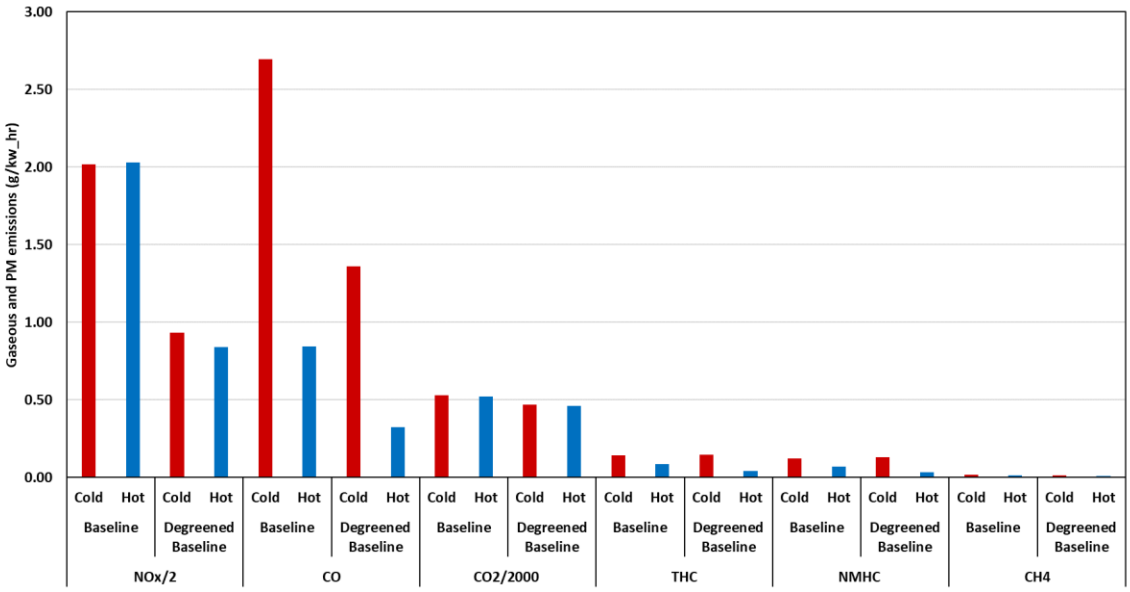

Figure 7-24 Gaseous results for skid steer engine NRTC cycle

Table 7-12 Gaseous results for skid steer engine C1 cycle

Baseline	THC (g/kW-hr)	NMHC (g/kW-hr)	CH_4 (g/kW-hr)	CO (g/kW-hr)	NOx (g/kW-hr)	CO_2 (g/kW-hr)	Energy Consumption (kW-hr)
Test 1	0.023	0.017	0.006	0.003	4.043	912.396	9.5536
Test 2	0.023	0.020	0.003	-0.014	3.807	913.572	9.5578
Test 3	0.022	0.021	0.002	-0.011	3.920	912.462	9.5564
Degreened Baseline	**THC (g/kW-hr)**	**NMHC (g/kW-hr)**	**CH_4 (g/kW-hr)**	**CO (g/kW-hr)**	**NOx (g/kW-hr)**	**CO_2 (g/kW-hr)**	**Energy Consumption (kW-hr)**
Test 1	0.000	-0.003	0.003	-0.014	0.777	848.968	9.3615
Test 2	-0.002	-0.003	0.002	0.019	0.891	848.342	9.3632
Test 3	-0.002	-0.003	0.001	0.025	0.896	848.432	9.3630
Ave	**THC (g/kW-hr)**	**NMHC (g/kW-hr)**	**CH_4 (g/kW-hr)**	**CO (g/kW-hr)**	**NOx (g/kW-hr)**	**CO_2 (g/kW-hr)**	**Energy Consumption (kW-hr)**
Baseline	0.023	0.019	0.004	-0.007	3.92	912.8	9.5559
Degreened Baseline	-0.001	-0.003	0.002	0.010	0.85	848.6	9.3626
Stdev	**THC (g/kW-hr)**	**NMHC (g/kW-hr)**	**CH_4 (g/kW-hr)**	**CO (g/kW-hr)**	**NOx (g/kW-hr)**	**CO_2 (g/kW-hr)**	**Energy Consumption (kW-hr)**
Baseline	0.000	0.002	0.002	0.009	0.12	0.7	0.0022
Degreened Baseline	0.001	0.000	0.001	0.021	0.07	0.3	0.0009
% Change Degreened Baseline to Baseline	-105.17%	-117.05%	0.00%	-230.34%	-78.21%	-7.04%	-2.02%

Table 7-13 Gaseous results for skid steer engine NRTC cycle

Baseline	THC (g/kW-hr)	NMHC (g/kW-hr)	CH_4 (g/kW-hr)	CO (g/kW-hr)	NOx (g/kW-hr)	CO_2 (g/kW-hr)	Energy Consumption (kW-hr)
Cold	0.141	0.124	0.018	2.694	4.034	1063.449	4.3602
Hot	0.085	0.072	0.013	0.844	4.058	1042.203	4.3618
Degreened Baseline	**THC (g/kW-hr)**	**NMHC (g/kW-hr)**	**CH_4 (g/kW-hr)**	**CO (g/kW-hr)**	**NOx (g/kW-hr)**	**CO_2 (g/kW-hr)**	**Energy Consumption (kW-hr)**
Cold	0.145	0.132	0.013	1.359	1.865	941.966	4.2949
Hot	0.043	0.033	0.010	0.323	1.682	921.818	4.2953
Cold	**THC (g/kW-hr)**	**NMHC (g/kW-hr)**	**CH_4 (g/kW-hr)**	**CO (g/kW-hr)**	**NOx (g/kW-hr)**	**CO_2 (g/kW-hr)**	**Energy Consumption (kW-hr)**
% Change Degreened Baseline to Baseline	2.53%	7.00%	0.00%	-49.56%	-53.77%	-11.42%	-1.50%
Hot	**THC (g/kW-hr)**	**NMHC (g/kW-hr)**	**CH_4 (g/kW-hr)**	**CO (g/kW-hr)**	**NOx (g/kW-hr)**	**CO_2 (g/kW-hr)**	**Energy Consumption (kW-hr)**
% Change Degreened Baseline to Baseline	-49.31%	-54.82%	0.00%	-61.73%	-58.54%	-11.55%	-1.52%

NOx emissions are the primary pollutant of interest in terms of emissions reductions for this SCRT system. For the baseline testing, the average NOx emissions levels were 3.923, 4.034, and 4.058 g/kw-hr, respectively, for the C1, NRTC cold start, and NRTC hot start tests. For the tests with the degreened SCRT, the average NOx emissions were 0.855, 1.865, and 1.682 g/kw-hr, respectively, for the C1, NRTC cold start, and NRTC hot start tests. Thus, the NOx emission reductions with the SCRT were 78.2%, 53.8%, and 58.5%, respectively, for the C1, NRTC cold start, and NRTC hot start tests.

To better understand these trends, real-time NOx emissions plots for the baseline and SCRT-equipped tests are shown in Figure 7-25, Figure 7-26, and Figure 7-27, respectively, for the C1, NRTC cold start, and NRTC hot start tests.

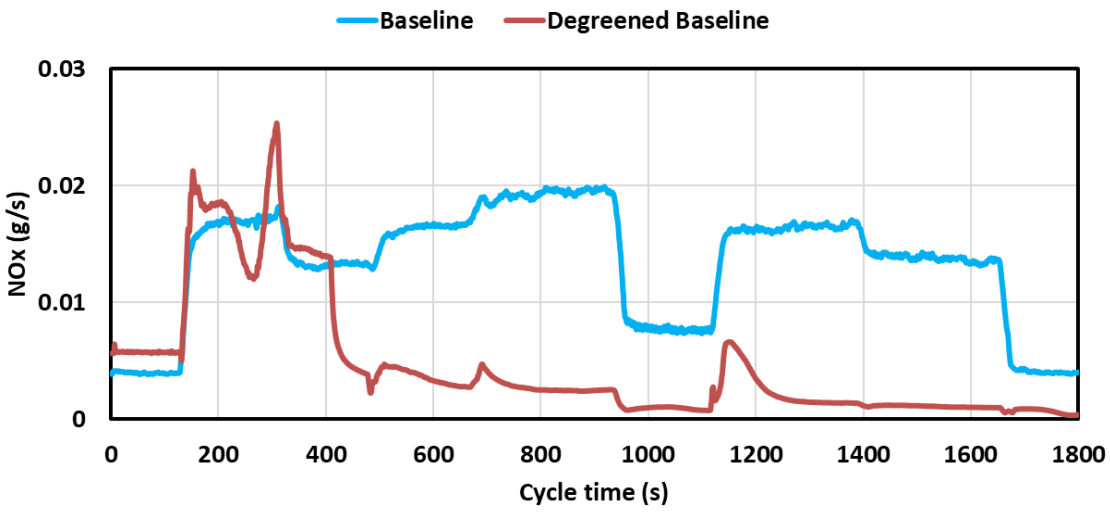

Figure 7-25 Real time NOx result for Ride Mower engine C1 cycle

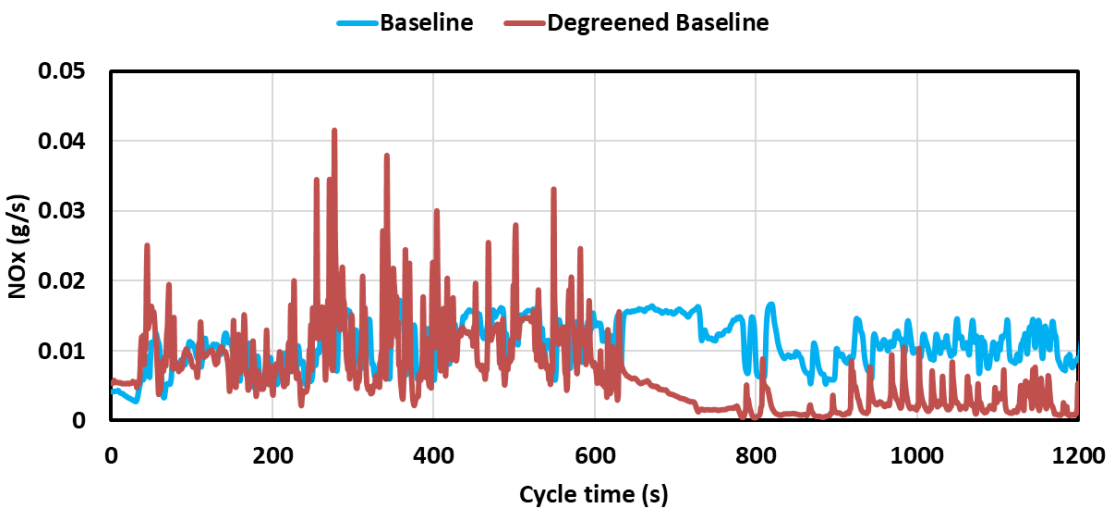

Figure 7-26 Real time NOx result for Ride Mower engine NRTC cycle cold start

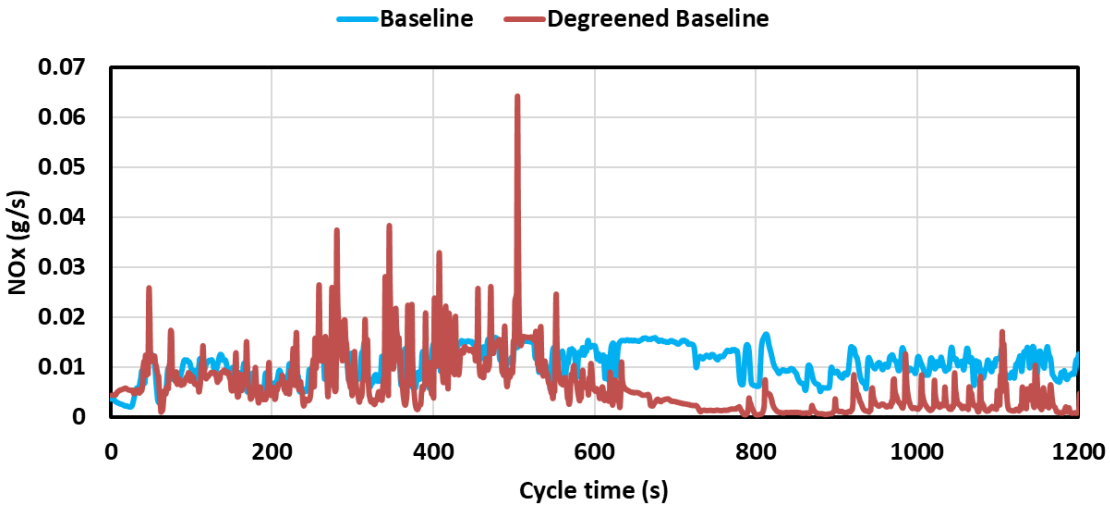

Figure 7-27 Real time NOx result for Ride Mower engine NRTC cycle hot start

The real-time plots show that the initial portions of the test do not show strong NOx reductions for the SCRT. This is due to the SCR not reaching the dosing temperature threshold of 190 °C. The period where the SCR not reach its dosing temperature is the shortest for the C1 cycle, since this cycles begins as a hot running cycle, where the engine is warmed up prior to starting the cycle. The C1 cycle is also longer in duration compared to the NRTC, so a small fraction of the total cycle is spend in a mode where the dosing

temperature is not reached. The NRTC test shows a low NOx conversion efficiency for almost first half does of the test because the SCR temperatures did not reach the dosing temperature threshold. As shown in the Figure 7-26 and Figure 7-27, the urea dosing starts ~10 minutes into the test run, and hence the overall NOx conversion efficiency comes out to be lower. If the engine is calibrated such that the engine-out exhaust temperatures are higher during transients, the SCRT can have a much better conversion efficiency. Also, the dosing control strategy for the SCRT system was developed using only feedforward control for urea dosing, since there was not sufficient time to do a full calibration that included the use of a storage control strategy. Using a storage control strategy helps the catalyst to reduce the NOx before the SCR reaches dosing temperature threshold, as it stores the ammonia on the catalyst based on absorption and adsorption phenomenon. Having the storage controls would help considerably during transients where the temperatures rise slowly, in that they would still provide for a good NOx conversion efficiency.

The average PM emissions were low for both the C1 and NRTC cycles, since this engine was originally equipped with an OEM DOC. The PM emissions were somewhat higher on an absolute level for the tests with the SCR, but still within the certification limits. For the regulated gaseous emissions, THC and NMHC, and CO emissions were also relatively low for the baseline testing, due to the OEM DOC, but showed some additional reductions for the SCR tests. For THC, the emissions were reduced by 100.0%, -2.53%, and 49.3%, respectively, for the C1, NRTC cold start, and NRTC hot start SCR-equipped tests. For NMHC, the emissions were reduced by 100.0%, 5.5%, and 17.2%, respectively, for the C1, NRTC cold start, and NRTC hot start SCR-equipped tests. CO emissions were

very low during the C1 cycle, but showed somewhat higher emissions during the cold start and hot start NRTC cycles. For CO, the emissions were reduced by 45.0%, 0.6%, and 23.7%, respectively, for the C1, NRTC cold start, and NRTC hot start tests. The CH4 emissions for these tests were at/below the background levels detection limit.

CO_2 emissions were comparable or slightly lower for the tests with and without the SCRT. CO_2 emissions rates for the C1 tests were within 7% for with and without SCRT tests. CO_2 emissions rates for the hot start and cold start NRTC tests with and without the SCR were within 11%. It should be noted that CO_2 emissions might be expected to increase slightly due to the additional back pressure from SCRT catalyst unit. Given the results, it is expected that the use of this SCRT configuration will not have a significant impact on fuel consumption over extended periods of use.

7.5. **Conclusions**

The objective of this study is to evaluate the potential effectiveness and feasibility of implementing regulations for small off-road diesel engines with rated powers of less than 37 kilowatts (kW) that will require the use of advanced emission control strategies, such as DPFs and SCR. The aftertreatment demonstrations for this study included the use of a DPF on a TRU engine, the addition of an SCR to an already DPF equipped ride mower, the use of a DPF on a mini-excavator engine, and the addition of a DPF and SCR on a skid steer engine.

PM emissions were the primary pollutant of interest in terms of emissions reductions for TRU engine and mini-excavator engine. For the baseline testing of TRU engine, the PM emissions level was at 0.149 g/kw-hr, which is comparable to the

certification value of 0.17 g/kw-hr for this engine. After installing the DPF and degreening it for 25 hours, the PM emissions were reduced to 0.003 g/kw-hr. Thus, the PM emission reductions with the DPF were about 98.1%. For the baseline testing of mini-excavator engine, the average PM emissions levels were 0.122, 0.128, and 0.125 g/kw-hr, respectively, for the C1, NRTC cold start, and NRTC hot start tests. For the tests with the degreened DPF, the average PM emissions were 0.003, 0.002, and 0.0004 g/kw_hr, respectively, for the C1, NRTC cold start, and NRTC hot start tests. Thus, the PM emission reductions with the DPF were 97.9%, 98.7%, and 99.7%, respectively, for the C1, NRTC cold start, and NRTC hot start tests. Our results show DPFs designed for SORDE applications can provide significant reductions in PM emissions. Other observations from the dynamometer testing included that exhaust backpressure increased with the DPF installed, and that the DPFs regeneration protocol is an important part of the DPFs operational performance profile.

NOx emissions were the primary pollutant of interest in terms of emissions reductions for ride mower and skid steer engines. For the baseline testing ride mower engine, the average NOx emissions levels were 5.07, 4.445, and 3.928 g/kw-hr, respectively, for the C1, NRTC cold start, and NRTC hot start tests. For the tests with the degreened SCR, the average NOx emissions were 1.50, 2.337, and 1.689 g/kw-hr, respectively, for the C1, NRTC cold start, and NRTC hot start tests. Thus, the NOx emission reductions with the SCR were 70.4%, 47.4%, and 57.0%, respectively, for the C1, NRTC cold start, and NRTC hot start tests. For the baseline testing of skid steer engine, the average NOx emissions levels were 3.923, 4.034, and 4.058 g/kw-hr, respectively, for

the C1, NRTC cold start, and NRTC hot start tests. For the tests with the degreened SCRT, the average NOx emissions were 0.855, 1.865, and 1.682 g/kw-hr, respectively, for the C1, NRTC cold start, and NRTC hot start tests. Thus, the NOx emission reductions with the SCRT were 78.2%, 53.8%, and 58.5%, respectively, for the C1, NRTC cold start, and NRTC hot start tests. Our results indicate SCR shows reasonable reduction on NOx emissions in the range of 47-78%. The lower reductions for the transient NRTC cycle can primarily be attributed to the lower SCR temperature being below the dosing threshold during the beginning of a NRTC cycle. For an actual commercial system, the operation of the SCR could be developed to minimize the impact of lower temperature operation on SCR efficiency with feedforward and storage control strategies, and thermal optimization.

7.6. **Acknowledgements**

The authors thank the following organizations and individuals for their valuable contributions to this study. We acknowledge funding from the California Air Resources Board under contract 13-315. We acknowledge Mr. Kurt Bumiller, Mr. Daniel Sandez, Mr. Mark Villela and Mr. Don Pacocha of the University of California, Riverside for their contributions in conducting the emissions testing for this program.

7.7. **References**

Dieselnet (2018). Tier 4 Emissions Standards. Accessed on 9/4/2018. https://www.dieselnet.com/standards/us/nonroad.php#tier4.

8. Controlling Emissions from an Ocean Going Vessel with a Retrofit Scrubber System

8.1. Abstract

Emissions from ocean going vessels (OGVs) are a threat to community health so global regulations have lowered the maximum allowed sulfur levels in fuels and mandated engines with lower emissions. Additionally, some environmentally sensitive areas require either burning fuels with a much lower sulfur content or installing an exhaust gas scrubber (EGS). As low-sulfur fuels cost about twice the fuels meeting global limits, many OGV owners are installing EGSs. While much is known about the EGS's high efficiency for controlling sulfur oxide (SOx) emissions, little is known about the control efficiencies for particulate mass (PM). Following standard protocols, this research measured SOx and PM control efficiencies for a scrubber retrofit to an existing OGV. The EGS reduced SOx by >95%; however, PM mass was reduced by ~2 to 12%. These findings are consistent with SO2 gas being absorbed by the EGS -droplets as simultaneously the SO3 gas is converted to a sulfuric acid particle that is too small to be removed by the EGS droplets. The results differ from others who find PM control efficiencies of ~75%. We explain how sampling methods for a system with condensable particles can account for the difference. The research suggests there is an immediate need for a PM emission limit and a measurement method to enforce the standard. Different EGS designs easily remove >95% SOx but if the number of EGS units on ships are multiplied ten-fold without regard to PM control, the air may not achieve the intended health benefits.

Figure: Graphic Abstract

8.2. **Introduction**

Global shipping represents over 80% of the volume and 70% of the value of goods traded (UNCTAD, 2015). As more goods are shipped, the local and global anthropogenic emissions and impact from shipping increases. International shipping can also contribute to increased mortality in coastal regions. Some have estimated this impact to be 60,000 deaths from cardiopulmonary and lung cancer per annum (Corbett et al., 2007, USEPA, 2016). Additionally, ship emissions are connected with climate change (Lawrence and Crutzen, 1999; Davis et al., 2001; Eyring et al., 2005).

International shipping is attractive because of the low cost per ton of delivered goods. One driver of the low delivery cost is that the diesel engines on ocean going vessels (OGVs) are designed to burn the lowest cost fuels available, so called bunker fuels. These fuels are a blend of distillable refinery streams with the non-distillable portions of crude and as a result have a high content of sulfur, polycyclic aromatic hydrocarbons and heavy metals. Burning this dirty fuel leads to high mass emissions of a particulate matter (PM)

composed of sulfate, organic/elemental carbon, metals, and black carbon (BC) and increased health concerns (Andreasen and Mayer, 2007; Schneider et al., 2005). The major pollutants in ship exhaust are PM with an aerodynamic diameter less than 2.5 μm (PM2.5), sulfur oxides (SOx), carbon monoxide (CO), and nitrogen oxides (NOx). Recently, BC emissions from ships have drawn attention due to its strong global warming effect (Corbett et al., 2007; Cappa et al., 2012).

Burning fuels with high sulfur contents lead to high levels of sulfur oxide emissions that can harm the respiratory system and make breathing difficult, especially for asthmatics (Li et al., 2014). Furthermore, SOx reacts with compounds in the atmosphere to form small particles that may penetrate deeply into sensitive parts of the lungs and cause additional health problems. Several investigators have reported a connection between fuel sulfur content and PM emissions (Fridell and Salo, 2014; Winnes and Fridell, 2009). For comparison, it should be noted that a switch from heavy fuel oil (HFO) to a marine gas oil (MGO) resulted in a 75% PM mass reduction (Winners and Fridell, 2009; Khan et al., 2012). Due to the increased concern about ship emissions near ports, the International Maritime Organization (IMO) reduced the maximum sulfur limit for marine fuels in 2012 to 3.5 wt% and in 2020 to 0.5 wt%, (IMO; Fridell and Salo, 2014).

In addition to lowering the sulfur levels for all marine fuels, the IMO also identified environmentally sensitive areas, called Emission Control Areas (ECAs), where after January 2015 SOx emissions had to be the same or less than if the ship burned a fuel with 0.1% sulfur. Currently, there are four ECAs around North America and Western Europe and more ECAs are planned. Within ECAs, vessels with exhaust gas cleaning system may

burn fuels with up to 3.5% sulfur as long as the ratio of SOx to C02 exhaust emissions are the same or less as if the ship burned a fuel with 0.1% sulfur.

When operating ships within ECAs, vessel owners have to decide whether to burn a fuel with <0.1% sulfur or install a scrubber in order to burn a fuels with up to 3.5% sulfur. Soon, in 2020, vessel owners will have to burn fuels with <0.5% sulfur globally or install an exhaust gas scrubber (EGS). For both cases, the choice of either low-sulfur fuel or a scrubber depends on a number of factors and is a tradeoff of operating versus capital expenses. Factors entering that decision include the relative cost of the fuels, the amount of time spent in ECAs, the ship's fuel consumption, its age and the cost of adding a scrubber (UNCTAD, 2015). The installed cost of a wet scrubber system is in the range of $2 to $5 million depending on vessel and scrubber design (UNCTAD, 2015). Many have found that installing a seawater scrubber to offset the higher operating expense of low sulfur fuel is a proven strategy (IMO, 2009). So, EGS use is expected to increase before 2020 when the new sulfur limits for marine fuels are implemented.

Many studies show that scrubbers were highly effective for controlling SOx at either the laboratory or power plant levels (Caiazzo et al., 2013; Andreasen and Mayer, 2007; Oikawa et al., 2003). However, ship results are sparse. Available results show SOx reductions > 95% and PM mass reductions ranging from 45-80%. (Fridell and Salo, 2014; Hansen, 2012; USEPA, 2011). The significant difference in scrubber efficiencies for SOx and PM is not surprising given that the mechanism and design principles for removing SOx and PM are different (Cooper and Alley, 2011) and that the vessels are installing scrubbers designed to remove SO2 rather than PM.

Given the ECA regulation, the approaching new sulfur limits and an increasing number of installed/planned EGS systems, there is an immediate need to understand whether EGS provides both the SOx and the PM emission control as intended in Regulation 14 of MARPOL Annex VI. Thus data from this research will provide information on whether EGS is an acceptable environmental path for both SOx and PM with the high-sulfur, residual marine fuels. Data can also be useful in the current debate on whether all marine fuels should be limited to 0.5% sulfur in 2020.

8.3. **Experimental Methods**

8.3.1. **Test Platform: Vessel and Fuels**

The ocean going vessel was a D7 class container vessel built in 1987 that moves up to 1,676 twenty-foot equivalent units (TEUs) and 249 reefers with a gross tonnage of 20,965. The vessel was equipped with one main engine (ME), two main generators (MGs), two auxiliary engines (AEs), one boiler and a wet EGS to allow the use of high-sulfur HFO fuels while operating in ECA areas. Only the ME and two MGs were connected to the scrubber. The ME is a model year (MY) 1986 Mitsui B&W 7L70, 7 cylinder 16.6 megawatt (MW) low speed, 2-stroke diesel engine with 177,962 operation hours. The MGs are both MY 1986 Wartsila 6R32D, 6 cylinder 2.1 MW medium speed 4-stroke diesel engines with 70,096 and 79,020 operation hours, respectively. This testing was scheduled between overhauls for the ME and MGs, so the PM emissions from this ship should be representative of a properly operating OGV.

Commercial marine heavy fuel oil meeting RMG-380 specifications and lubricants were used during testing. Selected fuel properties are shown in Table 8-1. The vessel used Mobilgard 300 for the ME cylinder oil and Mobilgard 560 for the ME camshaft oil.

Table 8-1 Selected Fuel Properties

Fuel Properties	Unit	Result	Specification
Density at 15°C	kg/m3	989.3	991.0 Max
Viscosity at 50°C	mm²/s (cSt)	306.6	380.0 Max
Carbon residue, micro	mass %	12.59	18.00 Max
Sulfur	mass %	1.89	3.5 Max

8.3.2. **Scrubber**

The retrofit scrubber system was designed and made by Alfa-Laval, and included: an exhaust gas inlet section, a high-pressure spray nozzle to create small droplets (~100µm), a jet section, and an absorber section. The jet section was designed to accelerate particles and gases to create greater mixing and a chance for SOx to be removed via absorption and PM by diffusion/impaction mechanisms. In the absorber section, the flow is slower, allowing time for collecting the mist with absorbed SOx and the PM by diffusion to the droplets. (Fridell and Salo, 2014). Demister pads follow the absorption section to remove larger water droplets before the gas is vented to the atmosphere.

The scrubber on this vessel was designed for both an open loop (OL) mode at-sea where the ocean water provides the alkalinity needed to meet the scrubber design and a closed loop (CL) mode during operation with low-alkalinity water. During CL, the scrubber water is fortified with added caustic solutions to boost alkalinity and re-circulated. This scrubber was designed to work with up to 3 wt% sulfur in the fuel. Above 3%, the

SOx absorption efficiency decreases with both decreasing salinity and alkalinity (Andreasen and Mayer, 2007).

8.3.3. Test and Measurement Methods

8.3.3.1. Engine Test Conditions

At sea, the flows of the main propulsion engine (ME) and up to 2 main power generators (MG) were combined before being treated by the EGS. Since there were no exhaust flow meters for each engine, the plan was to operate the MG at berth when the ME is not operating. This approach allowed the ME mass flow during sea operation to be determined by difference between the total and MG mass flows. MG data were collected at 26% and 50% loads while at port. At sea, ME operation followed the certification loads for the E3 cycle in International Organization for Standardization (ISO) 8178-4 as closely as possible during ship operations. The planned load/power points for the ME were 100%, 75%, 50% and 25% with the MG at 50%. Actual load points and tunnel dilution are listed in Table 8-2, where pre scrubber measured engine out and post scrubber measured a combined exhaust of ME and MG. It worth mentioning Test No. 10 is measured with only ME engine operating at the post scrubber location, this test point was used to calculate the scrubber efficiency and also to compensate for the load variability of the MG.

Table 8-2 Test Matrix and Sampling Location

Test No.	Sampling Source	Sampling Location	ME Load	MG Load	Sampling DR
1	MG	Pre-Scrubber	0%	29%	20
2	ME	Pre-Scrubber	51%	52%	12
3	ME	Pre-Scrubber	74%	55%	8
4	ME	Pre-Scrubber	94%	57%	20
5	ME	Pre-Scrubber	91%	57%	6
6	ME+MG	Post- Scrubber	77%	56%	6
7	ME+MG	Post- Scrubber	49%	56%	8
8	ME+MG	Post- Scrubber	75%	56%	20
9	ME+MG	Post- Scrubber	75%	56%	12
10	ME-only	Post- Scrubber	92%	57%	6
11	ME+MG	Post- Scrubber	75%	0%	8
12	MG	Post- Scrubber	0%	46%	20

The test points covered the range of the normal scrubber exhaust flow and represent about 85% of the weighting factor used for determining the overall emission factor. Prior to the first test, the engine was operated for 30 minutes at the highest power to stabilize emissions. At subsequent loads, we waited for the gas concentration values to stabilize and then the gaseous and PM mass were sampled continuously for 5 to 20 minutes, with time depending on the PM mass filter loading. Triplicate samples were taken.

8.3.3.2. **Measuring Gaseous and PM mass Emissions**

The exhaust duct configuration allowed the engine out emissions from the ME and MG to be measured separately; however, both streams were combined before the EGS unit so only combined emissions were monitored after the EGS. The post-scrubber sampling

port was located approximately 1 m above the absorber section of the EGS unit and 0.5 m below the vessel's continuous emissions monitor (CEMs).

Exhaust concentrations of carbon monoxide (CO), carbon dioxide (CO2), nitrogen oxides (NOx), oxygen (O2) and sulfur oxides (SOx) gases were continuously measured following the ISO 8178-2 protocol with a Horiba PG-350 portable multi-gas analyzer. The PG-350 utilizes Non-Dispersive Infra-Red (NDIR) detectors to measure CO, CO2, and SO2 and a chemiluminescence detector (CLD) for NOx measurement. The PG-350 analyzer was calibrated using EPA protocol gases several times during the testing and measured drift was factored during the analysis of the data. Instrument drift met the manufacturer's specification.

The PM2.5 mass emission measurements were made using a partial dilution system design based on the ISO 8178-1 protocol and on conditioning the diluted exhaust gas, as per 40 CFR Part 1065. The dilution system maintained PM2.5 sampling at 47 ± 5 0C. To avoid water condensation the system used heated dilution air, a heated sample line, and a heated tunnel body during both the pre and post scrubber testing. After sample conditioning, PM2.5 mass was collected on a Teflon filter and weighed offline daily with a Mettler Toledo ultra-balance placed in a Heraeus climate chamber until consecutive measurements were within 1%.

8.3.3.3. **PM mass Speciation**

$M_{2.5}$ mass was fractionated into sulfate, organic carbon (OC), elemental carbon (EC) and Black Carbon (BC) by several methods. Sulfate on the Teflon filter was sonicated with deionized water and a small amount of alcohol, and then analyzed for the sulfate using a

Dionex ICS-3000 ion chromatography. A thermal/optical method analyzed the carbon aerosol deposited on a quartz filter collected in parallel with the Teflon filter according to the National Institute for Occupational Safety and Health (NIOSH) 5040 reference method (Birch, 1999). The analysis reported elemental carbon and organic carbon (EC & OC). Black carbon was measured with an AVL Micro Soot Sensor (MSS) Model 483 that is based on the photoacoustic measurement principle and an AVL Smoke Meter (FSN) Model 415 SE filter paper method. The AVL MSS continuously monitored PM concentrations and was used to confirm that PM levels were stable before and during filter collection.

8.3.3.4. **Exhaust Flow Calculation**

The exhaust flow rate must be determined to calculate emission factors for the different engines. Exhaust gas flow rates can be calculated using both the air pump method and the carbon balance method. Engine power output in kilowatts (kW), engine revolutions per minute (RPM), boost pressure (bar), and intake manifold temperature ($^{\circ}$C) were recorded during the testing in order to calculate the engine exhaust flow via the air pump method (Miller et al., 2009). Fuel consumption by the engine was also measured enabling exhaust flow to be calculated by a carbon balance method. For this study, the results are based on exhaust flow rates from the carbon balance method, although the results for both methods are similar.

8.4. **Results**

Emissions were measured before and after the scrubber while the vessel was burning a high-sulfur HFO in an ECA zone and as it sailed from Tacoma, Washington to Anchorage, Alaska. Engine out mass flow rates and emission concentrations were collected

separately from the ME and from the MG before being combined and sent to the scrubber; thus, emission rates and emissions factors were determined directly. The overall scrubber efficiency was determined based on the combined flows of the ME and MG to and from the scrubber. An accurate determination of the overall scrubber efficiency depended on knowing the mass flow and this calculation was helped in that at 50% load the ME had 8-times the mass flow of the MG, with proportional deviations from there. Thus, the slight load variations seen for the MG in Table 8-2 should not significantly affect the results. In our calculations, no adjustment was made for the increase in exhaust flow due to water evaporation as the exhaust gas cooled in the EGS. While we did not measure the moisture content before and after the EGS, the estimated flow increase due to exhaust gas cooling and evaporation of water was <10% (Cooper and Alley, 2011).

8.4.1. **Modal and Overall Gaseous Emission Factors: NOx, CO, CO_2, and SO_2**

NOx, CO, CO2 and SO2 emission factors for the MG and ME before the scrubber are shown in Table 8-3 in units of g/kWhr. As planned, only the three highest loads in the ISO E3 cycle were tested for the ME due to the power needed for sailing. For calculating the overall emission factor, the emission factor at 25% load was assumed to be the same value as at 50% load, similar to the method used by Jayaram et al. (2011). Emissions at the highest three loads comprise 85% of the overall emission factor so deviations from this assumption weakly affect the overall factor. Triplicate results showed good repeatability with the coefficient of determination being <3%, which is an indication of a system under control (stable) during the measurement process.

Table 8-3 NOx, CO, and CO_2 Emission Factors for Engine Out in g/kWhr

MG Load	ME Load	NOx	CO	CO_2	SO_2
57%	94%	13.76±0.12	0.213±0.019	616.98±2.00	7.503±0.023
55%	74%	16.92±0.14	0.224±0.033	592.70±6.16	7.223±0.077
52%	51%	16.23±0.12	0.200±0.003	591.73±8.60	7.221±0.103
	ME ISO Weighted*	16.08±0.13	0.215±0.021	597.27±6.06	7.278±0.074
29%	0ff	14.96±0.19	1.34±0.053	763.06±0.12	6.61±0.054

*Assumed emission factor at 25% load is the same as 50% load

Results shows an overall NOx value of ~16.1 g/kWhr for the ME and a modal value of 15.0 g/kWhr for the MG; both values as expected for Tier 0 engines. The overall CO_2 emission factor of the more efficient, slow-speed ME is ~25% lower than the medium-speed MG, as expected. Emission factors for CO_2 agree with earlier reports and were used as the basis for calculating the SO_2 emissions factors. Although SO_2 concentrations were measured during the testing, the reported values did not match a mass balance for the sulfur entering the system. Thus SO_2 emission factors were calculated based on the mass balance methods, as allowed by ISO-8178-1.

8.4.2. PM Emission Factors: Mass, EC, OC, BC, and sulfate

Similar to the gases, the PM emissions were measured from each engine exhaust stream and the modal and overall weighted emission factors are listed in Table 8-4.

Table 8-4 PM Mass & PM Speciated Emissions Factors for Engine Out in g/kWhr

Loads	PM Mass	OC	EC	BC**	H_2SO_4*6.65H_2O
94% ME	1.23±0.02	0.075±0.002	0.0104±0.0011	0.0033±0.0000	0.934±0.024
74% ME	1.46±0.08	0.099±0.005	0.0103±0.0004	0.0037±0.0001	1.081±0.036
50% ME	1.13±0.02	0.113±0.000	0.0073±0.0000	0.0040±0.0000	0.841±0.020
ME ISO Weighted*	1.31±0.05	0.098±0.003	0.0094±0.0004	0.0037±0.0001	0.980±0.029
29% MG	0.90±0.13	0.172±0.009	0.0633±0.0047	0.0473±0.0013	0.468±0.009

*Assumed emission factor at 25% load to be the same as 50% load
**BC results based on the photoacoustic values from the micro-soot sensor (MSS)

Note sulfate is ~75% and the major contributor to the PM mass from the ME exhaust. Also the overall PM mass emission factor from the ME is about 145% of the MG value. Given that the ME engine is eight times the MG size, the primary flow of PM mass into the EGS is from the ME. Note EC emissions from the ME are small due to the higher fuel efficiency of a slow speed engine and <1% of total PM mass. However, EC from the MG is ~11 times higher at equal loads so similar amounts of EC from the ME and MG reach the scrubber.

8.4.3. Overall Scrubber Efficiency for Gaseous Emissions

The overall scrubber control efficiency for removing a gas is calculated based on the total mass flow entering from both the ME and the MG as compared with the mass flow exiting the scrubber using the formula:

$$\textit{Control efficiency, \%} = 100 - (g/hr)exit/(g/hr)enter$$

During the testing of the ME at sea, the MG was always operating about 50% power, as noted in Table 8-2. The scrubber efficiency for removal of NOx, CO and CO2 was <5%, as expected for weak acid gases, so attention was focused on SO2. Post scrubber SO2 concentrations were ~1-2 parts per million (ppm) and the overall reductions and scrubber control efficiencies for SOx were >97%, as shown in Table 8-5. With CO2 concentrations

ranging from 4-6%, the SO2/CO2 ratio are in the range of 0.19 to 0.64, and met the IMO requirements for EGS systems of < 4.3.

Table 8-5 SO_2 Flow Entering/ Exiting Scrubber in kg/hr and Control Efficiency

ME Load	SO_2 Entering (kg/hr)	SO_2 Exiting(kg/hr)	Scrubber Efficiency
50%	54.5	1.3	97.6%
75%	67.5	1.8	97.3%
90%	75.8	2.1	97.2%

8.4.4. Overall Scrubber Efficiency for Gaseous Emissions

The combined PM emission rates in kilograms/hour for the ME + MG are shown in Figure 8-1. For this analysis, the PM mass reduction was measured as well as that for elemental and organic carbon and sulfate. Table 8-6 shows the control efficiency of PM mass and other entities. Of particular note is the low control efficiency for PM mass. This is expected given that sulfate is the primary component of the PM mass and sulfate reduction is small. The OC removal was fairly consistent for all loads but the EC removal at ~50% load suggested a production of EC. Since the scrubber does not produce EC, the result was a consquence of EC being ~1% of the PM mass and a value calculated after subtracting two large numbers.

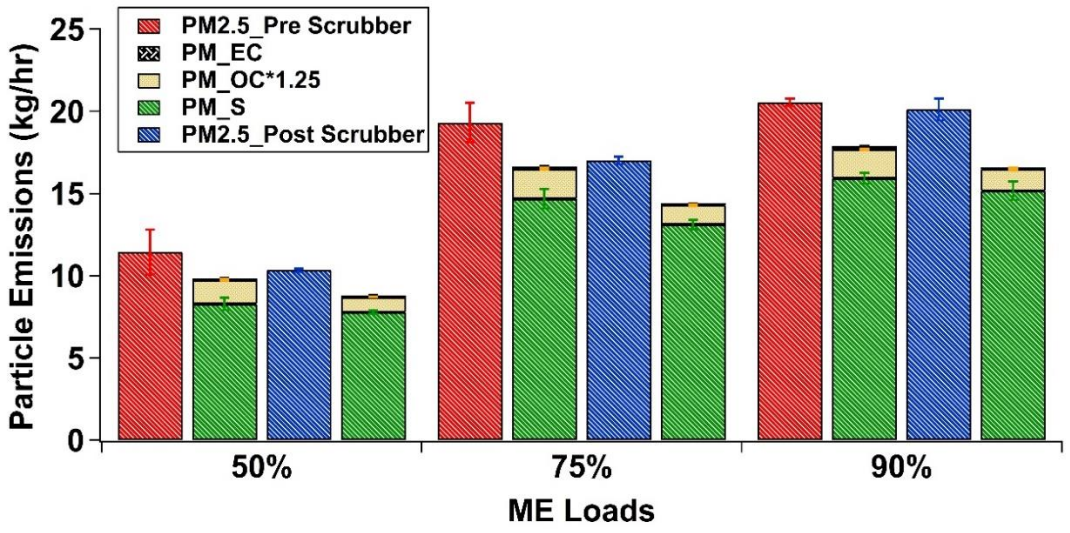

Figure 8-1 Emissions of $PM_{2.5}$ and PM Fractions Before and After the Scrubber in kg/hr

Table 8-6 Scrubber Control Efficiency for PM Fractions in Percent (%)

ME Load	PM mass	OC	EC	H2SO4*6.65H_2O
50	9.5%	36.5%	-21.7%	6.1%
75	11.9%	34.9%	32.9%	10.7%
90	2.1%	24.7%	49.2%	4.8%

8.4.5. Overall Scrubber Efficiency for BC Emissions

Calculating the BC scrubber efficiency mass flow rates from the in grams/hour entering and leaving the scrubber were compared using Equation 1 and results for the EGS control efficiency are shown in Table 8-7 for the MSS, FSN, and EC measurement methods. Remember that the BC mass flow from the ME and MG were nearly the same.

Table 8-7 Scrubber Control Efficiency (%) for Black Carbon Measured by Three Methods

ME Loads	MSS	FSN	EC
50	24.8%	14.1%	-21.7%
75	37.6%	17.8%	32.9%
90	29.4%	8.1%	49.2%

The results show BC control efficiencies between 8% to 49%, depending on the measurement method and load. Some differences could be attributed to the low levels of BC in the PM. The control efficiency measured with the MSS was generally higher than the FSN results, which is similar to the results from Jiang et al. (2018). The EC results from the thermal optical method were higher than both the FSN and MSS for the 50% and 90% loads. Since sulfate and organic PM contribute over 99.5% of the PM on the filter, high levels of sulfur species could potentially pyrolyze OC to BC in the very early heating stages of the NIOSH EC/OC method. This could affect the EC-OC split point, which could lead to higher EC readings. It has also been suggested that metals released during HFO combustion can enhance the oxidation of soot, which could potentially impact the NIOSH ECOC method (Kasper et al., 1999; Sarvi et al., 2011; Sippula et al., 2014). There is also a possibility that some metals could contribute more to the charring of the oxidized carbon species as well, especially when the fraction of EC on the filter is considerably less than OC (Wang et al., 2010; Panteliadis et al., 2015).

8.5. **Conclusion**

One of the most surprising and important findings in this research was the relatively low PM control efficiency (2-12%) for PM mass while the control efficiency for gaseous SO2 removal was ~98%. At first, this finding was difficult to explain since the precursor to sulfate particles is SO3, and that molecule absorbs faster into a sea water droplet than SO2 in a mass transfer controlled process. Furthermore, (Fridell and Salo, 2014; Hansen, 2007) studies measuring emissions from marine engines using a fuel with a high sulfur content report most of the sulfate was removed during the scrubbing process.

We suggest our results can be explained by following the SO2 and SO3 molecules in the exhaust. While both molecules are in the gas phase before the EGS, only the SO2 remains in the gas phase after reaching the EGS and where the SO2 is absorbed by the sea water droplets. By contrast when SO3 gas reaches the EGS, with the lower temperature, high humidity and field of sea water droplets, the SO3 combines with water molecules and changes from the gas to the particle phase as a sulfuric acid particle. Semi-volatile organic molecules also transfer to the particle phase either as distinct particles or coatings on solid PM. Several have reported that a particle phase is favored with rapid cooling, excessive moisture and low dilution (Schneider et al., 2005; Andreasen and Mayer, 2007; Lemmetty et al., 2006) of the exhaust. Such conditions are found in an EGS.

Knowing that SO2 is >95% of the sulfur leaving the engine and always is in the gas phase explains the overall >95% control efficiency. However, the same EGS unit that is designed to remove a high percentage of SO2 by absorption onto sea water droplets may only sparingly remove sulfuric acid and other condensable particles, as the design and collection principles for removing SO2 gas and particles are quite different (Cooper and Alley, 2011). While the SO2 gas is diffusing to the droplet surface, the nuclei-sized, condensable particles are imbedded in the stream flow and go around the droplet, unless close enough to the surface to diffuse there and be captured. The sulfuric acid particles are too small to be removed by impaction.

Many reasons can account for differences in reported PM generated from the combustion processes and collected with an EGS; for example, properties of fuel and the combustion unit, scrubber design and operating conditions, and measurement methods.

Further complicating the measurement of PM mass in a scrubber environment are the generation of condensable particles; for example, the SO3 (gas) into SO4*6.65H_2O (PM) and the partitioning of semi-volatile organic compounds to the particle phase. When exhaust contains both solid and condensable PM, it is well known that the sampling approach will affect the measured PM mass and properties. In this research, we collected PM on a filter, using a dilution ratio of 5-10 and dilution air at 47°C. Others (Fridell and Salo, 2014) used a two stage dilution unit with the first dilution being ~10/1 and air at 250ºC. Their second dilution increased the overall dilution from 64 to 106. Differences in sampling conditions can lead to differences in the penetration of condensable mass at the filter face and the overall measured PM mass. Both approaches will capture the solid PM mass but an approach with a lower dilution ratio and collection temperature will capture more of the condensable PM mass. For example, this research found more PM mass, thus the overall PM mass was reduced by 2-12% while Fridell and Salo (2014) found ~75% of the PM mass removed, suggesting that some of the condensable mass was lost using highly diluted high dilution with air at up to 250°C as the sulfuric and organic PM return to the gas phase and penetrate the filter.

The significance of these findings raise questions as to whether the intent of the IMO sulfur rule is being achieved in that the rule significantly lowered the sulfur content of fuels with the expectation there would be significant reduction in sulfur oxides and PM mass. The results confirmed the >95% reduction in sulfur oxides; however, by contrast PM mass removal was <12%. Since PM mass is driven by sulfate mass, and very little sulfate is removed, the result is as expected. We believe these findings raise several questions.

First, whether there needs to be a separate PM standard since processes and operating conditions will affect the PM mass generated in the process and collection efficiency, and second, whether there needs to be a standard method for measuring the PM before and after the scrubber. Without such a discussion, it is doubtful that the intended health benefits from the IMO sulfur rule will be achieved as more heavy fuel oil is burned and thousands of new scrubbers are installed.

8.6. **Acknowledgements**

The authors thank the following organizations and individuals for their valuable contributions to this study. We acknowledge funding from the International Council on Clean Transportation (ICCT). We acknowledge Mr. Eddie O'Neal and Mr. Mark Villela of the University of California, Riverside for their contributions in conducting the emissions testing for this program. We also thank Dr. Kevin Thomson and Dr. Stéphanie Gagné from National Research Council (NRC) Canada and Dr. Tak Chan from Environmental and Climate Change (ECC) Canada for their contribution. We acknowledge AVL for providing the Smoke Meter.

8.7. **References**

Agrawal, H., Malloy, Q. G., Welch, W. A., Miller, J. W., & Cocker, D. R. (2008). In-use gaseous and particulate matter emissions from a modern ocean going container vessel. Atmospheric Environment, 42(21), 5504-5510.

Agrawal, H., Welch, W. A., Henningsen, S., Miller, J. W., & Cocker, D. R. (2010). Emissions from main propulsion engine on container ship at sea. Journal of Geophysical Research: Atmospheres, 115(D23).

Andreasen, A., & Mayer, S. (2007). Use of seawater scrubbing for SO2 removal from marine engine exhaust gas. Energy & Fuels, 21(6), 3274-3279.

Berglen, T. F., Berntsen, T. K., Isaksen, I. S., & Sundet, J. K. (2004). A global model of the coupled sulfur/oxidant chemistry in the troposphere: The sulfur cycle. Journal of Geophysical Research: Atmospheres, 109(D19).

Birch, M. E. (1999). Elemental carbon (diesel particulate): Method 5040. NIOSH Manual of Analytical Methods (NMAM).

Cappa, C. D., Onasch, T. B., Massoli, P., Worsnop, D. R., Bates, T. S., Cross, E. S. & Kolesar, K. R. (2012). Radiative absorption enhancements due to the mixing state of atmospheric black carbon. Science, 337(6098), 1078-1081.

Caiazzo, G., Langella, G., Miccio, F., & Scala, F. (2013). An experimental investigation on seawater SO2 scrubbing for marine application. Environmental Progress & Sustainable Energy, 32(4), 1179-1186.

Cooper, C. D., & Alley, F. C. (2010). Air pollution control: A design approach. Waveland Press.

Corbett, J. J., Winebrake, J. J., Green, E. H., Kasibhatla, P., Eyring, V., & Lauer, A. (2007). Mortality from ship emissions: a global assessment. Environmental science & technology, 41(24), 8512-8518.

Davis, D. D., G. Grodzinsky, P. Kasibhatla, J. Crawford, G. Chen, S. Liu, A. Bandy, D. Thornton, H. Guan, and S. Sandholm (2001), Impact of ship emissions on marine boundary layer NOx and SO2 distributions over the Pacific Basin, Geophys. Res. Lett.,28, 235–238.

Entec UK Limited. (2002). Quantification of emissions from ship associated with ship movements between ports in the European Community. Final Report.

Eyring, V., Köhler, H. W., Lauer, A., & Lemper, B. (2005). Emissions from international shipping: 2. Impact of future technologies on scenarios until 2050. Journal of Geophysical Research: Atmospheres, 110(D17).

Fridell, E., & Salo, K. (2014). Measurements of abatement of particles and exhaust gases in a marine gas scrubber. Proceedings of the Institution of Mechanical Engineers, Part M: Journal of Engineering for the Maritime Environment, 1475090214543716.

Hansen JP. Exhaust gas scrubber installed onboard MV Ficaria Seaways (Public test report). København: Environmental Protection Agency, Danish Ministry of Environment, 2012.

International Maritime Organization (IMO), Marine Environment Protection Committee 184(59), adopted on July 17 2009, http://www.imo.org/blast/blastDataHelper.asp?data_id=26469&filename=184(59).pdf

International Maritime Organization (IMO), Sulphur oxides (SOx) – Regulation 14, accessed on October 10 2016, http://www.imo.org/en/OurWork/environment/pollutionprevention/airpollution/pages/sulphur-oxides-(sox)-%E2%80%93-regulation-14.aspx

IMO International: IMO Marine Engine Regulations, http://www.dieselnet.com/standards/inter/imo.php

IMO Nitrogen Oxides (NOx) – Regulation 13: http://www.imo.org/en/OurWork/Environment/PollutionPrevention/AirPollution/Pages/Nitrogen-oxides-(NOx)-%E2%80%93-Regulation-13.aspx

IMO Sulphur oxides (SOx) – Regulation 14: http://www.imo.org/en/OurWork/environment/pollutionprevention/airpollution/pages/sulphur-oxides-(sox)-%E2%80%93-regulation-14.aspx

Jayaram, V., Nigam, A., Welch, W. A., Miller, J. W., & Cocker III, D. R. (2011). Effectiveness of emission control technologies for auxiliary engines on ocean-going vessels. Journal of the Air & Waste Management Association, 61(1), 14-21.

Khan, M. Y., Giordano, M., Gutierrez, J., Welch, W. A., Asa-Awuku, A., Miller, J. W., & Cocker III, D. R. (2012). Benefits of two mitigation strategies for container vessels: cleaner engines and cleaner fuels. Environmental science & technology, 46(9), 5049-5056.

United States Environmental Protection Agency (USEPA). Exhaust gas scrubber washwater effluent. EPA-800-R-11-006, November 2011. Washington, DC.

Lawrence, M. G., & Crutzen, P. J. (1999). Influence of NOx emissions from ships on tropospheric photochemistry and climate. Nature, 402(6758), 167-170.

Li, R., Kou, X., Tian, J., Meng, Z., Cai, Z., Cheng, F., & Dong, C. (2014). Effect of sulfur dioxide on inflammatory and immune regulation in asthmatic rats. Chemosphere, 112, 296-304.

Miller, J. W., Agrawal, H., & Welch, W. A. (2009). Criteria Emissions from the Main Propulsion Engine of a Post-Panamax Class Container Vessel Using Distillate and Residual Fuels (CARB Report). University of California, USA.

Oikawa K, Yongsiri C, Takeda K, et al. Seawater flue gas desulphurization: its technical implication and performance results. Environ Prog 2003; 22: 67–73

Schneider, J., Hock, N., Weimer, S., Borrmann, S., Kirchner, U., Vogt, R., & Scheer, V. (2005). Nucleation particles in diesel exhaust: Composition inferred from in situ mass spectrometric analysis. Environmental science & technology, 39(16), 6153-6161.

United Nations Conference on Trade and Development (UNCTAD), Review of Maritime Transport 2015

United State Environmental Protection Agency (US EPA), MARPOL Annex VI, accessed on October 5 2016, https://www.epa.gov/enforcement/marpol-annex-vi

Winnes, H., & Fridell, E. (2009). Particle emissions from ships: dependence on fuel type. Journal of the Air & Waste Management Association, 59(12), 1391-1398.

8.8. **Supporting Information**

8.8.1. **Supplemental Tables**

Table S8-1 Test Sequence

Test No.	Sampling Source	Location to Scrubber	ME Load	MG Load	Sampling DR
1	MG	Pre	0%	29%	20
2	ME	Pre	51%	52%	12
3	ME	Pre	74%	55%	8
4	ME	Pre	94%	57%	20
5	ME	Pre	91%	57%	6
6	ME+MG	Post	77%	56%	6
7	ME+MG	Post	49%	56%	8
8	ME+MG	Post	75%	56%	20
9	ME+MG	Post	75%	56%	12
10	**ME-only**	Post	92%	0%	6
11	ME+MG	Post	75%	57%	8
12	MG	Post	0%	46%	20

8.8.2. **Supplemental Figures**

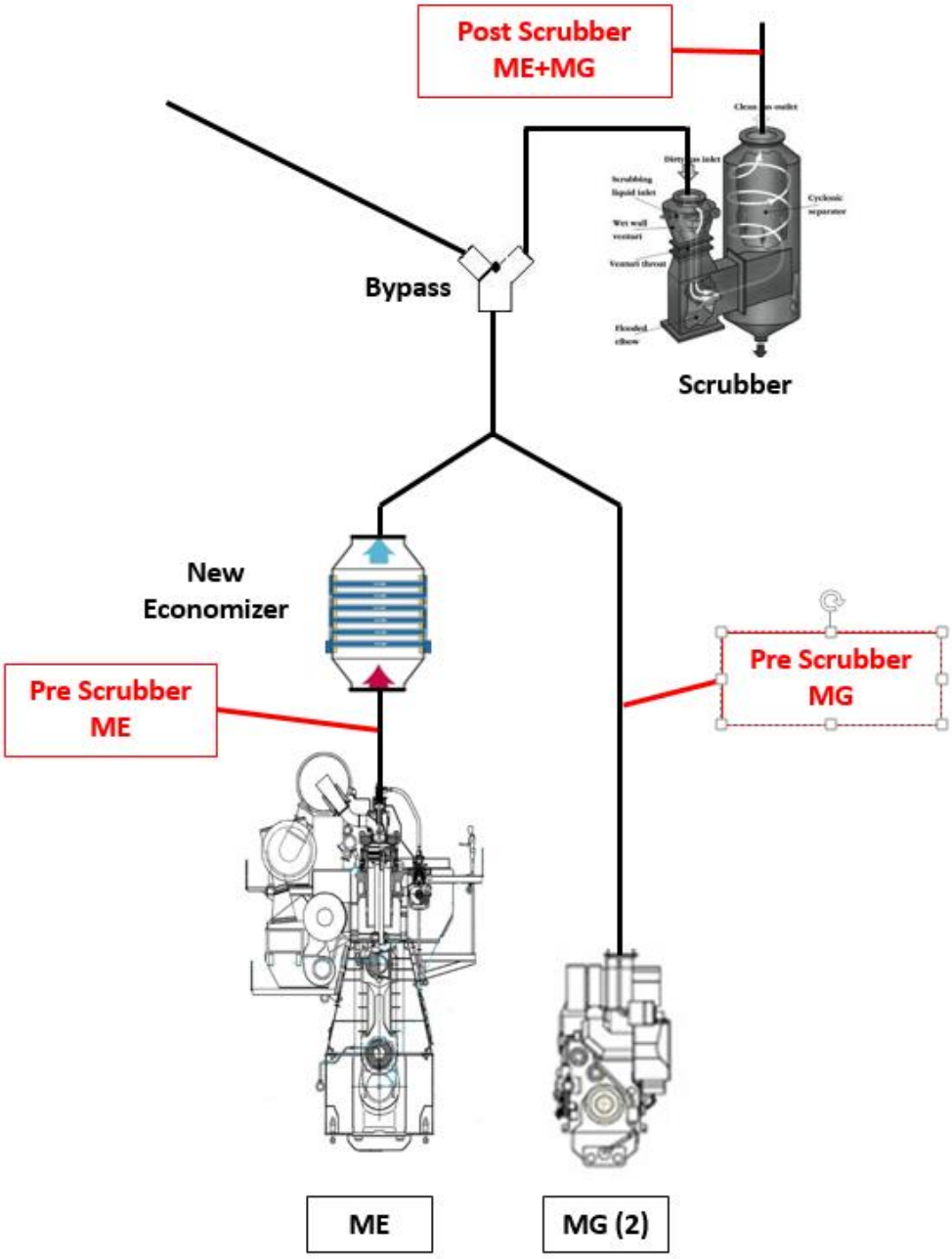

Figure S8-1 Schematic Diagram for the Tested OGV Engines Layout

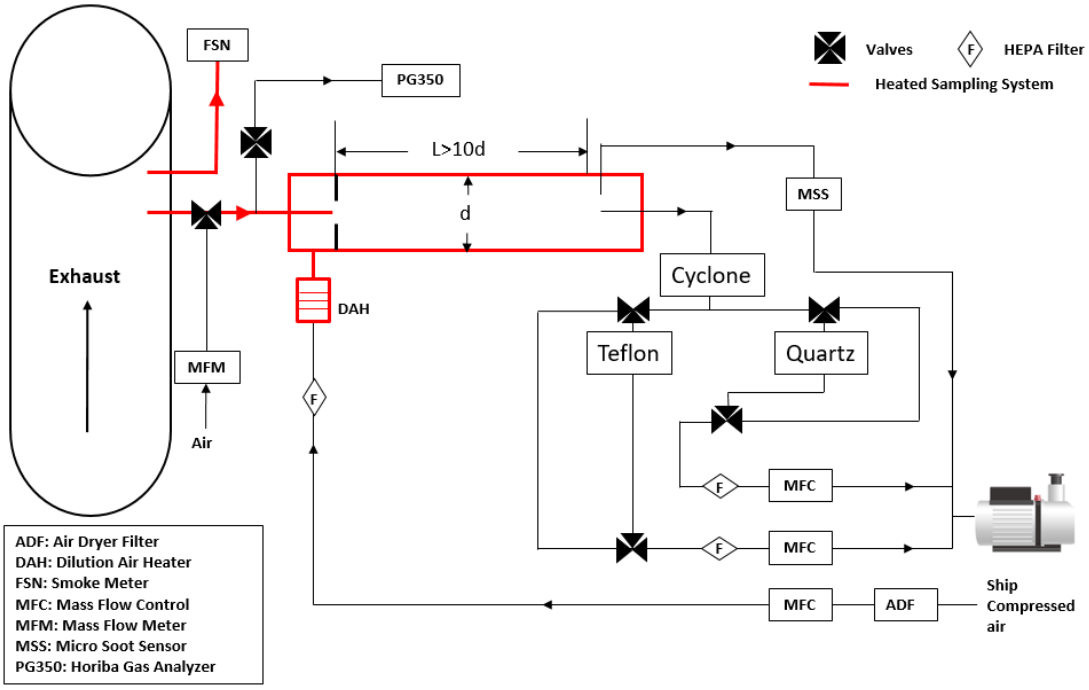

Figure S8-2 Schematic of the Dilution Sampling System

9. Conclusions

The main objective of chapters two to four in this research was to understand the PM emissions from light duty GDI vehicles, and how their emissions can controlled and monitored. Chapters two and three laid out PM control strategies with GPFs and higher ethanol content gasoline fuel. Chapter four investigated the PM toxicity from current technology GDI vehicles. Chapter 5 focused on the evaluation of sensors to see how accurate and robust they were compared to a fully 1065-compliant PEMS. The main objective of chapters six to eight in this research was also to evaluate the emissions reductions from advanced aftertreatment device and alternative fuels, but more focused on the diesel engines with the applications in on-road trucks, off road equipment, and large ocean going vessels.

Chapter two demonstrated that current technology GDI vehicles could be an important source for on-road ultrafine particles and black carbon emissions, and ultimately a contributor to urban air pollution. It was found that the use of catalyzed GPFs could significantly reduce the PM mass and black carbon emissions, as well as total and solid particle number emissions. This is without having a measurable impact on the vehicle's GHG emissions and fuel economy. This study showed that catalyzed GPFs could also improve the conversion efficiency for NOx, THC, and CO emissions. This is one of the few studies showing that GDI vehicles could significantly contribute to PAH and nitrated PAH emissions, and to our knowledge, the only one that looked at remediation of these toxics using a catalyzed GPF. The catalyzed GPF significantly reduced the particle-phase

PAHs and nitro-PAHs emissions, especially the less volatile or highly reactive PAH species. On the other hand, the vapor-phase PAHs did not show the same filtration efficiency as the PM-bound compounds. This study showed that GDI vehicle exhaust is characterized by diverse PAH distribution profile, ranging from 3-6 ring species. The projected increased penetration of GDI vehicles in the US market, suggests that future health studies aimed at characterizing the toxicity of GDI emissions are needed to understand the health risks associated with non-GPF-equipped GDI PM emissions.

Chapter three evaluated the gaseous and particulate emissions from a FFV equipped with a wall-guided direct injection gasoline engine with different level ethanol blends. The results reported in this study demonstrated strong emissions reductions for PM mass, black carbon, total and solid particle number with the higher ethanol blends and the lower PMI E10 fuel compared to the high PMI E10HA. The higher PMI fuel showed increased populations of accumulation mode particles, while the E78 blend had an almost unimodal particle distribution dominated by nucleation mode particles. Our results also showed that the use of higher ethanol blends resulted in lower THC, NMHC, CO, and NOx emissions from a current technology GDI FFV. The higher aromatic E10 fuel showed higher THC and NMHC emissions than the lower aromatic E10 fuel, suggesting the formation of these pollutants were more sensitive to fuel aromatics than CO and NOx emissions. The GHG emissions of CO_2 and CH_4 showed some increases with the E78 blend compared to the other fuels. This could potentially be a concern for high concentration ethanol blends considering the global warming potential for both the CO_2 and CH_4 gases. As expected, the vehicle experienced a fuel economy penalty with the higher ethanol blends due to their

lower energy content per gallon compared to the E10 fuels. Ethanol fuels showed a clear increase in acetaldehyde emissions, but mixed results for formaldehyde emissions. The fuel effect on BTEX and 1,3-butadiene emissions was particularly strong, with aromatics being the main driver for their formation. Fuels with lower aromatics and higher ethanol contents showed lower BTEX and 1,3-butadiene emissions. Overall, this study provided valuable insights on the impacts of ethanol content and gasoline composition on the exhaust emissions from a current technology GDI FFV.

Chapter four examined the physical and toxicological properties of particulate emissions from current technology GDI light-duty vehicles while operating over the LA92 driving cycle. Our results showed that three of the four GDI vehicles tested had PM emissions from 3 to 5 mg/mile, while one emitted about 0.2 mg/mile, thus showing the technical possibility for significant reductions for GDI vehicles with the latest technology. The toxicology metrics employed in this study indicate that at least for acute exposure, toxicity is relatively low in comparison to many ambient PM samples, both for reactive oxygen species (ROS) generation and for inflammatory potential. Dithiothreitol (DTT) and ROS followed a different activity profile across the samples, which is likely due to contrasts in PM composition, but additional studies with larger statistical power will be needed to better resolve those relationships. The overall suite of toxicology measurements suggests a likely role for small insoluble particles in inducing oxidative stress, either directly or by providing a catalytic particle surface. Ultrafine particles can also partition into the blood stream from the lungs and can travel to other organs including the brain. Whole animal studies will be needed to address these systemic effects. Effects on

macrophages can be especially important since the microglia in the brain share some responses that are key contributors in some neurodegenerative diseases.

Chapter five compared emissions measurements between a 1065 compliant AVL M.O.V.E.S. PEMS, and a current generation mini-PEMS capable of measuring NOx, PM, and solid PN. As recent findings have suggested, it is important to monitor vehicle emissions under a much wider range of conditions than can be duplicated in the laboratory. The comparisons between the 1065 compliant PEMS and the NCEM suggest that there could be applications for the NCEM or other mini-PEMS in areas where larger data sets of emissions data are needed, or where the cost of full laboratory or 1065 compliant PEMS testing is prohibitive. The NCEM could play a role in allowing for the testing of more vehicles under a broader range of conditions. For the NCEM in particular, a good comparison for NOx emissions was found, which suggests that the NCEM could be applied in a variety of areas where characterization of NOx is considered to be important, which could include in-use or I/M testing of light-duty or heavy-duty diesel vehicles. The PM emissions comparisons with the NCEM suggest that the NCEM could be effective in identifying potential situations where high PM emissions might be found for either GDI vehicles or diesel vehicles with DPFs in various stages of failure. Additional testing of PM emissions over a wider range of PM emissions levels would be needed to better understand this possibility.

Chapter six assessed the emissions performance of DMC when blended with typical on-road CARB ULSD in a 1991 DDC Series 60 engine over the FTP test cycle. PM emissions showed consistent, statistically significant reductions for all of the DMC blends.

PM emissions decreased with increasing DMC blend levels, ranging from 30 to 78% for 5% to 30% DMC blends. These reductions were significantly higher than those typically seen for biodiesel at a comparable blend level. This can be attributed to the higher oxygen content in the DMC molecule, with DMC's chemical structure and physical properties potentially also being of importance at the higher oxygen levels. Particle number emissions followed opposite trends to the PM mass, and showed increases with increasing DMC blending. The increases in particle number emissions for the DMC blends were statistically significant, with the exception of DMC5. Consistent with the particle number emission results, the application of DMC resulted in higher concentrations of nucleation mode particles compared to CARB ULSD, suggesting a suppression of soot particles available for condensation of semi-volatile species and a promotion of nucleation mode particles. Emissions of NO_x generally increased with increasing DMC, especially for the higher DMC blends. The same observation holds for the THC emissions, where the increases for the DMC blends relative to CARB ULSD were at a statistically significant level. As expected, BSFC showed increases with the DMC blends, as a result of the lower energy content of DMC compared to diesel fuel. On the other hand, CO emissions showed clear reductions with the use of DMC blends at a statistically significant level. Overall, the use of DMC led to increases in BTEX emissions and most VOCs relative to CARB ULSD, including carcinogenic benzene. It was observed that mono-aromatic and polyunsaturated hydrocarbons that are known soot precursors showed increases with increasing DMC blending. Formaldehyde and acetaldehyde were the predominant aldehydes in the exhaust, and the use of DMC resulted in higher aldehyde levels compared to CARB ULSD.

Chapter seven evaluated advanced emissions aftertreatment devices for four small off-road diesel engines, with applications for a TRU, ride mover, mini excavator, and skid steer. DPFs were added onto TRU and mini excavator engines, while a SCR was added onto a ride mover engine. A Skid steer engine was equipped with SCRT, where a DPF and SCR are combined. For the TRU and mini excavator engines, the PM reduction were over 97% for both engine with the addition of DPFs. Depending on the DPF designs and the way DPFs handled regeneration, the power output could be reduced up to 6% based on our results. For the ride mover engine with the SCR system, NOx emissions were reduced 70% for a C1 cycle and close to 50% for NRTC cycles. The lower reductions for the NRTC cycles were mainly due to the transient duty cycle, and that the SCR could not achieve the activation temperature during the first section of the cycle. So, the SCR was not functioning at the beginning of the cycle until the catalyst temperature reached 250℃. Similar trends were observed with the skid steer engine, where the NRTC showed lower reduction efficiencies compared to C1 cycle.

Chapter eight evaluated a cutting-edge scrubber system on sulfur emissions reductions for an OGV. The scrubber showed good reductions for SO_2 (>97%), but a relatively low control efficiency (2-12%) for PM mass. Since PM mass is driven by sulfate mass, and very little sulfate is removed, the result is as expected. The significance of these findings raise questions as to whether the intent of the IMO sulfur rule is being achieved. In particular, the rule required the sulfur content of fuels to be significantly reduced, unless a significant reduction in sulfur species can be obtained with an ECS. The regulations do not incorporate PM sulfate, however. These findings raise several questions. First, whether

there needs to be a PM standard since processes and operating conditions affect the PM control efficiency, and second, whether there needs to be a discussion of a standard method for measuring the PM before and after the scrubber. Without such a discussion, it is doubtful that the intended SOx and PM mass reduction will be achieved before 1,000 of new scrubbers are installed on OGVs.